UNIVERSITAT AUTÒNOMA DE BARCELONA

Programa de Doctorat en Ciencia i Tecnologia Ambientals

TESI PER OPTAR AL GRAU DE DOCTOR PER LA UNIVERSITAT AUTÒNOMA DE BARCELONA EN EL PROGRAMA DE CIENCIA I TECNOLOGIA AMBIENTAL

Barcelona, Juliol de 2015

Títol:

Tracing metal-CO_2(aq)-solid interactions from deep sources to shallow aquifers

---

Tesi presentat per: *Marco Agnelli*

Sota la direcció de: [a] *Dr. Fidel Grandia i Borràs i* [b] *Dr. Pere Masqué i Barri*

[a]*Amphos21 Consulting SL*

[b]*Universitat Autònoma de Barcelona*

SEVENTH FRAMEWORK PROGRAMME

MetTrans

MARIE CURIE ACTIONS

UNIVERSITAT AUTÒNOMA DE BARCELONA

Programa de Doctorat en Ciencia i Tecnologia Ambientals

Tracing metal-CO_2(aq)-solid interactions from deep sources to shallow aquifers

MARCO AGNELLI

Ph.D. Thesis

Barcelona, 2015

UNIVERSITAT AUTÒNOMA DE BARCELONA

Programa de Doctorat en Ciencia i Tecnologia Ambientals

Tracing metal-CO_2(aq)-solid interactions from deep sources to shallow aquifers

Memòria presentada per Marco Agnelli, sota la direcció del Dr. Fidel Grandia i Borràs i del Dr. Pere Masqué i Barri, per optar al grau de Doctor per la Universitat Autònoma de Barcelona en el programa de Ciencia i Tecnologia Ambiental.

Barcelona, Juliol de 2015

Vist i plau

Dr. Fidel Grandia i Borràs

Dr. Pere Masqué i Barri

Foreword:

This thesis is part of the European Project Met-Trans, a Marie Curie Initial Training Network of leading European research groups in both academic and industrial institutions, which addresses outstanding issues in the migration of metals in the environment.

The Network is dedicated to providing young scientists with high quality personalised training in both research and complementary skills. 12 early-stage researchers (ESRs), all registered for PhD degrees, have been recruited.

MetTrans is a €3.5 million project funded by the European Union under the Seventh Framework Programme.

Ringraziamenti:

Quando si arriva al momento dei ringraziamenti non si sa mai cosa scrivere, anche perché le persone da ringraziare sono molte e c'é pure il timore di dimenticarsene qualcuna. Sperando peró che questo non succeda, anche perché l'etá dovrebbe essere ancora un'alleata, vorrei iniziare dai miei ***genitori****. Mi avete accompagnato sempre durante questo ventennio di studi, sostenendomi ed appoggiandomi, finanziariamente e moralmente, nei momenti belli ed anche in quelli piú complicati, offrendomi sempre una visione ottimistica degli eventi, dandomi sempre la libertá di fare le mie scelte e regalandomi poi buoni consigli su come affrontare le varie asperitá. Vi ringrazio per la determinazione ed il coraggio che mi avete trasmesso e che continuate a trasmettermi, che mi hanno dato finora la forza e la grinta per portare a termine tutti i miei obiettivi con i migliori risultati e nei tempi prestabiliti.*

Parlando di genitori, spero che mi sará perdonato da quelli di sangue, ma non posso fare a meno di nominare anche il mio "padre geochimico" oltre che mentore scientifico che mi ha assistito nel corso di questi anni. Grazie ***Orlando*** *per tutti gli insegnamenti che mi hai dato e per aver acceso in me la scintilla della geochimica, per avermi dato la possibilitá di lavorare con te durante le mie tesi di laurea e per avermi assisito anche dopo di queste, pretendendo sempre il meglio da me e spingendomi a fare sempre di piú. Il tuo aiuto ed il tuo supporto in tutti questi anni, tanto nel "campo" quanto nella vita reale, mi sono stati davvero preziosi durante questi tre anni di dottorato. Mi hai insegnato che non devo sottovalutarmi e che valgo piú di quello che possa pensare (cosa che ho effettivamente capito da dopo il nostro primo viaggio a Calatrava).*

Hablando de mentores, no puedo dejar de nombrar a ***Fidel Grandia****. Antes de todo, gracias por la confianza que tuviste en mi eligiéndome para el doctorado de investigación. En estos tres años además de conocimientos científicos me has dado muchos conocimientos de vida empresarial, profesionalizándome y haciéndome entender con paciencia la diferencia que hay entre universidad y empresa. Me has enseñado no sólo como redactar un artículo o un informe sin que se parecieran a la Divina Commedia de Dante, sinó también como hablar con los clientes, gestionar proyectos y presupuestos. Quiero agradecerte también de haber estado una de las pocas personas a no pretender*

que hablara catalán después de sólo cinco días que vivía en Barcelona y de ayudarme para aprender bien el castellano.

*Parlando di mentori, non posso non nominare il buon **Fidel Grandia**. Prima di tutto, grazie per la fiducia che mi hai dato selezionandomi per il dottorato di ricerca. In questi tre anni oltre che di conoscienze scientifiche mi hai farcito di conoscienze di vita aziendale e impresariale, professionalizzandomi e facendomi capire con pazienza la differenza che c'è tra una universitá ed una impresa. Mi hai insegnato non solo come redattare articoli e relazioni senza che sembrassero la Divina Commedia, ma anche come parlare con clienti, gestire progetti e budget. E grazie per essere stato uno dei pochi a non pretendere che sapessi parlare in catalano dopo cinque giorrni che vivevo a Barcellona.*

Hablando de Barcelona y de idiomas aprendidos, tengo que agradecer a la dulcisima "Maria Rosa", la primera persona que habló conmigo en toda la empresa y que siguió haciéndolo también después de burlarme de su inglés. Gracias para acogerme a brazos abiertos y para haberme estado cerca durante de los primeros meses en esta fantástica ciudad, haciéndome sentir un poco menos solo.

*Parlando di Barcellona e di lingue apprese, non posso non ringraziare la dolcissima "**Maria Rosa**", la prima a rivolgermi la parola in tutta l'azienda e che ha continuato a farlo anche dopo che avessi deriso il suo inglese. Grazie per avermi accolto a braccia aperte e per essermi stata vicina nei primi momenti in questa fantastica cittá, facendomi sentire un po' meno solo.*

*Se si parla di appoggio morale non si puó non nominare dunque un sacco di altre persone, tra cui in primis i miei fratelli (di sangue e non) **Luca**, **Matteo**, **Inno** e **Alberto**. Dal giorno della mia partenza ad ora non mi avete abbandonato un attimo, standomi vicino e tranquillizandomi in una infinita quantitá di modi. Mi avete fatto sentire come a casa, anche se tra di noi c'erano 1200 Km e 11 ore di macchina. Siete venuti a trovarmi quando ancora non conoscevo nessuno nella metropoli e mi avete fatto compagnia ogni qual volta rientrassi dentro quelle sempre piú sconosciute quattro case della nostra cittá, liberandovi sempre dai vostri impegni, di lavoro o di altro tipo. Il frutto della tranquillitá che mi avete dato é la presente tesi.*

*Sempre nel girone dei familiari voglio ringraziare **Mauro**. Sei stato un compagno virtuale preziosissimo durante i campionamenti con freddo e nebbia mentre canticchiavo "la nebbia agli irti colli, piovigginando sale, e sotto il Maestrale urla e bincheggia il mare".*

*Come non parlare poi di **Giada**. Sei stata una alleata, amica, confidente, sorella e chi ne ha piú ne metta unica ed impagabile. Insieme abbiamo affrontato mille avventure e disavventure durante questi tre anni, sorbendoci reciprocamente scleri e unilateralmente discussioni scientifiche e filosofiche fino alle due di notte. Grazie per avermi sopportato e supportato per tutto questo tempo.*

*Hablando de Giada, tengo que hablar también de **Jordi Garcia** de la Universidad Autónoma de Barcelona. Gracias por los cafés tomados de vez en cuando, por haberme aconsejado académicamente y no solo. Ha sido un placer enfrentarme y delirar científicamente contigo.*

*Parlando di Giada allora devo parlare anche di **Jordi Garcia** dell'Universitá Autonoma di Barcellona. Grazie per i caffé presi di volta in volta, per avermi consigliato accademicamente e non solo ed avermi aiutato in momenti di difficoltá. É stato fantastico confrontarmi e delirare con te scientificamente.*

*Querría agradecer también a **Jordi Bruno**, **Lara Duro, Mireia Grivé** y a todo el staff de **Amphos 21**, cuya competencia y personalidad han sido de inspiración y aprendizaje para mí durante estos tres años.*

Un ringraziamento va anche Jordi Bruno, Lara Duro e Mireia Grivé e a tutto lo staff di Amphos 21. La vostra competenza e personalitá sono state di ispirazione ed insegnamento per me durante questi 3 anni.

*A questo punto mi resta solo una persona da ringraziare, a meno che l'etá non sia l'alleata che pensassi. Grazie **Amelia** per essermi stata accanto in quest'ultimo anno di dottorato. La tua presenza é stata non solo inaspettata, quanto fondamentale per me e per il buon esito di questa tesi. Mi hai dato coraggio e forza, credendo in me e nelle mie capacitá in maniera esponenziale, regalandomi allo stesso tempo tranquillitá e sicurezza e facendomi sentire una persona speciale.*

A ce stade, je souhaiterais encore remercier une dernière personne, à moins que l'âge ne soit pas l'allié que j'imaginais. Je te remercie ***Amélia*** *d'avoir été à mes côtés au cours de cette dernière année de doctorat. Ta présence a non seulement été inespérée, mais aussi fondamentale pour moi quant à l'accomplissement de cette thèse. Tu m'a donné courage et force, tu as cru en moi ainsi qu'à mes capacités de manière exponentielle, tu m'as enseigné le français et tu m'as offert en même temps tranquillité et sécurité, me donnant l'impression d'être une personne spéciale.*

Abstract:

Researchers and energy companies involved in CO_2 capture and storage (CCS) are presently discussing the impact on the environment of potential leakage after the injection of CO_2 in deep aquifers. The effects of gas-water-rock interaction occurring during the injection, storage and leakage are still under debate. Studies based on natural systems can provide valuable information on physical and geochemical processes occurring underground.

One of the most concerning aspects of the risk assessment of CCS is the potential impact on water resources in case of leakage, especially on shallow aquifers. The research on the effects of dissolved CO2 on the mobility of some metals in aquifers has been mainly focused on Fe(III) solubility, and experimental results match observations in naturals systems, where high Fe concentration can be found under oxic, circum-neutral solutions.

The main research objective of this Ph.D. project is the study of the capacity of aquifers to supply metals and metalloids from reactions with CO_2-bearing fluids, and their persistence in solution in the impacted aquifers. The research has been divided into three different parts.

The first part is a review of the variety of mechanisms for metal mobilization and transport in fluids characterized by a high amount of dissolved CO_2 and by circum-neutral pH. Since 1990, it is postulated that increased CO_2 concentrations in seawater would affect trace element mobility, and a large number of laboratory experiments have been performed in order to determine the influence of increased CO_2 concentrations in the mobility of a number of key trace metals, including Fe(II), Fe(III) and U(VI). In this work, a number of these laboratory experiments from literature have been selected, revisited and compared with data from some natural systems. Natural analogues, in fact, provide valuable information on the gas-water-rock interaction and subsequent metal release and transport. In addition, to complement literature data, a detailed systematic sampling along a stream in North Spain, called Font Groga, was performed from the source point to the end. The aim of this sampling was to understand the change on the dissolved metal load as a consequence of a steady degassing state. The degassing leads to changes in the water pH-Eh state that control the chemical speciation of most elements

in solution. The sampling was carried out dividing the stream into a number of equidistant sampling points starting from the spring and then considering each point as a separated system in equilibrium with a given CO_2 pressure. From each sampling site, the concentrations of anions, cations, trace metals, "free" CO_2 and dissolved gaseous species in aqueous phase were determined. Water chemistry was interpreted by using the equilibrium chemical-speciation/mass transfer model PHREEQC-3. The results show that as the gas concentration decreases, as a consequence of the degasification, the pH increases. In the field, the impact of degassing is well evidenced by the precipitation of ferrihydrite and, later, calcite throughout the course stream. Also, the concentration of Fe is positively correlated with pCO_2, indicating a strong link between both parameters. The thermodynamic analysis indicate that the dissolved CO_2 allows the solubilisation of Fe(III) by the forming aqueous Fe(III) carbonate complexes. The impact of these complexes, especially $FeOHCO_3$, is the increase of the solubility of Fe(III) by three orders of magnitude. Such an impact is very well illustrated by looking at the ferrihydrite saturation index (SI) with or without considering the formation of the aqueous Fe-carbonate complexes. CO_2 degassing makes these complexes unstable and iron is back in to solid phase by precipitating colloidal particles of ferrihydrite.

From experiments in literature, the enhanced solubility of iron and other metals such as U in CO2-bearing fluids has also been confirmed looking at the available thermodynamic data due to the formation of aqueous carbonate complexes. Other metals (e.g., Hg(II), Pb(II), Zn(II), Ce(III) and Ce(IV)) the increased pCO_2 has a positive effect in terms of stabilising their carbonate or hydroxocarbonato solid phases. This is the result of the formation of carbonate containing solid phases, which are more stable than the aqueous carbonate complexes. In the case of Cr(III) the increased pCO_2 has no effect, as no Cr(III) carbonate complexes have been reported in the literature.

The second part of the Ph.D. project deals with the release and transport of metals as a result of the intrusion of CO_2 flows into shallow aquifers. This is an important aspect in the risk assessment associated with CO_2 sequestration, and the understanding of the persistence of metal plumes is a very concerning aspect. This work has been carried out in the Campo de Calatrava region, an old volcanic field in central Spain, where CO_2 flows from mantle interact with shallow aquifers resulting in remarkable metal release. 12 sampling stations have been selected for gas and water analysis, 10 as bubbling pools and 2 as episodic "cold" geysers. These samples are characteristically much enriched in trace metals compared to CO2-free aquifers, being Fe the most abundant, (up to

6.08×10-4 mol·L-1). Also, high concentrations of Mn (up 8.01×10-5 mol·L-1), Zn (up to 1.46×10-6 mol·L-1), Ni (up to 1.19×10-6 mol·L-1), Co (up to 7.1×10-7 mol·L-1), Cu (up to 3.3×10-7 mol·L-1) and As (up to 1.4×10-7 mol·L-1). pH range is very close to 6 and Eh is quite oxidising. Gas composition is almost pure CO_2, with no detectable amounts of CH_4 and H_2S.

Thermodynamic calculations reveal that the formation of aqueous Fe(III) carbonate complexes, mainly $FeCO_3OH$, as a result of the CO_2-shallow aquifer interaction causes the dissolution of native $Fe(OH)_3$ releasing iron and all trace metals sorbed onto its charged surface. Then, neither acidification, "reducing" gas impurities, nor low Eh environments (i.e., making Fe(II) as predominant iron form) can be considered as the main drivers for the development of the metal plumes associated to gas inflows into shallow aquifers.

The persistence of these metal plumes, which is crucial in the risk assessment studies of CO2 underground storage, is predicted to be potentially long since Fe(OH)3 is the solubility-limiting phase not only for Fe but also for the other metals with an observed increase in concentration. The effect of the formation of aqueous metal carbonate is not as relevant in metals like Mn, Zn, Cu, Co, Ni, and except for Mn, the measured concentration in samples from the Campo de Calatrava are far from the saturation in solid carbonates.

The last part of the thesis is aimed to assess the potential use of metals *as an early detection tool of low-intensity leakage from CO_2 storage.*

Diffusive gradients in thin films (DGT) have been tested in some CO_2-rich, metal-bearing fluids to assess their applicability as a monitoring tool in onshore CO_2 storage projects. These films are capable of adsorbing metals and recording changes in their concentration in water, sediments, and soils. Considering that CO_2 dissolution promotes metal solubilization and transport, the use of these films could be valuable as a monitoring tool of early leakage. A number of DGT have been deployed in selected springs with constant metal concentration in the Campo de Calatrava region. The studied waters show high concentrations of Fe, as high as 1 × 104 μg·L–1, Ni, Co, Zn, Cu, and Mn. Comparing re-calculated metal concentration in DGT with metal water concentration, two different metal behaviours are observed: (i) metals with sorption consistent with the metal concentration (i.e. plotting close to the 1:1 line in a [Me]DGT: [Me]water plot), and (ii) metals with non–linear sorption, with some data showing metal enrichment in DGT compared with the concentration in water. Metals in the first group

include Fe, Mn, Co, Ni, and U, and metals in the second group are Zn, Pb, Cr, Cu, and Al. From this research, it is concluded that the metals in the first group can be used to monitor potential leakage by using DGT, providing effective leakage detection even considering low variations of concentrations, episodic metal release, and reducing costs compared with conventional, periodic water sampling.

Resum:

Tant a nivell acadèmic com a les indústries energètiques involucrades en la captura i emmagatzematge geològic de CO_2 (CCS) actualment s'està discutint l'impacte sobre el medi ambient de potencials fuites a conseqüència de la injecció d'aquest cas en aqüífers profunds. Els efectes de la interacció aigua-gas-roca durant la injecció, emmagatzematge i fuita estan encara en el camp del debat científic. Els estudis duts a terme en sistemes natures poden proporcionar una informació molt valuosa sobre els processos físico-químics que tenen lloc en profunditat.

Un dels aspectes més preocupants pel que fa a l'anàlisi de risc en el CCS és el potencial impacte en els recursos hídrics degut a fuites de gas, especialment sobre aqüífers somers. La investigació sobre els efectes del CO_2 dissolt en la mobilitat de metalls en aquests aqüífers ha estat focalitzada en la solubilitat del Fe(III), i els assajos experimentals en laboratori permeten explicar les observacions fetes a la natura on concentracions molt altes de Fe han estat detectades en solucions oxidants i de pH neutre.

El principal objectiu de la recerca en aquesta tesi doctoral és l'estudi de la capacitat dels aqüífers per alliberar metalls i metal·loides a partir de reaccions amb fluids rics amb CO_2 i analitzar la seva persistència com a fases solubles. Aquesta recerca ha estat dividida en tres parts diferents.

La primera part és una revisió dels mecanismes que permeten la mobilitat dels metalls en fluids amb concentracions elevades de CO_2 dissolt i amb pH pròxims a la neutralitat. Des de 1990, la comunitat científica ha postulat que l'increment de la concentració d'aquest gas en l'aigua dels oceans afectaria la mobilitat de metalls traça, i des de llavors, un nombre important d'experiments de laboratori han estat dissenyats per tal de determinar la influència d'aquest increment sobre metalls com ara Fe(II), Fe(III) i U(VI).

En el present treball, alguns d'aquests experiments duts a terme i publicats en la literatura científica han estat seleccionats, revisats i comparats amb dades procedents de sistemes naturals. Aquests sistemes naturals, sovint anomenats anàlegs naturals,

proporciones de fet una informació molt rellevant sobre la interacció gas-aigua-roca i el conseqüent alliberament de metalls des de la roca cap a l'aigua de l'aqüífer. Així, per tal de complementar aquesta revisió bibliogràfica, s'ha estudiat en detall un rierol de la comarca de La Selva (Girona), anomenat Font Groga com a anàleg natural de transport de metalls en aigües amb alts continguts de CO_2 dissolt. L'objectiu d'aquest estudi ha estat entendre el canvi en la solubilitat del ferro com a conseqüència de la desgasificació del CO_2. La desgasificació comporta canvis en el pH de l'aigua que, en el seu torn, controla l'especiació aquosa de molts del metalls en solució. El mostreig dut a terme a la Font Groga consta de 8 estacions de mostreig dividides equidistantment des del punt d'emissió fins al final del rierol, considerant cada un d'aquests punts de mostreig com equilibris aigua-roca aïllats. Per a cada punt de mostreig s'ha analitzat la concentració d'anions, cations, metalls traça, CO_2 "lliure" i gasos dissolts. La química de l'aigua ha estat interpretada i modelada amb l'ajuda del codi PHREEQC. Els resultats indiquen que a mida que la concentració del gas decreix degut a la desgasificació, el pH s'incrementa. En el rierol, el impacte de la desgasificació s'evidencia per la precipitació de ferrihidrita, i, després, de calcita aigües avall. A més, la concentració de Fe correlaciona positivament amb la pressió de CO_2 mesurada, indicant un fort lligam entre els dos paràmetres.

L'anàlisi termodinàmica indica que la dissolució de CO_2 permet la solubilització del Fe(III) mitjançant la formació de complexes aquosos carbonatats. L'impacte d'aquests complexes, especialment $FeOHCO_3$, és l'increment de la solubilitat del Fe(III) d'uns tres ordres de magnitud. Aquest impacte és ben evident observant l'índex de saturació de la ferrihidrita calculat considerant o no la formació d'aquests complexes. La desgasificació del CO_2 a mida que el rierol avança implica la desestabilització d'aquests complexes i el ferro re-precipita en forma de partícules col·loïdals de ferrihidrita i per aquest motiu el sediment del rierol presenta una característica coloració vermellosa.

A més del ferro, l'increment de la solubilitat d'altres metalls per la formació de complexes ha estat estudiat al detall i reportat en la literatura, principalment en el cas de l'urani. Altres metalls, com ara Hg(II), Pb(II), Zn(II), Ce(III) i Ce(IV), l'increment de pCO_2 implica l'estabilització de les seves fases sòlides carbonatades o hidroxicarbonatades, ja que són més estables que els complexos carbonatats aquosos.

Finalment, en el cas del Cr(III), no s'ha observat cap efecte ja que no es coneixen complexes carbonatats per aquest metall.

La segona part de la tesi tracta de la solubilització i transport de metalls com a conseqüència de la intrusió de fluxos de CO_2 en aqüífers somers. Aquest és un aspecte molt rellevant en l'anàlisi de risc del CCS, en especial en la persistència de plomalls amb concentracions elevades de metall ja que pot posar en risc la qualitat de recursos hídrics. Aquest treball ha estat desenvolupat a la regió de Campo de Calatrava, a la província de Ciudad Real, que constitueix un antic camp volcànic on fluxos de CO_2 des del mantell terrestre interaccionen amb aqüífers poc profunds, resultant en una important solubilització de metalls des de la roca encaixant dels aqüífers. En aquesta zona s'han seleccionat 12 estacions de mostreig de gas i aigua, 10 de les quals eren "bullidors" (basses on el CO_2 fa borbollejar l'aigua) i dues eren guèisers freds ocorreguts ocasionalment durant canvis en la pressió de gas en l'aqüífer i canalitzats en pous d'extracció d'aigua. Les aigües estudiades estan característicament molt enriquides amb metalls comparades amb els aqüífers que no han interaccionat amb CO_2. En tots els casos, el ferro és el metall de transició més abundant (fins a 6.08×10^{-4} mol·L^{-1}). A més, concentracions altes de Mn (fins a 8.01×10^{-5} mol·L^{-1}), Zn (fins a 1.46×10^{-6} mol·L^{-1}), Ni (fins a 1.19×10^{-6} mol·L^{-1}), Co (fins a 7.1×10^{-7} mol·L^{-1}), Cu (fins a 3.3×10^{-7} mol·L^{-1}) i As (fins a 1.4×10^{-7} mol·L^{-1}) han estat observades. El rang de pH és molt proper a 6 i l'Eh és força oxidant. La composició del gas revela que els fluxos són gairebé de CO_2 pur, i no s'han detectat concentracions analíticament significatives de CH_4 and H_2S.

Els càlculs termodinàmics indiquen que la formació de complexos aquosos carbonatats de Fe(III), principalment $FeCO_3OH$, com a conseqüència de la interacció del gas amb l'aqüífer, causa la dissolució de partícules de hidròxids de ferro (ferrihidrita) presents en la roca alliberant ferro i tots els metalls traça adsorbits en la seva superfície. En conseqüència, ni l'acidificació, ni la presència de impureses de gasos reductors en el flux de gas, ni la formació de condicions reductores, poden ser considerades com els principals causants del desenvolupament de plomalls de metalls en els aqüífers afectats.

La persistència d'aquests plomall amb concentracions altes de metalls, molt important en l'anàlisi de risc del CCS, es preveu que sigui llarga ja que la ferrihidrita és la fase sòlida que limita la solubilitat no només del ferro sinó d'aquells altres metalls

dels que s'ha observat un increment en la seva concentració. L'efecte de la formació de complexes aquosos carbonatats resulta poc rellevant en metalls com ara el Mn, Zn, Cu, Co, Ni, i excepte pel Mn, les concentracions mesurades a la zona del Campo de Calatrava es troben lluny de la saturació de les seves corresponents fases sòlides carbonatades.

La darrera part de la tesi té per objectiu l'avaluació del potencial ús dels metalls com a eina de detecció precoç de fuites de gas de baixa intensitat en projectes d'emmagatzematge geològic. Els anomenats DGT (Diffusive gradients in thin films) han estat provats en algunes de les déus d'aigua amb CO_2 per tal de determinar la seva eficiència com a detectors de canvis en la concentració d'aquest gas. Aquests films són capaços d'absorbir i registrar canvis en la concentració de metalls en aigües, sediments i sòls. Considerant que la dissolució de CO_2 incentiva la solubilització i el transport de metalls, el seu ús pot resultar en una eficient metodologia de control de fuites. En aquest treball, un conjunt de DGT han estat instal·lats en déus seleccionades a la regió del Campo de Calatrava, que presenten concentracions molt altes de metalls. Els resultats indiquen que, comparant la concentració de cada metall en els DGT amb la corresponent concentració en l'aigua, es poden distingir dos comportaments diferents. En el primer cas, s'observa una sorció lineal mentre que el segon no és lineal registrant en alguns casos un enriquiment de metall en el DGT comparat amb l'aigua. En el primer grup s'inclouen el Fe, Mn, Co, Ni, i l'U, mentre que en el segon hi trobem el Zn, Pb, Cr, Cu, i l'Al. Les conclusions d'aquest estudi permeten afirmar que els metalls en el primer grup poden ser utilitzats per monitoritzar fuites de CO_2 mitjançant els DGT, proporcionant una detecció efectiva fins i tot considerant variacions petites en la seva concentració, a un cost relativament reduït en comparació a altres mètodes com ara el mostreig periòdic d'aigües.

MOTIVATION AND Ph.D. DISSERTATION STRUCTURE

The capture and the storage of CO_2 (CCS) in deep subsurface reservoirs is one of the options currently being considered to mitigate the rising anthropogenic greenhouse gas concentrations in the atmosphere. The injection of CO_2 in aquifers has become, then, a recurrent topic of scientific discussion for academic researchers and industry in the last 15 years.

Despite the exhaustive efforts, some debate still exists in some aspects of the carbon underground storage. One of them is the impact of CO_2 on shallow aquifers in case of leakage, although this possibility is unlikely if the geological site investigation has been carried out properly. Field studies and laboratory tests indicate that significant metal plumes are released once CO_2 is injected, but the mechanisms of solubilisation are still under discussion. This process may jeopardize the quality of fresh water resources and, consequently, is of great concern in the risk assessment analysis of CCS.

The motivation of this Ph.D. project is to provide further knowledge on the impact of gas leakage in the metal release and mobilisation in shallow aquifers. For that aim, selected natural systems have been used. These systems provide valuable information on the gas-water-rock interaction and subsequent metal release and transport. The use of natural analogues to CCS allows the observation of geochemical processes under realistic conditions occurring in the geological media, which provide complementary data to that obtained from laboratory experiments and from model calculations.

This Ph.D. dissertation consists of a number of sections describing multiple aspects:

The first section describes the general concepts and the main objectives of this work, each of which have been published as a paper in a scientific journal and reported in the annexes of the present document.

The second section reports the sampling and analytical methods commonly performed during all the field campaigns, focused on water sample, dissolved gas and “free” CO_2

collection. Some sampling and analytical methods used only for specific cases and campaigns are exhaustively explained in the specific objective section.

The third section consists of a detailed explanation of each objective of Ph.D. project.

The last section provides general conclusions of the thesis, with a set of implications and recommendations for the risk assessment of geological storage of CO_2.

Table of Contents:

List of figures:

List of Tables:

XXX

Section One

1 GENERAL CONCEPTS:

1.1 CARBON CAPTURE AND STORAGE (CCS) AND CLIMATE CHANGES

In the last decade, the study of natural emissions of greenhouse gas from the Earth interior to the atmosphere through their migration in the geosphere, is a field of investigation that has become increasingly important. This is due the need to establish the relationship between anomalies of gas flow generated underground and tectonic structures that favor its ascent (Etiope, 1999; Etiope et al., 1999; Lewicki and Brantley, 2000), as well as the global budget of some carbon-bearing gaseous compounds (such as CO_2, CH_4 and C_6H_6) with high environmental impact (Lelieveld et al., 1998). In fact, the presence of the carbon in its gaseous form in the atmosphere contributes to the phenomenon of the greenhouse effect. As a beneficial phenomenon for life for several million years, the greenhouse effect has indeed helped maintain suitable temperatures for the development of human, animal and plant, accumulating gases such as CO_2, methane, steam water in the upper layers of the atmosphere and preventing leakage of infrared radiation to space by redirecting it to the Earth's surface. In particular, CO_2 gas is an important component in natural environments controlling the water pH, the total alkalinity and the trace metals speciation. The first models for the total budget of this species were based on indirect estimates of the flow spread assuming it to be equal to the amount consumed by the chemical alteration (Berner et al., 1983: Berner and Lasaga, 1989).

The main natural sources responsible for the natural emission of CO_2 are volcanoes. These structures are in fact capable of emitting CO_2 into the atmosphere both in periods of eruptive activity both in periods of quiescence by fumarolic activity (Allard et al., 1991; Chiodini et al, 1996b; Etiope and Klusman, 2002). Another significant natural contribution of CO_2 from underground is related to the activity of hydrothermal systems. In fact, it is well known that the amount of this compound emitted as gaseous form from areas not affected by active volcanism, mainly related to thermal-metamorphic processes of carbonate rocks, is comparable to that of the active volcanic areas (Mahon et al., 1980; Kerrick et al., 1995; Seward and Kerrick, 1996; Chiodini et al., 2004; Castaldi et al., 2005).

The increase in atmospheric concentration recorded in the last two centuries it is not only due to natural emissions. In fact, following two successive Industrial Revolutions of the nineteenth century, a high release of carbon dioxide into the atmosphere was due to the intensive production of energy through combustion of fossil fuels accompanied by a strong deforestation.

The content of CO_2 of the atmosphere was measured for the first time at the beginning of 19th century. CO_2 is progressively increasing with time with the superimposed seasonal oscillations. During the vegetative growing season (i.e, spring and summer in mid and high latitudes of the north hemisphere) the vegetation absorbs CO_2 from the air and the atmospheric CO_2 decreases. On the contrary, during the hibernation period, the terrestrial biomass loses carbon and the CO_2 concentration in air increases.

The atmospheric CO_2 concentration increased from 280 ppm in the preindustrial period to 364 ppm in 1997 when the Kyoto protocol was drawn (Indermühle et al., 1999) and hit 400 ppm in 2015. The increased thermal imbalances and devastating weather events over the entire surface of the globe that have affected the planet in the last two hundred years, called to scientific analysis of the possible causes and correlations with the increased emissions of anthropogenic CO_2 in the atmosphere and to find a solution to reduce them.

According to a "business as normal" scenario, the CO_2 concentration will reach levels of 700 ppm the year 2100 (Scenario IS92a, in Houghton et al., 1996).

An example of the consequences caused by the increase in the atmospheric CO_2 concentrations is found in the surface of the ocean, whose average pH is approximately 0.1 units lower today than in the preindustrial period (Zeebe and Wolf-Gladrow, 2001). These changes might have important consequences on the biogeochemistry of the environment, especially on the life cycle of aquatic species. Atmospheric carbon dioxide dissolves readily in water and some dissolved molecules escape from the sea to the air. Most of the dissolved carbon dioxide reacts with sea water to form carbonates, which settle on the ocean floor as calcium carbonate either in the form of inorganic precipitates (limestones) or fixed as skeletons of various forms of marine organisms.

This loss is partially balanced by the action of inland water which slowly dissolves limestone deposits and transports the dissolved carbonates to the sea.

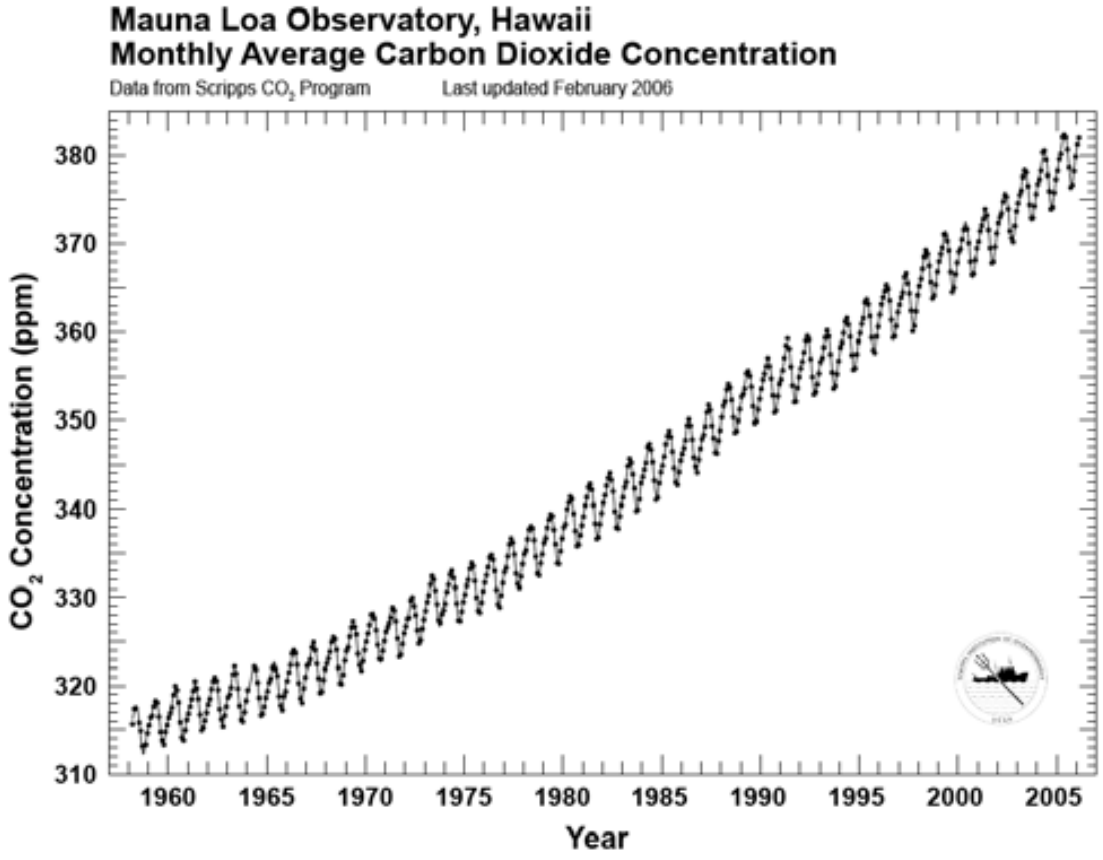

Fig. 1: Increase of CO_2 concentration in the atmosphere in the past 45 years, called Keeling curve (http://www.esrl.noaa.gov/gmd/ccgg/trends/)

In the last years, and as a result of the Kyoto protocol, a strong social and political debate has arisen on the use of energy sources different from those emitting CO_2 to the atmosphere, in order to reduce the existing CO_2 emissions.

Actually the main solutions to human reach and internationally recognized to long-term carbon trapping are: i) in the form of organic carbon from photosynthesis, and ii) as inorganic carbon from the physicochemical sequestration in deep geological formations.

1.2 *CARBON CAPTURE AND STORAGE (CCS) AS ENVIRONMENTAL AND ECONOMICAL OPTION*

The capture and the storage of CO_2 in deep subsurface reservoirs is one of the options currently being considered to mitigate the rising anthropogenic greenhouse gas concentrations in the atmosphere (e.g., European Commission, 2013). This option adds a set of proposed solutions to prevent global warming above 2°C such as energy efficiency, increased renewable energy and questioning the mode of consumption. These solution, on an industrial scale, should be applied at industrial sources of emissions (coal fired power plants and oil, oil refineries, cement plants, steel plants), to avoid significant new emissions from intensive, point-source industrial activities. This technique consists of three steps: i) separation and capture of CO_2 at the emitting industry, ii) transport as supercritical state and iii) its injection into geological reservoirs to store millions of tons of CO_2 over the long term (>10000 years).

The site selection of CO_2 storage reservoirs must be accurate enough to minimize the risks to human health and the environment (Rempel et al., 2011; Zheng et al., 2011).

Saline aquifers, exhausted and active hydrocarbon reservoirs (oil and gas), basaltic formations and coal seams represent the five possible types of geological reservoirs for the CO_2.

However, the reservoir capacity depends strictly on the performance (available volume) and on the geological stability of the reservoir (risks for seal formation failure and existing wells). Beyond the purely ecological aspect, the capture and geological storage of CO_2 can be also an economic benefit for oil and gas companies. In fact, the major advantage of geological storage in deep reservoirs of hydrocarbons is the enhanced recovery of oil and gas due to the piston effect during the injection activity (Fig. 2). In this way, unproductive reservoirs become interesting economically through CO_2 injection and subsequent production of hydrocarbons. Another enhancement of this concept is the Emission Trading System (ETS), in which low-emitting countries can sell emissions credits to more polluting states. Furthermore, CO_2-emitting industries could buy some emissions credits from those enterprises managing a CO_2 storage site.

Since the meeting in Japan in 2008 (34th G8 summit), there is the global common consensus for the selection of 20 pilot sites worldwide for the CO_2 geological storage,

with the aim to demonstrate both storage performances and security against potential leaks risks. The International Energy Agency estimates that $ 20 billion are needed for the development of the CCS worldwide. The set of chosen storage pilot sites in hydrocarbon reservoirs (Weyburn, Bahia) and saline aquifers (Sleipner, In Salah, Snøhvit) should allow the storage of ten million tons of CO_2.

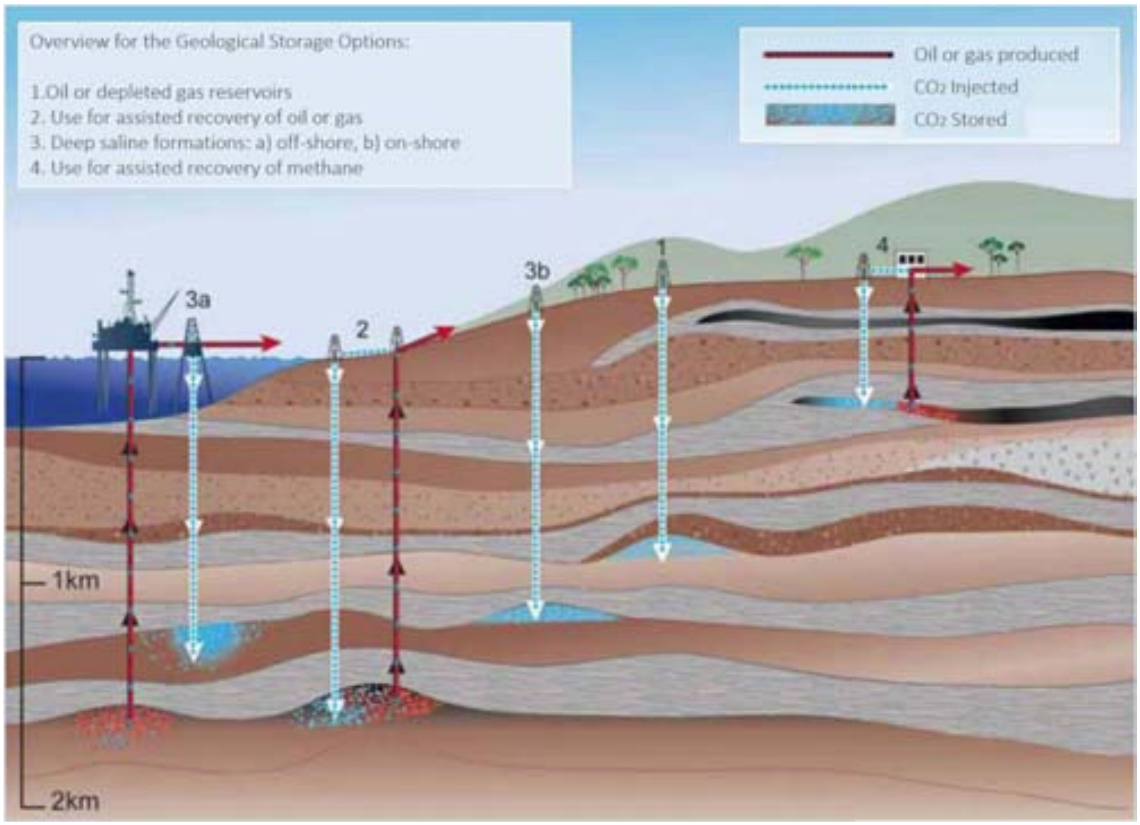

Fig. 2: The geological storage of CO2 (CGS), potential reservoirs and their theoretical capacity (modified from IPCC, 2005).

The challenge will then be to multiply the result by a factor of 100 during the next decade to arrive at that capacity of hundreds of millions of tons of stored CO_2 approved by experts (future SGC International Agency) to have a significant decrease in current anthropogenic footprint on the carbon cycle. The challenge is therefore double for the experts on geological storage of CO_2: i) Optimize storage performance to achieve CO_2 injected and trapped volumes in the order of hundreds of millions of tons and ii) Ensuring the safety of CO_2 sequestration in the reservoir for several thousands of years.

1.3 *CARBON CAPTURE AND STORAGE (CCS): GEOLOGICAL ASPECTS*

The steps of the CCS -collection, transport and storage- are three distinct areas of R&D for scientific and industrial world, but is in the storage where there are undoubtedly the greatest scientific challenges, including the prediction of the environmental impacts.. In fact, once CO_2 is injected at depths greater than 800 meters, the geochemistry and physics of the aquifer systems is strongly perturbed due to the interaction between CO_2 (+ trace gases), native water and host rock. These interactions occur in three main areas: i) The reservoir, a porous geological formation in which the CO_2 is directly injected as supercritical state forming a bubble and then migrating laterally and vertically, ii) Injection wells formed of steel layers and cement and iii) the cover, a very low permeability geological formation where the vertical migration CO_2 is limited or stopped naturally. Physical and chemical entrapment for the fluid operates during the injection for the long-term storage of supercritical CO_2 in the reservoir formation. These could be divided into i) structural trapping, by retention of the supercritical CO_2 into the pore space by capillary forces and at the interface of heterogeneous geological levels, ii) geochemical trapping, by dissolving the supercritical CO_2 in native fluids, increasing the density of the acidified solution and its migration to the deeper levels of the target aquifer and iii) mineralogical trapping, by precipitation of carbonate minerals due to the formation of carbonate and bicarbonate ions from the dissolution of CO_2. The wells also have a specific reactivity due to the presence of cement and iron-rich materials interacting with the acidified solution. However, depending on the geometry of the system, the injection pressure, the nature of the reservoir, alteration of the pipe lines and conduits and the period considered, some of the CO_2-rich phases can reach shallow aquifers, causing a variety of geochemical reactions.

The storage of CO_2 in deep subsurface reservoirs must be accurate enough to minimize the risks to human health and the environment. In fact, the possibility of CO_2 leakage cannot be completely ruled out, in which case the stored CO_2 could migrate following preferential pathways upward into overlying shallow groundwater resources or directly emitted to atmosphere (Fig. 3). The dissolution of CO_2 leads to a decrease of the pH and, in turn, to an increase on the dissolution, mobilization and re-precipitation of metals and other rock-forming elements.

In fact, acidification and carbonation of water could induce Fe-, Cr-, Zn-, Pb-, Ni- and Mn-bearing minerals dissolution that increases the concentration of these metals in water (e.g., Czernichowski-Lauriol et al., 2006; Kharaka et al., 2006; Wigand et al., 2008; Kharaka et al., 2009; Fischer et al., 2010).

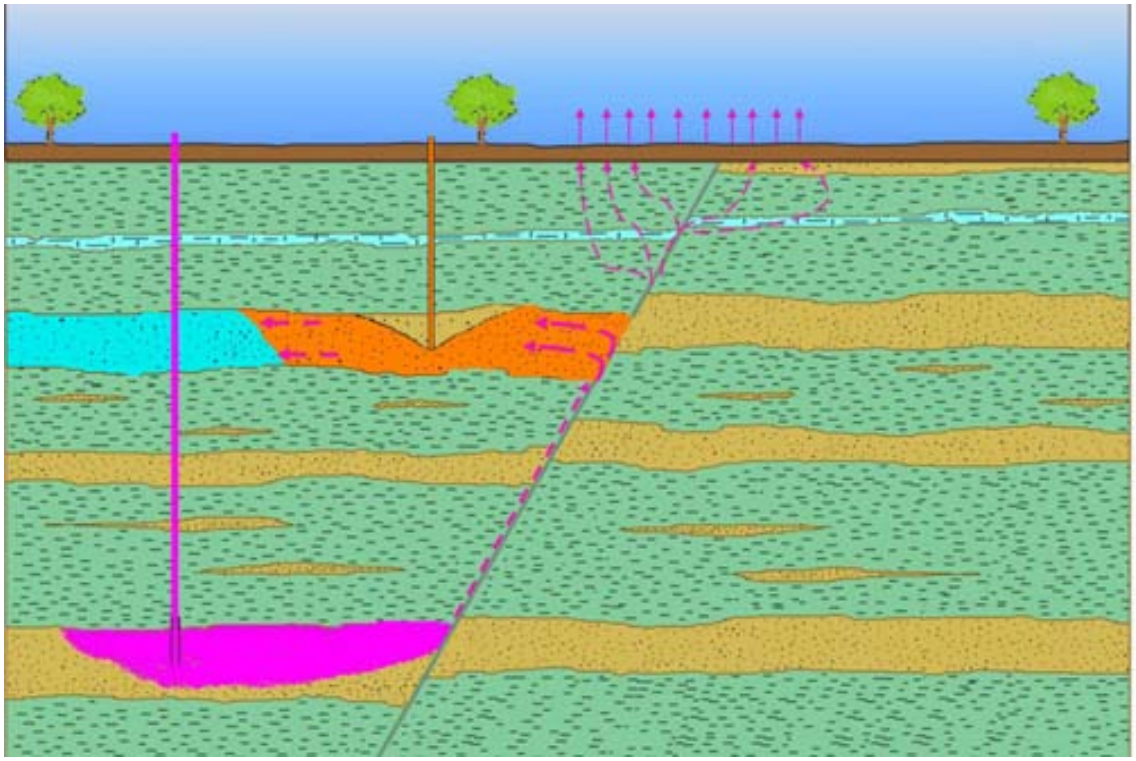

Fig. 3: Possible scenario of CO_2 leakage. The stored CO_2 could migrate following preferential pathways (i.e. fractures or faults) upward into overlying shallow groundwater resources leading to a decreasing of the pH and so to an increase on the dissolution, mobilization and re-precipitation of metal or diffuse naturally from the soil.

1.4 *CHEMICAL ASPECTS OF CARBON STORAGE:*

1.4.1 H_2O - CO_2 SYSTEM: Dissolution of CO_2 and system acidification

The reservoir and cover rocks are naturally filled with pore fluids that are mainly in equilibrium with the mineralogical composition of the host rock under the existing environmental conditions of the system (temperature, pressure). Once injected, the CO_2 migrates into the reservoir under supercritical state (>37 °C; >73 bars).

During injection, as well as during a potential leakage episode, the CO_2 present in its hydrated form $CO_{2(aq)}$ reacts with water to form carbonic acid H_2CO_3 (eq. 1). This acid dissociates into protons H^+ and bicarbonate ion HCO_3^- (eq. 1) for the interaction with the surrounding solution (initial pH > 6.00), decreasing the pH.

$$CO_{2(aq)} + H_2O \rightarrow H_2CO_3 \rightarrow H^+ + HCO_3^- \quad \text{pKa1 = 3.58, pKa2 = 6.37 (25°C)} \quad \text{eq.1}$$

$$H^+ + HCO_3^- \rightarrow 2H^+ + CO_3^{2-} \quad \text{pKa3 = 10.3 (25°C)} \quad \text{eq.2}$$

The predominant carbon species in the system depend on the acidity and alkalinity (Fig. 4).

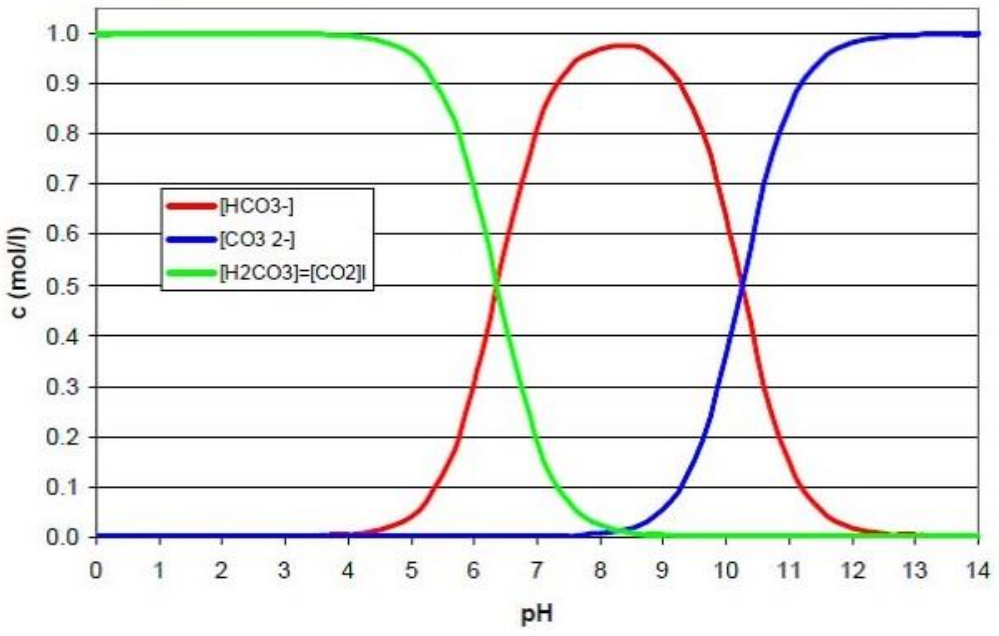

Fig. 4: Predominance diagram of the C(IV) species in water at 25 ° C.

1.4.2 H_2O - CO_2 SYSTEM: Metals solubility and mobility

In the last thirty years, the study of the trace metal mobiity in natural waters affected by carbon dioxide is a field of investigation that has become increasingly important. The pioneering works were by Hietanen and Högfeldt (1976) on mixed hydroxo-carbonate complexes of Hg(II), by Ferri et al. on Zn(II) (1987a) and on Pb(II) (1987b) mixed hydroxo carbonate complexes, and by Bruno et al. (1987) on the Be(II) hydroxo carbonate system. They early established that metal mobility in natural waters is affected by carbon dioxide content through the formation of mixed hydroxo-carbonate complexes.

The reaction of metal bridging OH groups with CO_2 to build carbonate bridges has been further studied for Cu(II) (Kitajima et al, 1990), for Zn(II) (Murthy and Karlin, 1993) and for a series of divalent organometallic(II) complexes, including Mn, Fe, Co, Ni, Cu and Zn, in Kitajima et al (1993). This research is particularly relevant in the case of zinc since the Zn(II) enzyme carbonic anhydrase catalyses the reversible reaction CO_2 hydration to produce bicarbonate, a process that is essential to remove CO_2 from tissues in mammalian respiration process. More recently, Huanga et al. (2011) have proposed a similar mechanism for the fixation of CO_2 onto a Ni(II) pyridine hydroxo complex which occur at remarkable fast rates ($10^6 \cdot M^{-1} \cdot s^{-1}$) compared to rates obtained for the transformation of metal hydroxides onto metal carbonates which are 1000 times slower.

1.4.2.1 Fe(III) Solubility and Mobility

Iron is a key metal ion in biological and geochemical systems as it regulates many key processes, including the scavenging and release of critical trace metals in natural water systems. The biogeochemical cycling of iron through the global reservoirs (atmosphere, oceans, soils, and sediments) depends on a number of physical, chemical and biological processes and it is regulated to a large extent by electron transfer processes (Fig. 5).

In all reservoirs, iron-bearing solids are present with high surface area to volume ratios. Surface-controlled reactions are, therefore, of great significance in regulating the composition of the reservoirs and they influence the mass fluxes of elements from one reservoir to another. The cycle of iron is often kinetically coupled with the cycles of P, S, heavy metals, O_2 and C, and depends on the biota and the energy and intensity of the light (Luther et al., 1992; Stumm and Sulzberger, 1992).

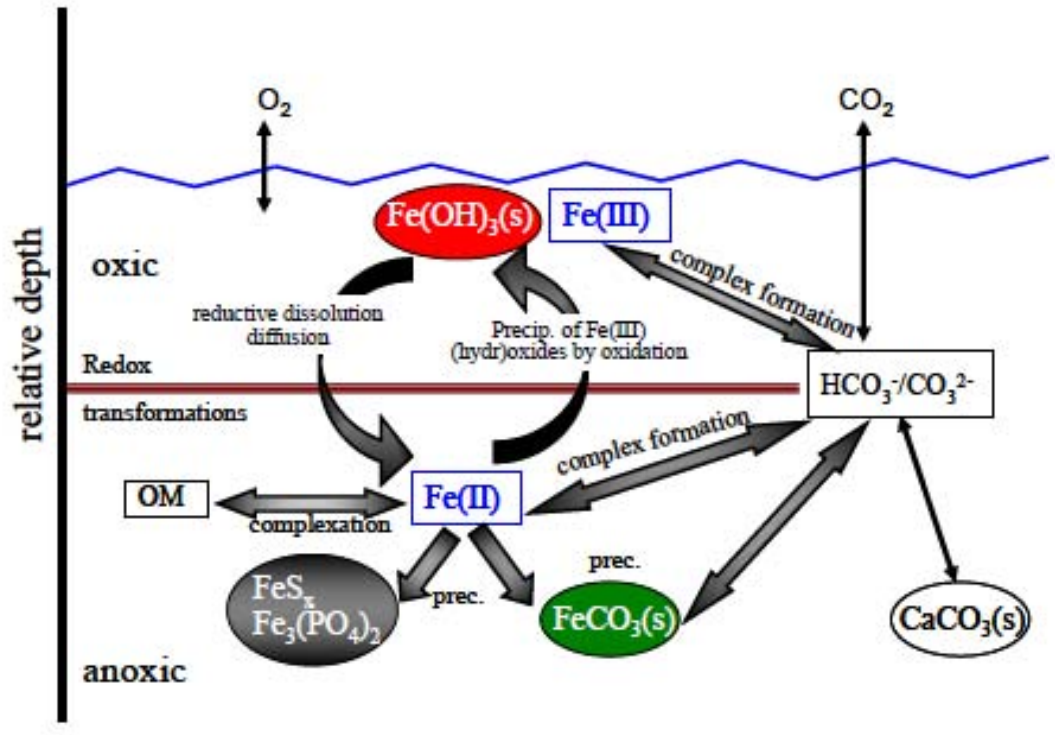

Fig. 5 Schematic diagram of important processes controlling the fate of dissolved iron at an oxic-anoxic boundary in a water column (Grivé, 2005).

The linkage between the iron and the carbon cycles is of paramount importance to understand and quantify the effect of increased CO_2 concentrations in natural waters on the mobility of iron and associated trace elements. The cycles of iron (Stumm and Sulzberger, 1992) and carbon (Berner and Lasaga, 1989) are also the drivers of the mobility and retention of trace elements involved in natural weathering processes of minerals as well as in the anthropogenic activities. This is especially critical in the biosphere/geosphere interface, where atmospheric oxygen and carbon dioxide undergo the main part of their transformation processes. Among them, the coupled dissolution precipitation of Fe(III) hydroxides and calcium carbonate are very dynamic processes in underground environments and can be normally approached assuming local equilibrium.

The oxygen-rich upper zone is a source of Fe(III) oxide solid phases, which settle downwards. In the other hand, the anoxic bottom waters are a source of dissolved Fe(II), which diffuses upwards. The oxidation of Fe(II) is accompanied by precipitation, and the reduction of Fe(III) oxy-hydroxides is accompanied by processes of dissolution. Precipitation and dissolution of Fe(III) oxy-hydroxides is normally fast in the order of hours-day time scale and the transformation of the ferric phases can lead to immobilization-mobilization of associated trace components. Therefore, the understanding of the effect of the different parameters affecting the dynamics of the Fe(III) system is critical to address the migration of the trace components potentially affected by this system. Nevertheless, there are at least two parameters affecting the oxic part of the cycle, (i.e., the stability of Fe(III) oxides under oxic conditions), which are not yet well known from a quantitative point of view. First of all the solid particle size of Fe(III) oxy-hydroxide that is the most important physical property of the solid that may affect solubility. Among the different iron oxides forming in nature, ferrihydrite is of particular interest because it may be considered to be the first iron oxide typically occurring in natural aqueous environments, undergoing further ageing to more crystalline forms like hematite or goethite (Schwertmann and Cornell, 1991; Cornell and Schwertmann, 1996). It is a poorly-ordered iron oxi-hydroxide that, due to its small grain size, shows a high specific surface area. This makes it an important constituent for surface-related processes in nature as well as in catalytic processes (Dzombak and Morel, 1990; Jambor and Dutrizac, 1998; Cornell and Schwertmann, 2003).

Precipitation of this mineral does not only control the concentration of iron in surface waters, but also removes many dissolved metals from the aqueous solution through co-

precipitation and adsorption processes (Schultz et al., 1987; Ford et al., 1997). Although numerous efforts have been devoted to measuring the solubility product constants of ferrihydrite, a wide range of solubility data has been reported. This wide range of variation in the solubility of ferrihydrite has been normally attributed to differences in the crystallinity of the solid.

The second parameter affecting the oxic part of the cycle is the carbonate concentration.

Dissolved carbonate is ubiquitous in aquifers and groundwater systems, often in equilibrium with CO_2 at partial pressures 100 to 1000 times higher than ambient atmosphere (Hem, 1989). Although the carbonate equilibrium contributes to regulate master variables as pH or alkalinity in most natural water systems, the coupling between the carbonate and the iron cycles in these systems is not completely understood. In groundwater, carbonate contributes to the mobilization of iron under reducing conditions by forming aqueous Fe(II) carbonate complexes and some thermodynamic data at the Fe(II)-CO_2-H_2O system are available from the literature (Larson, 1967; Mattigod and Sposito, 1977; Fouillac and Criaud, 1984; Nordstrom and Puigdomenech, 1986; Bruno et al., 1992). However, the available information on the influence of carbonate system in the iron cycle under oxic conditions is limited (Bruno et al., 1992; Bruno and Duro, 2000; Hummel, 2000; Grivé et al., 2014).

Despite the attention that has been already devoted to Fe(III) aqueous speciation, the thermodynamics of some species such as Fe(III) carbonates are still not well known, particularly in the pH range of natural waters (i.e., Bruno et al., 1992).

Recently, experiments conducted on the ferrihydrite under a different pCO_2 but maintaining the same circum-neutral pH, gave different iron concentrations (see Fig. 6) in equilibrium with ferrihydrite, indicating a dependence of iron measurements on the pCO_2 (Grivé et al., 2014).

Thus, the no-dependence on the pH but the clear dependence on pCO_2 suggests that aqueous iron species in equilibrium with ferrihydrite at this pH should be neutral and might be $FeOHCO_3(aq)$, as previously suggested (Bruno et al., 1992; Bruno and Duro, 2000).

As suggested by Grivé et al. (2014), the dissolution of ferrihydrite is therefore affected thermodynamically by the carbonate system, increasing its solubility in carbonated solutions.

The measured experimental data are well explained by assuming the formation of two aqueous Fe(III) species: $FeOHCO_3(aq)$ and $Fe(CO_3)_3^{3-}$. The dominant speciation for ferric iron may be shifted from hydrolysed species to $FeOHCO_3$ and $Fe(CO_3)_3^{3-}$ in groundwater environments, where pCO_2 reaches 10^{-2} atm.

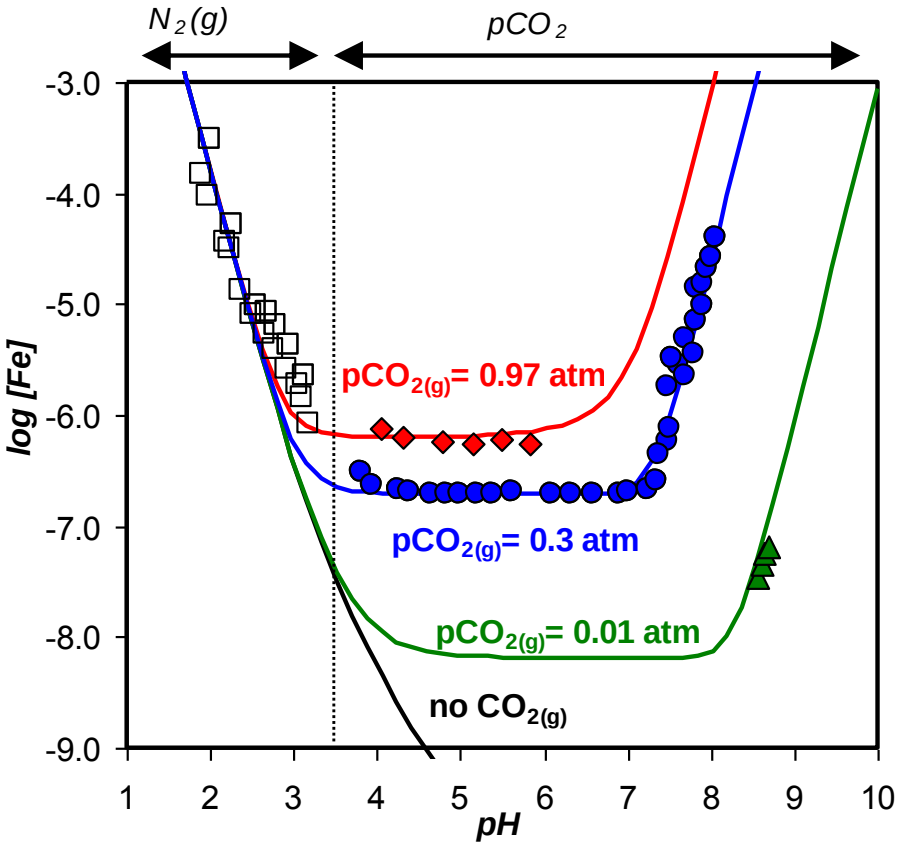

Fig. 6: Dependence of concentration of iron on pCO_2 inf the experiments conducted in equilibrium with ferrihydrite (from Grivé, 2005).

In principle, the metal transport capacity of CO_2-bearing fluids in shallow aquifers should dramatically decrease as pH increases due the buffering with aquifer rocks and also due to the relative high Eh favouring very low iron solubility. However, the formation of Fe(III) carbonate complexes, that are stable at circumneutral pH's, make that the iron being more persistent in time and space in the geological media. The experimental results match observations in natural systems, where high Fe(III) concentration can be found under oxic, circum-neutral solutions where iron concentration is up to 3 orders of magnitude higher than that expected in CO_2-free solutions (Bruno et al., 2009).

One example illustrating on how the mixed Fe(III)-carbonate aqueous species predicted in Bruno et el. (1992) and Grivé (2005) and Grivé et al. (2014) might explain the high measured aqueous iron concentrations in some CO_2-bearing springs is given below (see Figure 7, data from Vilanova, 2004). As it can be observed, when those species are not taken into account, the calculated and measured iron concentrations are in total disagreement.When these species are considered in the calculations with the constants reported in Grivé (2005) and Grivé et al. (2014), the measured iron concentrations are in total agreement with the predicted (calculated) ones.

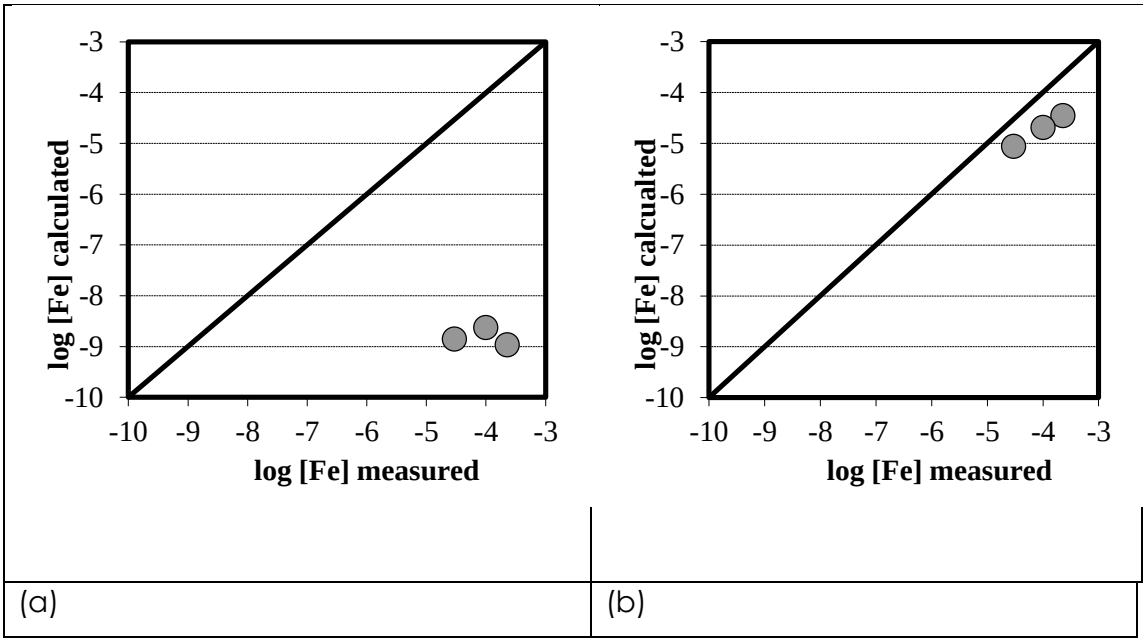

Fig. 7: Plot of the calculated iron (III) concentrations in some springs in the La Selva basin (Font de Bell-Lloch, Font Panedes and Font del Ferro), in front of the iron (III) measured concentrations (from Vilanova 2004)(a) No iron (III) aqueous carbonate species included in the thermodynamic database used (b) Effect of the consideration of iron (III) carbonate species proposed in Grivé (2005) and Grivé et al. (2014) in the thermodynamic database used in the calculations.

1.4.2.2 Secondary trace elemental mobility as a result of Fe(III) dissolution under oxic conditions

The enhanced solubility of Fe(III) has an additional and unwanted side effect: the inhibition of the precipitation of $Fe(OH)_3(am)$ (ferrihydrite), which is the main sink for many trace and minor elements in shallow aquifers. Then, CO_2-bearing solutions are particularly rich not only in iron but also in many other metals and metalloids, increasing the pollution impact of affected aquifers. The $Fe(OH)_3$ inhibition is gone due to CO_2 degassing related to fluid ascent to surface, and eventually part of all these metals may be precipitated back into solid phases but still some of the metal load is under solution.

The association of trace elements to Fe^{3+} oxy-hydroxides through sorption processes has also been very well established and the compilation by Dzombak and Morel(1990) summarizes the rationalization of these interactions through surface complexation reactions. Therefore, any effect of CO_2 on the solubility of the Fe(III) oxy-hydroxides cascades into the release of trace metals associated to these solid phases. In addition, for some trace metals, the formation of mixed hydroxocarbonato or carbonate aqueous complexes enhances their dissolution and consequently their mobility.

One of the trace elements that better exemplifies this is uranium. In oxic environments uranium is present in the hexavalent form and is rather soluble in natural water conditions.

However, U(VI) has also a strong tendency to sorb onto Fe(III) oxy-hydroxide phases and depending on the circumstances may even co-precipitate with these solid phases (Bruno et al, 1995). The presence of increased CO_2 concentrations has a double effect on this retention mechanism. On one hand, as we have seen in the previous section, carbon dioxide may destabilize the precipitate Fe(III) oxy-hydroxide releasing the attached U(VI) and in addition, increased total carbonate has the result of building stable U(VI) carbonate complexes. Duro (1996) studied the effect of increased HCO_3^- concentration in the kinetics of dissolution of $U(VI)/Fe(OH)_3$ co-precipitates. The kinetic data in terms of the U(VI) dissolved had a direct linear correlation with the dissolved HCO_3^- concentration, with a rate constant of the order of 10^{-3} moles $Ug^{-1}h^{-1}$. The comparison of the rates of congruent dissolution of the U/Fe co-precipitate and the pure schoepite indicated that the co-precipitate had a protective action against dissolution. This is that the rates in the presence of bicarbonate were three orders of magnitude slower in the case of the co-precipitate than the pure schoepite phase. However, the co-precipitate was

destabilized also in the presence of bicarbonate, indicating that in the long run, increased CO_2 and consequently larger bicarbonate concentrations would have a deleterious effect on metal-iron oxy-hydroxide co-precipitated phases.

Grivé (2005), investigated the effect of the carbonate system on the kinetics of dissolution of ferrihydrite, as representative of one of the most widespread oxides in nature behaving as a sink of trace metals, on the kinetics of dissolution of schoepite, which is one of the main secondary phases of uranium to form under oxidizing conditions, and on the kinetics of dissolution of a co-precipitate of Fe(III) and U(VI), given that the formation and dissolution of Fe minerals can imply the incorporation of U into these Fe oxide structures or the sorption of U onto these newly formed minerals. The mechanism for the ligand-promoted dissolution of ferrihydrite, schoepite and Fe(III)-U(VI) co-precipitate in bicarbonate solutions was ascertained in that thesis (Grivé, 2005) suggesting a three-step mechanism in the case of ferrihydrite and schoepite, and a two-step mechanism in the case of the co-precipitate. The applicability and validity of the model presented in the case of the co-precipitate was tested against independent data from Duro (1996) (see Grivé et al., 2005).

1.4.3 ENHANCED METAL TRANSPORT IN CO_2-BEARING FLUIDS: Leassons learned from laboratory experiments and natural analogues evidences

In recent years the focus of the research on CCS has shifted towards the potential environmental effects of the geological storage of CO_2 and in particular in the metal mobilization in aquifers affected by potential leakage from the storage complex. The effects of a potential CO_2 leakage from a carbon storage reservoir are one of the key environmental concerns related to the geological storage of CO_2. There is a large body of experimental, natural analogue and modelling studies in this respect (see Keating et al, 2013, and references therein)

An illustrative example of the impact of CO_2 dissolution on the iron transport is found in the aquifers affected by CO_2 flows from deep underground natural sources (i.e., mantle degassing, thermal decarbonation). This gas-water-rock interaction has been recently studied in detail in the environmental impact assessment of potential CO_2 leakage from geological storage (e.g., Zheng et al., 2009; Kharaka et al., 2010; Spangler et al., 2010). In addition, injection tests of high-pressured CO_2 have resulted in an increase of iron and other metals in the reservoir (e.g., Peter et al., 2012; Trautz et al., 2013). In this context, there are two issues to be concerned about. On one hand, increased CO_2 concentrations may induce increased acidity in poorly buffered systems where acidity increases of three orders of magnitude have been observed (Trautz et al, 2013). This increased acidity may result in the release of metals bound on the existing solid phases.

On the other hand, the increased CO_2 concentrations will result in the increase of the total carbonate of the system and consequently in the build-up of metal hydroxo carbonate and metal carbonate complexes, which will result in increased metal concentrations. In both scenarios, the metal mobilization has been commonly related to acidity increase and the relative high solubility of Fe(III).

How and where such leakage can be detected very early is then challenging. Natural systems provide evidence of metal increase in solution as a response of CO_2 intrusion but these are in most cases very mature in terms of hydrogeology and water-to-rock interaction processes. Instead, early intrusion may lead to a transient state in which neither CO_2 ascent nor geochemical reactions are constant in time. The detection of metal changes in shallow aquifers can be done by periodic water collection and analysis in wells

within an area that should cover the potential spreading of CO_2 plume in the deep reservoir. In general, the extension of this area should be at least some hundreds of km^2, including dozens of sampling points to be regularly monitored through the operational and post-closure stages. In this context, depending on the nature of early intrusion, there is a chance of not detecting leakage even considering a tight, regular water sampling. To illustrate this, three scenarios could be drawn: i) No CO_2 intrusion, ii) episodic intrusion, and iii) constant intrusion. Assuming that CO_2 dissolution and metal release is fast, the periodic collection and analysis of a particular well close to the intrusion point should yield different results if inputs of CO_2 react with the water aquifer (Fig. 8).

Episodic intrusion of $CO_2(g)$ or CO_2-rich deep groundwater into shallow aquifers has been recently reported by Piqué et al. (2010) from the Caldes de Malavella geothermal field (NE Spain). In one of the studied stations (shallow aquifer DW-5), a remarkable increase in bicarbonate concentration was recorded (Fig. 9a), coupled with a sharp increase in metal concentration, mainly iron (Fig. 9b) but also U, V, Cu, Zn, Th, and Al. In contrast, pH did not significantly change through the sampling period (9 months). The CO_2-rich groundwater was geothermal in origin, showing a very similar chemistry with geothermal springs nearby.

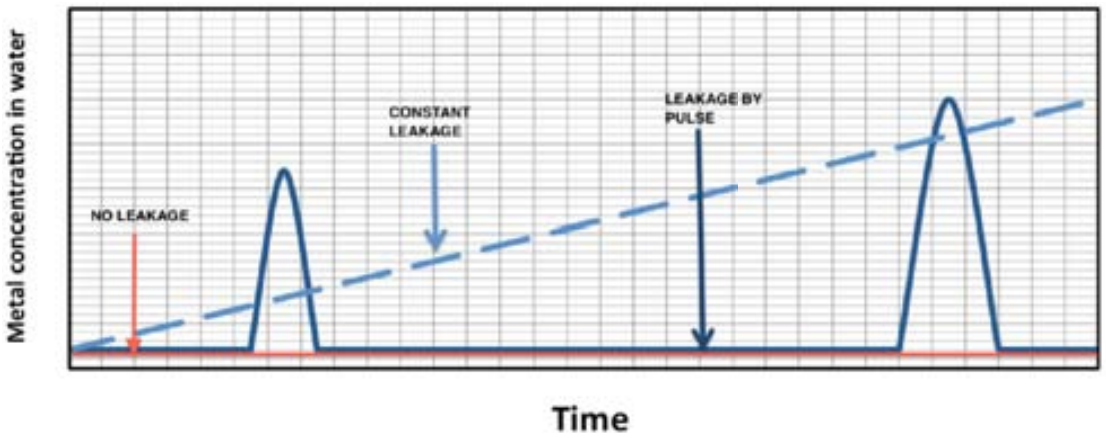

Fig. 8: Example of expected metal release from water- rock interaction as detected in a well close to a CO_2 intrusion point considering an episodic intrusion and a constant intrusion.

(a)

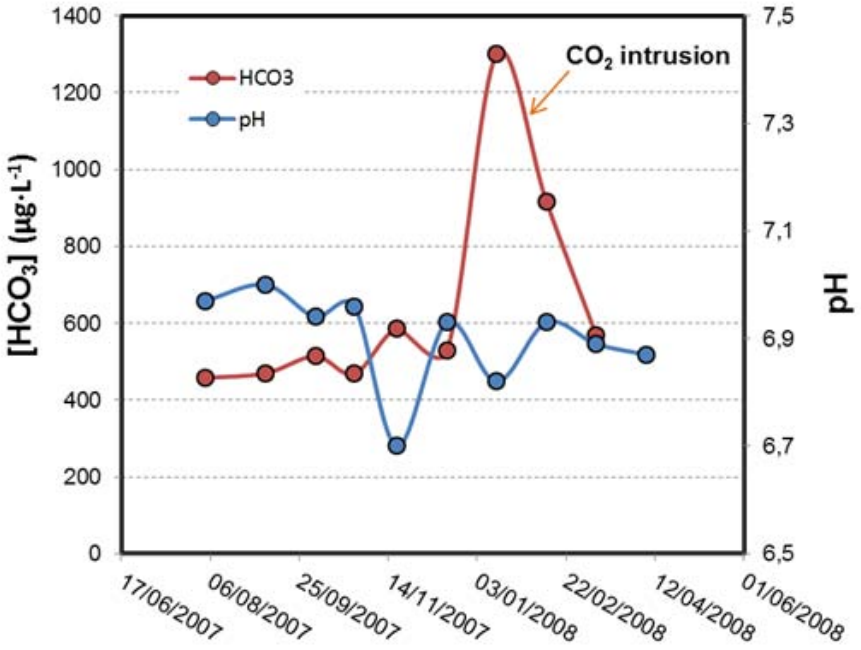

(b)

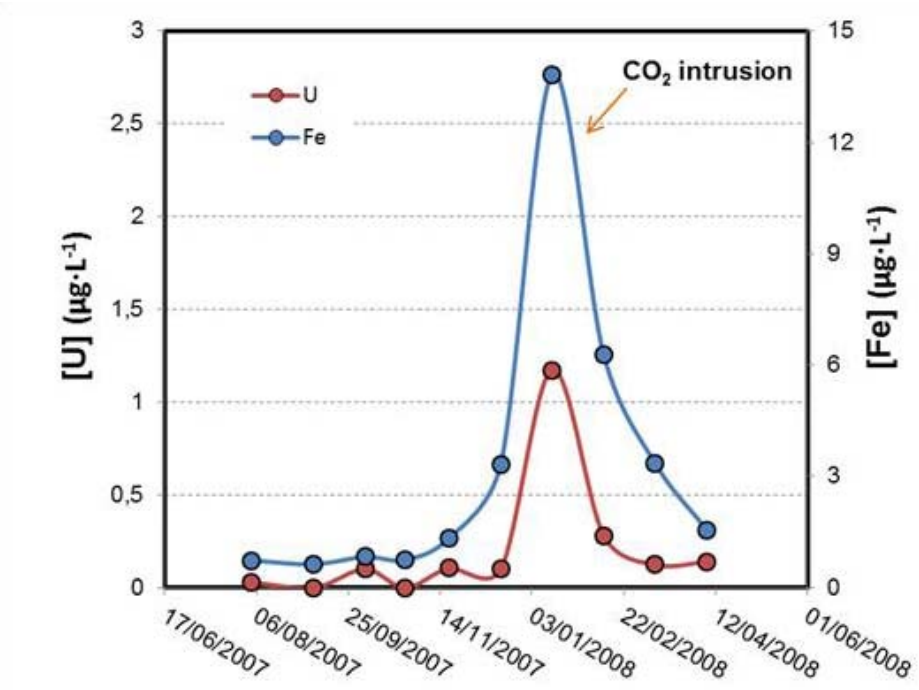

Fig. 9: a) Episodic intrusion of CO_2-rich deep groundwater into a shallow aquifer at Caldes de Malavella geothermal field (station DW-5 from Piqué et al. 2010). Note that pH does not significantly change. *b) Increase in Fe and U in shallow aquifer as a response of an episodic intrusion of CO_2-rich deep groundwater at Caldes de Malavella geothermal field (station DW-5 from Piqué et al. 2010).*

1.5 GEOLOGICAL FRAMEWORK OF CO_2 NATURAL EMISSIONS

Plate boundaries are characterized by high heat flow and large-scale vertical-expulsion, through a number of mechanisms (Person and Baumgartner, 1995; Kerrick, 2001; and references therein), of hot and deep pressurized fluids from volcanic and geothermal systems as well as active faults (i.e., Oliver, 1986). Volcanoes, fumaroles, mofettes, mud pools, geysers, thermal springs are typical surface features of such fluid expulsion, of material mostly recycled by subduction (i.e., Peacock, 1990) and partly having a ‘‘juvenile’’ mantle origin (i.e., Hawkesworth et al., 1991). Such thermal fluid discharges, focused around volcanic and geothermal areas, mix with topographically driven downward and laterally flowing non-thermal ground waters as they move towards the oceans (Sverjensky and Garven, 1992). Where the meteoric versus thermal fluid ratio is high enough, volcanic and geothermal fluids condense, and a free, non-condensable gas may form and rise along faults and fractures to spread in shallow aquifers. Because this non-condensable (or scarcely condensable) phase is rich in acidic compounds (such as CO_2, HCl and H_2S), its partial solubilisation enhances the water-rock interactions in shallow ground waters. By this mechanism, progressive de-carbonation of carbonaceous minerals in orogenic areas or direct mantle degassing can produce huge quantities of CO_2 (Minissale et al., 2004). Non-volcanic CO_2 would be released as small- to-powerful emissions (dry vents or bubbling pools), diffuse degassing and CO_2-enriched spring waters, sometimes spectacular in terms of both the amount of CO_2 released to the atmosphere (up to several tons/day) and the capability of CO_2 to displace the water gurgling in up to the height of 1 m (Chiodini et al., 1999; Minissale et al., 2000; Minissale 2004).

Mechanism of gas migration:

The gas migration through the geosphere, generally constituted by a prevailing gas (usually CO_2 or CH_4) and secondary components, among which the main hydrocarbons (benzene and toluene) and rare gas (Rn, He), is closely linked to the presence of a source (deep aquifer fluids, hydrocarbons in sedimentary basins, presence of geothermal fluids in volcanic areas or in areas related to igneous or metamorphic phenomena) and the existence of preferential paths of movement which allow the gas to migrate both in vertical and horizontal direction (Gold and Soter, 1985).

The preferential paths are usually linked to the zones of greater permeability, where the gas can migrate horizontally (i.e., sandy levels within a sequence of clay), and tectonic discontinuities (i.e., faults and fractures) through which the gas tends to migrate vertically.

The nature of the driving force of the migration can change several times during the ascent of the gas due to the geological and physico-chemical conditions (changes in temperature, pressure, precipitation and chemical reactions that may change the permeability of the crossed formations).

In addition, the rocks and the fluids contained in it may be subjected to enormous loads, phenomena of compaction (subsidence) and tectonic stress that can change the way migration unpredictably.

The interaction of all these factors can give rise to migration processes varying in time in a manner such that the escape of gas to the earth's surface should be considered, at least to the geological time scale, an episodic phenomenon.

One can assume that the movement of gases in the subsurface can be induced by two kinds of forces: pressure gradients or concentration gradients.

2 GENERAL OBJECTIVES OF THE Ph.D.:

The research objective of this Ph.D. project is the study of the capacity of aquifers to supply metals and metalloids from reactions with CO_2-bearing fluids and the effect of trace gases in the metal transport. This is a fundamental issue in the risk assessment of present-day and future commercial projects of CO_2 storage in deep aquifers, since potential leakage may jeopardize the quality of fresh water resources. The research on the effects of dissolved CO_2 on the mobility of some metals in aquifers has been mainly focused on Fe(III) solubility in CO_2-bearing fluids, and experimental results match observations in naturals systems, where high Fe concentration can be found under oxic, circum-neutral solutions. This project focuses on the fate of iron and other trace metals and metalloids once they are released from the rocks until they are precipitated back or adsorbed on minerals or organic substances.

The expected outcome is to fix a set of implications and recommendations for the risk assessment of geological storage of CO_2.

The development of the project is based on the next interrelated research activities:

- Review the various mechanisms for metal mobilization and transport in fluids characterized by high amount of dissolved CO_2 and circum-neutral pH, with a special focus on iron.

- Determine the gas-water-rock interaction time for the formation of metal plumes in CO_2-bearing waters and the influence of carbonate species on iron solubility.

- Assess the possibility to use metals as an early detection tool of low-intensity leakage from CO_2 storages

Section Two

3 SAMPLING AND ANALYTICAL METHODOLOGIES

The sampling stations selected in natural analogues in this work consist of bubbling pools, rivers and cold geysers. The sampling of the two geysers was carried out in order to collect deep waters not affected by a long-term degasification, able to give direct information of the redox state and metal content of the aquifer. The degasification, in fact, can lead to changes in the pH and redox state of a water that control the chemical speciation of many chemical elements (e.g. Fe, Mn, As) and so the chemistry and the structure of many metal complexes, colloids and particles present in solution. For the same reason, a detailed systematic sampling was performed at the Font Groga stream (La Selva Basin) (see section 3 in this volume), with the aim of understanding the change on the metal amount from the source point to the end of the stream as a consequence of a steady degassing state.

3.1 WATER SAMPLING

From each sampling site, 4 aliquots of water were collected (Fig. 10): *i)* 125 mL in a plastic bottle for the determinations of anions; *ii)* 50 mL in a plastic bottle for the determination of cations, previous acidification with 0.5 mL of Suprapur HCl and filtration using 0.45 μm filters; iii) 50 mL in a plastic bottle for the determination of trace metals, previous acidification with 0.5 mL of 1M HNO_3 and filtration using 0.1 μm filters; iv) a 50 ml. glass bottles where 5 mL of a 1M Na_2CO_3 solution was previously added for the Free CO_2. The pH-Eh measurements where performed in the field using a Crison portable pH-Eh meter with a platinum electrode for the redox determination.

3.2 FREE CO_2 COLLECTION AND ANALYSIS

When high CO_2 flow is present, free CO_2 bubbles can be observed. "Free" CO_2 is CO_2 present in water as both gas micro-bubbles (CO_2 gas) and dissolved phase (CO_2 aq), the latter being CO_2 not yet transformed into HCO_3^-, which is the largely dominant ionic carbonate compound in water at pH ranging between 4.5 and 8. The kinetics of the CO_2-HCO_3^- reaction is independent on the CO_2 concentration. Therefore, high concentrations of "free" CO_2 correspond to high CO_2 recharge rate from bacterial activity and/or other possible sources, i.e. mantle and/or thermometamorphism suffered by carbonate formations. As a consequence, free-CO_2 is a useful parameter to detect "active" CO_2 inputs in aquifers.

The concentration (in mg/L) of "free" CO_2 is calculated on the basis of the analysis of total alkalinity, carried out with a 0.5M HCl solution, on water samples collected in 50 mL glass bottles where 5 mL of a 1M Na_2CO_3 solution was previously added. The carbonate solution is used to increase the water pH to >12, allowing the entrapment of free CO_2 within the liquid phase as CO_3^{2-}.

Fig. 10: Bottles and filters used to collect the aliquots of water.

3.3 DISSOLVED GASSES:

In order to determine the main dissolved gaseous species in aqueous phase and their partial pressures, a dedicated sampling was performed using a new method setup by the CNR-IGG Unit of Geochemistry (Tassi et al., 2008) for which the determination of dissolved gases is carried out at equilibrium conditions (Fig. 11). The sampling is operated by using gas tubes with a capacity of 200-300 mL with a Teflon stopcock. In the laboratory the gas vials are pre-evacuated by a rotary pump with a vacuum value of 10^{-1}-10^{-2} Pa. By immerging the gas vial into the water and opening the Teflon stopcock, the water is forced to enter the vial by decompression. Normally, <70% of the tube volume has to be filled with water in order to allow the chemical and determination.

a) b) c)

Fig. 11: a) Glass tube used to sampling dissolved gasses and b, c) schematic representation of the sampling methodology). By immerging the gas vial into the water (b) and opening the stopcock, the water is forced to enter the vial by decompression (c).

3.4 MAJOR AND MINOR ELEMENTS CONCENTRATION

The measurement of the concentration of major anions, e.g., chlorides, sulphates, bromides, nitrates, fluorides, and phosphates, and major cations, e.g., Ca, Mg, Na and K, were performed at the laboratories of the Department of Earth Sciences of the University of Florence using the ion chromatography technique. The chromatograph used is the Metrohm 761 Compact IC for the anions and the Metrohm 861 Advanced Compact IC for cationic species.

The sample is fed into the circuit of the instrument using a syringe, and then, enters inside of a separation chromatographic column filled with an ion exchange resin.

The instrument uses the resistance that the ions encounter when crossing the resin in relation to their size and their affinity with the eluent, consisting, respectively, of 0.329 g of Na_2CO_3 and 0.084 g of $NaHCO_3$ for the anion chromatograph and 34.6 mL of HNO_3 0.65% for the cation chromatograph for each liter of MilliQ water.

The eluent, introduced by peristaltic pump, allows the various ionic species to move through the column, acquiring different speeds depending on their molecular size. The analytes come to the detection system, constituted by a conductivity meter, at successive times, characteristic of each species.

Within the suppressor of the anion chromatograph, placed downstream of the chromatographic column and upstream of the conductivity meter, an exchange between the cations present and the hydrogen ions of the regenerating (consisting of Milli-Q water and 2.5 mL of H_2SO_4 95-97%) also takes place, causing a consequent decrease in the intensity of the background signal and an enhancement of the anions' peak.

An integrator collects the signals provided by the conductivity, relative to the various ionic species, according to the order of arrival, and is also able to provide the maximum value of conductivity (height) and the area of each peak. Through the responses obtained from solutions of known, of which height and peak area are known, it is possible to build a calibration curve and through this trace the concentrations of the species investigated.

3.5 TRACE ELEMENTS

Trace elements (Al, As, B, Ba, Be, Bi, Cd, Co, Cr, Cs, Cu, Fe, Hg, Li, Mn, Mo, Ni, P, Pb, Rb, Sb, Sc, Se , Si, Sr, Tl, U, V, W, Y, Zn and Zr) were analyzed at the Universitat Autònoma de Barcelona (UAB) laboratories and ActLabs Laboratories® (Canada).

The technique uses a plasma torch to produce the ICP ionization and a mass spectrometer for the separation and detection of the ions produced.

The spectrometer uses a quadrupole mass analyzer, the component responsible for the instrument to direct the ions of the sample to the detector (electron multiplier), on the basis of their mass/charge ratio (m/z). Once transmitted, only the ion beam having the "m / z" ratio selected produces a signal proportional to its concentration, which is then determined by calibration with a standard. The relatively low resolution of the quadrupole mass filter is sufficient to completely separate the peaks relating to atomic species with mass numbers contiguous, but not those due to polyatomic ions with small mass differences, which can produce interference in a particular m/z <40.

3.6 DISSOLVED GASES:

The composition of inorganic compounds dissolved in the gas phase (CO_2, N_2, O_2, Ar, Ne, H_2 and He) was determined by a gas chromatograph (Shimadzu 15a), equipped with a Thermal Conductivity Detector (TCD); methane was determined by a gas chromatograph Shimadzu 14a equipped with a Flame Ionization Detector (FID) (Tassi et al., 2004). The composition of the volatile species in the liquid phase is a function of the Henry's Law and it can be calculated, follows (eq. 3.1):

$$C_{i(liq)} = P_i \times K_i \qquad (3.1)$$

Where C_i(liq) is the concentration (in mol/L) of i-species in the liquid phase, K_i is the solubility of the i-species at room temperature (25 °C); P_i is the partial pressure (in atm) of the i-species in the head space of the gas vial.

From P_i we have (eq. 3.2):

$$P_i = P_{tot} \times X_{i\,(\%gas)} \qquad (3.2)$$

Where P_{tot} is the total pressure (in atm) of the exsolved gases in the vial head space; X_i(%gas) is the concentration (% by vol.) with respect to the total of the exsolved gases of the i-species in the gas phase.

The concentration of the different gas compounds is determined as follows (eq. 3.3):

$$C_{i(gas)} = X_{i\,(\%gas)} \times \frac{C_{tot(gas)}}{100} \qquad (3.3)$$

C_i(gas) is the concentration (in mmol/L) of the i-species in the gas phase; C_{tot}(gas) is the total amount (in mmol/L) of gas in the vial head space. In turn, C_{tot}(gas) is calculated on the basis of the Law of the Perfect Gases from eq. 3.4:

$$C_{tot(gas)} = P_{tot} \times \frac{V}{RT} \qquad (3.4)$$

The remaining gas can be finally used to determine the isotopic composition of CO_2 and/or helium.
Determination of gaseous compounds was performed at the Department of Earth Sciences of the University of Florence.

3.7 ALKALINITY AND FREE CO_2:

The potentiometric titration was used to measure alkalinity, corresponding to the concentration of the bicarbonate, and the "free" CO_2. The analyses were performed with a Metrohm 794 Basic Titrino at the Department of Earth Sciences of the University of Florence. The instrument is equipped with a combined glass and calomel electrode, of automatic burette and magnetic stirrer.

3.7.1 BICARBONATES:

The concentration of the bicarbonates in the samples was obtained from the acidimetric titration curve, registered by an automatic titrator. The combined glass electrode used in this analysis is simultaneously measuring and reference. The titrant is 0.01M HCl.
The concentration of the bicarbonate is obtained from the formula in eq. 3.5:

$$\frac{mL_{TITRANT} \times TITRAND}{mL_{SAMPLE}} \times 1000 \qquad (3.5)$$

The number of mL of titrant is read on the acidimetric curve at the inflexion point, indicating complete transformation from bicarbonate to carbonic acid according to the reaction eq. 3.6:

$$HCO_3^- + H^+ = H_2O + CO_2 \qquad (3.6)$$

3.7.2 "FREE" CO_2:

The concentration was derived from the aliquots, weighed pre- and post-sampling, to which were previously added 5 ml of Na_2CO_3 (1M) solution.

The "free" CO_2 is obtained by the following formula (eq. 3.7):

$$\left[\frac{CO_{2(Tot)} \times \text{Weight of Sample}}{\text{Weight of Sample} - 5} - [HCO_3]^-\right] \times \frac{1}{2} \qquad (3.7)$$

The weight of the sample was obtained by subtracting to the weight of the bottle with the sample inside (glass + carbonate + sample) the weight of the single bottle + 5 mL solution of sodium carbonate, measured on the scale before sampling.

Section Three

4 Objective 1:

Review of the various mechanisms for metal mobilization and transport in fluids characterized by high amount of dissolved CO_2 and circum-neutral pH, with a special focus on iron.

Article 1: The effect of increased CO_2 concentrations on trace metal mobility: field and laboratory experiences

Marco Agnelli[a], Jordi Bruno[a,*], Lara Duro[a], Fidel Grandia[a], Mireia Grivé[a], Javier Olmeda[a]

[a]*Amphos 21 Consulting SL, Passeig Garcia Faria 49-51, 08109 Barcelona*

Abstract:

Already in 1990 it was postulated that increased CO_2 concentrations in seawater would affect trace element mobility. Some 24 years later, CO_2 levels have further increased and the acidity of seawater is also increasing. In this article we revise the effects of increased CO_2 concentrations on the iron(III) mobility and associated trace elements with particular emphasis on the environmental consequences of CO_2 geological storage.

The outcome of this work would indicate, by comparison between field and laboratory experiences, that increasing in dissolved CO_2 solubilises Fe(III) oxyhydroxides and triggers secondary mobility of the trace metals associated to these phases with special focus on uranium(VI).

Keywords

Trace metal mobility; Iron solubility; CO_2 geological storage; Carbonate content; Dissolved CO_2; Seawater acidity.

Submitted to scientific journal: Applied Geochemistry

4.1 INTRODUCTION

Back in 1990 was already postulated that increased CO_2 concentrations would have an effect on trace metal mobility, particularly in seawater (Bruno, 1990). At that time the CO_2 concentrations in the atmosphere as measured in the Manua Loa observatory were around 350 ppmv, while at present they reach the 400 ppmv (Tans and Kieling, 2014). The measured CO_2 concentrations in surface sea water appear to follow the increased trend of atmospheric concentrations with some variability depending on sea water temperature (Bates et al. 2014). This has critical consequences for seawater acidification as the oceans constitute the largest CO_2 sink. An example of the consequences caused by the increase in the atmospheric CO_2 concentration in the surface of the ocean is that its mean pH is approximately 0.1 units lower today than in the preindustrial period (Zeebe and Wolf-Gladrow, 2001) and these trends are confirmed by the multisite oceanographic study by Bates et al. (2014).

Since the publication in 1990, a large number of investigations have been performed in order to determine the influence of increased CO_2 concentrations in the mobility of a number of key trace metals, including Fe(II) (Bruno et al., 1992a) and Fe(III) (Bruno et al., 1992b; Duro, 1996 ; Bruno and Duro, 2000; Grivé et al., 2014a, b) and U(VI) (Bruno et al., 1995; Duro, 1996; Grivé, 2005).

The linkage between uranium mobility and the influence of CO_2 on Fe(III) mobility was specifically studied in Duro (1996) and Grivé (2005). The outcome of these studies was clear in the sense of demonstrating the influence of increased CO_2 concentrations on the dissolution of Fe(III) oxyhydroxides and consequently on the mobilisation of trace metals attached to these very relevant and ubiquitous surfaces. This was later confirmed by a number of evidences from the geochemical modelling of trace element solubility in a number of sites that were investigated as natural analogues to geological repositories of spent nuclear fuel (Miller et al., 2000), particularly, in the *Poços de Caldas* and the *El Berrocal* sites (Duro, 1996; Bruno et al., 2002; Grivé, 2005).

In recent years, the focus of our research has shifted towards the potential environmental effects of the geological storage of CO_2 and in particular in the metal mobilisation in aquifers affected by potential leakage from the storage complex. In this context, there are two issues to be concerned about. On one hand, increased CO_2 concentrations may induce increased acidity in poorly buffered systems where acidity increases of three orders of

magnitude have been observed (Trautz et al., 2013). This increased acidity may result in the release of metals bound on the existing solid phases. On the other hand, the increased CO_2 concentrations will result in the increase of the total carbonate of the system and consequently in the build-up of metal hydroxo carbonate and metal carbonate complexes, which will result in increased metal concentrations. The two effects are difficult to separate in natural system studies, but some dedicated laboratory tests, particularly in relation to effects on marine systems may give some interesting clues.

In this paper the findings from the early publication in the light of the research conducted in these two decades, will be revised and updated with the aim to clearly confirm the link between increased carbon dioxide, iron(III) solubility and trace metal mobility by the comparison of laboratory results and field experiences, discussing the implications for trace metal mobility in the present emissions scenario with constantly increasing CO_2 levels.

4.2 FIELD EXPERIENCE

An illustrative example of the impact of CO_2 dissolution on the iron transport is found in the aquifers affected by CO_2 flows from deep underground sources (i.e., mantle degassing, thermal decarbonation). These gas-water-rock interactions have been recently studied in detail in the environmental impact assessment of potential CO_2 leakage from geological storage (e.g., Zheng et al., 2009; Kharaka et al., 2010; Spangler et al., 2010). In addition, injection tests of high-pressured CO_2 have resulted in an increase of iron and other metals in the reservoir (e.g., Peter et al., 2012; Trautz et al., 2013). In both cases, the metal mobilisation has been commonly related to acidity increase and the relative high solubility of Fe(II). However, the role of carbonate complex formation has also been discussed (Lions et al., 2014). Many CO_2-bearing aquifers carry high amounts of iron and other metal even at circumneutral pH and oxidising Eh, in which Fe(III) is the dominant redox state. In these cases, the low solubility of iron(III) oxyhydroxide phases should prevent the dissolution of significant amounts of Fe(III) but the formation of aqueous carbonate complexes allows the concentration of Fe(III) to reach values higher than 10^{-4} mol·L^{-1}. (e.g., Agnelli et al., 2013). In order to better understand that increasing in dissolved CO_2 solubilises Fe(III) oxyhydroxides and triggers secondary mobility of the trace metals associated to these phases, a detailed systematic sampling was performed, from the source point to the end, at the Font Groga stream (La Selva Basin, NE Spain).

4.2.1 GEOLOGY OF LA SELVA BASIN (NE SPAIN)

La Selva basin is a tectonic depression of Tertiary age surrounded by Paleozoic massifs located in the province of Girona (NE Spain) (Fig. 12). It is a graben of tectonic origin, part of the so-called Prelitoral Catalan depression, which extends from the NE rift of Vallès basin, to the south of Transversal Mountains. La Selva basin is surrounded by a number of elevated tectonic blocks: the massif of Guilleries to the west, the Transversal ranges to the north,the Gavarres range to the east, and the Selva Marítima mountains to the south. It covers an area of approximately 331.1 km^2. The depression of La Selva originated in the Neogene, during the distensive phase of the Alpine orogeny,. These movements originated magmatic episodes into the depression, leading to the formation of some volcanic structures at surface, e.g., Esparra, Riudarenes, Sils, Maçanet de la Selva and Vidreres (Donville, 1976; Pallí i Roqué, 1995). The main fault trend in the area is NW-SE, with other relevant faults oriented NE-SW and N-S. The NW-SE faults could be considered as the most relevant of the La Selva depression and determine its eastern border with Gavarres and the western with Guilleries and the Massanet trough. Finally, a set of N-S faults crosses the depression from Girona city to Caldes de Malavella town (Pallí et al., 1983; Mas-Pla, 1986; Pous et al., 1990). All these fractures have led to an irregular basement, consisting mainly of Paleozoic materials. The collapse originated in the Neogene, allowed the filling of the depression with materials from the erosion of adjacent beds, mainly covered by the most recent alluvial deposits. The characteristics of these Neogene materials depend mainly on the source area, as well as the type of sedimentary processes. The north of the depression is predominantly characterized by clay materials, while in the rest of the depression consists of coarser material of colluvial origin, sand and conglomerates with clasts of metamorphic or granitic composition and with sandy or clay matrix (Menció i Domingo, 2005). The thickness of these Neogene materials depends on the shape and depth of the bottom of the basin. At the western margin, the thickness reaches up to 300 m, whilst in the central part of the basin, thickness is up to 175 m.

The water and gas discharges:

A large number of CO_2-bearing springs are found in La Selva basin, mainly located in the fault system that borders the basin. CO_2 isrelated to mantle degassing ascending through these deep fractures. All these groundwaters have a circumneutral pH (between 6 and 7) and show a relatively oxic Eh (Vilanova, 2004; Piqué et al., 2010). The degree of water-gas-rock interaction is though to be high as proved by the elevated concentration of solutes such as Cl, Na, K, Li and F (up to 5.9 10^{-2} $mol \cdot L^{-1}$). Characteristically, these waters are iron-rich, with concentration up to 10^{-4} $mol \cdot L^{-1}$. One of the best-known CO_2-bearing groundwater in the area is the Font Groga stream, located in the north margin of the basin.

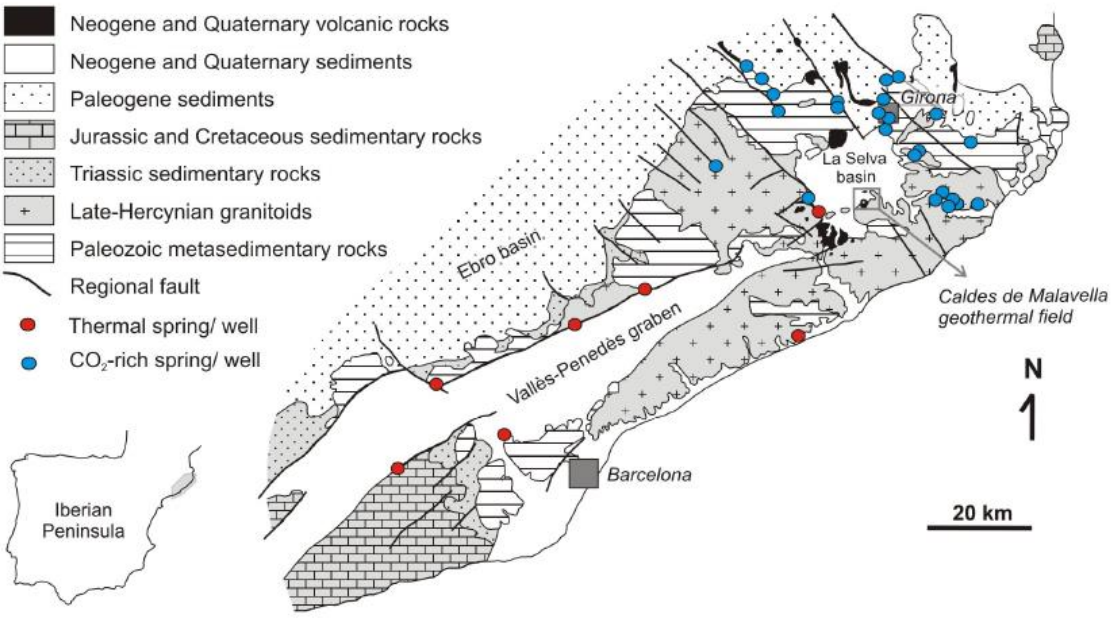

Fig. 12: Geological map of the northern part of the CCR, with the location of the Caldes de Malavella geothermal field, and other CO2-rich cold springs and wells and thermal springs.

4.2.2 WATER AND GAS SAMPLING:

The sampling was carried out dividing the initial 60 m of the stream into 9 equidistant sampling points starting from the spring and then considering each point as a separated system in equilibrium with a given CO_2 pressure (Fig. 13 and Fig. 14).

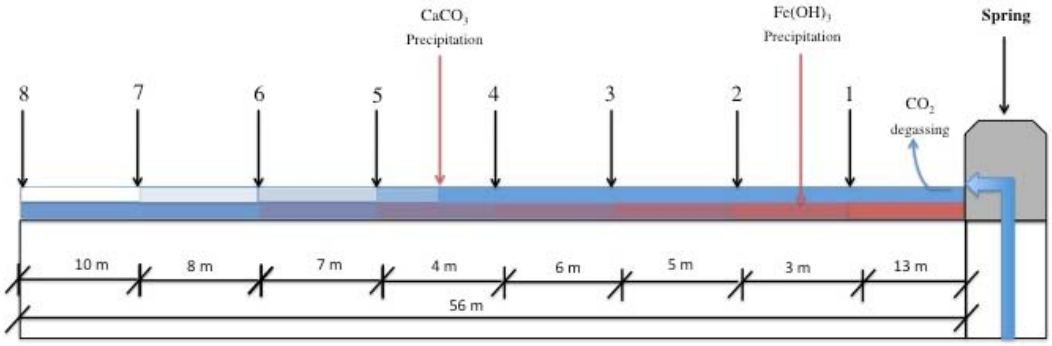

Fig. 13: Sketch of the sampling in the Font Groga stream. Observable precipitation of ferrihydrite and calcite has been indicated as a reddish and bluish colour, respectively.

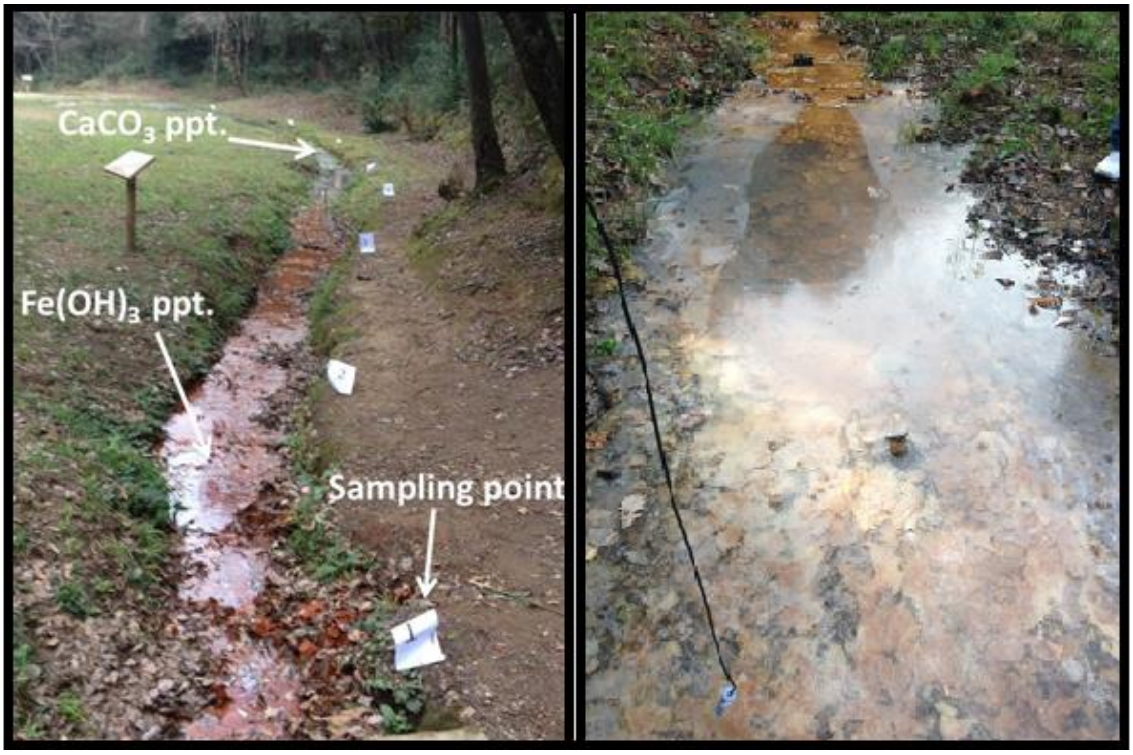

Fig. 14: View of the sampling in the Font Groga stream. Precipitation of ferrihydrite (left) and calcite (right) is clearly observed.

4.2.3 GEOCHEMICAL MODELLING:

Water chemistry was interpreted by using the equilibrium chemical-speciation/mass transfer model PHREEQC-3 (Parkhurst and Appelo, 2013). The thermodynamic calculations were performed using the Sit.dat database, based on the ThermoChimie v.7.c (Giffaut et al., 2014), in order to determine both the $Fe(OH)_3$ saturation indexes and the amount of Fe-carbon-complexes formed as a function of the pCO_2 and pH.

Input data for each sampling point include measured values of metal (Fe_{tot}) and major elements (HCO_3^-, SO_4^{2-}, Cl^-, K^+, Na^+, Mg^{2+}, Ca^{2+}) concentrations, temperature, pH and alkalinity.

For each sampling point a simulation has been performed using both measured pCO_2 values and the calculated ones by using the HCO_3^- amounts determined in the water. This double step was carried out to verify whether the simulation result obtained with the measured values does not deviate from the theoretical result and to detect any problems caused by sampling. The degree of saturation is expressed as the saturation index (SI), where SI is equal to the difference between logarithms of product ion activity and constant solubility (SI = log IAP − log Ksp). To determine the ferrihydrite SI was used the log K_{sp} from the Minteq.V4 dataset (log_k = 3.19) instead of the original one of the SIT dataset (log K_{sp} = 1.19). This change was done taking in mind the variability of the thermodynamic properties referring to a poorly crystalline mineral in natural systems.

4.2.4 RESULTS:

4.2.4.1 Gas and Water Chemistry:

The physical parameters, the chemical composition of water in terms of major, minor and trace elements and an aliquot of dissolved gases were sampled for each point. The results are shown in Table 1. From the spring to the last sample point, the stream is characterized by an electrical conductivity ranging from 6470 $\mu S \cdot cm^{-1}$ up to 6600 $\mu S \cdot cm^{-1}$ and by pH values that increase from 6.4 to 7.3.

Eh ranges from 168 mV to 214 mV. The main metal characterizing the spring is Fe, in a range of $2.5x\,10^{-1}$ $mg \cdot L^{-1}$ ($4.47x10^{-3}$ $mmol \cdot L^{-1}$) to 6.4 $mg \cdot L^{-1}$ ($1.15x10^{-1}$ $mol \cdot L^{-1}$). The

studied samples also show rather high concentrations of Mn (up to 652 $\mu g \cdot L^{-1}$, 11.9 $\mu mol \cdot L^{-1}$), Zn (up to 14.6 $\mu g \cdot L^{-1}$, 2.23 $x10^{-1}$ $\mu mol \cdot L^{-1}$), Ni (up to 6.4 $\mu g \cdot L^{-1}$, 1.09 $x10^{-1}$ $\mu mol \cdot L^{-1}$) and Co (up to 3.38 $\mu g \cdot L^{-1}$, $5.73x10^{-2}$ $\mu mol \cdot L^{-1}$).

The main dissolved gas dominating is CO_2 (Table 2), with a range from 96.2% (6.56 $mmol \cdot L^{-1}$) to 65,5% (1.58 $mmol \cdot L^{-1}$). The remaining gas portion is mainly characterized by the occurrence of N_2, CH_4 and Ar.

A comparison between CO_2 amount and pH in each sampling station (Fig. 15) shows that as the gas concentration decreases, as a consequence of the degasification, the pH increases. In the field, this trend is well-evidenced by the precipitation of $CaCO_3$ throughout the stream (Fig. 13 and Fig. 14). The same comparison has been done for CO_2 and Fe concentrations (Fig. 16). As for the pH, the plot shows how Fe reduces its concentration as CO_2 decreases.

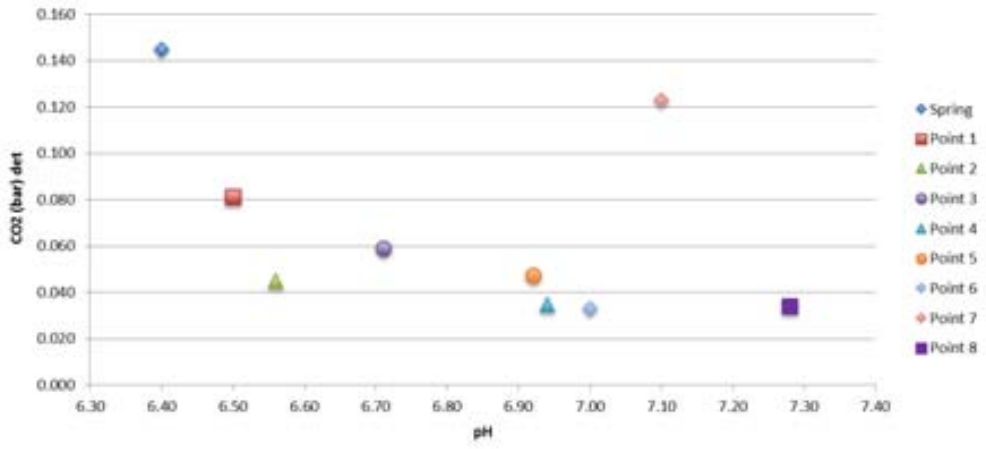

Fig. 15 : CO_2 pressre vs pH sampled along the Font Groga stream

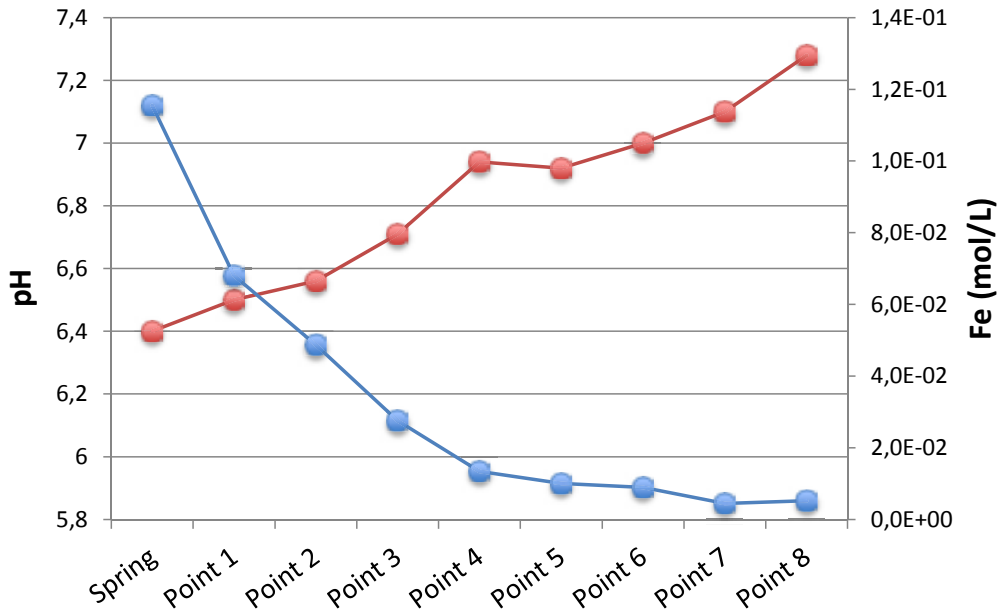

Fig. 16: Evolution of pH (red line) and Fe_{tot} concentration (blue line) downstream in the Font Groga River sampling stations.

Table 1: Chemistry of the water samples at Font Groga stream (La Selva basin).

Sample	Distance (m)	T (°C)	pH	Eh (mV)	Cond. ($\mu S \cdot cm^{-1}$)	HCO_3^- (mmol/l)	Cl (mmol/l)	SO_4^{2-} (mmol/l)	Ca (mmol/l)	Mg (mmol/l)	Na (mmol/l)	K (mmol/l)	F (mmol/l)	Fe (mmol/l)
Spring	0.0	17.1	6.4	168	6470	55.9	18.7	3.0	8.3	3.4	59.1	0.8	0.05	0.170
Point 1	13.2	16.3	6.5	189	6620	55.0	19.7	3.1	9.2	3.4	58.9	0.9	0.02	0.068
Point 2	16.2	15.2	6.6	195	6630	56.0	19.1	3.1	8.5	3.4	58.5	0.8	0.02	0.048
Point 3	21.2	15.8	6.7	198	6570	55.9	19.3	3.1	8.6	3.4	58.9	0.9	0.02	0.027
Point 4	27.2	15.5	6.9	188	6640	57.6	19.4	3.1	8.1	3.4	58.7	0.7	0.03	0.013
Point 5	30.9	15.3	6.9	180	6660	56.9	18.9	3.1	8.6	3.3	57.6	0.8	0.02	0.010
Point 6	38.3	15.0	7.0	189	6630	57.3	19.2	3.2	8.4	3.5	60.6	0.8	0.02	0.009
Point 7	46.8	14.6	7.1	197	6630	57.5	19.7	3.3	7.9	3.4	58.3	0.8	0.02	0.004
Point 8	56.0	13.7	7.3	214	6560	55.9	18.9	3.0	8.0	3.3	58.1	0.8	0.03	0.005

Table 2: Chemical composition of the dissolved gases sampled in the Fong Groga stream station

Sample	CO_2 ($mmol \cdot L^{-1}$)	N_2 ($mmol \cdot L^{-1}$)	Ar ($mmol \cdot L^{-1}$)	CH_4 ($mmol \cdot L^{-1}$)	O_2 ($mmol \cdot L^{-1}$)	CO_2 (%)	N_2 (%)	Ar (%)	CH_4 (%)	O_2 (%)
Spring	6.564	0.213	0.006	0.0005	0.043	96.16	3.12	0.08	0.0073	0.63
Point 1	3.685	0.411	0.010	0.0002	0.015	89.41	9.97	0.24	0.0049	0.37
Point 2	2.047	0.405	0.010	0.0016	0.052	81.37	16.10	0.40	0.0636	2.07
Point 3	2.698	0.395	0.010	0.0008	0.041	85.79	12.56	0.32	0.0254	1.30
Point 4	1.588	0.615	0.015	0.0001	0.208	65.45	25.35	0.62	0.0041	8.57
Point 5	2.165	0.316	0.008	0.0011	0.057	85.01	12.41	0.31	0.0432	2.22
Point 6	1.515	0.588	0.014	0.0001	0.116	67.84	26.33	0.63	0.0045	5.19
Point 7	5.623	0.255	0.006	0.0002	0.022	95.21	4.32	0.10	0.0034	0.36
Point 8	1.554	0.319	0.008	0.0007	0.0890	78.86	16.19	0.41	0.0355	4.52

4.2.4.2 Thermodynamic Modelling results:

From the chemistry data from gas and water analysis, the SI for calcite and ferrihydrite have been calculated. The results shown that the SI calculated using the sampled pCO_2 fit reasonably better with field observations than those obtained using the calculated pCO_2 (Fig. 17 to 19). Moreover, a undersaturation with respect with calcite generally corresponds to an oversaturation in ferrihydrite. This is consistent with the field observation since ferrihydrite precipitation stops between sampling points 3 and 4 and the calcite precipitation starting at the same points (Fig. 13 and Fig. 14).

Under the pH-Eh conditions in the studied samples, iron is present as Fe(III). The solubility of this species is commonly low in shallow aquifers and surface waters due to the precipitation of $Fe(OH)_3$. However, the dissolution of CO_2 allows the enhanced solubilisation of Fe(III) by the formation of aqueous Fe(III) carbonate complexes. The impact of these complexes, especially $FeOHCO_3$, is illustrated in Fig. 20, since the solubility of Fe(III) increases three orders of magnitude. Such an impact is very well illustrated looking at the ferrihydrite saturation index (SI) (Fig. 21) obtained in the set of simulations performed using the sampled pCO_2 (pCO_2 det) and the calculated one (pCO_2 calc) and with or without the aqueous Fe-carbonate complexes formation. In fact, the SI values calculated without the aqueous Fe-carbonate complexes always show an unrealistic oversaturation of $Fe(OH)_3$ along the river, independently of the pCO_2 used. Introducing the aqueous carbonate complexes, the SI dramatically decreases to normal saturation values.

Table 3: Sampled CO_2 pressure values and recalculated (PhreeqC) by using the HCO3- amounts determined in Font Groga stream stations.

Sample	**CO_2 (bar) (sampled)**	**CO_2 (bar) (PhreeqC)**
Spring	0.145	0.662
Point 1	0.081	0.562
Point 2	0.045	0.512
Point 3	0.059	0.407
Point 4	0.035	0.269
Point 5	0.048	0.281
Point 6	0.033	0.239
Point 7	0.123	0.194
Point 8	0.034	0.131

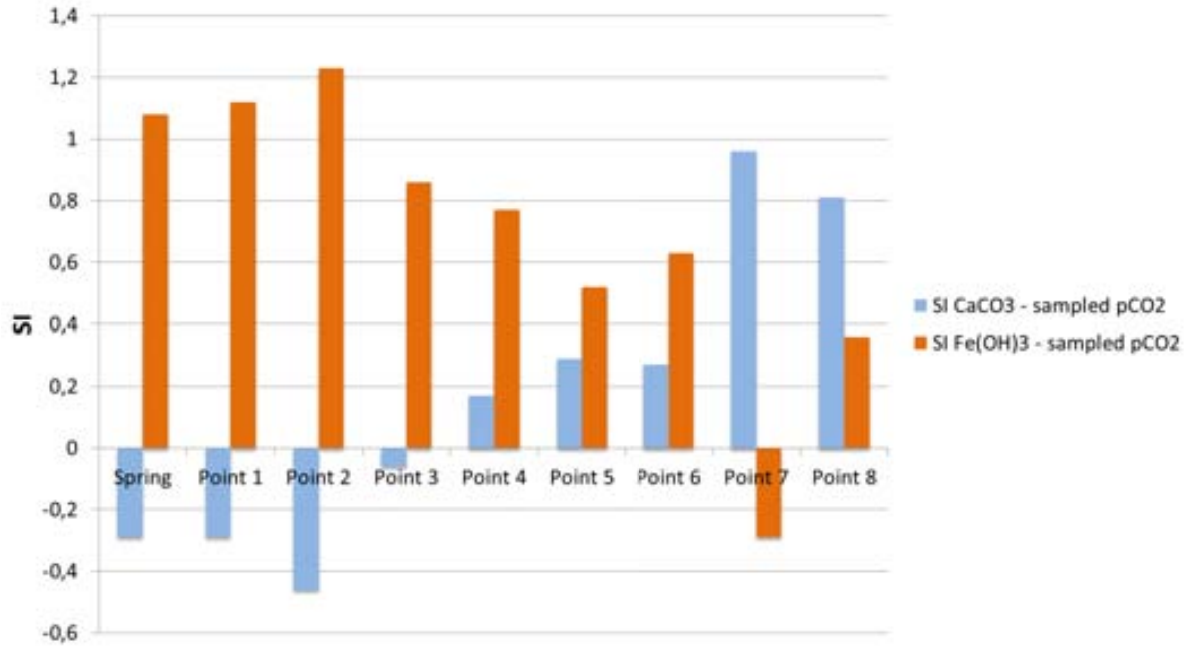

Fig. 17: Comparison between SI $Fe(OH)_3$ and SI $CaCO_3$ calculated using the sampled CO_2 pressures.

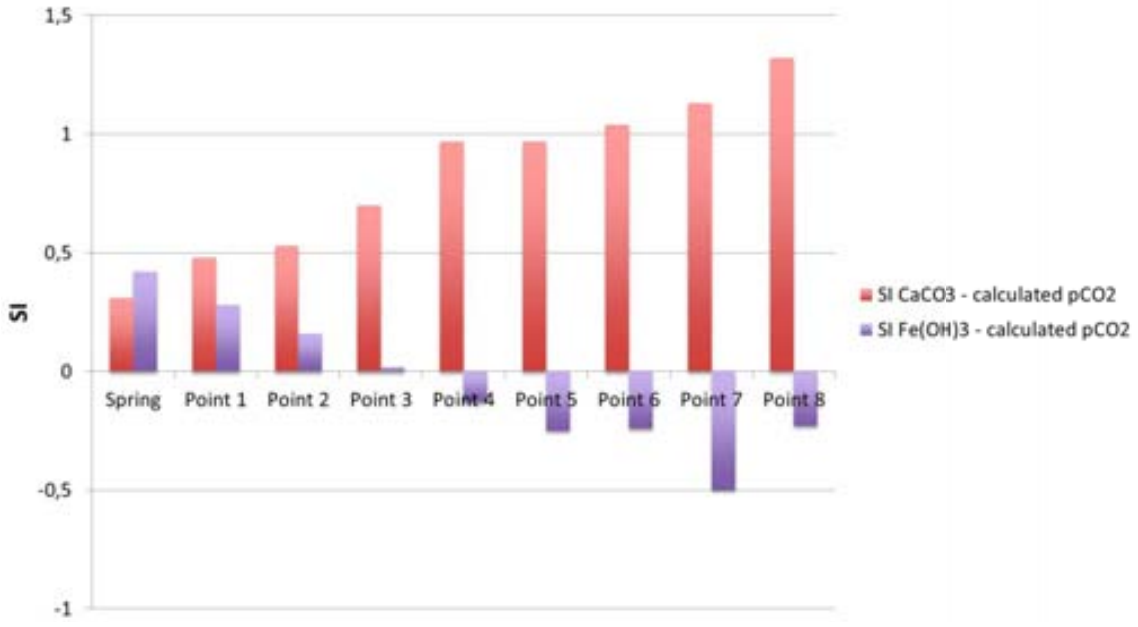

Fig. 18: Comparison between SI $Fe(OH)_3$ and SI $CaCO_3$ calculated using the calculated CO_2 pressures.

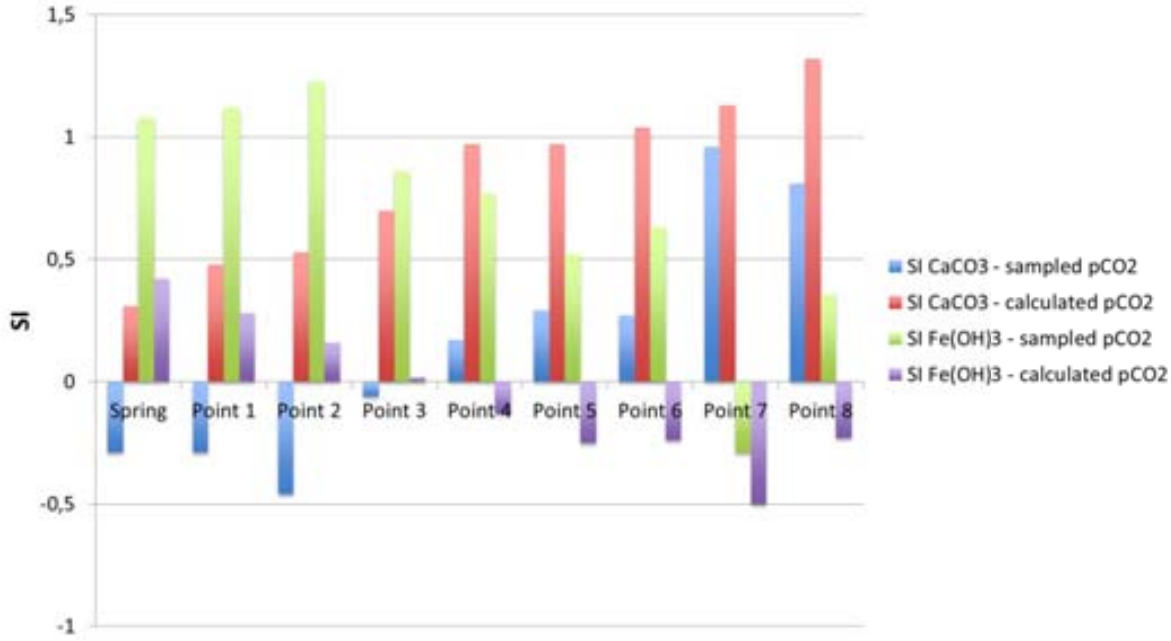

Fig. 19: Comparison between SI $Fe(OH)_3$ and SI $CaCO_3$ as a function of pCO_2

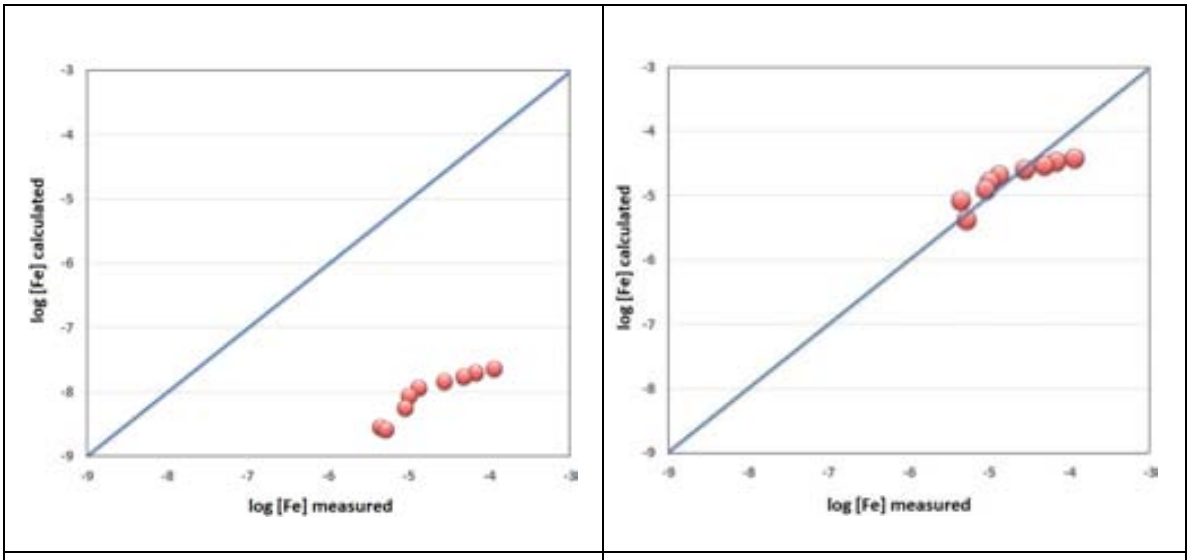

(a) (b)

Fig. 20: Plot of the calculated iron (III) concentrations in the samples from the Font Groga stream in front of the iron (III) measured concentrations (a) No iron (III) carbonate species in the thermodynamic database used (b) Effect of the incorporation of iron (III) carbonate species proposed in Grivé (2005) and Grivé et al. (2014a) in the thermodynamic database used in the calculations.

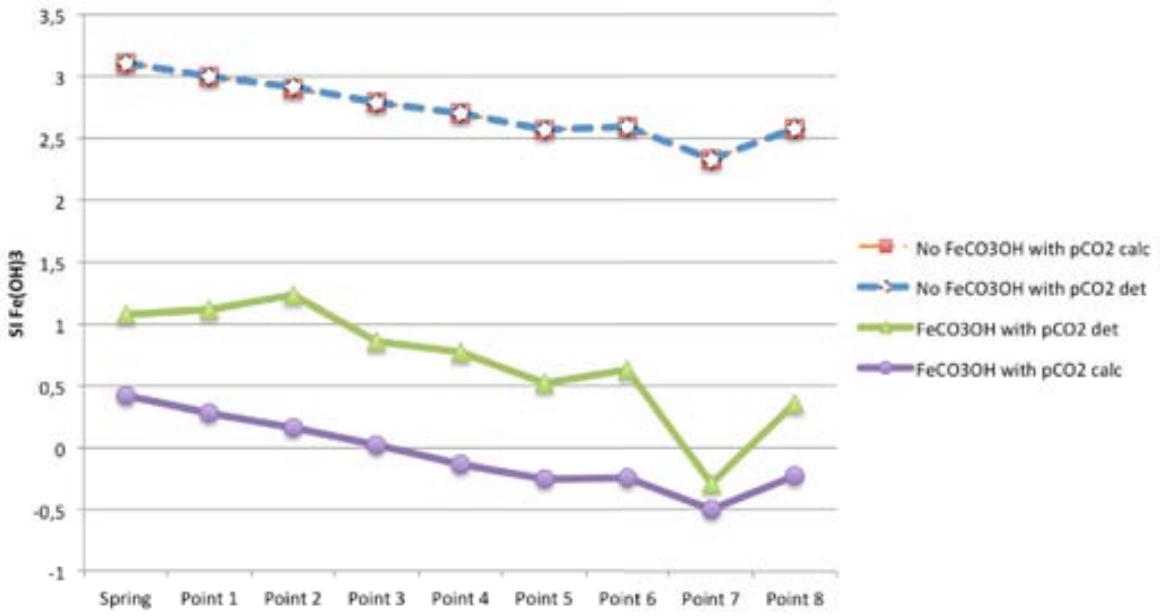

Fig. 21: Ferrihydrite saturation index (SI) calculated in the simulation performed with or without considering the Fe(III)-carbon-complexes formation, using the sampled CO_2 pressure (pCO_2 det) and the calculated one (pCO_2 calc).

4.3 EVIDENCES FROM LABORATORY STUDIES RELATED TO CO_2 STORAGE:

4.3.1 TRACE METAL BEHAVIOUR IN SYSTEMS WITH INCREASED CO_2 CONCENTRATION.

Ardelan et al. (2012) reported a particularly interesting study in connection with the effects of CO_2 seepage from sub-seabed geological storage. In this study the authors have used a titanium pressure tank, to simulate a high-pressure release of carbon dioxide in a sediment-sea water system. The sediments used in the experiment were extracted from the Trondheimsfjord and placed in contact with seawater extracted from the same site at 90 m depth. The seawater was flown into the tank and out for sampling at a flow rate of 1 l min^{-1}. Pure CO_2 was pumped into the system at 10 bar.

The conditions of the experiment were carefully controlled and the inflowing and outflowing waters were analysed for pH, dissolved inorganic carbonate (DIC), pCO_2 and trace metal concentrations as collected in diffusive gradient thin-film (DGT) units.

The inflow sea water composition was: pH=8.1; $pCO_2=3.38\cdot10^{-3}$ atm and DIC=2.13 milimolar. The outflowing seawater composition was pH=6.9; pCO_2=6.6 atm and DIC=2.635 milimolar. One of the striking observations is that the acidity of the system is rather well buffered, due to the sediment-water interactions that control the pH, in this case most probably through the $CO_2/CaCO_3$(s) buffer system. Cruz Payán et al. (2012) made similar observations in their investigations of the effects of CO_2 interactions with seabed sediments from the Cantabria Sea, where they observed a strong buffering effect of the sediments when put in contact with water at pH between 5 and 7, although they could also observe a substantial release of trace metals contained in the sediments.

In spite of the relative acidity buffering effect, Ardelan et al. (2012) observed a strong mobilisation of Al, Cr, Co, Pb, Ce, As and U when compared with similar high pressure tests run with N_2 as blanks.

In order to discern to which extent this effect is the result of the acidification and/or the carbonate complexation, a simple modelling exercise was performed in this study.

The solubility and speciation of a number of trace metals was calculated as a function of pCO_2 at the outflow pH=6.8 reported by Ardelan et al (2012). The code used was the Spana package developed by Puigdomènech (last update, April 2013) together with the

ThermoChimie database (Giffaut et al., 2014a; Grivé et al., 2014b; http://www.thermochimie-tdb.com/).

The results of the calculations are shown in Figure 21.

The outcome of these simple calculations would indicate that for most trace metals (Hg(II), Pb(II), Zn(II), Ce(III) and Ce(IV)) the increased pCO_2 has a positive effect in terms of stabilising their carbonate or hydroxocarbonato solid phases. This is the result of the formation of carbonate containing solid phases, which are more stable than the aqueous carbonate complexes. In the case of Cr(III) the increased pCO_2 has no effect, as no Cr(III) carbonate complexes have been reported in the literature. It is only in the case of Fe(III), when increased pCO_2 clearly results on a solubilisation of the Fe(III) oxyhydroxide or Fe(III) oxide phases resulting not only into increased iron concentrations but also triggering the dissolution of a number of trace metals sorbed onto the Fe(III) oxyhydroxide phases. This is clearly in line with the observations in the Font Groga stream and other data, previously discussed.

In the case of uranium(VI), the presence of very stable hydroxocarbonate and carbonate complexes results in the increase of uranium solubility as a function of pCO_2. This effect, together with the destabilisation of Fe(III) oxyhydroxides results in a net release of U(VI) in CO_2-rich waters as described in the results here reported, as well as in Grivé (2005) and references therein.

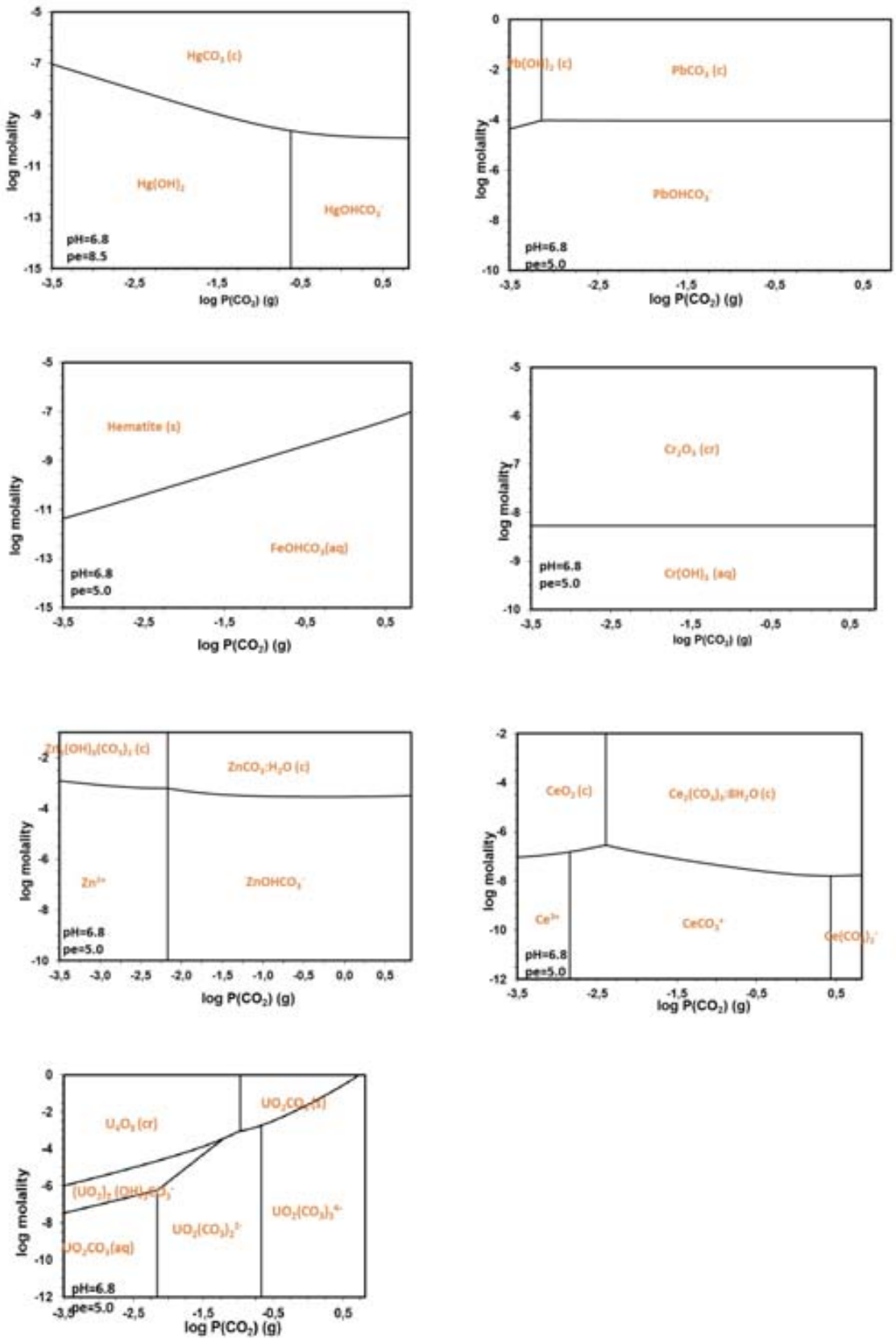

Fig. 22: Predominance diagram of Hg(II), Pb(II), Zn(II), Fe(III), Cr(III), U(VI), Ce(III) and Ce(IV) species at pH=6.8 and pe=8.5 as a function of pCO_2, reflecting the outlet conditions of the experiments performed by Ardelan et al. (2012).

4.3.2 SECONDARY TRACE ELEMENTAL MOBILITY AS A RESULT OF Fe(III) DISSOLUTION IN OXIC CONDITIONS

The association of trace elements to Fe(III) oxyhydroxides through sorption processes has also been very well established and the compilation by Dzombak and Morel (1990) summarises the rationalisation of these interactions through surface complexation reactions. Therefore, any effect of CO_2 on the solubility of the iron(III) oxyhydroxides cascades into the release of trace metals associated to these solid phases. In addition, for some trace metals, the formation of mixed hydroxocarbonate or carbonate aqueous complexes enhances their dissolution and consequently their mobility.

One of the trace elements that better exemplifies this is uranium. In oxic environments uranium is present in the hexavalent form and is rather soluble in natural water conditions. However, U(VI) has also a strong affinity to sorb onto iron(III) oxyhydroxide phases and depending on the circumstances may even co-precipitate with these solid phases (Bruno et al., 1995). The presence of increased CO_2 concentrations has a double effect on this retention mechanism. In one hand, as we have seen in the previous sections, carbon dioxide may destabilise the iron(III) oxyhydroxide (ferrihydrite, $Fe(OH)_3(am)$) releasing the attached uranium(VI) and, in addition, the increased total carbonate has the result of building stable U(VI) carbonate complexes.

Duro (1996) studied the effect of increased HCO_3^- concentration in the kinetics of dissolution of U(VI)/$Fe(OH)_3$ coprecipitates back in 1996. To this aim, coprecipitates of $Fe(OH)_3$/U(VI) were synthesised at a nominal 3% U:Fe ratio $(2.71\pm0.1)\cdot 10^{-2}$ determined by total dissolution and ICP analyses. 5 different experiments with the same solid phase were setup, by contacting 0.4 g of solid with 200 mL of a 0.1M$NaHCO_3$ solution, previously equilibrated with 1 atm $CO_2(g)$. The experiments were kept under a constant bubbling of 100% $CO_2(g)$ at different pH values (in the range 5 to 7), as shown in Table 4. Another experiment, equilibrated with atmospheric $CO_2(g)$ was set up to reach a more alkaline pH of 9.2. Solution samples were taken at different time intervals for uranium analysis and pH monitoring until steady state uranium concentration was reached. No important pH changes were observed (the uncertainty in Table 4 stands for the maximum pH variation in each experiment). For the sake of comparison with a pure uranium solid phase, an experiment mimicking the previous ones, but by using schoepite ($UO_2(OH)_2(s)$) instead of a $Fe(OH)_3$/U(VI) coprecipitate, was set up.

Table 4: Experimental conditions used in the dissolution experiments of a coprecipitate and schoepite samples.

Exp	Solid phase	Gas	pH
Exp 1	$Fe(OH)_3$/U(VI) coprecipitate	100% CO_2	5.58 ± 0.04
Exp 2	$Fe(OH)_3$/U(VI) coprecipitate	100% CO_2	6.16 ± 0.12
Exp 3	$Fe(OH)_3$/U(VI) coprecipitate	100% CO_2	6.66 ± 0.06
Exp 4	$Fe(OH)_3$/U(VI) coprecipitate	100% CO_2	7.03 ± 0.07
Exp 5	$Fe(OH)_3$/U(VI) coprecipitate	Atmospheric CO_2	9.18 ± 0.04
Exp. 6	Schoepite	100% CO_2	6.03 ± 0.04

The results obtained are shown in Fig. 22, showing an initial stage of fast uranium dissolution is followed by a slow down until a steady-state is established (note the logarithmic scale in the plot).

The influence that bicarbonate has on the dissolution of uranium from the coprecipitate can be clearly observed when representing the initial dissolution rates versus the concentration of $[HCO_3^-]$ in the system (Fig. 23 a) from where a direct linear correlation with the dissolved HCO_3^- concentration is observed. The best fit to the data renders a calculated rate constant in the order of 10^{-3} moles $U \cdot g^{-1}h^{-1}$ (see eq. 4.1):

$$R_o = (1.1 \pm 0.2) \cdot 10^{-3} \cdot [HCO_3^-]^{(1.06 \pm 0.12)} \text{ moles U } g^{-1}h^{-1} \qquad (4.1)$$

Bruno et al. (1992) established the formation of a surface complex on the surface of ferrihydrite in the presence of $CO_2(g)$: $>FeOH\text{-}HCO_3^-$. According to their study, the rate of dissolution of hematite was linearly dependent on the concentration of this surface complex. By assuming congruent dissolution of the co-precipitate, and calculating the concentration of the surface complex in experiments 1 to 5, it is possible to observe a direct correlation between the rate of dissolution of iron from the coprecipitate and the concentration of this surface species (see Fig. 23b). The comparison of the rates of congruent dissolution of the U/Fe coprecipitate and the pure schoepite indicated that the coprecipitate had a protective action against dissolution. The rates of uranium dissolution in the presence of bicarbonate were three orders of magnitude slower in the case of the coprecipitate than for the pure schoepite phase. Kinetic data for schoepite was only

possible to obtain until 120 hours, given that a solid phase transformation to (UO_2CO_3(s)) occurred after 200 hours of contact between the solid and the solution, confirmed by XRD (see Fig. 25).

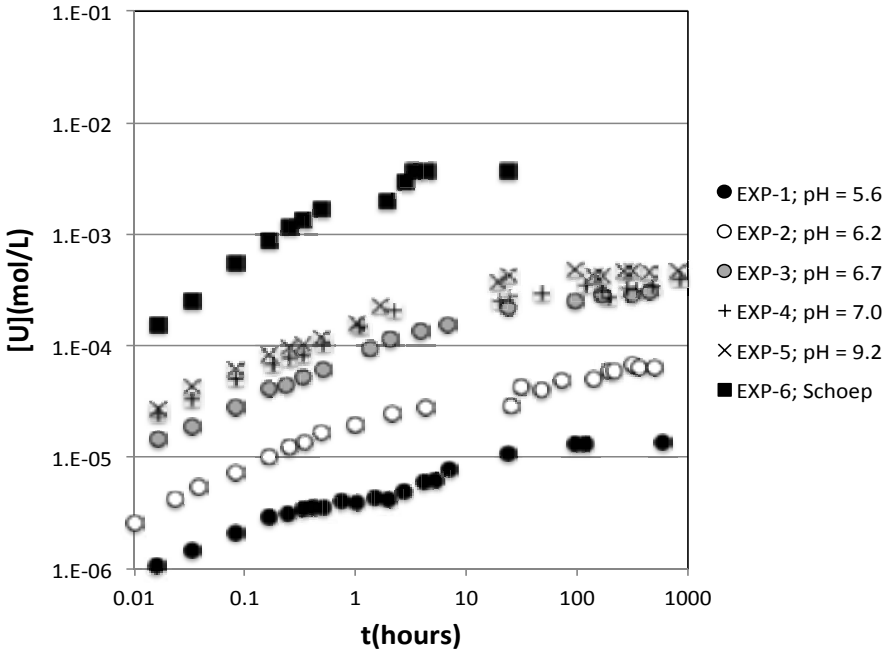

Fig. 23: Evolution of the concentration of uranium in solution with time in experiments 1 to 5 in Table 4.

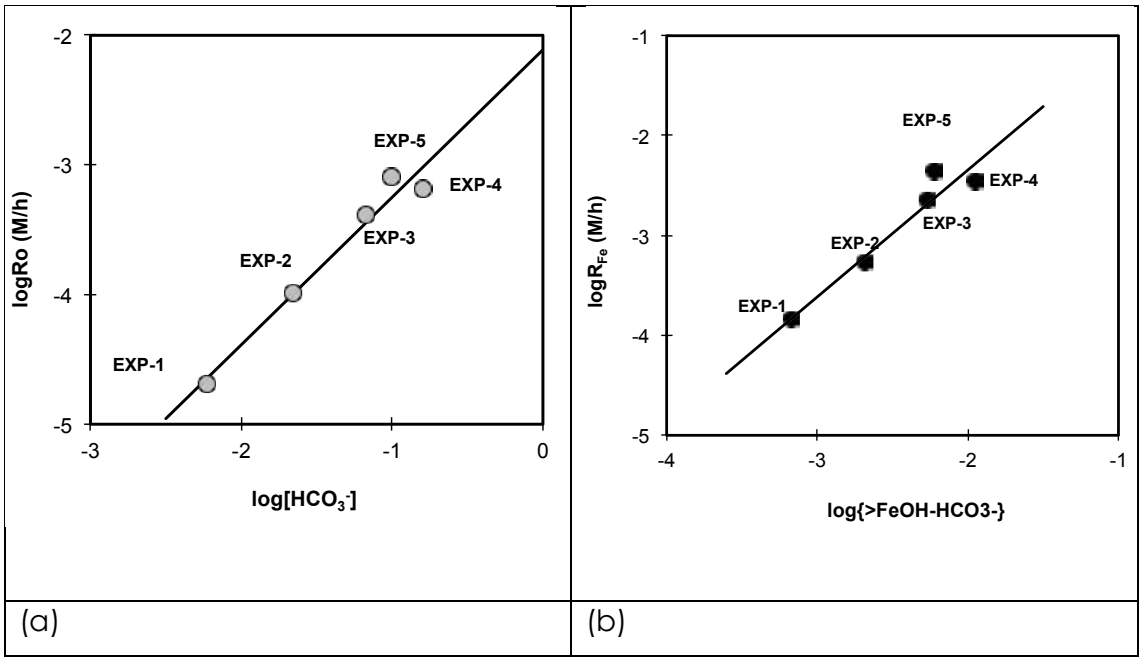

Fig. 24 (a) Plot of the initial rates of uranium dissolution from the co-precipitates versus the concentration of bicarbonate in the system; (b) plot of the initial rates of iron dissolution from the co-precipitates versus the calculated concentration of >FeOH-HCO_3^-

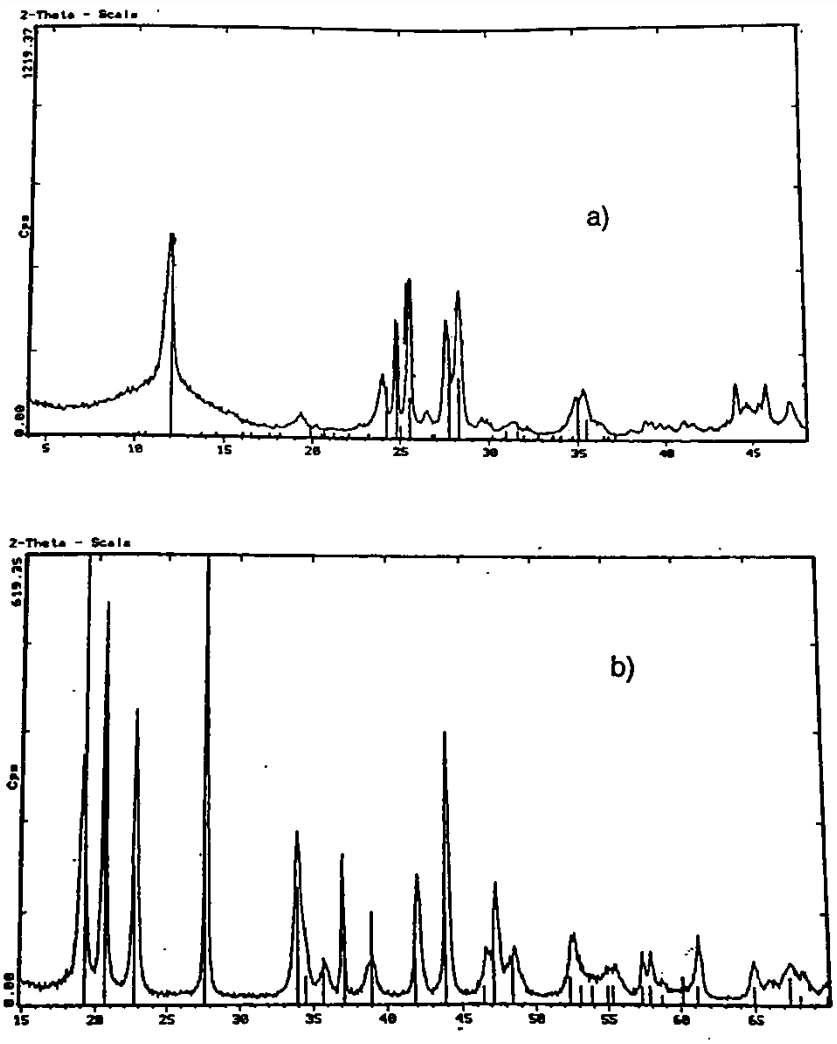

Fig. 25: XRD of the initial schoepite solid phase used in Exp-6; (b) XRD of the solid phase in Exp-6 after 200 h ours o f contact with th e solution, s howing th e pattern o f the uranyl carbonate R utherfordine ($UO_2CO_3(s)$).

The concentrations of uranium reached at steady state from Experiments 1 to 5 in Table 4, could be properly explained by invoking the dissociation of the following carbonate surface complex (eq. 4.2), with its associated equilibrium constant (Fig. 25):

$$FeO\text{-}UO_2OH\text{-}HCO_3^- + 3\ H^+ \Leftrightarrow >FeOH + UO_2^{2+} + CO_2(g) + 2\ H_2O \quad (\log K = 13.42 \pm 0.5) \qquad (4.2)$$

which is in agreement with a similar complex defined by Waite et al. (1994) with a log K = 14.43.

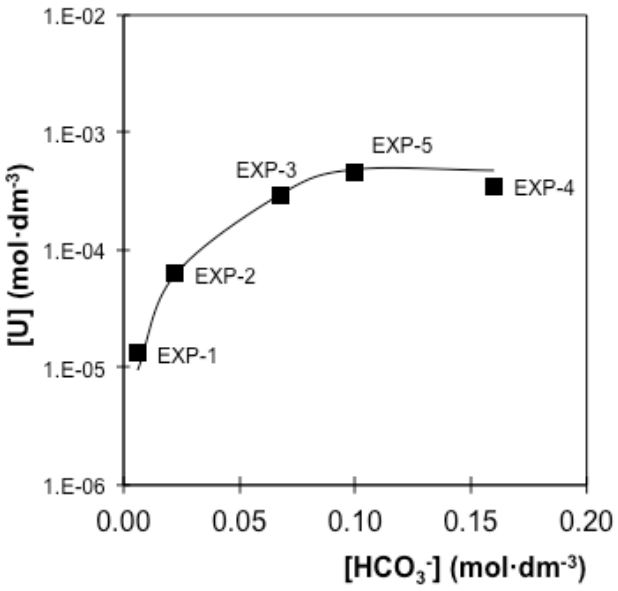

Fig. 26: Steady state concentrations of uranium in solution from the dissolution of a coprecipitate (see Table 4) versus the concentration of hydrogenocarbonate in solution. Symbols stand for experimental data and line for the calculated solubility obtained by considering the formation of the surface species in eq. 2.

These results highlight again the relevance of carbonate not only on the kinetics of the release of trace metals associated with major mineral phases, such as U(VI) with ferrihydrite, but also on the equilibrium (or steady-state) concentrations in the system.

In order to remove the effect of phase transformation and to expand the study to lower $pCO_2(g)$, more representative of natural conditions, Grivé (2005) investigated further the previous system by means of flow-through experiments. This author assessed the effect of the carbonate system on the kinetics of dissolution of ferrihydrite, schoepite and U(VI)/$Fe(OH)_3$ co-precipitate in bicarbonate solutions through flow-through experiments. The results suggested a three-step mechanism in the case of ferrihydrite and schoepite, and a two-step mechanism in the case of the co-precipitate. The applicability and validity of the model presented in the case of the co-precipitate was tested against independent data from Duro (1996) (see Grivé, 2005).

4.4 DISCUSSION:

4.4.1 GENERAL ASPECTS:

4.4.1.1 The effect of CO_2 on trace metal complexation:

Already in 1986 it was postulated that trace metal mobility in natural waters is affected by carbon dioxide content through the formation of mixed hydroxo-carbonate complexes (Bruno, 1986), as it had been established by the pioneering work of Hietanen and Högfeldt (1976) on mixed hydroxo-carbonate complexes of Hg(II) and the one by Ferri and co-workers on Zn(II) and Pb(II) (Ferri et al., 1987a, b) mixed hydroxo-carbonate complexes and the work on the Be(II) hydroxo carbonate system (Bruno et al. 1987).

The co-authors of this paper proposed that mechanism for the transition between metal hydroxo complexes to metal hydroxo carbonate complexes involved the attack of the dissolved CO_2 onto the metal hydroxide bridges to build bicarbonate and carbonate bridges. This was based on the kinetic work performed by Chaffe et al (1973), Dasgupta and Harris (1977), Spitzer et al. (1982) and Sadler and Dasgupta (1987) on the formation of ternary organo-hydroxo-carbonato complexes in the presence of CO_2.

Later, the reaction of metal bridging OH groups with CO_2 to build carbonate bridges has been further studied for Cu(II) (Kitajima et al. 1990), for Zn(II) (Murthy and Karlin, 1993) and for a series of divalent organometallic(II) complexes, including Mn, Fe, Co, Ni, Cu and Zn, in Kitajima et al. (1993). This research is particularly relevant in the case of zinc since the Zn(II) enzyme carbonic anhydrase catalyses the reversible reaction CO_2 hydration to produce bicarbonate, a process that is essential to remove CO_2 from tissues in mammalian respiration process.

More recently Huanga et al. (2011) have proposed a similar mechanism for the fixation of CO_2 onto a Ni(II) pyridine hydroxo complex by a combination of spectrophotometric measurements and density functional theory (DFT) calculations which occurs at remarkable fast rates (10^6 $M^{-1}s^{-1}$) compared to rates obtained for the transformation of metal hydroxides onto metal carbonates which are 1000 times slower.

From all this information, we can conclude that the formation of metal carbonate complexes is kinetically enhanced by increased CO_2 concentrations and that it is favoured

by the occurrence of metal hydroxide complexes normally occurring at the pH ranges of natural water systems. According to the work performed on divalent organometallic complexes, the presence of organic matter could largely accelerate the reaction.

Iron is a key metal ion in biological and geochemical systems as it regulates many key processes, including the scavenging and release of critical trace metals in natural water systems. The cycle of iron is often kinetically coupled with the cycles of P, S, heavy metals, O_2 and C, and depends on the biota and the energy and intensity of the light (Luther et al., 1992; Stumm and Sulzberger, 1992).

The cycles of iron (Stumm and Sulzberger, 1992) and of carbon (Berner and Lasaga, 1989) are also the drivers of the mobility and retention of trace elements involved in natural weathering processes of minerals as well as in the anthropogenic activities. This is especially critical in the biosphere/geosphere interface, where the atmospheric oxygen and carbon dioxide undergo the main part of the transformation processes. Among them, the coupled dissolution-precipitation of iron (III) hydroxides and calcium carbonate are very dynamic processes in natural water systems with characteristic reaction times which are in the range of days.

The role of the iron cycle on trace metal mobility in natural water systems has been traditionally associated to the oxic/anoxic redox transitions and the effect of increased CO_2 concentrations has been mainly explained by the formation of Fe(II) carbonate complexes in anoxic/reducing conditions. However, already in 1992, the effect of increased CO_2 on Fe(III) oxyhydroxide dissolution by the formation of mixed Fe(III) hydroxocarbonato complexes was established (Bruno et al., 1992b; Bruno and Duro, 2000). The stoichiometry and stability of the mixed hydroxocarbonato complexes was firmly determined by Grivé in her PhD Thesis (2005) and it has been recently published (Grivé et al., 2014a, b). In this work was shown that the solubility of Fe(III) is enhanced some 3 to 4 orders of magnitude as $CO_2(g)$ is increased from present atmospheric to 1 bar at the pH range of most natural waters. This is mainly due to the formation of one mixed hydroxocarbonato complex, $Fe(OH)CO_3(aq)$, predominant in the circumneutral pH range and a very stable Fe(III) carbonato complex, $Fe(CO_3)_3^{3-}$, in the alkaline pH range.

4.5 CONCLUSIONS:

Increased atmospheric CO_2 concentrations have an effect on the aquatic chemistry of seawater by increasing the total carbonate content and increasing the acidity.

The buffering capacity of the oceanic system is quite large but a clear increase of acidity and of the dissolved CO_2 content can be seen, provided a careful date analyses is performed in a long time series (Bates et al., 2014)

The effect of increased acidity in trace elemental solubility is obvious but the net effect of increased carbon dioxide concentrations is more complex. The increased dissolution due to the formation of aqueous carbonate complexes can be compensated by the formation of carbonate solid phases. However, as the kinetics of the carbonate complex formation is faster than the build up of carbonate solid phases, in a dynamic situation a net metal release could be observed when the partial pressure of CO_2 is increased.

Our observations from several CO_2-rich systems would indicate that there is a marked increase of Fe(III) solubility due to the formation of aqueous hydroxo carbonate and carbonate complexes (Agnelli et al., 2013; Grive et al., 2014). This increase on Fe(III) solubility cascades in the release of trace elements associated to Fe(III) oxyhydroxide solid phases.

An analysis of the observations by Ardelan et al. (2012) on the effect of increased CO_2 on increased trace metal dissolution would indicate that most of the trace elemental mobility is due to secondary dissolution as a result of the destabilisation of Fe(III) oxyhydroxides and/or the competing kinetics between aqueous and solid metal carbonate complex formation.

5 Objective 2:

Characterisation of the gas-water-rock interaction time for the formation of metal plumes in CO_2-bearing waters and the influence of carbonate species on iron solubility

Article 2: Metal enrichment in shallow aquifers due to $CO_{2(g)}$-rich fluids intrusion: the influence of carbonate aqueous species on iron solubility and metal plumes in natural systems

Marco Agnelli [a], Fidel Grandia [a], David Soler [b], Álvaro Sáinz - García [a,c], David Brusi [b], Manel Zamorano [b], Jordi Bruno [a]

[a] *Amphos 21 Consulting S.L., Passeig Garcia i Fària, 49-51, 08019 Barcelona – Spain.*

[b] *Centre de Geologia i Cartografia Ambiental (GEOCAMB), Departament de Ciències Ambientals, Facultat de Ciències, Universitat de Girona. Campus de Montilivi s/n, 17071 Girona – Spain.*

[c] *Université Toulouse III - Paul Sabatier - Route de Narbonne 118, 31062- Toulouse – France*

Abstract:

The interaction between carbon dioxide gas flows and groundwater leads to the dissolution, mobilization and re-precipitation of metals and metalloids. The potential for metal release associated with CO_2 leakage from underground storage formations into shallow aquifers is an important aspect in the risk assessment associated with CO_2 sequestration, and the understanding of the persistence of metal plumes is a very concerning aspect. In the Campo de Calatrava region, an old volcanic field in central Spain, CO_2 flows from mantle interact with shallow aquifers resulting in remarkable metal release. 12 sampling stations have been selected for gas and water analysis, 10 as bubbling pools and 2 as episodic "cold" geysers. These samples are characteristically much enriched in trace metals compared to CO_2-free aquifers, being Fe the most abundant, (up to 6.08×10^{-4} mol·L^{-1}). Also, high concentrations of Mn (up 8.01×10^{-5} mol·L^{-1}), Zn (up to 1.46×10^{-6} mol·L^{-1}), Ni (up to 1.19×10^{-6} mol·L^{-1}), Co (up to 7.1×10^{-7} mol·L^{-1}), Cu (up to 3.3×10^{-7} mol·L^{-1}) and As (up to 1.4×10^{-7} mol·L^{-1}). pH range is very close to 6 and Eh is quite oxidising. Gas composition is almost pure CO_2, with no detectable amounts of CH_4 and H_2S.

Thermodynamic calculations reveal that the formation of aqueous Fe(III) carbonate complexes, mainly $FeCO_3OH$, as a result of the CO_2-shallow aquifer interaction causes the dissolution of native $Fe(OH)_3$ releasing iron and all trace metals sorbed onto its charged surface. Then, neither acidification, "reducing" gas impurities, nor low Eh environments (i.e., making Fe(II) as predominant iron form) can be considered as the main drivers for the development of the metal plumes associated to gas inflows into shallow aquifers.

The persistence of these metal plumes, which is crucial in the risk assessment studies of CO_2 underground storage, is predicted to be potentially long since $Fe(OH)_3$ is the solubility-limiting phase not only for Fe but also for the other metals with an observed increase in concentration. The effect of the formation of aqueous metal carbonate is not as relevant in metals like Mn, Zn, Cu, Co, Ni, and except for Mn, the measured concentration in samples from the Campo de Calatrava are far from the saturation in solid carbonates.

Keywords: Carbon storage, leakage, metal transport, natural analogue, Campo de Calatrava

Submitted to scientific journal: Chemical Geology

5.1 INTRODUCTION:

The capture and storage of CO_2 in deep subsurface reservoirs is one of the options currently being considered to lower the industrial emissions of this greenhouse gas to the atmosphere. The site selection of CO_2 storage reservoirs must be accurate enough to minimize the risks to human health and the environment (Rempel et al., 2011; Zheng et al., 2011). However, the possibility of CO_2 leakage cannot be completely ruled out, in which case the stored CO_2 could migrate following preferential pathways upward into overlying shallow groundwater resources. The presence of high carbon dioxide content into an aquifer leads to chemical interactions between the CO_2, brine and reservoir rock, leading the dissolution, mobilization and re-precipitation of metals and metalloids (Czernichowski-Lauriol et al., 2006; Fischer et al., 2010; Kharaka et al., 2006; Kharaka et al., 2009; Wigand et al., 2008). The potential for metal release associated with CO_2 leakage from underground storage formations into shallow aquifers is an important aspect in the risk assessment associated with CO_2 sequestration. The effects of increased CO_2 concentrations on the release of metals like Zn, Cu, Co and Ni in shallow aquifers have been studied using numerical simulation (Apps et al., 2010; Atchley et al., 2013; Navarre-Sitchler et al., 2013; Siirila et al., 2012; Wang and Jaffe, 2004; Wilkin and DiGiulio, 2010; Zheng et al., 2012), laboratory experiments (Frye et al., 2012; Little and Jackson, 2010; Lu et al., 2010; Romanò et al., 2013; Wei et al., 2011) and few field studies (Agnelli et al., 2013; Kharaka et al., 2009; Trautz et al., 2013). In most studies, the exposure of aquifer materials to CO_2 increased the aqueous concentrations of metals, although in some cases such increase was episodic (Lu et al., 2010). In other cases, the concentration of some metals decreased altogether (Little and Jackson, 2010). In principle, the metal transport capacity of CO_2-bearing fluids in shallow aquifers should increase as pH decreases; another potential mechanism is the formation of low Eh environments due to the presence of "reducing" trace gases (e.g., H_2S and CH_4). More recently, Grivé et al. (2014) showed that Fe(III) solubility in CO_2-bearing fluids can significantly increase due to the formation of Fe(III) carbonate complexes that are stable at circumneutral pH's, and, therefore, being more persistent in time and space in geological media. The enhanced solubility of Fe(III) has an additional and unwanted side effect: the inhibition of the precipitation of $Fe(OH)_3$ (am), which is a major sink for many trace and minor elements. The $Fe(OH)_3$ precipitation is favoured when CO_2 starts degassing due to loss of pressure (i.e., fluid ascent to surface through faults or by well production) and, eventually, part of

all these metals may precipitate back into solid phases; but some of the metal load is still dissolved.

The high solubilisation of metals can be used as a monitoring tool of CO_2 leakage episodes. Time-lapse measurement of metal contents in shallow aquifers can help in the early detection of seal failure of CO_2 storage site because the concentration of all these metals in shallow and surface waters is commonly very low, and tiny changes in such a concentration could be indicative of early leakage (Agnelli et al., 2013; Romanò de Orte et al., 2013; Wunsch et al., 2013).

Constraining the duration and intensity of metal release to the aquifer is fundamental in the risk assessment of the geological storage because such metal increase, if fast and intense, can jeopardise the quality of water resources. The rates of metal release due to CO_2(g)-water interaction are believed to be quite fast in view of laboratory experiments and from few pilot plant-scale injection operation. Recently, Romanò de Orte et al. (2013) found, in a laboratory experiment, how Fe content in water increased 85% and persisted in water due to a decrease of pH from 7 to 5.5 in 10 days, showing that short time interaction between CO_2(g) and water is sufficient to dramatically increase the metal concentration in the water. Furthermore, in natural systems, some examples of episodic intrusion of deep natural CO_2 into shallow aquifers provide evidence of quick metal increase in solution (Piqué et al., 2010).

In this research article, the interaction of deep CO_2 fluxes with shallow aquifers is investigated through the geochemistry of CO_2-bearing waters and gas emissions in natural systems in the Campo de Calatrava region in central Spain. A ubiquitous feature of the CO_2-rich waters in this area is the reddish color due to the formation of iron hydroxide colloids. The quality of these springs and aquifers is not acceptable in terms of metal content and represents an illustrative example of the impact of potential leakage from deep geological storage. The role and importance of the aqueous Fe(III) carbonate complexes in metal mobility is assessed and compared against other mechanism of metal solubilisation, such as acidity or reducing gases.

5.2 THE CAMPO DE CALATRAVA GEOLOGICAL SETTING:

The Campo de Calatrava is located a few hundreds of kilometers south of Madrid and about 25 km south-east from Ciudad Real. This area is geologically interesting since it does contain a volcanic field with a large number of gas+water discharges. These springs are often accompanied by conspicuous and gentle gas bubbling generally dominated by CO_2. This area can probably be regarded as one of the most important natural emitting zone of CO_2 in the whole Peninsular Spain, along with that of La Selva-Empordà basin in north-eastern Spain (Catalunya).

The geological setting of this area can be summarized into three main units (Fig. 27):

- A basement of Paleozoic rocks that define the higher relief, with small ridges that are arranged with preferred orientations E–O, NNE-SSO and NO-SE.

- Tertiary basins opened over the Hercynian material, with the occurrence of normal faults, forming depressions (sometimes closed, sometimes open towards the plain of La Mancha) refilled by alluvial and lacustrine sediments aged between Miocene and Quaternary.

- The volcanic material from Campo de Calatrava, is a product of an eruptive phase that began in the area in the late Miocene (between 7 and 8 Ma), with the most important peak of activity taking place between the upper Pliocene and lower Pleistocene (between 3.7 and 1.75 Ma) (Ancochea, 1982). Traditionally, this volcanism has been associated to an extensional setting or of "aborted rifting", but some authors suggested that this activity could be related to flexural processes of the lithosphere, through which the mantle would rise and partially melt.

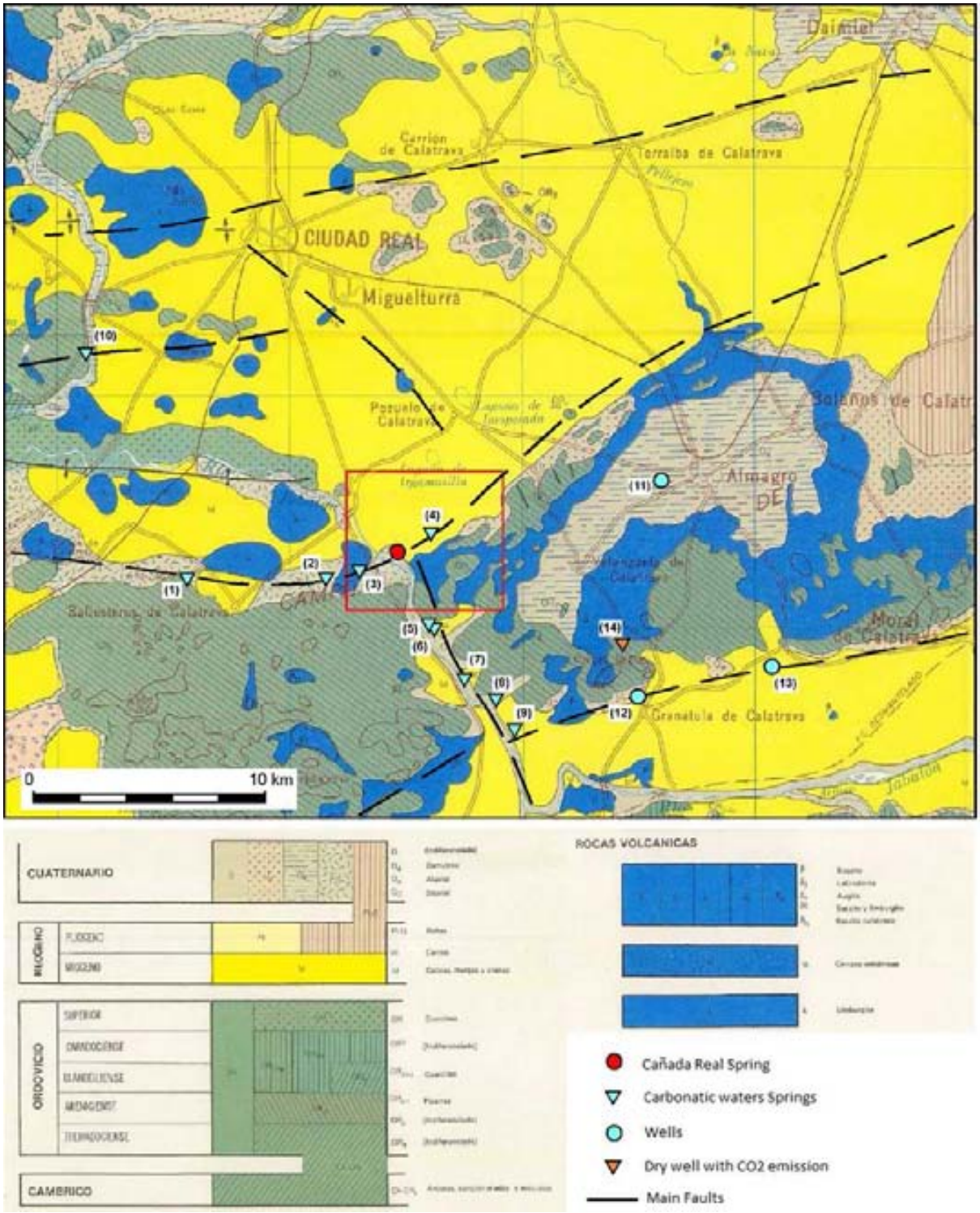

Fig. 27: Geological map of the central area of Campo de Calatrava (extracted from IGME, 1983). In the map are shown the main faults and sites characterized by CO_2 emissions. (1): Villar del Río; (2): Villafranca; (3): Fuensanta; (4): San Cristóbal; (5): El Chorrillo; (6): Piedra de Hierro; (7): Jabalón-La Nava; (8): Fontecha; (9) Baños del Barranco, Aldea del Rey; (10): Fuentillejo; (11): Hoya de Almagro; (12): El Bombo; (13) El Chorro de Granátula de Calatrava; (14): La Sima.

The materials emerging in the proximity of the study area consist predominantly of quartzites. The thickness of this unit ranges from 200 to 300 m and it is believed to be of Ordovician age (IGME, 1988). In the field, this unit forms the main reliefs and showing some strata that locally allow the observation of structures of folds and small fracture displacements.

Above the Hercynian basement it is possible to find levels of breccias, conglomerates and sandstones with ferruginous cement, alternating with stretches of pelitic dominance (Fig. 28). Occasionally it's possible to observe crusts and concretions of iron and manganese oxides.

Fig. 28: Detrital levels of lower Pliocene age

The rest of the sedimentary deposits filling basins are those that have a greater extent of surface outcrops. These deposits consist mainly of detrital formations dominated by silts and sands with different degree of cementation related to sedimentation in wetlands. Carbonate-rich horizons are also present (IGME, 1988 a,b) (Fig. 29).

Concerning the volcanic materials of the Campo de Calatrava province, these are a set of more than 200 eruptive centers. The main eruptive features of the many volcanic edifices that characterize the Campo de Calatrava are dominated by strombolian and hydromagmatic events.

This area is characterized by several gas and water discharges that are distributed almost through the whole volcanic provinc e. It is interesting to be point ed out that the geochemical and isotopic features of the gas seeps indicate a high concentration of CO_2 (up to 98% by vol.) and helium isotopic ratios affected by a deep(mantle)- related source. The Campo de Calatrava volcanic province along with that of Selva-Empordà (NE Spain) likely represent the highest output zone of CO_2 in the whole continental Spain.

Fig. 29: Blocks of calcarenite accumulated near the river Jabalón (left) and details of the internal organization into the calcarenite (right).

5.2.1 THE WATER AND FLUID DISCHARGES:

The CO_2-bearing emission sites in the Campo de Calatrava area are mainly located in its southern part. By a nalyzing the distribution of the different emission sit es, it c an be observed that most of them seep out from the main volcanic centers. Furthermore, these fluid discharging sit es are a pparently aligned a long we ll-defined tec tonic li neaments: NW-SE and NNW-SSE and subordinately, ENE-WSW.

Geophysical investigations have revealed the pre sence of crustal and mantle anomalies that support the correlation between CO_2 discharges and the volcanic activity.

A peculiar a nd sp ectacular fe ature o f the Campo de C alatrava Vol canic F ield is that during well drillings some gas blasts have recently occurred, leading to the formation of "cold geisers". The most famous episode oc curred in spring 2000 in Granátula de Calatrava when a gas blast emitted a column of water and gas up to 60 m high, caused by illegal drilling (Fig 30). These events are strongly indicative of a geopressurized (CO_2-

rich) reservoir that may have at least two important implications. The first one is related to the need of ensuring a proper protocol while drilling wells in the area in order to prevent such gas blasts that may have fatal effects on the people in vicinity of the drilling operation. The second one is that the presence of a pressurized reservoir at depth may suggest weak diffuse soil degassing in the Campo de Calatrava Volcanic Field.

An important feature for the geological and hydrogeological characterization of the area is the formation of iron and manganese crusts, with economically relevant concentrations of cobalt (Crespo, 1992; Poblete, 1992). In fact, it is likely that the rise of CO_2 contributes or contributed to the formation of metal plumes that are the origin of these deposits (Fig. 31).Spring waters of the Campo de Calatrava share a number of geological and geochemical features (Poblete, 1992; Pérez et al., 1996; Yélamos et al., 1999). The waters are hyperthermal (<33 °C), bicarbonate or sulphate-carbonate and characterized by moderate electrical conductivity (1 to 6.7 mS/cm), slightly acid pH (5.5-6), high concentrations of Fe and Mn and high CO_2 concentration (up to 2990 mg/l) (Calvo et al., 2010; Vaselli et al., 2013; Elío et al., 2015). The isotopic composition of oxygen and hydrogen suggests a meteoric origin for the water, while those of carbon and helium indicate a significant contribution from the mantle in the dissolved gas.

Fig. 30: The gas blast occurred in July 2011 close tu Almagro.

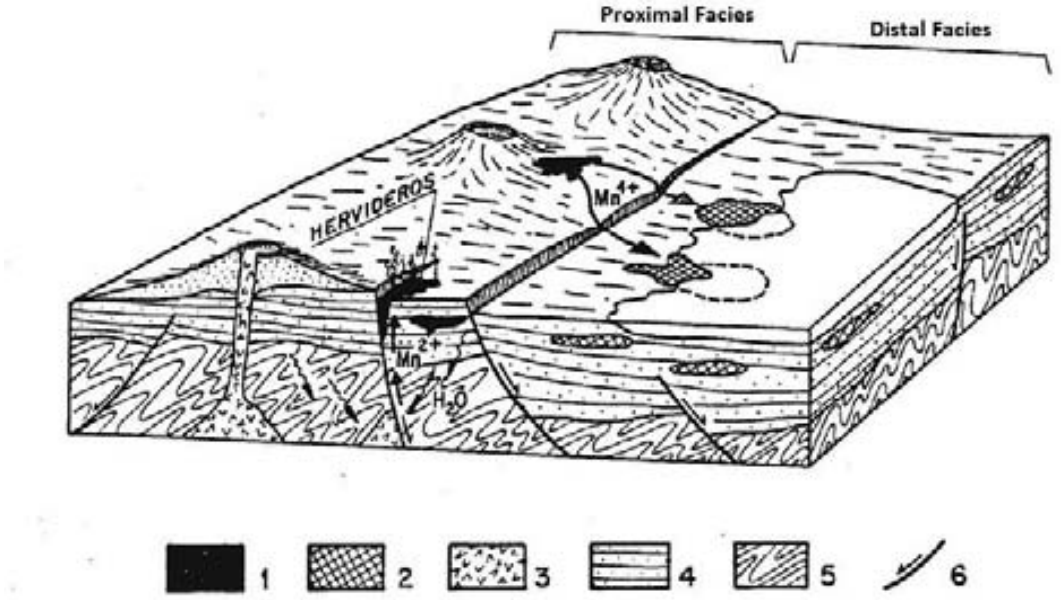

Fig. 31: Geological outline of the types of oxide mineralization Fe-Mn-Co and fractures associated to the volcanism of Campo de Calatrava. 1: Proximal Mn deposit, 2: Distal Mn deposit; 3: Volcanic rocks, 4: Pliocene and Quaternary sediments, 6: Faults. (Adapted from Crespo, 1992).

5.3 GEOPHYSICAL PROSPECTING:

5.3.1 GENERAL ASPECTS:

In order to constrain ground geology and hydrogeology related to the CO_2-bearing water emission points, electrical resistivity tomography (ERT) investigations were carried out at the Cañada Real site (see location in Fig. 32), the largest CO_2 discharge in CCVF. The geophysical prospecting techniques aim to characterize the subsurface in a non-invasive way, from measuring a physical parameter that may be related with characteristics of geological materials or other entities under the soil's surface. In the case of prospecting electrical the parameter investigated is the electrical resistivity, usually expressed in ohm per meter (Ωm). It can be defined as the resistance that a material opposes to the passage of electric current through it, and is equivalent to the inverse of electrical conductivity. The electrical resistivity of the material depends on its mineral composition, the internal structure, the presence of fluid in the pores (typically air or water), and ion's concentration. The two-dimensional electrical tomography gets a quite accurate model of the variations in resistivity on the ground, based on large number of measurements from the surface. The measuring device consists of a cable which connects a certain amount of metallic electrodes stuck to the floor in regular distances, defining an ideally straight profile. The measuring equipment, typically placed in a central position of the profile, consists of an amperemeter that can regulate the intensity of the current injected in the ground and a potentiometer that measures the potential loss of the electric field generated. This apparatus was usually integrated into a Resistivity, equipped with filtering systems for the environmental electrical noise and powered by an external DC source. Every resistivity reading involves two current and two potential electrodes in a "tetraelectrodical" configuration characterized by a known distance (spacing) between the four points. The resistivity measurement represents an average value of real resistivity of all the materials that are in the focus of the four electrodes. The automated recording of all possible combinations of the device results in a pseudo-section of points of apparent resistivity of the ground distributed in consecutive data levels, which, broadly speaking, has the shape of inverted triangle. The arrangement of the electrodes and their separation determines the degree of resolution and depth of study. Closer electrodes yield a shorter profile but with a higher resolution, while greater separation permit to cover more surface and go deeper but with a loss of data.

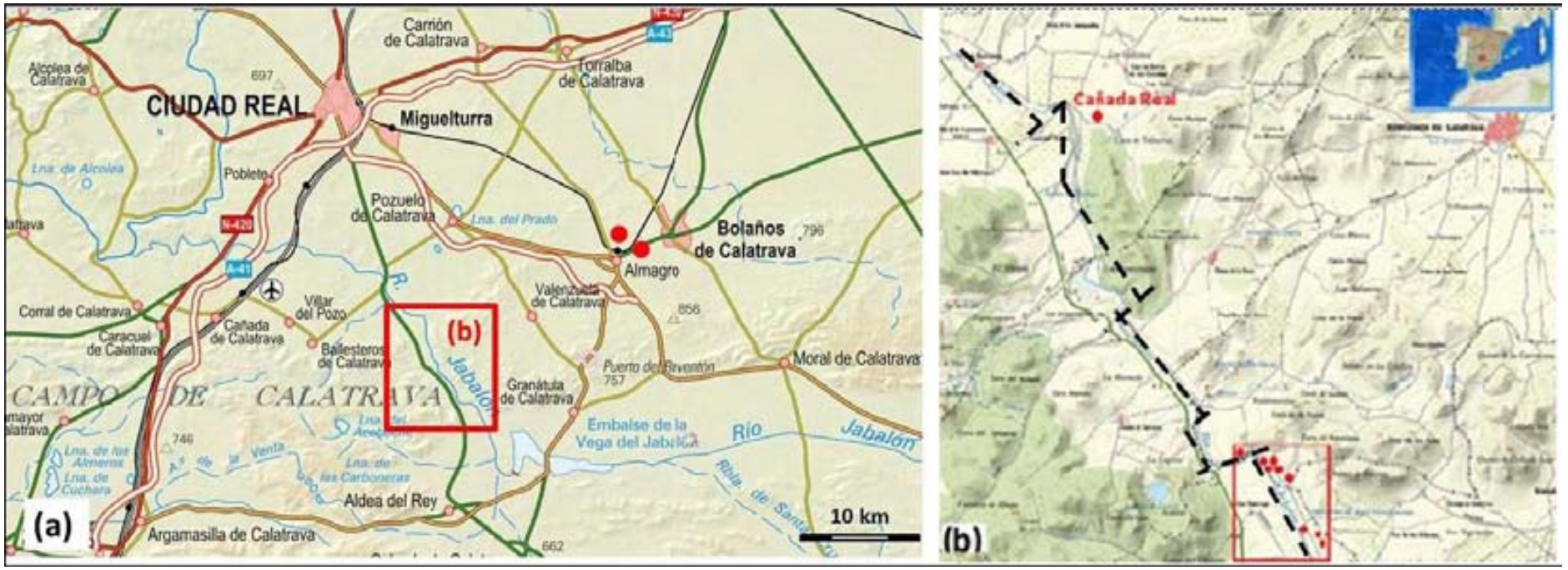

Fig. 32 Location of sampling stations in the Jabalón river basin in the Campo de Calatrava region (from Visor Iberpix IGN, http://www.ign.es/iberpix2/visor).

5.3.2 FIELD WORK:

5.3.2.1 ERT profiles:

As part of a wider campaign of data acquisition around the Cañada Real (Fig 34), on 6th and 7th of May 2014, five electrical resistivity tomography profiles, among 200 m and 600 m in length, have been made (ERT-1 to ERT-5). The details of the geometry of each profile are shown in Table 5, while its location and geometry can be seen in Figure 33.

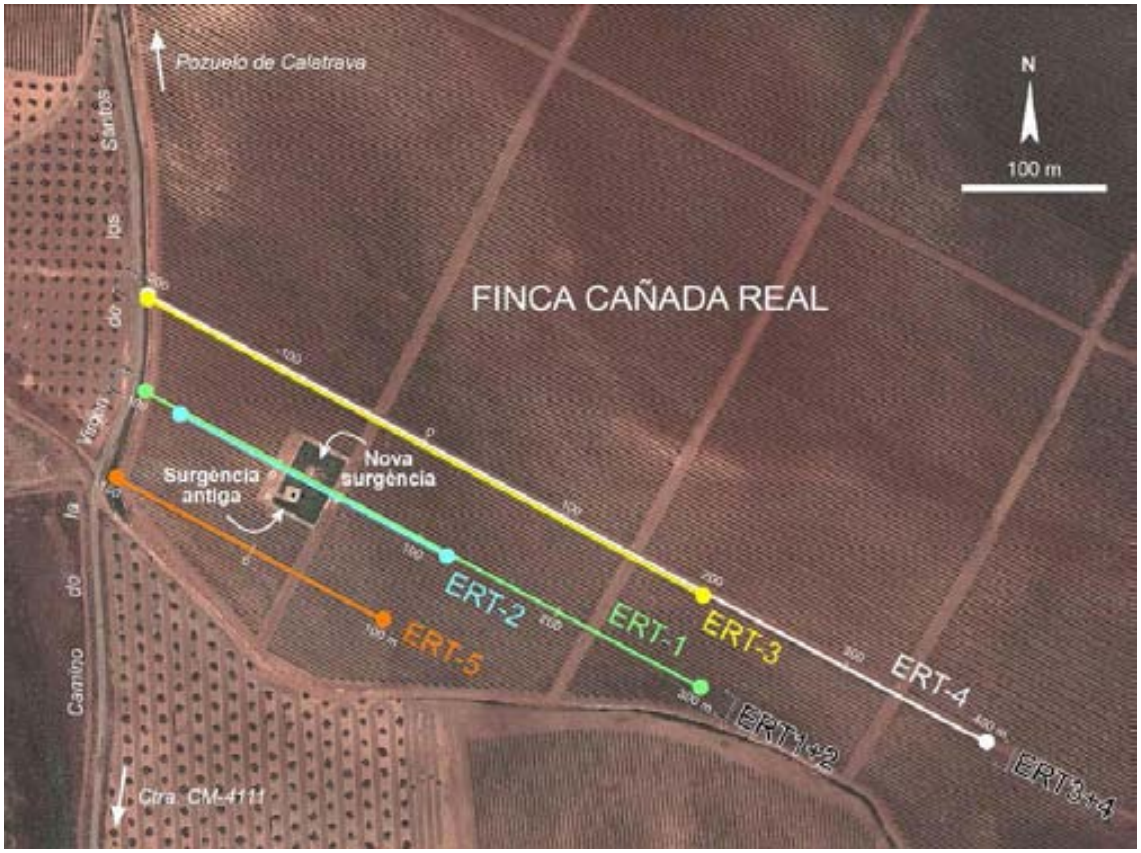

Fig. 33: Location of the geoelectrical profiles performed on the farm Cañada Real.

Table 5: Characteristics of electrical resistivity profiles performed. (a) Distance between electrodes corresponding to the protocol as long and short, respectively. (b) Does not include the time of assembly and disassembly

Profile	Date	Length (m)	Spacing (m) (a)	Electrodes positions	Measuring times(b)	Points of apparent resistivity	Data Levels
ERT-1	06/05/2014	400	10 and 5	71	3h 10min	947	26
ERT-2	06/05/2014	200	5 and 2,5	61	2h 15min	744	26
ERT-3	07/05/2014	400	10 and 5	61	2h 47min	745	26
ERT-4	07/05/2014	600	20 and 10	51	2h 04min	572	23
ERT-5	07/05/2014	200	5 and 2,5	61	2h 25min	741	26

Fig. 34: Geometry of the Cañada Real CO_2-bearing spring.

The apparatus used for measuring it's a Lund Imaging System (ABEMAT Instrument AB), formed by a Terrameter Resistivity System SAS1000 and automatic channel selector ES10-64. The electricity has been provided by a standard battery of 12V and 60Ah and has been transmitted to the ground by galvanized steel electrodes stuck to the floor of 15-20 cm, connected by stainless steel clamp wiring.

The electrode configuration protocol used in the data acquisition was the Wenner-Schlumberger type in which the current electrodes are the external ones and potential are the two interiors. This combination offers a good resolution and sensitivity in horizontal and vertical, and was chosen precisely because was expected that the study area presents both horizontally and vertically geological structures.

For each measurement cycle, the individual registration of resistivity corresponds to the arithmetic average between two and four stacks of three pulses of current injection with each polarity reversal. The device automatically discards all resistivity values that are negative or having a variation coefficient greater than 2.5%.

All profiles were arranged parallel to each other, crossing the space between the rows of vines on the estate and following a direction close to NO-SE.

Apart from the constraints imposed by the location, this approach was considered adequate enough to intercept perpendicularly what is expected to be the geophysical anomaly associated with the regional fracture that runs through the area, considered the main cause of the rise of CO_2 in the sector.

The data acquisition was done independently for each profile, but has taken advantage of those electrodes that, according with the corresponding spacing, have position in both profiles.

5.4 WATER AND GAS SAMPLING:

12 sampling stations have been selected for gas and water analysis, 10 as bubbling pools and 2 as episodic "cold" geysers. The sampling of the two geysers was found relevant because they provide a unique opportunity to collect aquifer waters not affected by a long-term degassing, and, therefore, to collect more pristine water from the impacted aquifer. Degassing leads to the formation of Fe(III) hydroxide colloids that can trap metals by surface sorption, lowering the metal concentration in solution (Fig. 35).

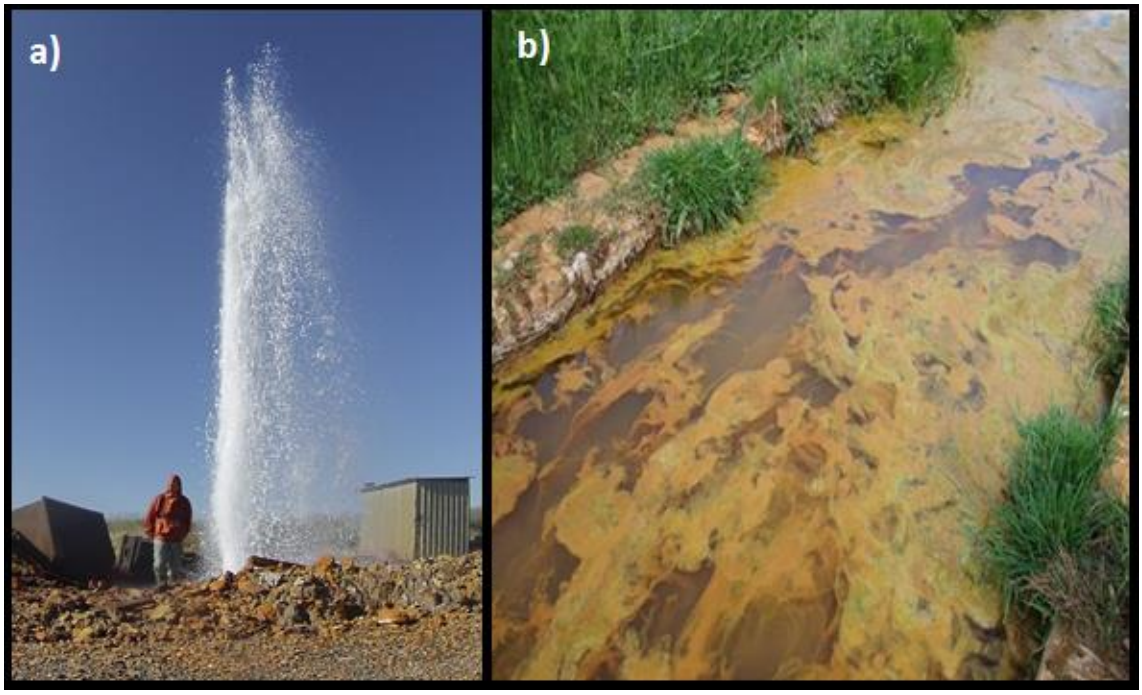

Fig. 35: Gas and water eruption at sampling station "Chorro Glicerio" near Almagro village in 2014 (a) and the formation of iron hydroxide colloids and algae growth over the water table due to the degassing (b).

5.5 RESULTS:

5.5.1 ERT RESULTS:

Results of the three electrical resistivity tomography profiles at Cañada Real provide an insight into the subsurface characteristics and hydrodynamics of the emplacement (Fig. 36). According to the resistivity distribution along the model sections, three zones can be differentiated with respect to their significance about lithology, geological structure, pore-water content and its salinity. Just for explanatory purposes, resistivity values have been arbitrarily classified into four categories: very low (<4 Ωm), low (4 - 16 Ωm), medium (16 - 64 Ωm) and high (>64 to ≈650 Ωm). The uppermost resistive unit defines a roughly continuous level parallel to the surface in all the profiles, with a minimum thickness of 5-7 m and a maximum of 15 m. It shows medium to high resistivity in the western and central parts of the prospected area, and low-medium values in the eastern half of ERT#2. The unit is attributed to Upper Pliocene calcarenites (IGME, 1988a, 1988b). In fact, a laminated porous calcarenite crops out in the perimeter of the spring below a thin surficial mixture of anthropogenically disturbed colluvial-alluvial sands and pebbles. At the nearby Jabalón river valley slopes, abundant joints divide up calcarenites into slightly shifted meter-sized blocks. This observed pattern may explain the irregular shape of basal contact of the unit, and also the pronounced horizontal contrasts in resistivity. Groundwater table is located within this unit at depths mostly ranging between 4.5 and 5.5 m from the surface. Underlying the previous materials, a second resistive unit is characterized by very low to low resistivity values with some low-medium resistivity patches in its eastern upper zones. Presumably it is made up of Upper Pliocene sediments (IGME, 1988a, 1988b), consisting in sands and gravels with varying contents of silt and clay, in an alternation of layers and lenses typical of proximal alluvial facies. Equivalent lithologies can be directly seen about 3 km to the south. Since these materials unconformably cover a paleo-relief defined by the rocky basement, they undergo strong differences in thickness. Minimum values of 7-8 m are found in the western area around the spring zone (ERT#1 and ERT#3), and approximately 10 m are detected in the easternmost part of ERT#2. In these areas the unit has a sharp contact with the basement. Conversely, in the centre of sections ERT#1 and ERT#2 the unit reaches up to 40-50 m in what is believed to represent an infilled valley. In accordance with the low resistivity values and the existence of springs, it may be assumed that the unit is saturated in

groundwater. Moreover, taking into account the source's outflow, water within the aquifer must stay somewhat confined. The bottom of the geo-electrical sections forms a third resistive unit attributed to the Ordovician quartzite basement that actually crops out in all the nearby hills. Medium to high resistivity values delineate a convex shape in the western and eastern areas, gradually passing into lower resistivities in the central concave zone of lines ERT#1 and ERT#2. This pattern may be attributed to rocky topographic highs located at both sides of a nearly vertical fault zone where materials affected by fracturing and weathering present low-medium resistivity values. The fault has WSW-ENE orientation, a width of about 50 m perpendicularly to its trace, and acts as the main source for the ascending CO_2 in the area. Upward migration of gas would cause a progressive decrease in resistivity of the Neogene sediments as it gradually becomes dissolved into groundwater, increasing its electrical conductivity and hence, giving rise to very low resistivity areas. The size and distribution of these most conductive lenses probably reflect the stratigraphic position of higher porosity zones (i.e. sand-gravel lenses with lesser fine content) which represent preferential pathways followed by the CO_2-bearing water to spread across the aquifer. A detailed inspection of resistivity distribution in the vicinity of the spring zone (X coordinates 25 to 35 m in line ERT#1) reveals distinctive features that can be directly linked to the process of groundwater upward migration and gas release (Fig. 36 and Fig. 37). Here, the uppermost calcarenitic unit hosts a negative anomaly that suddenly disrupts the horizontal continuity of prevailing high resistivity values. Under the first 3-4 m from the surface (18-30 Ωm), resistivity rapidly decreases to 4-16 Ωm, depicting a sort of hemispherical convex shape up to about 8-9 m depth. The anomaly extends even deeper inside the underlying detrital sediments, where it becomes a nearly vertical neck-shaped positive anomaly of low-medium values (8-20 Ωm) horizontally surrounded at both sides by two very low resistivity elliptical zones (<4 Ωm). No more distortion of the resistivity isolines is detected below 20-22 m deep, so the Paleozoic basement does not seem to be involved here in the dynamics that causes this particular anomaly. Slightly increased resistivity within the aquifer in the vertical of the spring may be interpreted to be due to a loss of dissolved ionic content (i.e. HCO_3^- passing into CO_2 gaseous phase). Ascent of water across the fractured calcarenites would cause a marked reduction of their resistivity and originate the plume-like shape related to localized elevation of the water table. Finally, near-surface massive water degassing would increase again resistivity values immediately below the bubbling.

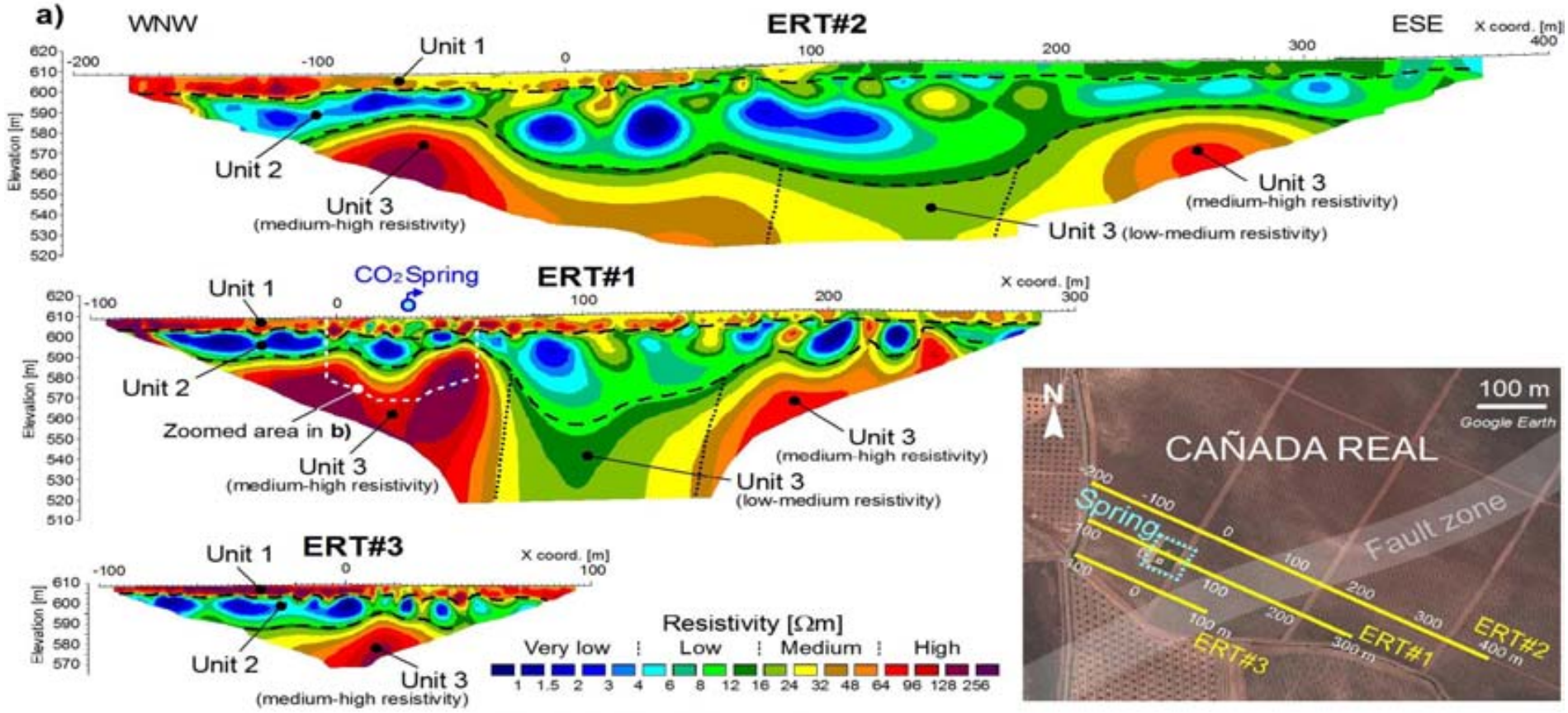

Fig. 36 (a): Location and model sections of the three electrical resistivity tomography profiles measured at Cañada Real in May, 2014. The two existing bubbling springs are placed inside a green grassy rectangular area, surrounded by brown vineyard's terrain. The inferred cartographic trace of the CO_2 source fault zone is also indicated in the map. Resistivity scale in the sections is divided into four classes only for descriptive clarity. Black dashed lines delineate contacts between resistivity units 1, 2 and 3, whereas dotted lines indicate different resistivity areas within Unit 3. (b) Zoomed view of the resistivity section ERT#1 along the spring zone. Color scheme is adjusted to four discrete resistivity intervals in order to emphasize different features related to the CO_2 dynamics: (b1) uses the same scale as in Fig. 4a for a more detailed general perception; (b2) highlights very low and low resistivity values in Unit 2; (b3) calls attention to the convex shape defined by the ascending CO_2-bearing water plume across Unit 1; and (b4) illustrates horizontal spreading of gas and water in the near-surface.

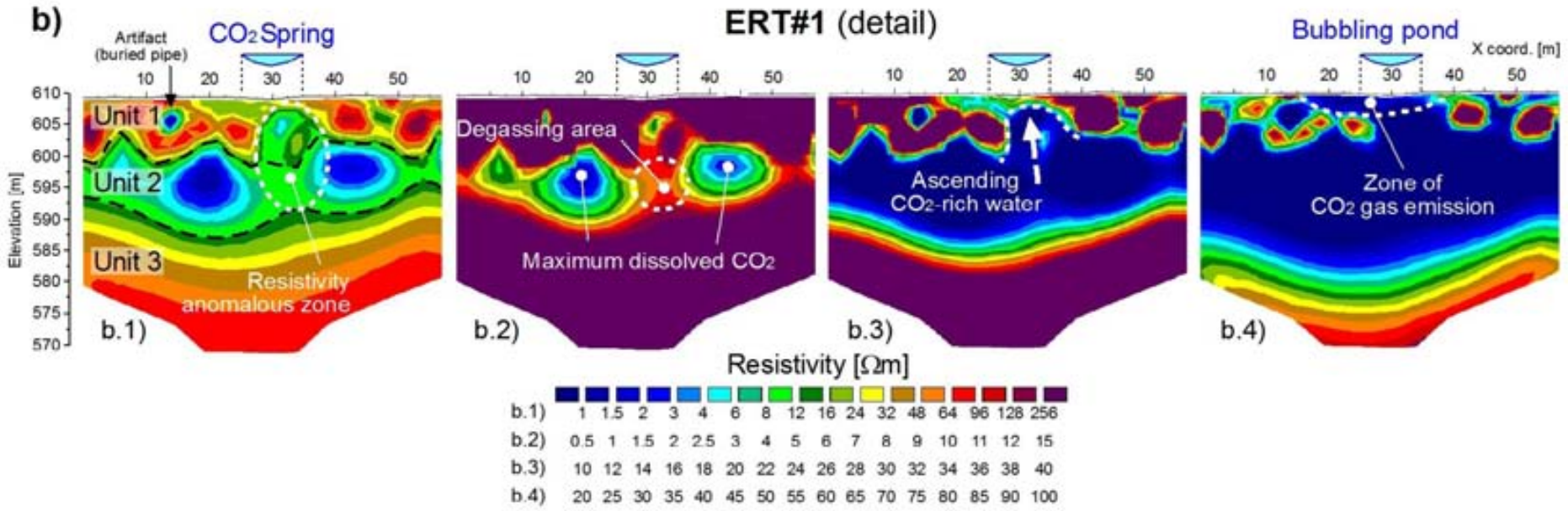

Fig 36 (b): Zoomed view of the resistivity section ERT#1 along the spring zone. Color scheme is adjusted to four discrete resistivity intervals in order to emphasize different features related to the CO_2 dynamics: (b1) uses the same scale as in Fig. 4a for a more detailed general perception; (b2) highlights very low and low resistivity values in Unit 2; (b3) calls attention to the convex shape defined by the ascending CO_2-bearing water plume across Unit 1; and (b4) illustrates horizontal spreading of gas and water in the near-surface.

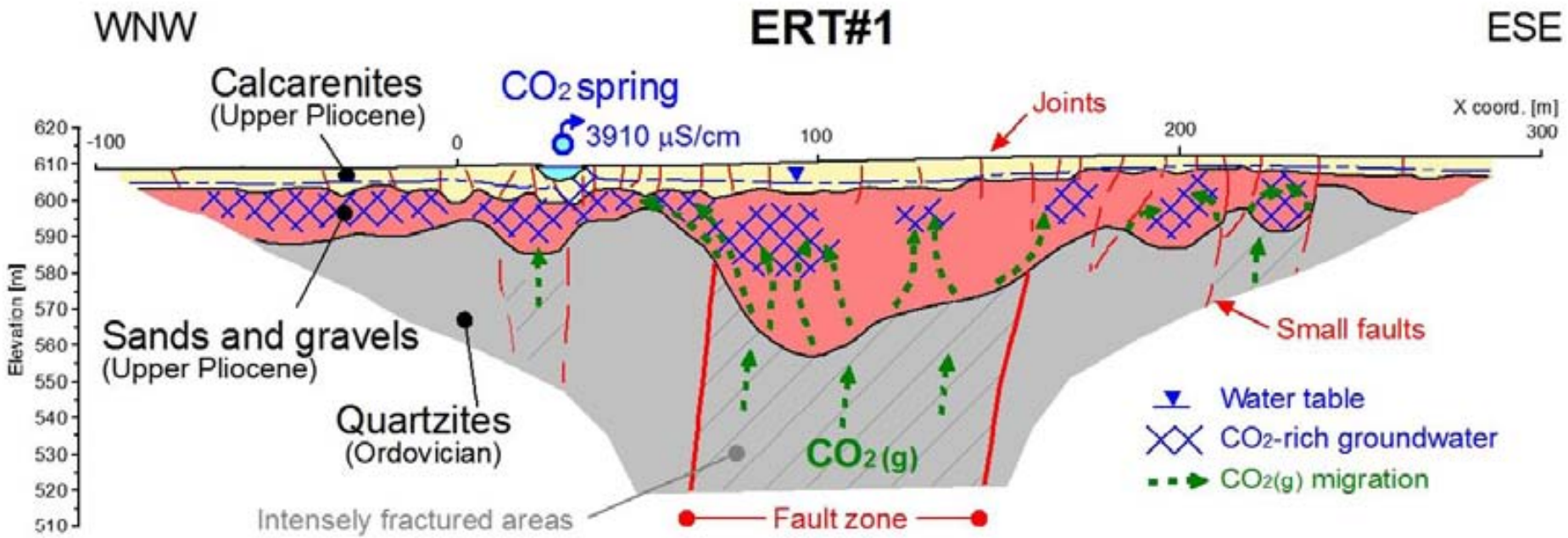

Fig. 37: Interpretative model of CO_2 migration and its emanation on profile ERT#1. CO_2 gas ascending across the fractured and fine grained materials of the main fault zone and other minor faults enters the water-saturated Neogene sands and gravels, where it partly dissolves. Emission into the atmosphere at the bubbling spring may be linked to a stationary upward water-gas plume below it.

5.5.2 WATER AND GAS COMPOSITION:

The temperature and the chemical composition of major, minor and trace elements of the waters have been determined for all the springs (Table 6). Spring waters are characterized by a circumneutral pH in the range of 5.9 to 6.4, an electrical conductivity ranging from 1345 $\mu S \cdot cm^{-1}$ up to 3910 $\mu S \cdot cm^{-1}$ and Eh values in the range of 167.2 mV to 360.2 mV. Only in one station, Baño Chiquillo, a more reduced Eh value has been measured (-52 mV). Temperature at sampling point is 16.9 and 27 ºC. Major ion composition is Mg-Ca-HCO_3, with minor Na-Cl-SO_4 (Fig. 38, and Table 6). Dissolved CO_2 (mainly as bicarbonate) is the main anion in solution (up to 2110 $mg \cdot L^{-1}$, 34.6 $mol \cdot L^{-1}$, in the Cañada Real site) (Fig. 38). These data are quite similar as CO_2-free aquifers in the region (Table 7), although a general increase in the solute content is observed when CO_2 is present, suggesting some degree of water-gas-rock interaction.

Concerning the chemical composition of the dissolved gases (Table 8), CO_2 is by far the most abundant gas species, ranging from 85.77% to 99.92%, followed by N_2 and Ar. H_2S content was always less than the detection limit. These compositions are consistent with those reported in a previous study by Vaselli et al. (2013). The authors suggested that a mantle-sourced signature of these volcanic products is apparently preserved in many CO_2-rich (up to 99% vol) gas discharges in the Calatrava Volcanic Province, whose carbon and helium isotopic signature is characterized by values between -6.8 and -3.2 ‰ (V-PDB) and up to 2.7 R/Ra, respectively. The authors also found that nitrogen and argon are related to an atmospheric component, with values between that of the air (83) and that of ASW (Air Saturated Water).

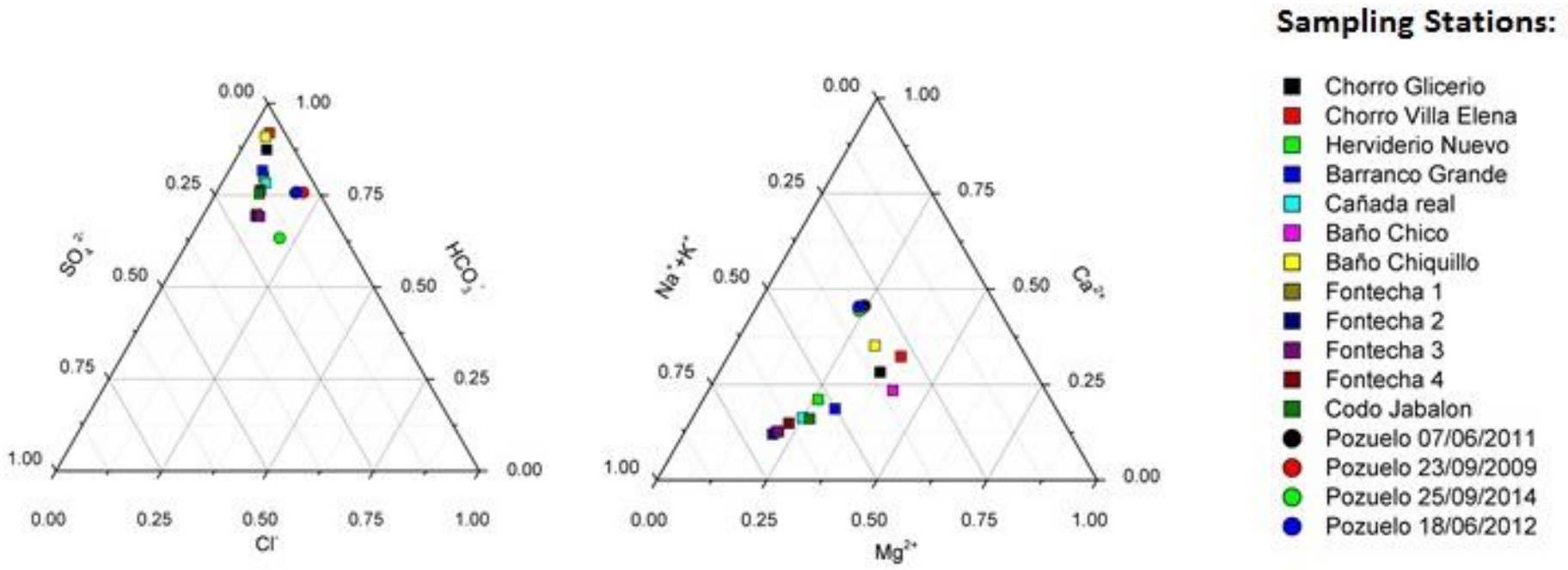

Fig. 38: Triangular diagrams showing the chemical composition of the major elements in CO_2-bearing water samples, and in non-impacted aquifers in the Campo de Calatrava region. See Tables 3 and 4 for complete chemistry of these waters.

Table 6: Chemistry parameters of the CO_2-bearing springs sampled in Campo de Calatrava area. All the concentrations are expressed as mg·L^{-1}.

Sample	T °C	pH	Eh (mV)	Cond. El. ($\mu S \cdot cm^{-1}$)	HCO_3^-	F^-	Cl^-	Br^-	SO_4^{2-}	Ca^{2+}	Mg^{2+}	Na^+	K^+
Chorro Glicerio	16.9	6.2	181	3660	2482	0.42	173	0.49	186	237	308	229	66
Chorro Villa Elena	18.8	6.1	180	2390	1586	0.52	78	0.29	62	165	201	97	48
Fontecha 1	18.4	5.9	207	2430	997	0.58	178	0.38	251	65.9	109	301	43.8
Fontecha 2	22.4	5.9	295	2310	1022	0.72	187	0.40	267	65	111	324	43.2
Fontecha 3	21.5	6.2	313	2440	1052	0.86	206	0.31	262	68.2	115	313	42.8
Fontecha 4	27.1	5.9	17	1720	831	0.47	110	0.30	147	55.7	85	199	36
Cañada Real	21.8	6.1	282	3910	2111	0.47	281	0.77	305	151	232	466	80.2
Baño Chico	21.6	6.1	360	1600	1009	0.57	45.2	0.180	55.8	71.5	128	78.4	27.4
Baño Chiquillo	25.2	6.4	-53	1714	1105	0.78	49.3	0.1	61.1	124	113	84.9	31.1
Codo Jabalon	18.2	5.9	211	1345	975	0.60	134	0.33	184	68.3	114	212	31.9
Barranco Grande	21	6.1	167	2000	1054	0.57	103	0.20	134	76.3	128	166	39.7
Hervidero Nuevo	21	6.0	213	1626	676	0.73	77.8	n.d.	92.4	54.7	68.2	111	26.4

Table 7: Chemistry of the representative spring not affected by CO_2 in Campo de Calatrava. All the concentrations are expressed as mg L^{-1}. Data from Confederación Hidrográfica del Guadiana (www.chguadiana.es).

Sample	Date	pH	HCO_3^-	Cl^-	SO_4^{2-}	Ca^{2+}	Mg^{2+}	Na^+	K^+
Pozuelo de Calatrava	mar-09	7.2	211	29.1	8.7	42.9	21.2	26.9	3.6
	sep-09	7.1	210	33	8.2	41.3	22.2	24.8	3.9
	aug-10	7.3	123	88.1	168	61.2	33.8	46.7	6.1
	nov-10	7.4	209	23.3	8.3	43.7	22.6	24.6	3.5
	jun-12	7.3	210	30.4	11.4	42.5	21.7	25.6	3.9
	dic-12	7.2	213	26.2	9.9	41.8	20.8	26.5	3.6
	jun-13	7.2	210	27.8	9.3	39.9	22.1	24.2	3.8
	dic-13	7.2	213	28.5	10.9	42.8	22.4	24.6	3.9
	oct-14	7.4	144	44.8	24.9	43.3	14.0	31.6	-
	nov-14	7.3	168.5	66.4	31.1	55.6	16.4	37.4	-

***Table 8*: Chemical composition of the dissolved gases sampled. All the values are reported in %.**

Sample	CO_2	N_2	Ar	O_2
Barranco Grande	85.77	13.41	0.32	0.48
Chorro Glicerio	91.16	8.23	0.20	0.40
Chorro Villa Elena	88.35	11.25	0.16	0.30
Cañada Real	99.53	0.42	0.01	0.01
Hervidero Nuevo	88.50	11.12	0.23	0.14
Fontecha 1	92.00	7.66	0.17	0.16

5.5.2.1 Determination of alkalinity: CO_2 measured vs calculated

One of the key parameters in the assessment of the mobility of metals in the CO_2-impacted aquifers is the correct determination of the CO_2 pressure once dissolved. Such data are obtained by direct sampling of the gas phase since most sampling stations show gentle bubbling meaning that active degassing is occurring or gas flows are bubbled through the groundwater. In both cases, direct collection of the gas phase may lead to overestimation or underestimation of the CO_2 pressure in equilibrium with water. In this work, gas pressure data from direct sampling has been compared with CO_2 pressure calculated from alkalinity of water samples. The calculation has been done using the PHREEQC-3 code (Parkhurst and Appelo, 1999), and with the ThermoChimie v.9 database (Giffaut et al., 2014), including the SIT approach for ionic strength correction. The compared pressures for each sampling station are shown in Table 9. Calculated pressure is in general similar as measured in the field, although in some stations the difference is remarkable. This suggests that sampling is performed under gas-water disequilibrium, assuming that no degassing occurs after water collection.

Table 9: Sampled CO_2 pressure value vs. calculated (PhreeqC) pressure in the sampling stations.

Sample	Sampled CO_2 pressure (bar)	Calculated CO_2 pressure (bar)
Baño Chico	0.400	0.281
Baño Chiquillo	0.200	0.223
Barranco grande	0.200	0.295
Cañada Real	0.733	0.602
Chorro Glicerio	0.022	0.478
Chorro Villa Elena	0.020	0.457
Fontecha 1	0.029	0.316
Fontecha 3	0.700	0.288
Fontecha 4	0.600	0.281
Hervidero Nuevo	0.024	0.208

Gas pressure is important to quantify the impact of CO_2 on the aquifers in terms of water-gas-rock interaction. The nature of shallow aquifers receiving CO_2 discharges in the Campo de Calatrava region is not well constrained but thermodynamic equilibrium calculation from water chemistry can provide clues on the mineral assemblage. For sample "Pozuelo de Calatrava", considered as a representative example of non-impacted shallow aquifer in the region, the saturation index calculation indicates that these waters are undersaturated with carbonate minerals (calcite and dolomite) but close to saturation (Table 10). This suggests that some carbonate components are part of the mineralogy of the aquifer, and, therefore, some potential of CO_2 buffering could exist. In contrast, equilibrium with silica is not attained, likely due to the very slow dissolution kinetics of silicon-bearing phases at low T and circumneutral pH. The intrusion of CO_2 (either already dissolved or as a gas phase) into the shallow aquifers in Campo de Calatrava leads to a decrease in pH and dissolution of carbonate phases. However, such dissolution is not significant as a pH buffer since all samples become even more undersaturated in carbonate minerals (Fig. 39).

Table 10: Saturation indexes with respect calcite, dolomite, gypsum and silica of the aquifer not affected by CO_2 intrusion in Campo de Calatrava (central Spain). All the concentrations are expressed as mg·L^{-1}. Data from Confederación Hidrográfica del Guadiana (www.chguadiana.es).

Sample	Date	pH	SI Calcite	SI Dolomite	SI Gypsum	SI SiO_2(am)
Pozuelo de Calatrava	mar-09	7.2	-0.22	-0.37	-2.80	-0.57
	sep-09	7.1	-0.34	-0.57	-2.85	-0.54
	aug-10	7.3	-0.28	-0.44	-1.48	-0.90
	nov-10	7.4	-0.02	0.06	-2.82	-0.57
	jun-12	7.3	-0.15	-0.19	-2.68	-0.53
	dic-12	7.2	-0.22	-0.38	-2.76	-0.54
	jun-13	7.2	-0.25	-0.38	-2.80	-0.56
	dic-13	7.2	-0.22	-0.34	-2.71	-0.52
	oct-14	7.4	-0.18	-0.46	-2.32	-0.59
	nov-14	7.3	-0.12	-0.39	-2.16	-0.59

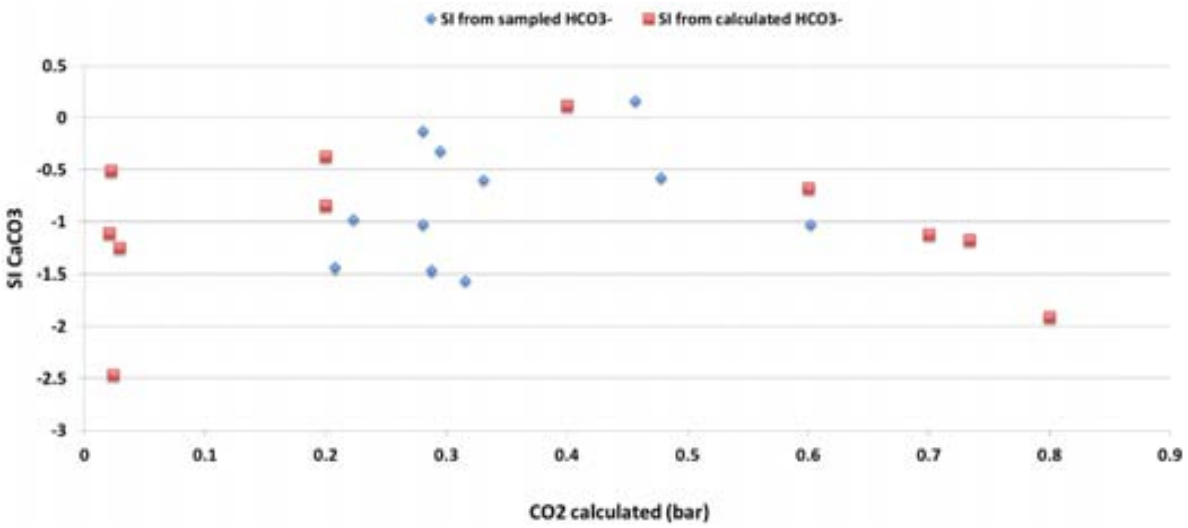

Fig. 39: Calcite saturation indexes (SI) trend calculated using the sampled and calculated CO_2 pressure.

5.5.2.2 Trace (transition, post-transition) metals and metalloids

All the studied samples are characteristically much enriched in trace metals compared to CO_2-free aquifers (Table 11). Iron is by far the most abundant, ranging from 2.5×10^{-2} mg·L^{-1} (4.47×10^{-7} mol·L^{-1}) to 34 mg·L^{-1} (6.08×10^{-4} mol·L^{-1}) (Fig. 40). They also show high concentrations of Mn (up to 4.4 mg·L^{-1}, 8.01×10^{-5} mol·L^{-1}), Zn (up to 96 μg·L^{-1}, 1.46×10^{-6} mol·L^{-1}), Ni (up to 70 μg·L^{-1}, 1.19×10^{-6} mol·L^{-1}), Co (up to 42 μg·L^{-1}, 7.1×10^{-7} mol·L^{-1}), Cu (up to 21 μg·L^{-1}, 3.3×10^{-7} mol·L^{-1}) and As (up to 11 μg·L^{-1}, 1.4×10^{-7} mol·L^{-1}) (Fig. 41). In general, uranium is not significantly enriched except in the sample from the cold geyser called "Chorro Glicerio", with 12 μg·L^{-1}(5.1×10^{-8} mol·L^{-1}).

Table 11: Concentration of trace metals and metalloids in impacted and non-impacted shallow aquifers.

Sample	Fe (tot) (mg/l)	Mn^{2+} (mg/l)	Cr^{3+} (μg/l)	Ni^{2+} (μg/l)	Co^{2+} (μg/l)	Cu^{2+} (μg/l)
Pozuelo de Calatrava	< 0.05 < 0.05 < 0.1 < 0.1 < 0.1 < 0.1 < 0.1 < 0.1 < 0.1 < 0.1	< 0.1 < 0.1 < 0.1 < 0.1 < 0.1 < 0.1 < 0.1 < 0.1 < 0.1 < 0.1	< 0.02 < 0.02 < 0.02 < 0.02 < 0.02 < 0.02 < 0.02 < 0.02 < 0.02 < 0.02	< 0.05 < 0.05 < 0.05 < 0.05 < 0.05 < 0.05 < 0.05 < 0.05 < 0.05 < 0.05	< 0.05 < 0.05 < 0.05 < 0.05 < 0.05 < 0.05 < 0.05 < 0.05 < 0.05 < 0.05	< 0.05 < 0.05 < 0.05 < 0.05 < 0.05 < 0.05 < 0.05 < 0.05 < 0.05 < 0.05
Chorro Glicerio	7.0	4.4	4.0	70	42	1.3
Chorro Villa Elena	16	1.2	6.7	41	14	1.3
Fontecha 1	34	0.8	2.1	56	16	20
Fontecha 2	29	0.7	2.2	34	10	21
Fontecha 3	0.08	0.26	2.2	27	3.7	21
Fontecha 4	2.6	1.0	1.1	46	20	9.8
Cañada Real	0.9	0.4	5.2	17	5.7	1
Baño Chico	1.4	0.9	1.2	36	22	13
Baño Chiquillo	0.02	0.6	1.4	57	17	11
Codo Jabalon	22	0.6	2.0	43	13	20
Herviderio Nuevo	21	1.0	1.8	48	19	17
Barranco Grande	34	1.4	1.9	37	20	19

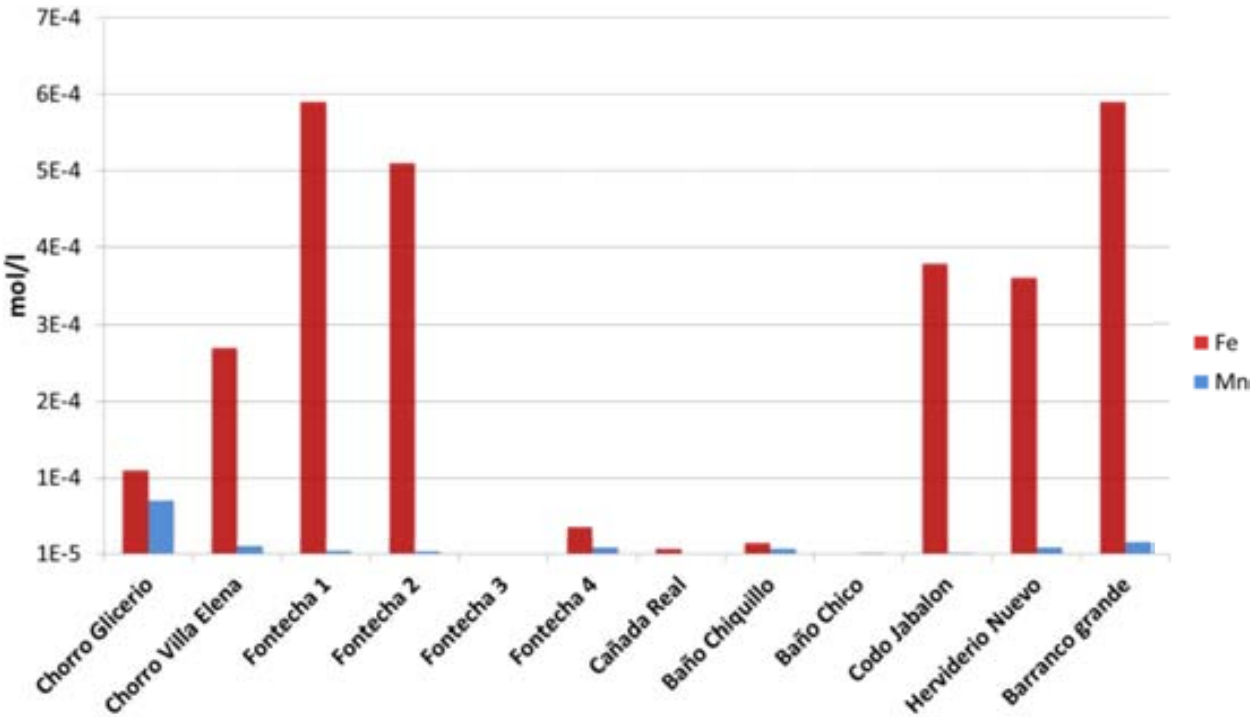

Fig. 40: Fe and Mn concentration of the sampled CO_2-bearing sampling stations.

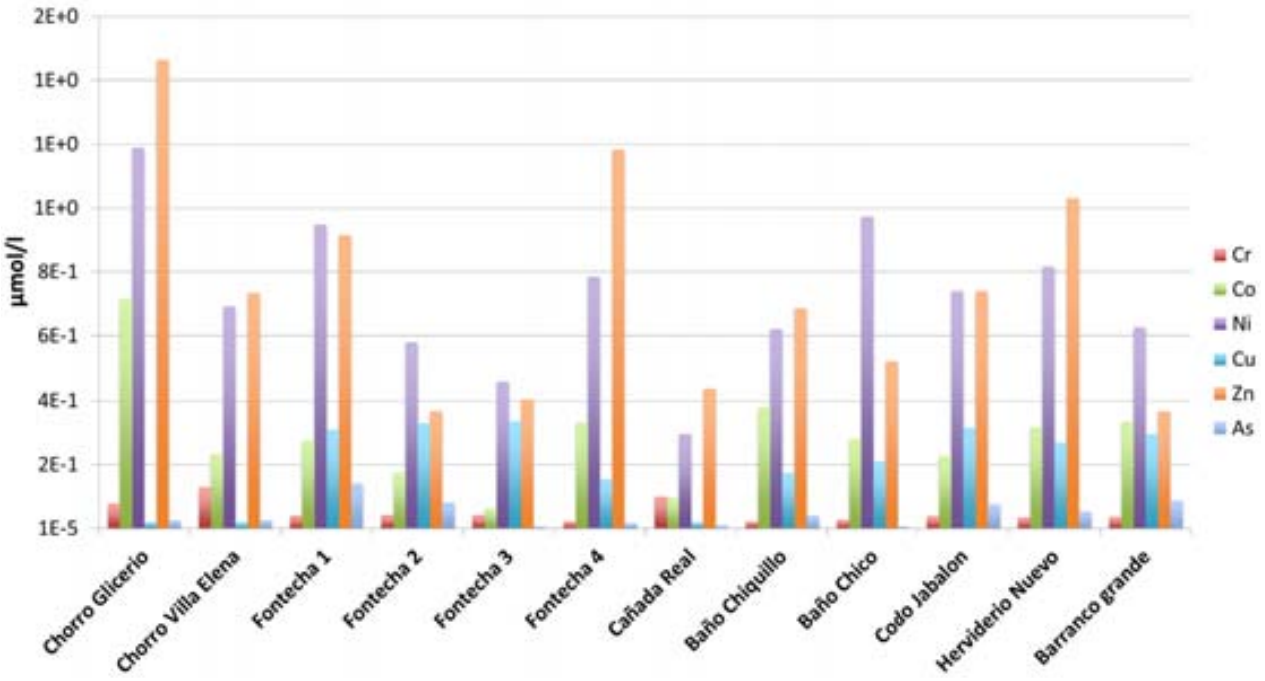

Fig. 41: Main trace metal and metalloid concentration of the sampled CO_2-bearing sampling stations.

The increase of iron and trace metals in solution is neither directly correlated with pH or CO_2 pressure (actually both parameters should be strongly related since CO_2 is the main contributor to water acidity) (Fig. 48). In a similar way, trace metals content do not show any positive correlation (Fig.42 to Fig. 44). In contrast, a good linear correlation between Ni, Zn and Co concentrations is observed (Fig. 45), suggesting a similar geochemical behaviour and source for all them.

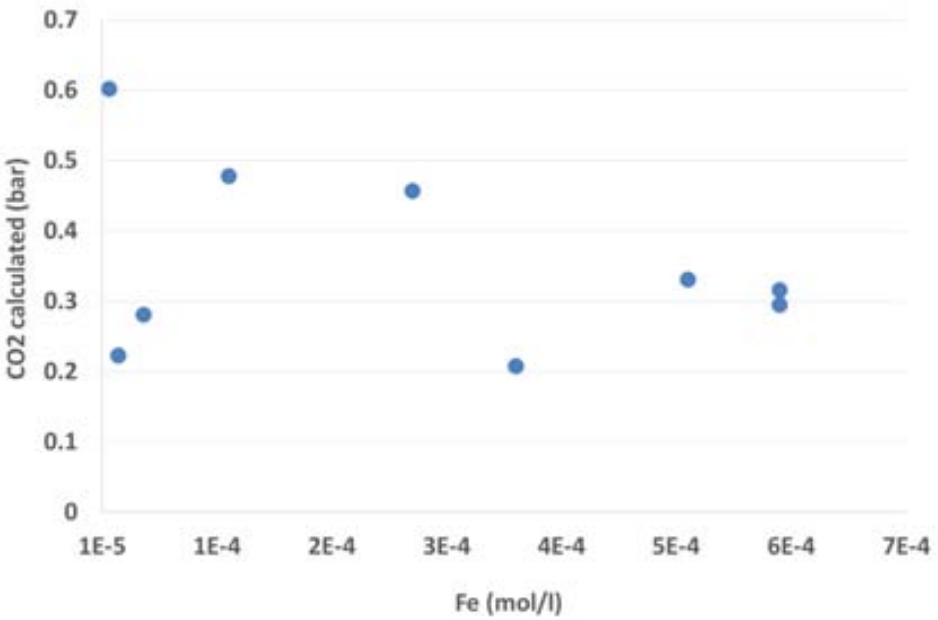

Fig. 42: Diagram of Fe_{tot} concentration vs. CO_2 pressure in the CO_2-bearing sampling stations.

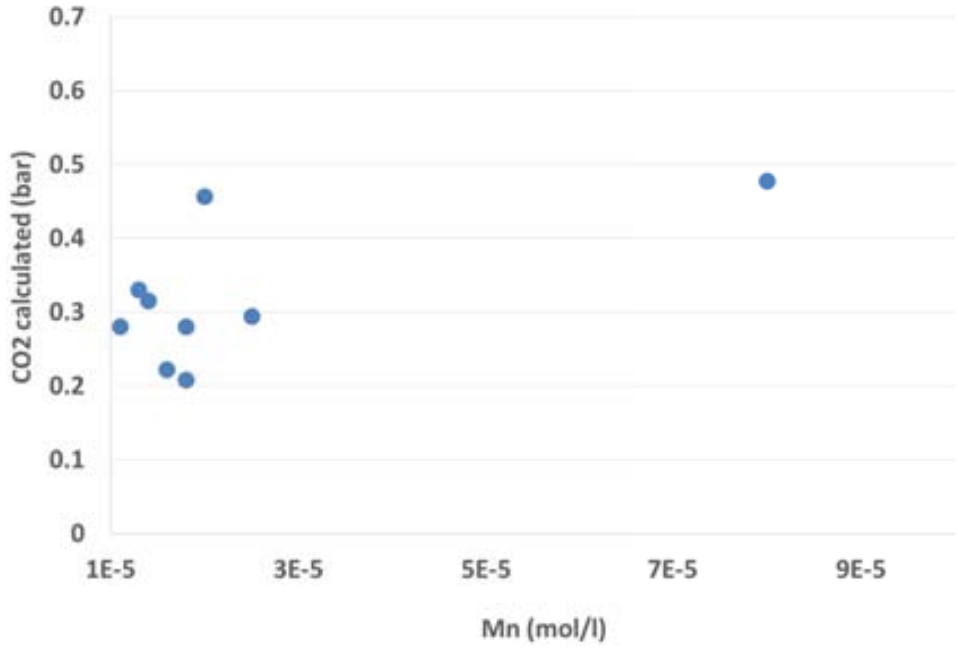

Fig. 43: Diagram of Fe_{tot} concentration vs. CO_2 pressure in the CO_2-bearing sampling stations.

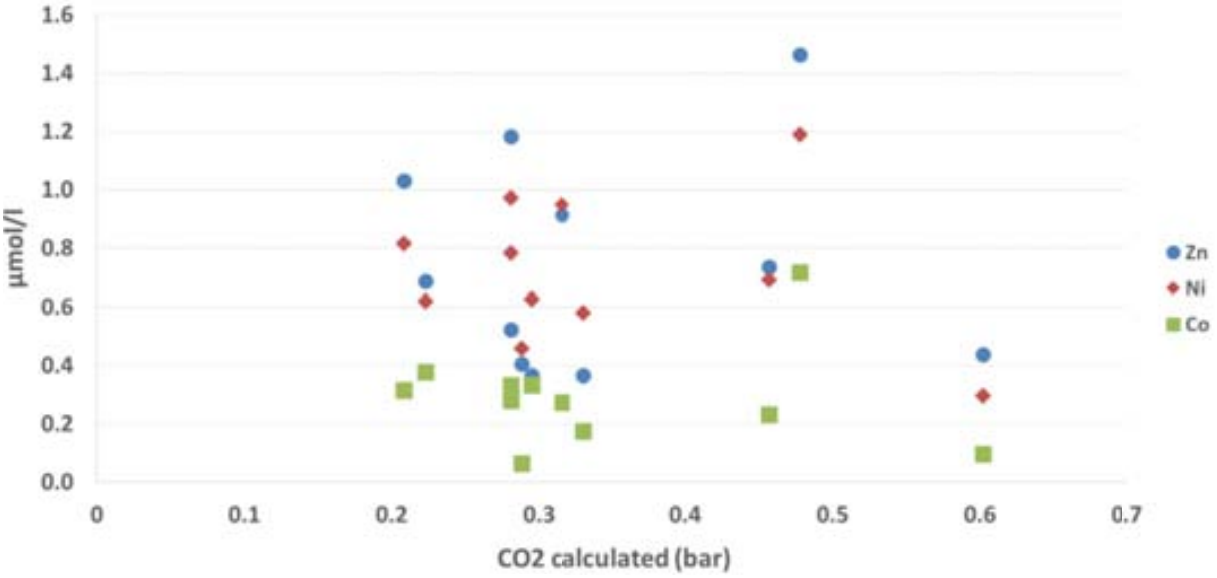

Fig. 44: Diagram of Ni, Zn and Co concentration vs. CO_2 pressure in the CO_2-bearing sampling.

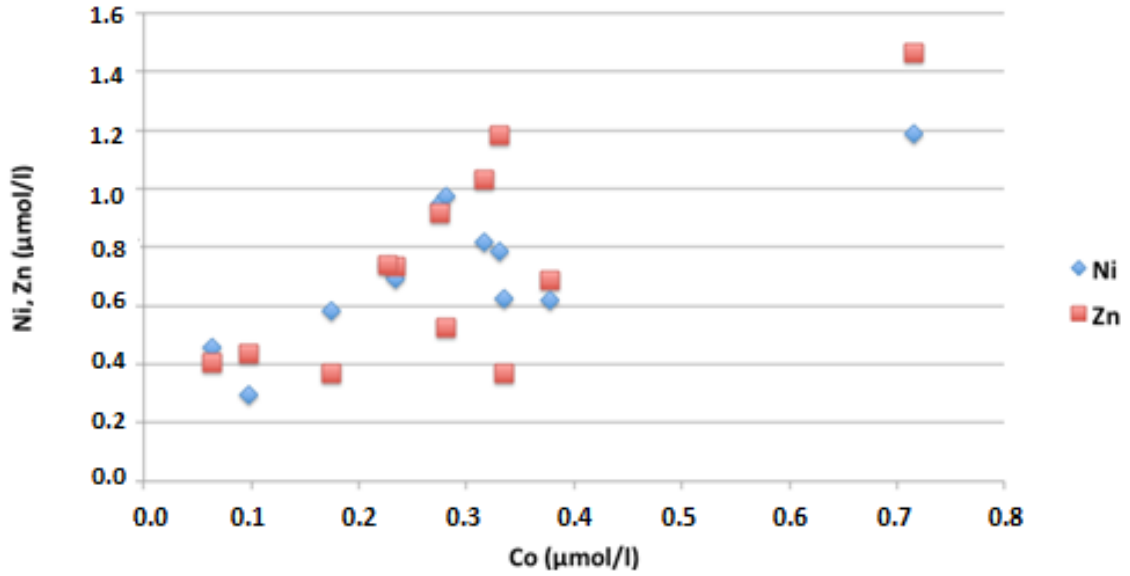

Fig. 45: Correlation diagram of Ni, Zn and Co concentration sampled in the CO_2-bearing sampling stations.

5.6 GEOCHEMICAL MODELLING: release and mobility of Fe(III), Mn and trace metals

The mobility of iron in low-CO_2, surface water and shallow groundwater is very limited due to the slightly solubility of Fe(III) at circumneutral pH and oxidizing conditions. In general, iron concentration under these conditions is lower than 1×10^{-6} mol·L^{-1} due to the equilibrium with iron (III) oxihydroxides. Higher concentrations are commonly observed in acidic environments from oxidative Fe-sulphide dissolution (e.g., acid mine drainage) or in anoxic waters due to the higher solubility of Fe(II). The observation that CO_2-bearing waters are commonly rich in iron has been reported from many natural systems and the formation of Fe(III) carbonate complexes accounts for its enhanced solubility (Grivé et al., 2014; Table 12).

The role of Fe(III) carbonate complexes is illustrated in Table 13 and Fig. 46, which shows the sharing between main aqueous Fe species in the samples. In all them, almost all Fe is found as carbonate $FeCO_3(OH)$, allowing a much higher iron concentration in equilibrium with $Fe(OH)_3$ existing in the aquifer. Figure 47 shows the saturation index (SI) with respect to $Fe(OH)_3$ considering the presence and absence of these two Fe(III) carbonate aqueous species. It is clearly observed that the solubility of solid $Fe(OH)_3$ is enhanced up to three order of magnitude if the formation of Fe(III) carbon complexes is taken in account. In general, most shallow groundwaters affected by CO_2 intrusion in Campo de Calatrava are saturated with respect $Fe(OH)_3$. However, it is worth considering that the crystallinity of these Fe(III) minerals is highly changeable, and in turn, its solubility product can also vary from one site to another. Therefore, the calculation of SI is just indicative of the necessary role of aqueous carbonate complexes.

Table 12: Solubility of Fe(III) carbonate aqueous complexes and ferrihydrite ($Fe(OH)_3$ (am)). Data from Grivé et al. (2014) and Schindler et al. (1963).

$FeCO_3OH \leftrightarrow Fe^{3+} + H^+ + CO_3^{2-} + H_2O$, log K= -10.76

$Fe(CO_3)_3^{3-} \leftrightarrow Fe^{3+} + 3CO_3^{2-}$, log K= -24.24

$Fe(OH)_3$ (am) + $3H^+ \leftrightarrow Fe^{3+} + 3H_2O$, log K= 2.54

Table 13: Percentage of iron species in solution in the studied samples.

Stations	$FeCO_3(OH)$ (%)	Fe^{+2} (%)	$Fe(CO_3)_{(aq)}$ (%)	$Fe(OH)_{3\ (aq)}$ (%)
Baño chico	93.5	5.9	0.6	0.002
Baño chiquillo	98.4	1.2	0.3	0.003
Barranco Grande	92.2	7.1	0.6	0.002
Cañada Real	94.0	5.3	0.7	0.001
Chorro Glicerio	98.9	0.7	0.3	0.001
Chorro Villa Elena	92.8	6.5	0.7	0.001
Fontecha 1	79.2	19.9	0.8	0.002
Fontecha 2	77.5	21.7	0.9	0.002
Fontecha 3	93.9	5.5	0.6	0.002
Fontecha 4	75.9	23.2	0.8	0.002
Hervidero Nuevo	83.0	16.2	0.7	0.003

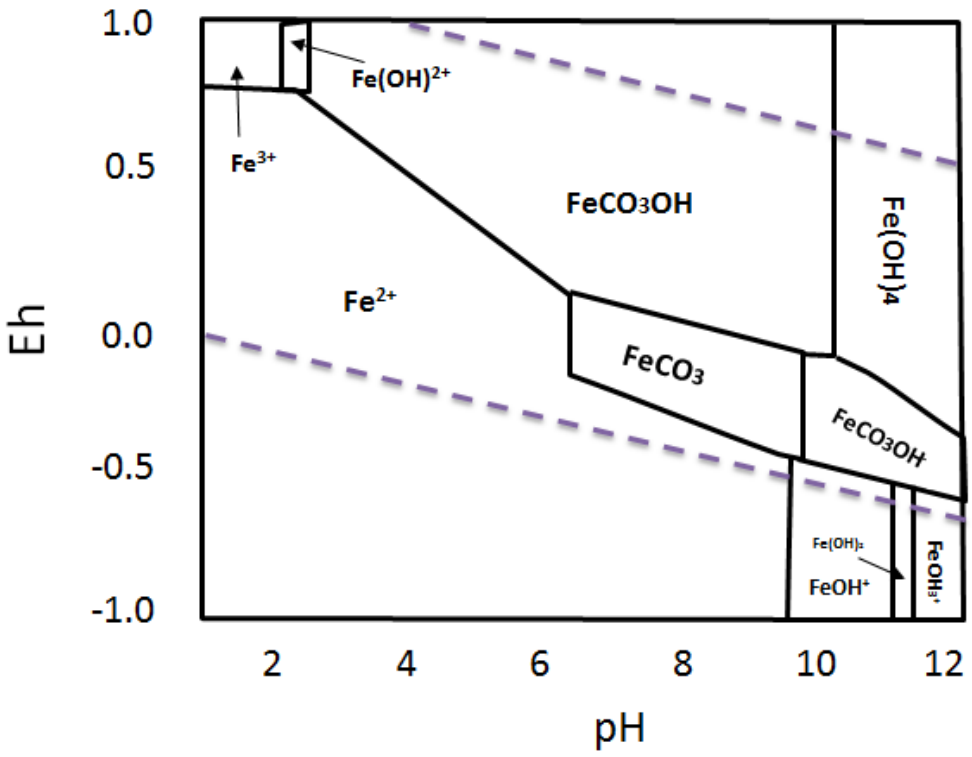

Fig. 46: pH-Eh diagram of the aqueous speciation of iron considering the pCO_2 found in shallow groundwaters in Campo de Calatrava.

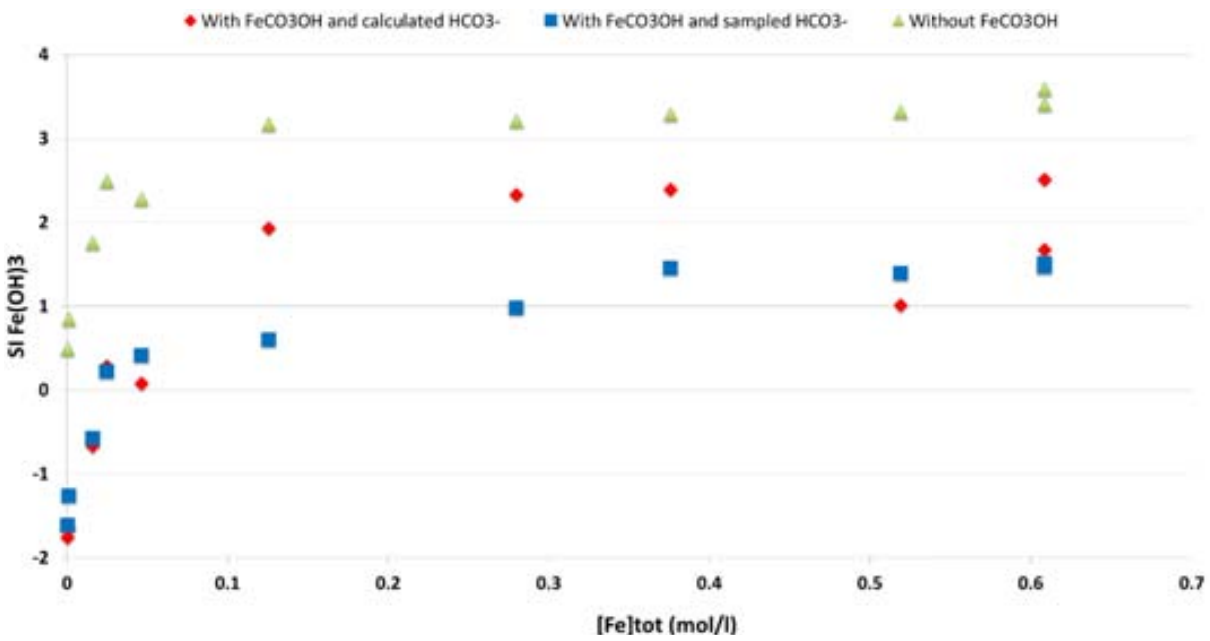

Fig. 47: $Fe(OH)_3(am)$ saturation indexes (SI) trend calculated using the sampled and calculated pCO_2 compared with the theoretical values obtained excluding the formation of Fe(III) carbonate complexes.

The source of iron in the Campo de Calatrava shallow CO_2-bearing groundwaters is likely the iron(III) oxihydroxides in the aquifer host rocks, which are widespread in sedimentary rocks. A numerical model of a gas-water-rock reaction supports such hypothesis. The impact of pH, CO_2 pressure and iron solubility increase was simulated using PHREEQC. 1 mol of $CO_2(g)$ has been progressively added, in steps of 1×10^{-3} moles, to an aquifer with the initial chemical composition of the water "mar-09" from the regional aquifer (Table 4 above). The aquifer is considered in equilibrium with $Fe(OH)_3$ (am) and to account for the potential variability in the solubility product of $Fe(OH)_3$ (am), a range of Log K has been considered (Log K = 4, 3.5, 3 and 2.2 respectively). The numerical simulation has been compared with the data collected from the CO_2-bearing waters, assuming the sampled CO_2 pressure. The results indicate that the intrusion of CO_2 gas can account for the observed pH and CO_2 pressure even assuming a significant loss of accuracy in sampling due to the bubbling during the water and gas collection (Fig. 48).

Concerning the iron release and solubility, the simulation results show that most measured [Fe] can be explained by the dissolution of Fe(III) solids due to the inflow of $CO_2(g)$ (Fig. 49). Again, the role of aqueous Fe (III) carbonate complexes is essential to reach the observed iron concentrations since the decrease in pH is not sufficient (see green dashed line in Fig. 50).

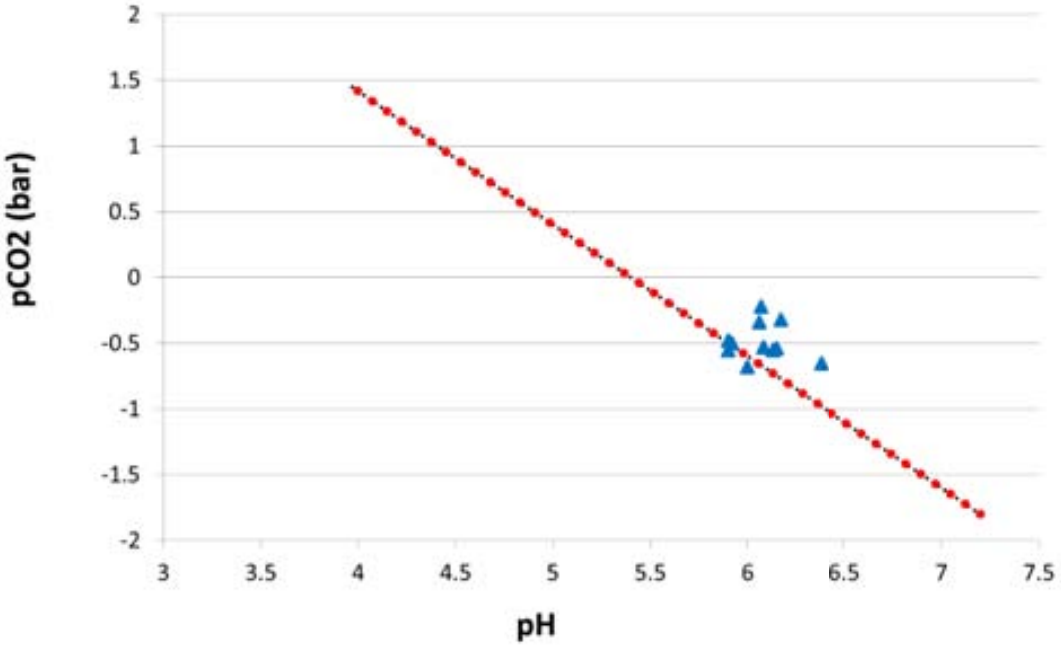

Fig. 48: Predicted increase of pCO_2 and decrease in pH in an aquifer as a response of CO_2 gas intrusion. Blue triangles are the data from Campo de Calatrava CO_2-bearing sampling stations.

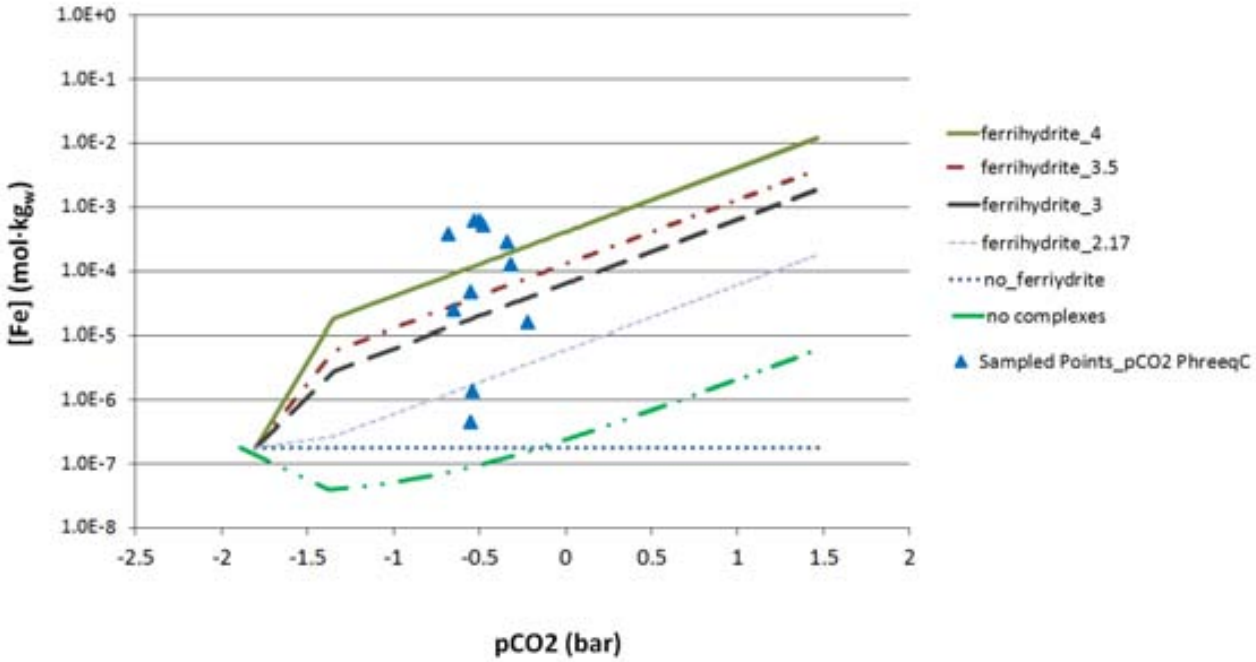

Fig. 49: Predicted concentration of iron from $Fe(OH)_3(am)$ (ferrihydrite in the label) dissolution due to the intrusion of $CO_2(g)$. Lines are the reaction path considering different $Fe(OH)_3(am)$ solubility products (Ksp= 4, 3 and 2.17, respectively). Dashed line corresponds to the simulation with no consideration of aqueous Fe(III) carbonate complexes. Iron concentration and corresponding pCO_2 of sampled shallow groundwaters in Campo de Calatrava are included in the plot for comparison.

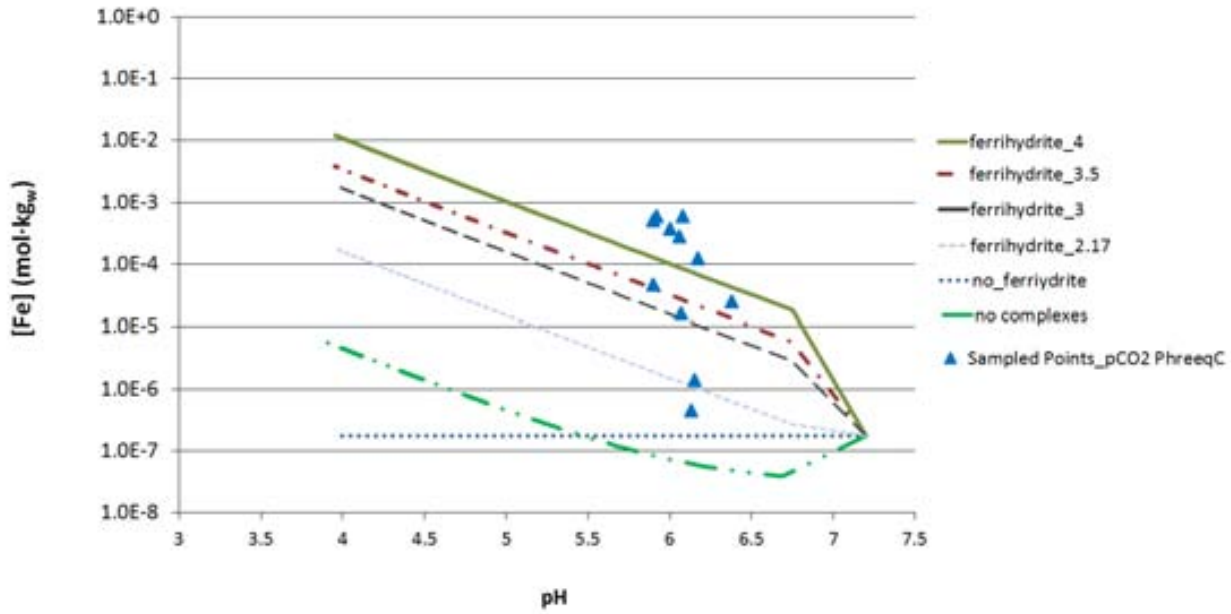

Fig. 50: Predicted concentration of iron from $Fe(OH)_3(am)$ dissolution due to the intrusion of $CO_2(g)$ vs. pH. Lines are the reaction path considering different $Fe(OH)_3(am)$ solubility products (Ksp= 4, 3 and 2.17, respectively). Dashed line corresponds to the simulation with no consideration of aqueous Fe(III) carbonate complexes. Iron concentration and corresponding pH of sampled shallow groundwaters in Campo de Calatrava are included in the plot for comparison.

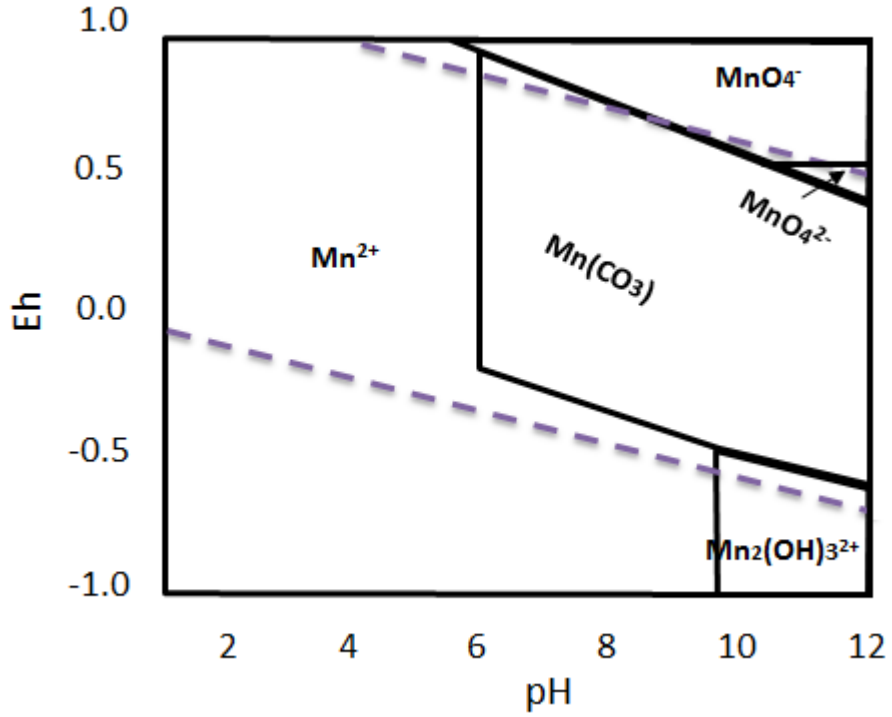

Fig. 51: pH-Eh diagram of the aqueous speciation of Mn considering the pCO_2 found in shallow groundwaters in Campo de Calatrava.

Manganese is also released in shallow aquifers in Campo de Calatrava. According the existing thermodynamic data, the speciation of Mn in fresh, oxidising waters is essentially as Mn^{2+}. In CO_2-impacted aquifers, the formation of $MnCO_3$(aq) is enhanced (Fig. 51). In the studied waters, carbonate aqueous Mn species are in the same order of magnitude as free Mn^{2+}, being predominant is some samples up to 75% of the dissolved Mn (Table 14). The solubility of Mn is limited by the precipitation of $MnCO_3$(s) (rhodocrosite) as suggested by the SI of these samples; Mn oxides and hydroxides are significantly much soluble.

Table 14: Percentage of Mn free cations and aqueous carbonate species in the studied samples. Saturation indexes of the solubility-limiting phase (rhodocrosite) are also listed.

Stations	Mn^{2+} %	$MnCO_3$ %	$MnHCO_3^+$ %	SI rhodocrosite ($MnCO_3$) %
Baño chico	56.6	37.7	4.1	-0.59
Baño chiquillo	34.3	61.1	3.6	-0.51
Barranco Grande	57.9	33.3	4.0	-0.44
Cañada Real	48.2	41.3	5.5	-0.97
Chorro Glicerio	23.6	70.8	4.4	0.38
Chorro Villa Elena	55.3	38.5	5.1	-0.44
Fontecha 1	70.1	18.8	3.4	-0.93
Fontecha 2	70.4	17.8	3.4	-1.00
Fontecha 3	53.4	36.1	3.9	-1.14
Fontecha 4	74.0	17.1	3.2	-0.87
Hervidero Nuevo	72.4	20.8	3.0	-0.79

The trace metal contents from the analysis of the CO_2-bearing fluids reveal a clear enrichment mainly in Zn, Co, Ni, Cu and, in a minor extend, U. Unlike Fe (III), whose enhanced concentration is a combination of release from the iron minerals and the formation of soluble Fe(III) aqueous carbonate complexes, the high concentration of these trace metals seems to be only related to a dissolution of the their source, i.e., $Fe(OH)_3$. Considering the aqueous species for Co and Ni included in Thermochimie v.9 database, and Minteq-v4 (U.S. Environmen tal Protection Agency, 1998) for Zn and Cu (since Cu and Zn carbonate and hydrolised species are not defined in Thermochimie v.9). This is the reason behind the selection of Minteq-v4., the impact on transport of the formation of aqueous metal carbonate complexes is less relevant, and divalent free cations are much predominant for Co, Ni and Zn (Table 15). In contrast, Cu carbonate species are predominant in some samples.

Table 15: Percentage of Co, Ni, Cu and Zn free cations and aqueous carbonate species in the studied samples.

Stations	Co^{2+} %	$CoHCO_3^+$ %	Ni^{2+} %	$NiHCO_3^+$ %	Cu^{2+} %	$CuCO_3$ %	$CuHCO_3^+$ %	Zn^{2+} %	$ZnHCO_3^+$ %
Baño chico	75.1	22.3	88.4	8.5	38.1	47.0	9.4	85.6	10.6
Baño chiquillo	67.9	29.3	84.7	11.8	20.6	68.2	7.4	80.3	14.5
Barranco Grande	74.0	20.6	85.8	7.7	38.6	42.1	9.2	83.4	10.0
Cañada Real	63.4	29.6	79.1	11.9	27.4	43.7	11.0	75.5	15.3
Chorro Glicerio	54.2	41.8	75.7	18.9	12.9	72.6	8.7	68.9	23.3
Chorro Villa Elena	71.1	26.8	86.9	10.6	35.9	46.6	11.5	83.4	13.4
Fontecha 1	75.3	14.9	83.2	5.3	46.6	23.7	7.9	82.1	7.0
Fontecha 2	75.1	14.7	82.8	5.3	46.8	22.4	7.9	81.7	6.9
Fontecha 3	70.0	20.7	80.9	7.7	32.7	41.1	8.1	78.7	9.8
Fontecha 4	79.1	13.9	86.8	4.9	53.3	22.9	7.8	85.6	7.2
Hervidero Nuevo	81.0	13.8	89.1	4.9	52.3	28.4	7.5	87.7	6.3

5.7 DISCUSSION:

The impact of CO_2 solubilisation on metal transport has been a topic thoroughly studied in the last decade due to the intention of store this greenhouse gas underground. A complete literature review on this topic has recently been performed by Lions et al. (2014). In general, most lab and field studies agree that iron and manganese are easily mobilised when an aquifer is impacted by CO_2, already dissolved in water or as supercritical gas in the storage formation (Kharaka et al., 2010; Trautz et al., 2013; Lu et al., 2010; Little and Jackson, 2010; Humez et al., 2013). However, there is still some debate on the driving processes of this metal mobilisation. Acidification is commonly invoked as a releasing and transport mechanism (Kharaka et al., 2009). Another proposed metal-releasing mechanism is the ascent of low-Eh, deeper fluxes and subsequent displacement of native, oxidising fluids, leading to, e.g., the reduction of Fe(III) to a more mobile Fe(II) form (Hem, 1985; Yardley et al., 2003; Kharaka and Hanor., 2007; Birkholzer et al., 2008; Keating et al., 2010). Finally, the occurrence of minor gases in the gas mixture such as CH_4 or H_2S may favour the development of microbially-driven reactions causing metal reduction (McMahon and Chapelle, 1991, 2008; Lions et al., 2014 and references therein).

The chemistry of the shallow groundwaters affected by CO_2(g) fluxes in Campo de Calatrava reveals that none of the above mechanisms is the main driver for metal release and solubilisation, since (1) all of them have circumneutral pH (close to 6), (2) they have oxidising Eh, and (3) the gas flow is almost pure CO_2 and free of "reducing" minor gases. The measured pH is likely controlled by the dissolution of gas into the shallow aquifer rather than mineral dissolution, as supported by numerical thermodynamic calculations, but gas fluxes are not intense enough to cause very acidic (pH<4) plumes in the affected aquifers. Geophysical profiles reveal that gas mixes at shallow depths with groundwater and part of this gas directly flows to the atmosphere. However, the suspected short interaction time between gas, water and host rocks is enough to dissolve iron hydroxides and form plumes of iron and other trace metals. The source of these trace metals are likely the iron hydroxides themselves since these minerals present charged surfaces where trace metals are immobilised by sorption. The lack of correlation between the concentration of iron and these metals could be found in the variable composition of the surface sites in the sampling stations.

Although part of the metal load precipitates back as colloids if some degree of degassing occurs, the metal concentration is still much higher than expected for circumneutral, oxidising waters. Therefore, the role of aqueous Fe(III) carbonate complexes becomes crucial for the persistence of this metal content in solution. In the samples studied in the Campo de Calatrava area, the theoretical impact of iron mobility calculated from laboratory experiments is well proved, and, contrary to the current opinion in the scientific community, the impact of CO_2 fluxes into shallow aquifers leading to relatively low CO_2 pressure is very significant and worth taking into consideration in the risk assessment.

Manganese is usually reported to be mobilised along with Fe in CO_2 injection test in aquifers. Interestingly, the role of carbonate complexes in Mn mobilisation is quite different from iron: at high pCO_2, a significant part of dissolved Mn predicted to be found as $MnCO_3(aq)$ but, in turn, the solution is approaching the equilibrium with solid Mn carbonate. Therefore, the competition between the formation of soluble Mn carbonates and the precipitation of solid $MnCO_3$ controls the solubility of Mn in these aquifers.

The general consensus on the release of Fe and Mn is not shared for other trace metals since the reported data shows a disparity of sets of metals released either in laboratory or from field tests (see review in Harvey et al., 2012). According to the analysis performed in this work, the formation of trace transition metal plumes in CO_2-impacted shallow waters is basically related to the occurrence of such metals in surface sorption sites in solid $Fe(OH)_3$, and their transport is eventually controlled by the precipitation of solid carbonates, in a similar way as Mn. In the studied samples in Campo de Calatrava, the thermodynamic calculations predict that these waters are far from the equilibrium with these carbonates (more than 2 orders of magnitude below the saturation) suggesting that the concentration of these metals is actually related to the source rather than to the transport. Their solubilisation is, then, maintained as long as the aquifer system keeps $Fe(OH)_3$ undersaturated.

Compared to results from literature, it is remarkable the similarity with the experimental data from Little and Jackson (2010), obtained from the same pH range. In both datasets, the trace metals with a significant increase are the same, i.e., Fe, Mn, Zn, Co, Ni, Cu and U. Only barium has not found to be mobilised in the present work.

5.8 CONCLUSIONS:

The CO_2 (g) flows into shallow aquifers cause severe changes in shallow, fresh aquifer chemistry since lead to the release and solubilisation of metals, mainly Fe and Mn but also of a set of many other metals in minor or trace amounts. In most cases, such amounts are not acceptable in terms of water consumption. The persistence of these metal plumes, which is crucial in the risk assessment studies of CO_2 underground storage, is under debate since subsequent water-rock interaction may lead to a decrease of acidity and, in turn, the metal load is then back to the rock. However, the observations from this work reveals that such persistence is clearly enhanced due to the formation of aqueous Fe(III) carbonate complexes, which has not been considered in the past in the risk assessment of the impacts of CO_2 (g) flows into shallow aquifers. These complexes modify the water-rock equilibrium in the aquifer forcing the dissolution of $Fe(OH)_3$, and, in turn, the release of the sorbed trace metals. These trace metals are dissolved with amounts lower than those necessary to precipitate pure metal carbonate and they are predicted to persist until they sorbed again in iron hydroxides. Consequently, the formation of iron carbonate complexes can be considered as the main driver of metal transport in the CO_2-impacted shallow aquifers.

6 Objective 3:

Assessment of the use of metal concentration changes as an early detection tool of low-intensity leakage from CO_2 storage

Article 3: Use of diffusive gradients in thin films (DGT) as an early detection tool of low-intensity leakage from CO_2 storage

Marco Agnelli[a], Fidel Grandia[a], Anthony Credoz[a], Andrea Gasparini[b], Jordi Bruno[a,c]

[a]Amphos 21 Consulting S.L., Barcelona, Spain

[b] Istituto Nazionale di Geofi sica e Vulcanologia (INGV), Rome, Italy

[c]Fundaciòn Ciudad de la Energìa (CIUDEN), Ponferrada, Spain

Abstract:

Diffusive gradients in thin films (DGT) have been tested in CO_2-rich, metal-bearing fluids from springs in the Campo de Calatrava region in Central Spain, to assess their applicability as a monitoring tool in onshore CO2 storage projects. These films are capable of adsorbing metals and recording changes in their concentration in water, sediments, and soils. Considering that CO_2 dissolution promotes metal solubilization and transport, the use of these films could be valuable as a monitoring tool of early leakage. A number of DGT have been deployed in selected springs with constant metal concentration. The studied waters show high concentrations of Fe, as high as 1×10^4 $\mu g \cdot L^{-1}$, Ni, Co, Zn, Cu, and Mn. Comparing re-calculated metal concentration in DGT with metal water concentration, two different metal behaviors are observed: (i) metals with sorption consistent with the metal concentration (i.e. plotting close to the 1:1 line in a [Me]DGT: [Me]water plot), and (ii) metals with non–linear sorption, with some data showing metal enrichment in DGT compared with the concentration in water. Metals in the first group include Fe, Mn, Co, Ni, and U, and metals in the second group are Zn, Pb, Cr, Cu, and Al. From this research, it is concluded that the metals in the fi rst group can be used to monitor potential leakage by using DGT, providing effective leakage detection even considering low variations of concentrations, episodic metal release, and reducing costs compared with conventional, periodic water sampling.

Keywords: Campo de Calatrava; CO_2 storage and leakage; DGT; metal leakage; metal transport; trace metals.

Scientific journal: Greenhouse Gases Science Technology. 1–13 (2013); DOI: 10.1002/ghg

6.1 INTRODUCTION:

The capture and the storage of CO_2 in deep subsurface reservoirs is one of the options currently being considered to mitigate the rising anthropogenic greenhouse gas (GHG) concentrations in the atmosphere (European Commission, 2013). The site selection of CO_2 storage reservoirs must be accurate enough to minimize the risks to human health and the environment (Rempel et al., 2011; Zheng et al., 2011). However, even considering a thick, impervious seal formation, the possibility of leakage via preferential pathways (fracture or wells) cannot be completely ruled out, and its early detection is essential to avoid major impacts. In this respect, the changes in the geochemistry of shallow groundwater may provide evidence of CO_2 intrusion in such aquifers. These changes can be promoted by the chemical interactions between the CO_2 and shallow groundwater, leading to the dissolution, mobilization, and re-precipitation of metals and metalloids (Czernichowski-Lauriol et al., 2006; Kharaka et al., 2006; Kharaka et al., 2009 ; Wigand et al., 2008; Fisher et al., 2010). In principle, the metal transport capacity of CO_2-bearing fluids in shallow aquifers should dramatically decrease as pH increases due the buffering with aquifer rocks and also due to the relative high Eh favoring very low iron solubility. However, the Fe(III) solubility in CO_2-bearing fluids can be significantly increased due to the formation of Fe(III) carbonate complexes that are stable at circum-neutral pHs, and, therefore, being more persistent in time and space in the geological media (Grivé et al., 2013). The experimental results match observations in natural systems, where high Fe(III) concentration can be found under oxic, circum-neutral solutions where iron concentration is up to 3 orders of magnitude higher than that expected in CO_2-free solutions (bruno et al., 2009). The enhanced solubility of Fe(III) has an additional and unwanted side effect: the inhibition of the precipitation of $Fe(OH)_3$(am), which is the main sink for many trace and minor elements in shallow aquifers. Then, CO_2-bearing solutions are particularly rich not only in iron but also in many other metals and metalloids, increasing the pollution impact of affected aquifers. The $Fe(OH)_3$ inhibition is gone due to CO_2 degassing related to fluid ascent to surface, and eventually part of all these metals may be precipitated back into solid phases but still some of the metal load is under solution. Monitoring of metal contents in shallow aquifers can, therefore, be valuable in the early detection of failure of containment of a CO_2 storage site because the concentration of all these metals in shallow and surface waters is commonly very low, and tiny changes in such a concentration could be indicative of early leakage.

DGT have long been used as recorders of ion pollution in waters, soils and sediments (Zhang et al., 1995).

They are commonly used to detect changes of metal concentration through time. Recently, Ardelan and Steinnes (2010) and Ardelan et al. (2012) used DGT to record the increase in metal concentration in CO_2-seepage chamber as a test of potential impact of CO_2 leakage on seafloor in off shore storage. Their results show that many metals were remarkably increased in their concentration after CO_2 dissolution in seawater, especially U and Ce, whose dramatic increase permits the use of these metals as chemo-indicators for CO_2 seepage. They concluded that the enhanced Fe, Co and Mn can also be used as supportive chemo-indicators for a possible CO_2 seepage in oxic waters. In this paper, DGT have been tested in CO_2-rich, metal-bearing fluids from shallow aquifers and springs in the Campo de Calatrava region in Central Spain, to assess its applicability as a monitoring tool in on-shore storage projects.

6.2 DIFFUSIVE GRADIENTS IN THIN FILMS (DGT) METHODOLOGY

Diffusive gradients in thin films (DGT), developed in Lancaster University in 1993, are devices capable of accumulating dissolved substances and provide the *in situ* concentration at time of deployment, measuring trace metals, phosphate, sulfide and radionuclides in waters, soils and sediments. When deployed in water, DGT measures labile species. DGT consist of a plastic base (2.5 cm diameter) loaded with a resin gel, a diffusive gel, and filter, and then the plastic top securely push fits over it to leave a 2.0 cm diameter window. The mouldings have been designed to accommodate a 0.4 mm Chelex resin gel layer, 0.8 mm diffusive hydrogel layer and 0.135 mm filter (0.45 μm) (Fig. 52).

The simple plastic DGT is deployed for a known time and then the mass of metal on the resin layer is measured after elution with acid by, for example, AAS or ICP-MS. DGT devices have usually been deployed by simply suspending them from a rope or string.

Above a low threshold value, the measurement is independent of solution flow. DGT has been deployed *in situ* in rivers, lakes, estuaries, and the deep sea. Its in-built pre-concentration gives it excellent sensitivity (10–12 $mol \cdot L^{-1}$) and avoids contamination problems. DGT can be kept under water from hours to several weeks, depending on the

metal concentration of water and the potential metal saturation of the Chelex resin. While Chelex is a robust and tolerant resin, it works very well in the pH range of 5 to 9 for most metals. Below or above these values the resin is prone to modify its physical characteristics. For Cu, the resin operates effectively over a broader range of 2–11.

DGT provides time-averaged concentrations that are ideal for regulatory monitoring. In water, the determination of the average concentration C_{DGT} of each metal given by DGT device, and the mass *m* of each metal adsorbed in the Chelex resin, are calculated from eq (6.1):

$$D_{DGT} = \frac{m \times \Delta g}{D \times t \times A} \quad with\ m = Ce \times \frac{\left(V_{HNO3} \times V_{gel}\right)}{f_e} \tag{6.1}$$

where Δg is the thickness of the diffusive gel plus filter (0.8 mm plus 0.14 mm respectively), *D* is the specific diffusion coefficient in the diffusive gel for each metal at the sampling temperature ($m^2 \cdot s^{-1}$), *t* is the duration of deployment, *A* is the area of exposure (3.14 cm^2), *Ce* is the concentration in the 1.0 M HNO_3 elution solution, *VHNO*3 is the volume for acid elution (average of 1 mL), *Vgel* is the volume of gel (0.15 mL), *fe* is the elution factor (0.8). The diffusion coefficient *D* used for each metal was selected as a function of the sampling point temperature and are those recommended by DGT Research Ltd. (2003) (Table 16).

Table 16: Diffusion coefficients (D, $\times 10^{-6}$ cm^2 s^{-1}) for each studied elements in the T range between 10 and 27 °C.

Temp	D (10^{-6} cm^2/s)										
°C	Al	Cr	Mn	Fe	Co	Ni	Cu	Zn	Cd	Pb	U
10	3,04	3,23	3,74	3,91	3,80	3,70	3,99	3,89	3,90	5,14	-
12	3,25	3,45	4,00	4,18	4,06	3,94	4,26	4,15	4,16	5,49	-
13	3,35	3,56	4,12	4,31	4,19	4,07	4,39	4,29	4,30	5,67	-
14	3,46	3,67	4,26	4,45	4,32	4,20	4,53	4,42	4,43	5,85	-
15	3,57	3,79	4,39	4,59	4,46	4,33	4,68	4,56	4,57	6,03	-
16	3,68	3,91	4,52	4,73	4,60	4,47	4,82	4,70	4,72	6,21	-
17	3,79	4,03	4,66	4,87	4,74	4,60	4,97	4,85	4,86	6,40	-
20	4,14	4,39	5,09	5,32	5,17	5,02	5,42	5,29	5,30	6,99	-
25	4,75	5,05	5,85	6,11	5,94	5,77	6,23	6,08	6,09	8,03	-
27	5,01	5,32	6,17	6,45	6,27	6,09	6,57	6,41	6,43	8,47	6,41

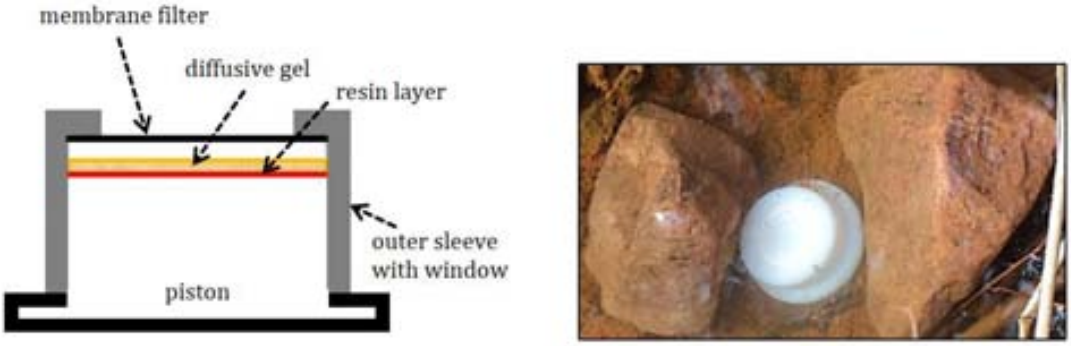

Fig. 52: Schematic drawing of DGT device (left) and deployment in CO_2-bearing spring (right).

6.3 CO_2 LEAKAGE SCENARIOS

Assuming that CO_2 dissolution and metal release is fast, the periodic collection and analysis of a particular well close to the intrusion point should yield different results if inputs of CO_2 react with the water aquifer (Fig. 53).

In a steady state the composition of water remains the same during the passing time, without significantly variation in terms of chemical composition and metal concentration. At the contrary, in the case of a constant leakage, the concentration of metals increase linearly with the increasing of time (brushed line), while in case of a pulse, the raise is strictly associated to the pulse event with the concentration in water that grows instantly at the beginning of the pulse to decrease later reaching the initial concentration until a new event takes place.

These different scenarios produce different responses in terms of metals mass sorbed into the DGT resin gel.

In fact in a "no intrusion" state, from the positioning to the collection, the DGT resin records a linear increase of the mass sorbed during the sampling time, with a slope that is directly related with the metal concentration in water (Fig. 54).

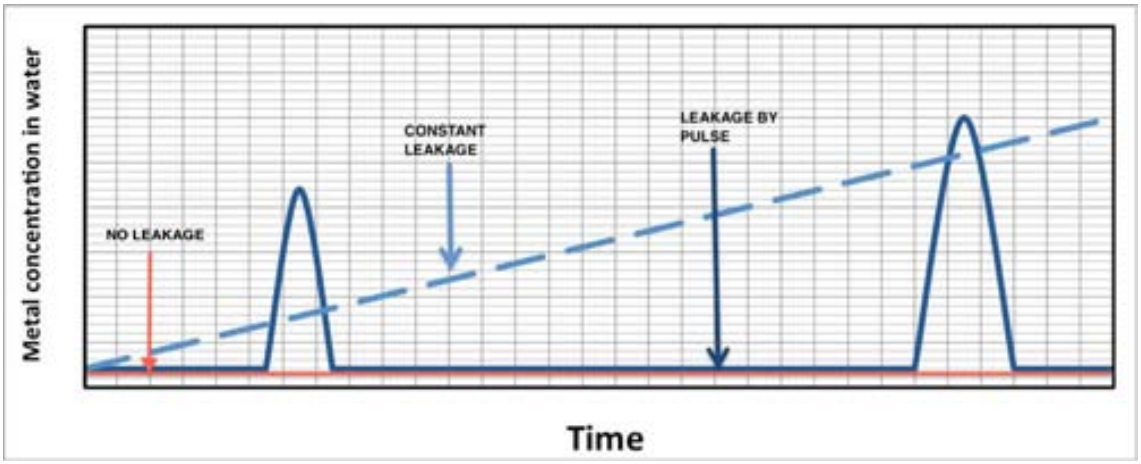

Fig. 53: Different scenarios of CO_2 leakage.

A similar trend is recorded when a constant leakage take place, with the mass of the sorbed metals that grows in time but, in this case, as a function of the increasing of the metals concentration in water (Fig. 55). In case of leakage by pulses the mass sorbed in the DGT resin gel show a particular trend. As shown by diagarams (Fig. 56), until that the first pulse takes place, the DGT resin sorbs metals with a slope depending on the original concentration in water, like in a no-leakage event. When the first pulse arrives, the slope representing the mass of metals sorbed in the resin increases for the increasing of the metals concentration in the water. As the pulse ends, the DGT follows to sorb metals with the same slope of the beginning but recording the rise of the mass caused by the pulse event. By the conversion from mass of metal sorbed in DGT resin gel to average concentration C_{DGT} (eq.1) it could be noted that, in case of a steady state, the metal concentration determined in water samples is equivalent to that sampled using the DGT device, and the comparison between the two concentrations gives a straight line with slope 1. Instead, in case of leakage by pulses, the metal concentration determined in water samples would be lower than the DGT ones and this results in a straight line characterized by a slope >1. So, by the comparison between the metals concentrations in water and DGT is possible to mark the presence (slope >1) or not (slope =1) of a metal leakage during the time, thanks to the capacity of DGT to record these events that wouldn't be recorded or only partially observed by a periodical water sampling carried off in time (Fig. 57). The use of DGT is intended to reduce costs of sampling and to avoid missing metal release episodes (Fig. 58).

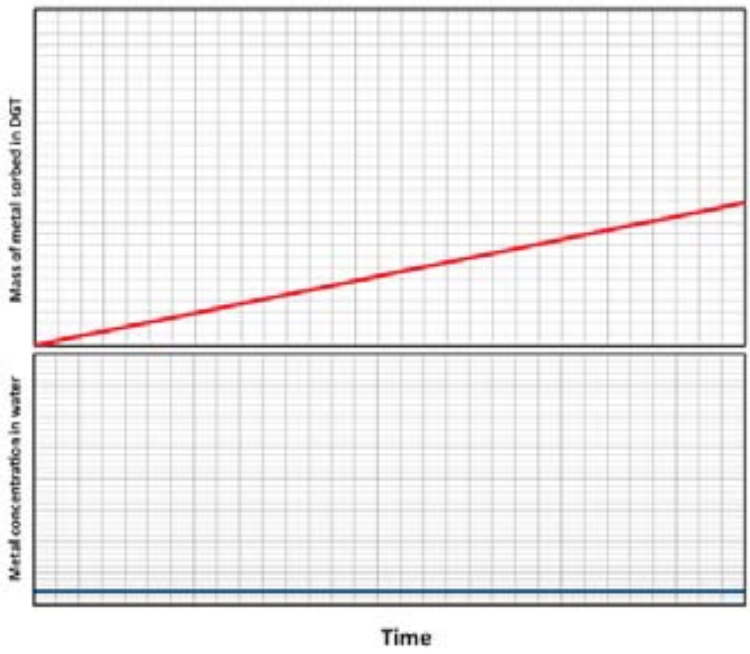

Fig. 54: No intrusion scenario. The slope is directly related with the metal concentration in water

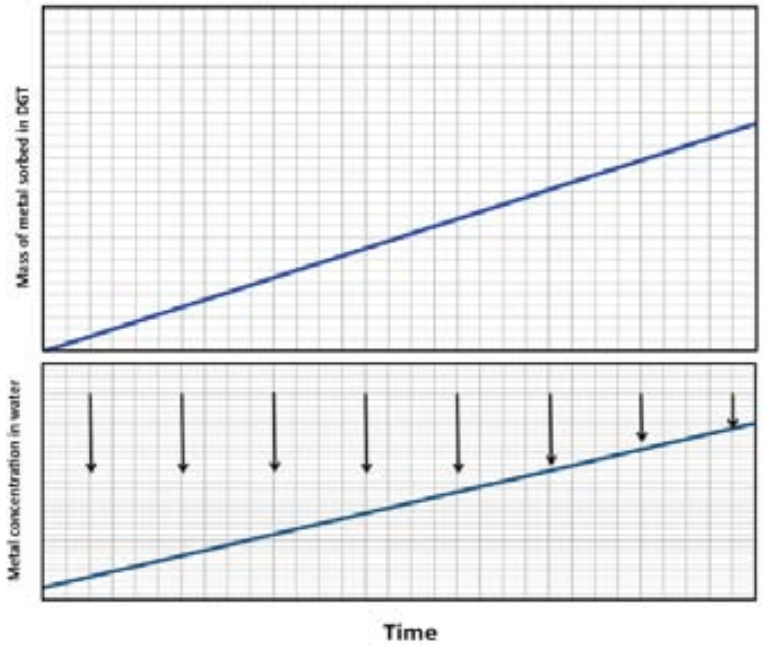

Fig. 55 Constant leakage scenario. The slope depend on the increase of metal concentration in water during the time.

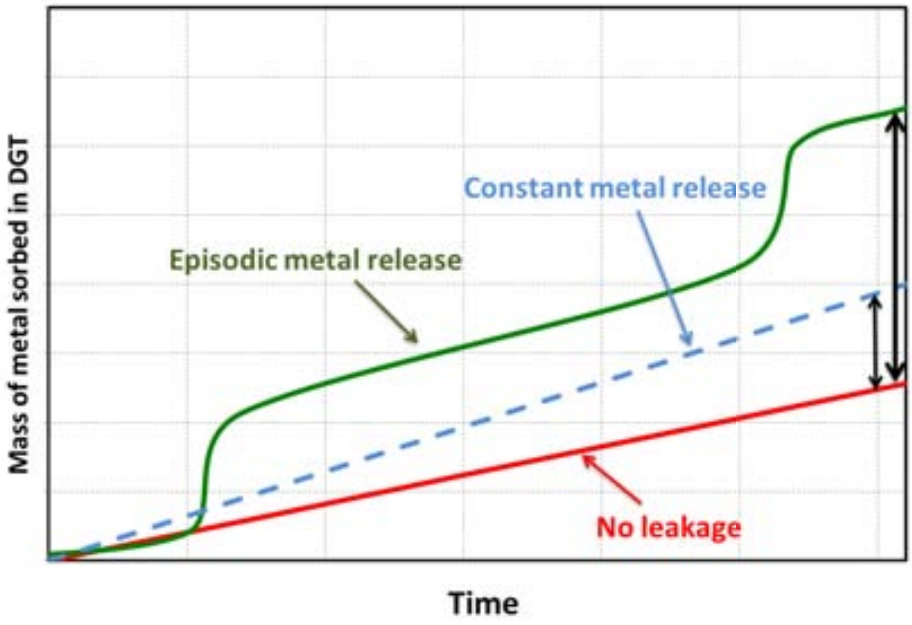

Fig. 56: Evolution of the mass of metal sorbed in DGT deployed in a well close to a CO_2 intrusion point in the three scenarios discussed in the text and illustrated in Fig. 53.

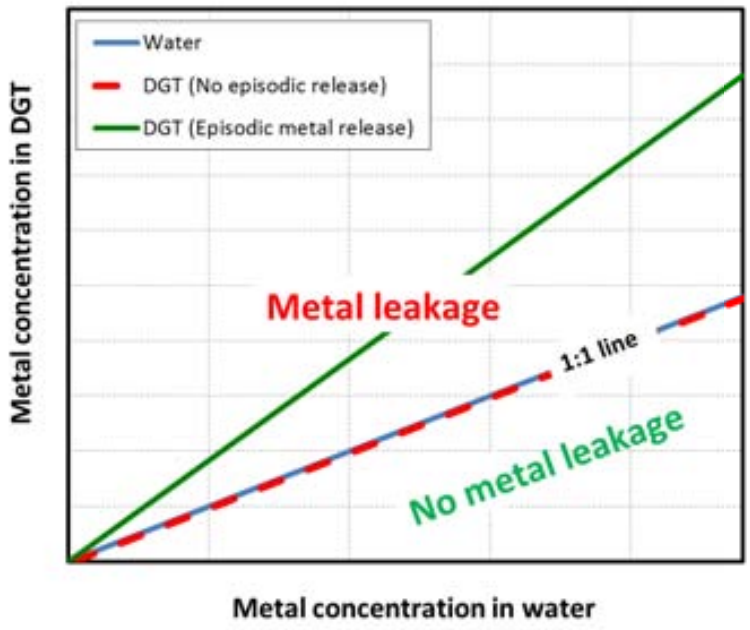

Fig. 57: [Me] sorbed in DGT per liter of water vs. [Me] in water plot. Potential leakage will yield data plotting above the 1:1 line.

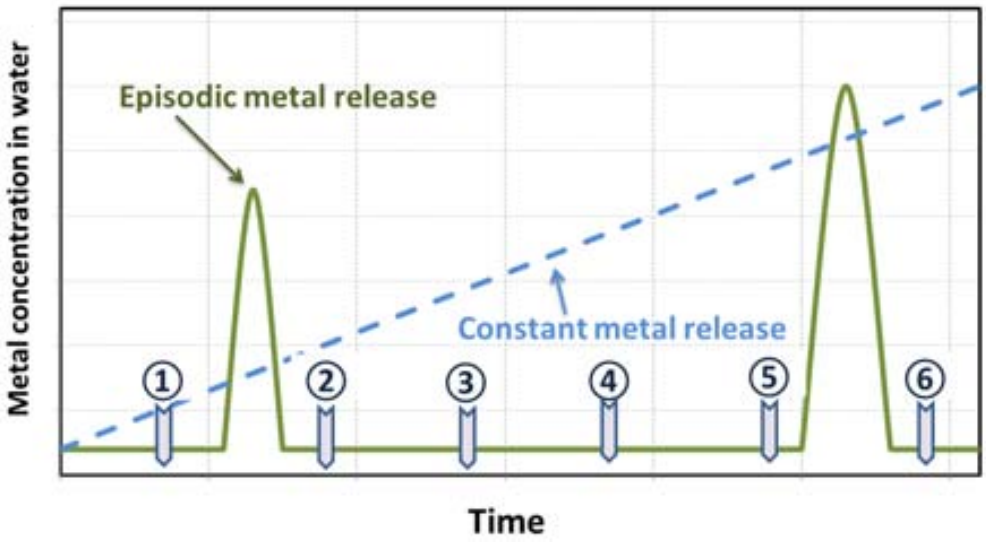

Fig. 58: Example of expected metal release from water-rock interaction as detected in a well close to a CO_2 intrusion point considering an episodic intrusion and a constant intrusion. Numbers refer to a periodic sampling that misses the detection of the metal release episodes.

6.4 VALIDATION OF DGT IN NATURAL ANALOGUE OF CO_2 SEEPAGE

The use of DGT to detect early leakage in commercial storage has been tested in natural CO_2-bearing, metal-rich groundwater in the Campo de Calatrava region in Central Spain. The objective is to quantify the sorption behaviour of a number of metals in DGT resins compared to the corresponding concentration in water. This must help to the selection of those metals showing an almost ideal behaviour, i.e., 1:1 relationship in a time-averaged $[Me]_{DGT}/L_{water}$ vs $[Me]_{water}/L_{water}$ plot (Fig. 57), that can be latter used in a monitoring campaigns in commercial storage. In the Campo de Calatrava region, CO_2 intrusion from mantle in shallow aquifers leads to significant changes in the chemistry of the water in terms of metal content. The metal concentration of these fluids can be considered stationary (e.g., no significant changes through time are expected in the fluid chemistry) in individual sampling point, at least in the sampling period. Interestingly, concentration gradients have been observed in these aquifers and a relatively large difference in the metal concentration is measured between sampling points. The reason behind such gradients is likely related to the channelled nature of the CO_2 migration and to particular geochemical reactions at the sampling sites.

The deployment of DGT and monitoring of trace metals have been studied in nine

sampling stations in the Jabalón river basin, in the Ciudad Real province (Fig. 59).

All stations, except one corresponding to the Jabalón river bed, are CO_2-bearing springs. Before deployment DGT devices were preserved in the fridge in a plastic bag filled with deionized water to avoid drying. Under these conditions, they have an optimal life of 6 months. During the field campaign, they were taken out from the bag, disposed and kept with a nylon string deep in the sampled spring. They were deployed from 24 hours (CO_2-bearing springs) to 30 days (river bed and station 9). After collection, DGT surface was washed with deionized water, disposed in the original bag and preserved in the fridge until the laboratory treatment and analysis. Chelex resin was submerged 24 h in 1 M Suprapur HNO_3 solution to desorb metals. The mass of metal on the resin layer were measured by ICP-MS.

In parallel to DGT withdrawal, sampling of spring and river water was performed in the same sites. Since CO_2 degassing at springs leads to formation of Fe(III) oxyhydroxide colloids, special care was taken in collecting colloid-free samples using 0.1µm filters.

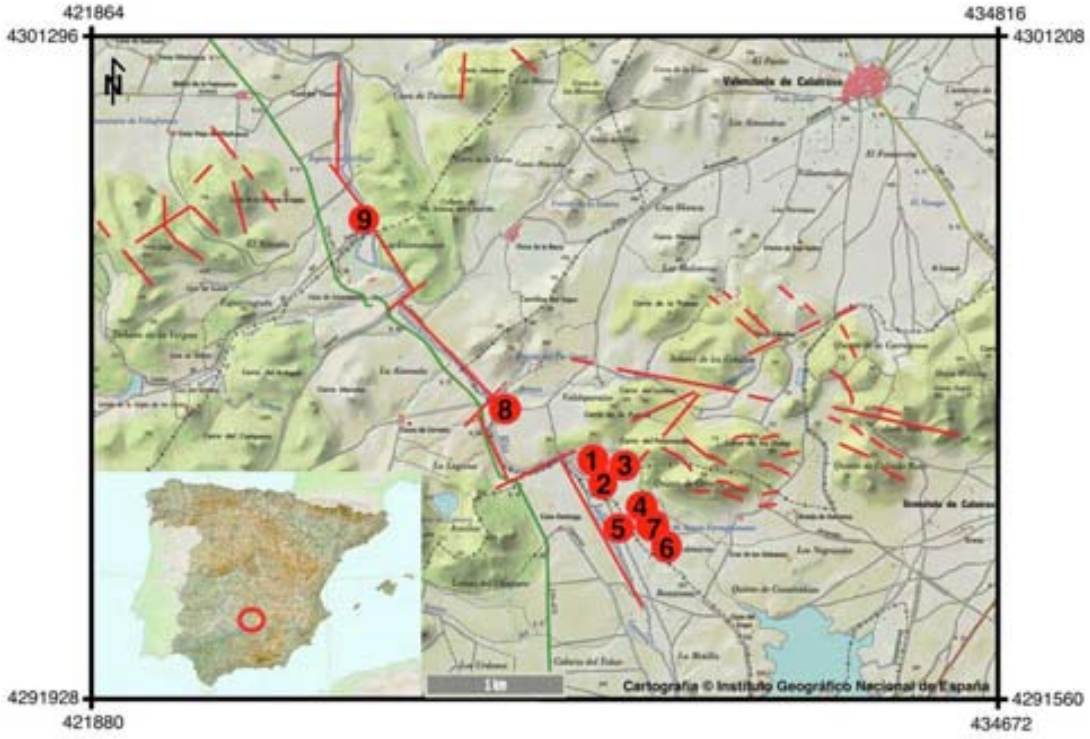

Fig. 59: Location of sampling stations in the Jabalón river basin in the Campo de Calatrava region. Red lines are major fracture zones.

6.5 RESULTS

Metal ratios are quite similar of the nine stations of Jabalon basin for both water and DGT in spite of their different ranges of concentration (Table 17). Metal concentration in the Jabalon River (point 8) and in the Chorrillo site (point 9) are one order of magnitude lower than the CO_2-bearing springs since they are much more diluted waters in spite of the continuous metal release due to CO_2 degassing.

Sampled spring waters are slightly acidic with pH in the range of 5.4 to 5.9. Water from Jabalon River has a pH of 8.16. Electrical conductivity is above 1000 $\mu S \cdot cm^{-1}$ in all the springs except in sampling point 9, reaching values above 2000 μS in points 1, 2 and 3.

The collected samples contain high Fe concentrations, up to 1×10^4 $\mu g \cdot L^{-1}$ (5.8×10^{-4} mol・L^{-1}) (Table 17). The concentration in sample 5 only reaches 60 $\mu g \cdot L^{-1}$ (1.0×10^{-6} mol・L^{-1}). This value is not consistent with the whole chemistry of the sample, and it is concluded that some error occurred during analysis.

River water (sample 8) has a lower concentration (180 μg・L^{-1}, 3.2×10^{-6} mol・L^{-1}). The redox state of these waters is quite oxidizing and Fe is found under its ferric form. Then, considering the low solubility of Fe(III) in CO_2-free waters, the elevated Fe concentration in these samples illustrates well the role ofaqueous Fe(III) carbonate complexes.

The studied samples also show high concentrations of Ni (up to 60 μg・L^{-1}, 1.1×10^{-6} mol・L^{-1}), Co (up to 24 μg・L^{-1}, 4.1×10^{-7} mol・L^{-1}), Zn (up to 157 μg・L^{-1}, 2.4×10^{-6} mol・L^{-1}), Cu (up to 22 μg・L^{-1}, 3.4×10^{-7} mol・L^{-1}), and Mn (up to 1 mg・L^{-1}, 1.8×10^{-5} mol・L^{-1}).

In river sample, the concentration of all these elements is at least 1 order of magnitude lower. On the other hand, metals such as Pb, Cr, U (Table 17), and metalloids (As) do not show elevated concentrations. Comparing re-calculated metal concentration in DGT (from eq. 6.1; Table 17) with metal water concentration, two different groups of metals are observed (Figs 60 and 61): (i) metals with sorption close to the ideality (plotting close to the 1:1 line) or with lower sorption, and (ii) metals with non-linear sorption, with some data with [Me]DGT: [Me]water >1. Metals in the first group include Fe, Mn, Co, Ni and U (Fig. 60). Metals in the second group are Zn, Pb, Cr, Cu and Al, with most data showing ‘excess’ of sorption compared to the concentration in water (Fig. 61).

Table 17: ***Metal concentration in the samples from the Campo de Calatrava CO_2-bearing springs and in DGT devices after collection. All concentrations are µg L^{-1}.***

Ref	Temp (ºC)	pH	Conductivity (µS)	Depth (m)	DGT/ Water	Al (µg·L^{-1})	Cr (µg·L^{-1})	Mn (µg·L^{-1})	Fe (µg·L^{-1})	Co (µg·L^{-1})	Ni (µg·L^{-1})	Cu (µg·L^{-1})	Zn (µg·L^{-1})	Pb (µg·L^{-1})	U (µg·L^{-1})
Detection limits						2	0.5	0.1	10	0.005	0.3	0.2	0.5	0.01	0.001
1	17	5.9	2170	0.05	DGT	478.68	4.59	204.32	632.76	5.95	25.83	10.11	65.68	0.61	0.29
					Water	1230.00	6.40	803.00	32400.00	19.20	59.60	21.80	157.00	3.96	0.61
2	13	5.7	2300	0.05	DGT	615.82	5.03	258.52	4099.61	7.66	24.65	5.31	36.18	0.68	0.01
					Water	66.00	4.50	745.00	> 10000	12.20	40.50	3.40	10.20	0.03	0.04
3	12	5.8	2250	0.1	DGT	681.99	5.83	219.74	137.34	4.89	28.33	4.72	54.32	0.78	0.21
					Water	12.00	3.80	349.00	190.00	6.88	39.20	2.40	22.30	0.03	0.29
4	16	5.7	1216	0.05	DGT	557.13	4.77	459.24	4234.74	13.74	34.87	4.25	94.77	0.63	0.16
					Water	204.00	3.00	973.00	> 10000	22.40	53.80	1.50	81.10	0.07	0.67
5	15	5.8	1733	0.2	DGT	608.90	6.48	516.45	4769.96	15.60	40.15	10.74	70.88	0.67	0.22
					Water	70.00	4.10	841.00	6860.00	18.30	43.30	1.80	73.60	0.06	0.30
6	14	6.1	1429	0.5	DGT	645.03	6.23	524.71	122.36	18.88	58.04	4.09	163.21	0.71	0.25
					Water	27.00	2.90	693.00	60.00	23.60	63.80	1.10	55.60	0.06	0.35
7	14	5.8	1421	0.05	DGT	623.36	5.15	445.33	8372.71	21.65	54.98	19.78	106.68	0.72	0.19
					Water	53.00	4.70	763.00	8760.00	24.30	56.70	2.90	63.50	0.17	0.25
8	10	8.1	1244	0.5	DGT	23.02	0.21	50.17	173.30	0.66	0.65	0.40	2.01	0.03	0.16
					Water	4.00	4.00	78.90	180.00	0.56	6.90	3.70	3.80	0.05	3.98
9	17	5.4	960	0.5	DGT	30.40	0.15	2.25	4.85	0.18	1.11	0.24	2.62	0.05	0.29
					Water	38.00	4.00	33.20	40.00	0.48	10.70	1.10	12.80	0.09	0.33
Blanc	15	-	-	-	DGT	556.50	4.43	5.85	64.60	0.05	2.28	3.59	394.49	0.77	0.0002

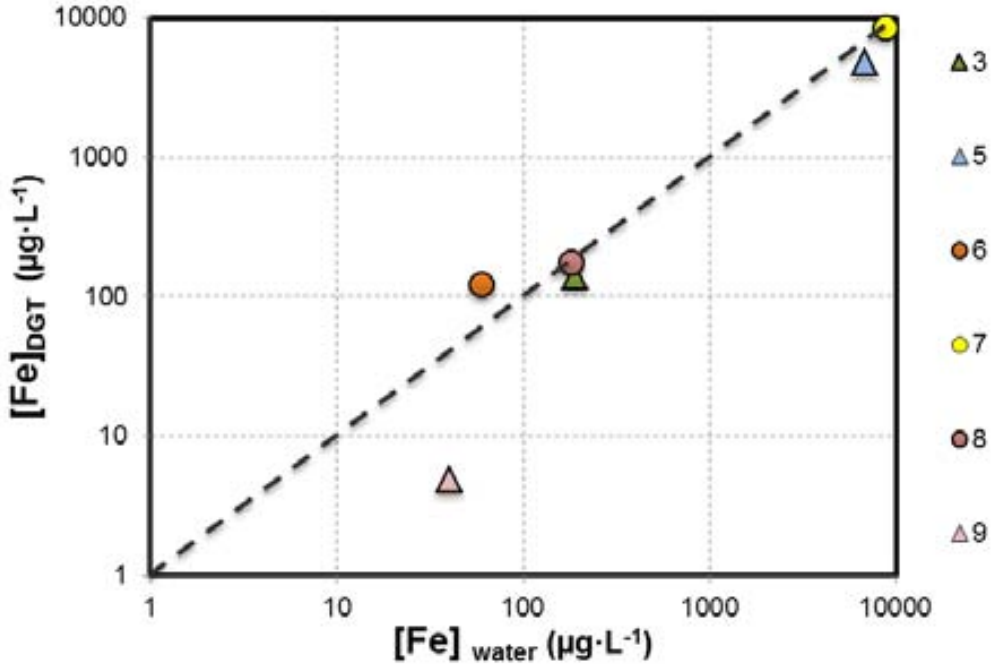
10000
1000
100
10
1
[Fe]DGT (µg·L-1)
1
10
100
1000
10000
[Fe] water (µg·L-1)
3
5
6
7
8
9

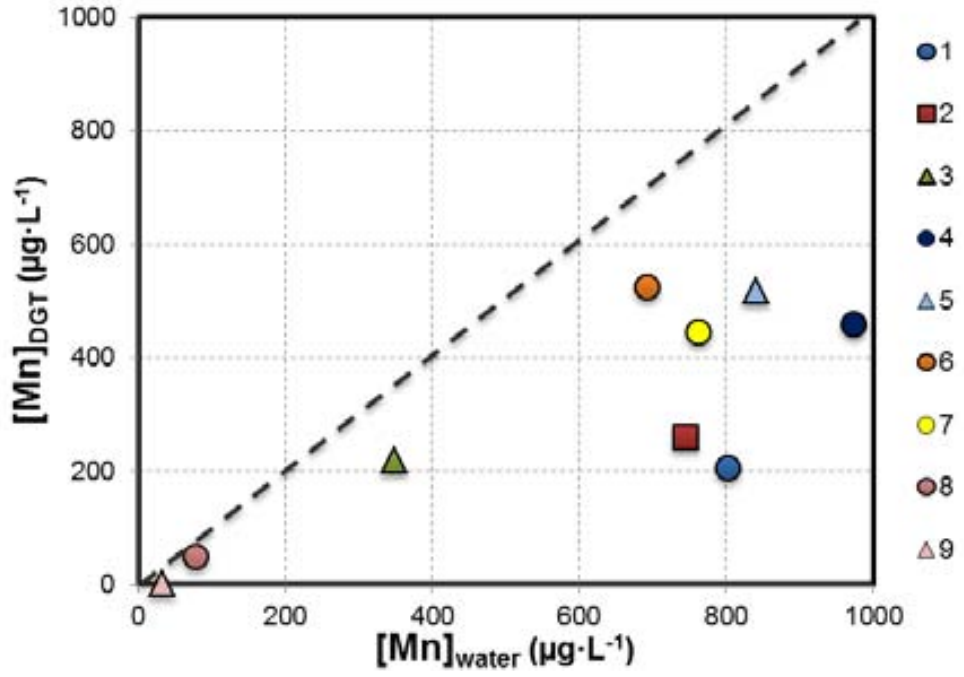
1000
800
600
400
200
0
[Mn]DGT (µg·L-1)
0
200
400
600
800
1000
[Mn]water (µg·L-1)
1
2
3
4
5
6
7
8
9

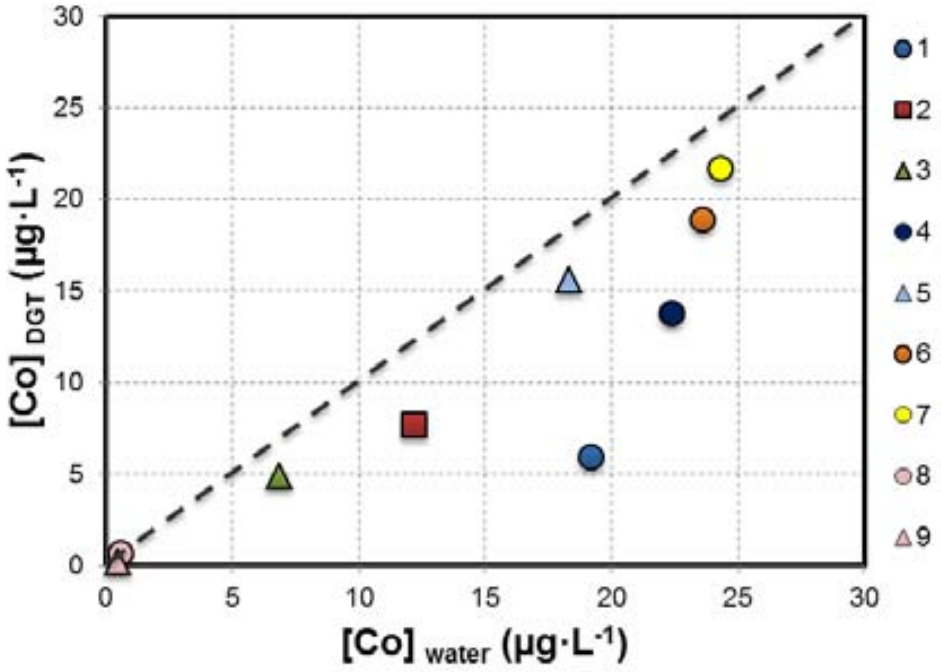
30
25
20
15
10
5
0
0
5
10
15
20
25
30
[Co] DGT (µg·L-1)
[Co] water (µg·L-1)
1
2
3
4
5
6
7
8
9

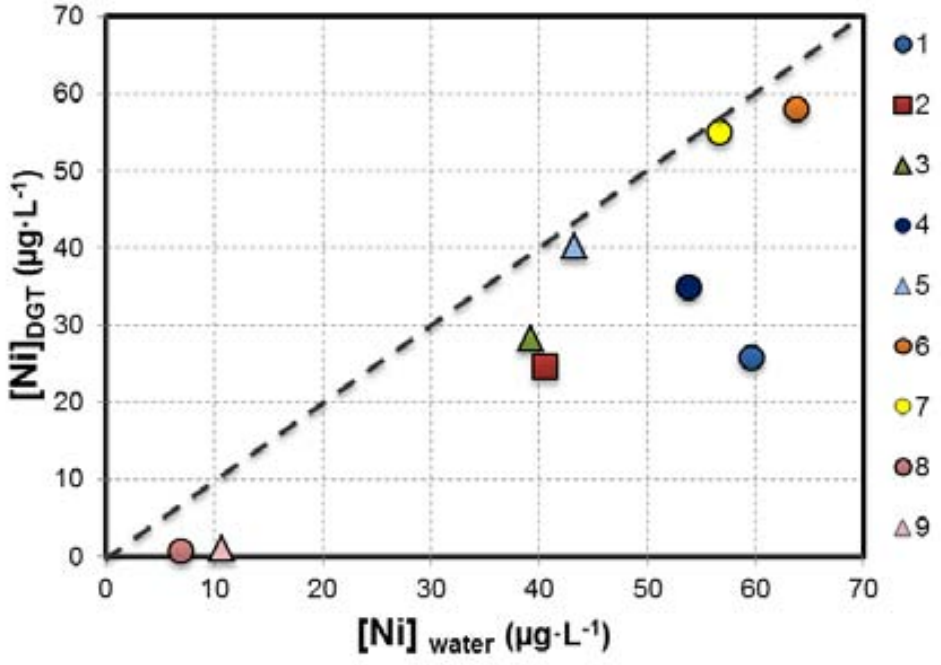
70
60
50
40
30
20
10
0
0
10
20
30
40
50
60
70
[Ni]DGT (µg·L-1)
[Ni] water (µg·L-1)
1
2
3
4
5
6
7
8
9

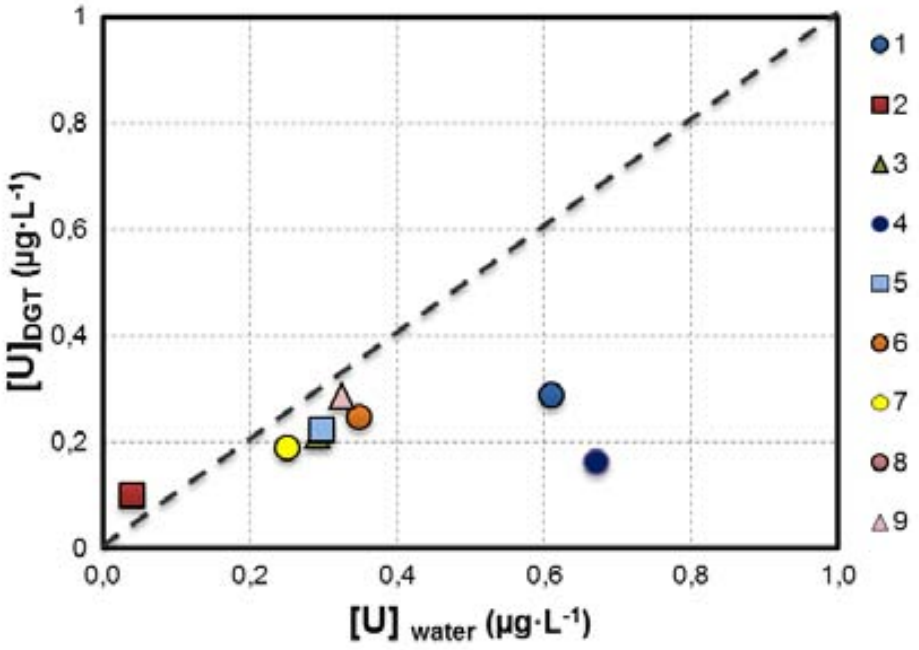

Fig. 60: [Me] sorbed in DGT per liter of water vs. [Me] plot in water corresponding to Fe, Mn, Ni, Co and U, in samples collected in the Campo de Calatrava region. These metals show typically data plotting below the 1:1 line. Symbol numbers are the sample station.

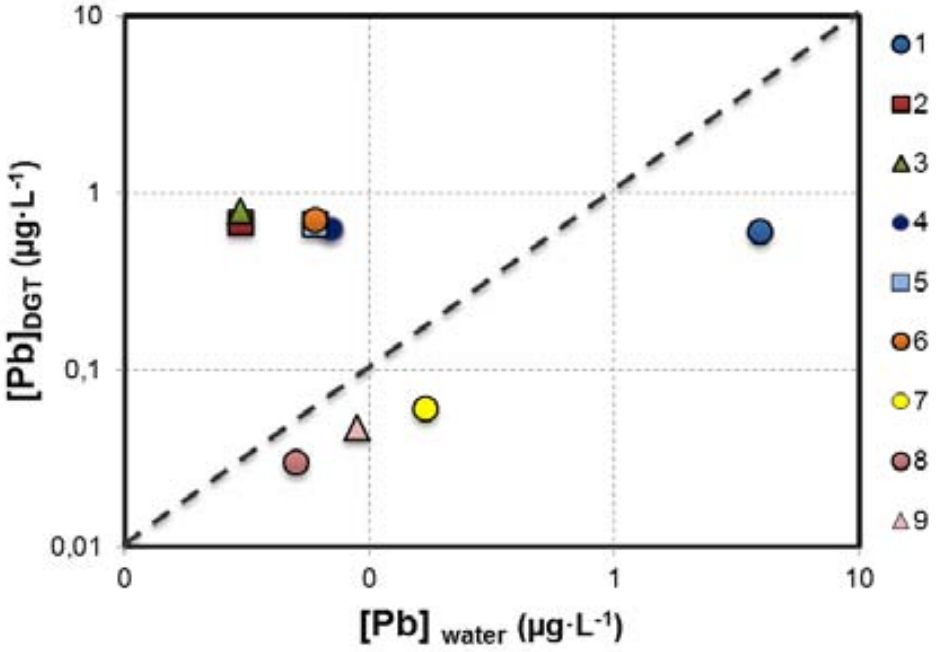
10
1
0,1
0,01
0
0
1
10
[Pb]DGT (µg·L-1)
[Pb] water (µg·L-1)
1
2
3
4
5
6
7
8
9

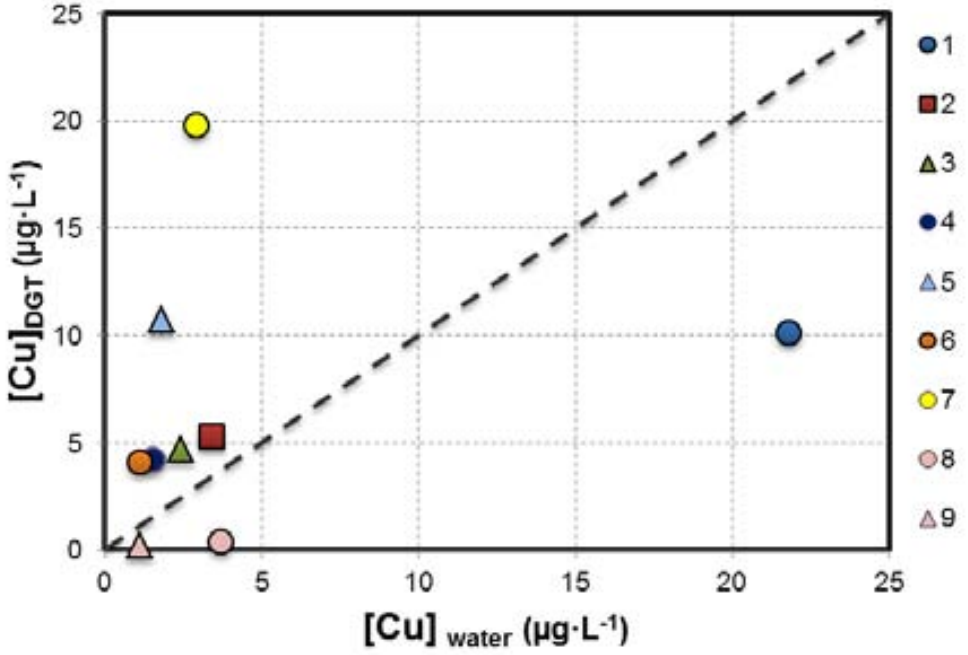
25
20
15
10
5
0
0
5
10
15
20
25
[Cu]DGT (µg·L-1)
[Cu] water (µg·L-1)
1
2
3
4
5
6
7
8
9

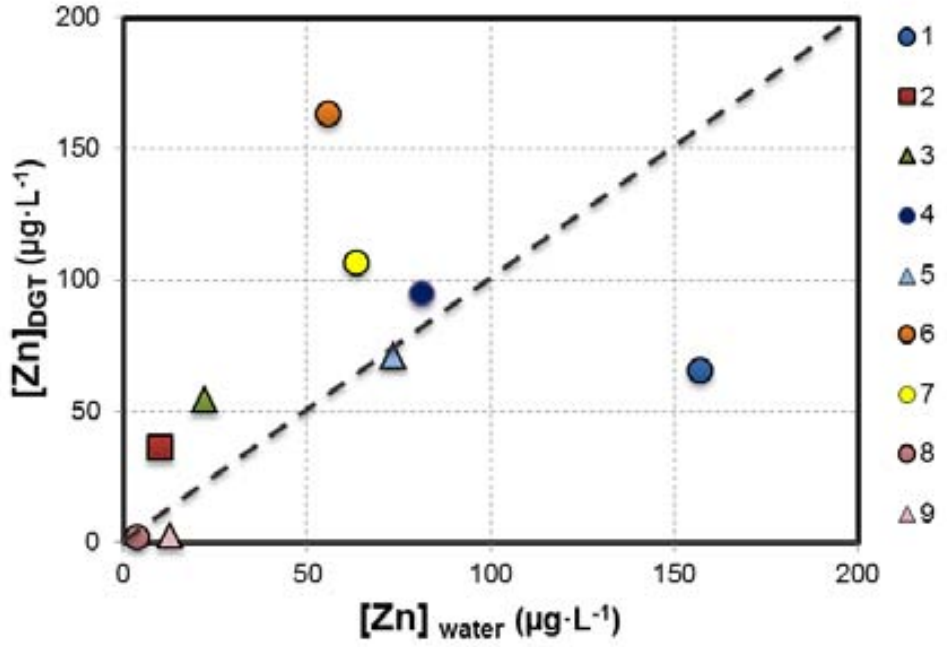
200
150
100
50
0
0
50
100
150
200
[Zn]DGT (µg·L-1)
[Zn] water (µg·L-1)
1
2
3
4
5
6
7
8
9

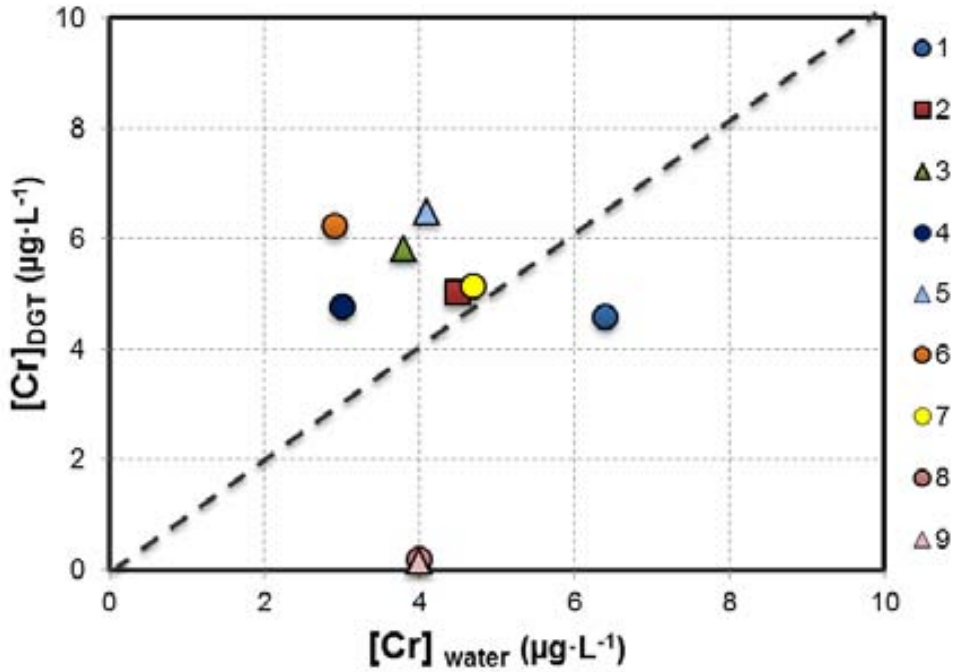
10
8
6
4
2
0
0
2
4
6
8
10
[Cr]DGT (µg·L-1)
[Cr] water (µg·L-1)
1
2
3
4
5
6
7
8
9

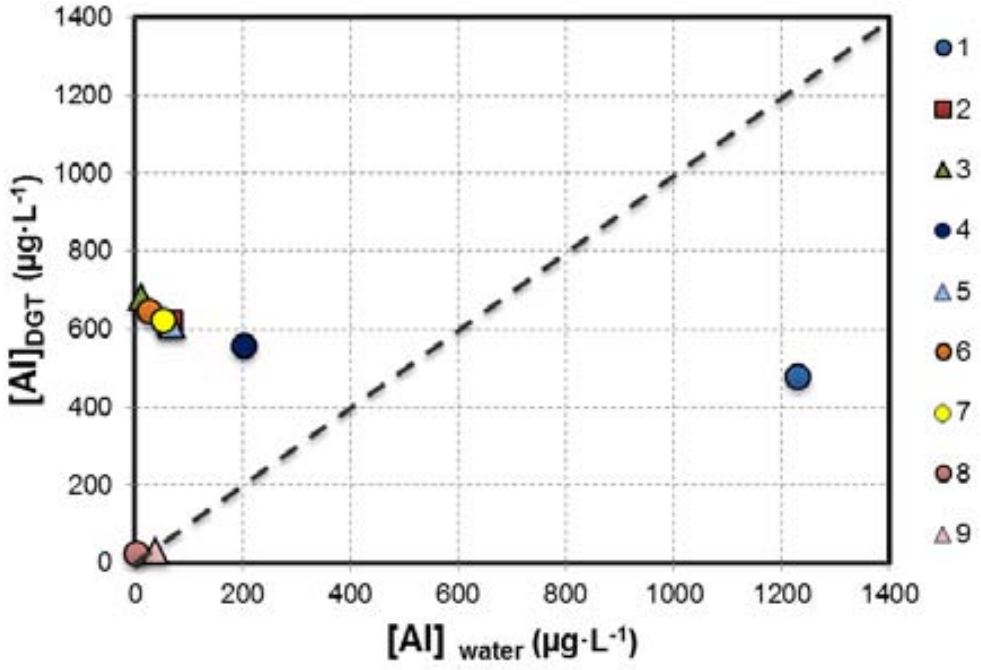

Fig. 61: [Me] sorbed in DGT per liter of water vs. [Me] plot in water corresponding to Al, Cr, Zn, Pb and Cu, in samples collected in the Campo de Calatrava region. These metals show most data plotting above the 1:1 line. Symbol numbers are the sample station.

6.6 DISCUSSION:

The use of DGT for conventional surface monitoring in the influence area of CO_2 geological storage is apparently cost-effective for operators and regulators.

Considering one-year long monitoring campaign, DGT could be deployed during a couple of times with water sampling at each deployment and collection time. In contrast, a traditional monitoring campaign of periodic water sampling is much more expensive in both sample analysis and field work, and less reliable for detecting slight changes in metal contents.

A strong point of DGT films is their capacity to bear tough environmental conditions (e.g. intensive rainfall and water level increase in river and lake, biological activity). However, the sorption of metals in DGT could not be complete due to a number of processes and this is something to take into consideration during monitoring and in the data interpretation. It is worth mentioning that DGT Chelex resin is selective for labile species that form inorganic complexes or small organic complexes (Davison and Zhang, 1994).

Large organic complexes diffuse differently through the resin and their presence may underestimate the calculated amount of metals in solution.

It is also remarkable the effect of colloid formation, which can reduce the sorption of mainly Fe and Mn in DGT, since particles larger than 0.45 μm will be excluded. In addition, all metals sorbed onto colloids cannot pass through the filters. However, the impact of colloid formation is minimized if a [Me]DGT/Lwater vs [Me]water/Lwater plot is used, since water collection also include colloid retention in filters. The formation of biofilm growth on DGT device can limit metal retention. Dunn et al. (2003) observed that DGT labile metal concentrations could be 3 to 5 times below the concentrations of 0.45 μm filtered samples for some elements such as Ni, Pb, Cu and Zn.

They suggested that biofilm growth on DGT could act to increase the thickness of the diffusive path-length above that estimated, which would mean that DGT labile metal concentrations calculated are proportionally underestimated. In the time of DGT exposure (24 h to one month) in the studied springs, biofi lm did not significantly grow to have a significant retardation effect on metal diffusion into the monitoring device. Operators would have to adapt the time of exposure of DGT to potential biofouling effect in backwater.

From the monitoring perspective, the limitation of DGT resins seems to be, thus, the behavior of the metal sorption depending on the metal speciation in the studied waters. The results from the tests in Campo de Calatrava suggest that some metals (Fe, Co, Ni, and U) are basically transported as labile inorganic forms and they are almost fully adsorbed in the DGT, as revealed by the [Me]DGT/Lwater vs [Me]water/Lwater ratios close to 1. For these metals, data plotting far below 1:1 line suggest problems with clogging of the DGT filters or metal uptake by mineral precipitation prior to the sorption in the DGT resin.

This could be the case of sample 1 since DGT is always much depleted in any metal.

In contrast, other metals (Zn, Pb, Cr, Al) show large discrepancies between the measured and expected metal sorption in DGT, with [Me]DGT/Lwater vs [Me]water/Lwater ratios typically higher than 1.

The reason behind such discrepancies is not clear and commonly proposed hypotheses are not conclusive.

First of all, the formation of colloidal particles could overestimate the metal concentration in DGT. In this work, two different filters have been used for DGT and for filtering the water samples, 0.45 and 0.1 μm, respectively. Therefore, some colloid-borne metals can

be retained and analyzed in DGT and excluded from the water collection. However, since most colloids in the studied samples seem to be Mn-, Fe-oxyhydroxides, the overestimation of metals in DGT should also be seen for iron and manganese, and also for other trace metals sorbed in their surfaces (including U, Ni, and Co), which is not the case. For Al, the presence of clay colloids could account for the excess in the DGT, since these minerals are abundant in the precipitates around the CO_2-rich springs.

Another hypothesis to explain preferential metal sorption on DGT could be a variable metal concentration in water through sampling time (up to one month) due to, for example, dilution in the aquifer.

However, this variability also should be seen in all metals. The formation of carbonate mineral precipitates inside the DGT device which could be also dissolved during the laboratory treatment could account for the data for Zn and Pb since calcite may uptake these metals in its lattice. Nevertheless, calcite can also fix metals with similar geochemical properties, i.e. Co and Ni, which are not enriched in excess in the DGT analysis.

6.7 CONCLUSIONS:

The enhanced metal transport due to CO_2 dissolution makes the changes in metal contents in surface waters and shallow aquifers a potential good indicator of leakage from deep geological storage. The early stages of such metal increase may not be constant in time and, consequently, of difficult detection. The use of DGT films appears to be a cost-effective monitoring tool to be used as a regular technique in commercial on-shore projects. Tests in CO_2-bearing, metal-rich springs in the Campo de Calatrava region in Central Spain reveal that DGT record well the concentration of some metals such as Fe, Ni, Co and U since a remarkable correlation between metal concentration in water and metal contents in DGT is observed. Therefore, these metals can be considered as favourable tracers for detection of early leakage by using DGT films. On the other hand, metals such as Zn, Pb, Al do not show a clear correlation between adsorbed contents in DGT and water concentration. The reason behind such lack of correlation is not clear and it is suggested that the use of these metals could lead to misinterpretation of early CO_2 leakage from deep sources.

Section Four

7 GENERAL CONCLUSIONS:

From literature review, field work in natural analogues and thermodynamic modelling, this Ph.D. work has provided clear evidences that metal release from aquifer rocks due to the interaction with $CO_2(g)$ is readily occurring, causing significant changes in the chemistry of the impacted aquifers. The reason behind such release is the dissolution of native $Fe(OH)_3$ (or ferrihydrite) which is widely believed to be the source and solubility-limiting phase for many trace metals through surface sorption.

The main contribution of this work, in addition to confirm that metal mobilisation is a real concern in the environmental safety assessment of CO_2 geological storage, is the demonstration that the formation of stable aqueous Fe(III)-carbonate complexes is the driving force in the metal release and transport (at least iron) when the $CO_2(g)$-water-rock interaction occurs at shallow depths, i.e., at oxisiding conditions. These complexes had been found in laboratory experiments but their "observation" in natural systems had been limited. The formation of these aqueous complexes helps making unstable ferrihydrite grains in the aquifer host-rock since the Fe(III) activity is strongly decreased. The impact of the formation of stable aqueous Fe(III)-carbonate complexes had not been previously considered by the CCS scientific community and, now, it can be stated that the persistence of high metal concentration plumes is extended to geological environments with higher pH and Eh conditions since these complexes are stable under oxidising and circum-neutral pH conditions, which are prevalent in shallow aquifers. Previous hypotheses, i.e., acidification, reducing trace gases in the gas flow or microbial activity leading to Fe reduction, are now believed to be less important in the transport of metal in these shallow waters.

This work also supports the idea, many times call it into question, that natural analogues can provide valuable information on processes that are expected to occur in commercial geological storage, not only of CO_2 but also of other wastes or energy-producing substances. Therefore, the collection of data from laboratory experiments, process observation in natural environments and numerical simulation is a powerful combination for scientists.

Finally, this thesis has also contributed to the monitoring strategy of carbon storage reservoirs by taking advantage of the lessons learned in the lab and in the field. The

confirmation that DGT films are able to detect tiny changes in the concentration of some metals related to CO_2 leakage is the base of a new monitoring methodology.

The research of the metal transport in CO_2-bearing fluids has not, obviously, completed with this work, and some aspects remain open. Among them, the impact of trace gases included in the gas flow is a topic in line of the research carried out in this work. The trace gases are present in the captured flue gas from industrial sources that is later injected and stored. The reactivity of these gases with the metals released once injected in the aquifer is a subject to be broadly investigated in natural systems. Actually, many CO_2 gas flows interacting with shallow aquifers are H_2S, CH_4 and other hydrocarbon-bearing, being the most prominent examples in western Italy. So this is the next frontier.

Bibliography:

ABEM, 2009. Instruction Manual. Terrameter SAS 4000 / SAS 1000. ABEM Instrument AB, Sundbyberg, Sweden. ABEM Printed Matter No. 93109, pp. 136. Accessed 2015-06-09 from (http://www.abem.se/files/upload/manual_terrameter.pdf).

Agnelli M, Grandia F, Credoz, A, Gasparini A, and Bruno J, 2013. Use of diffusive gradients in thin films (DGT) as an early detection tool of low-intensity leakage from CO_2 storage. Greenhouse Gases: Science&Technology 1:1-13.

Allard P, Carbonelle J,Dajlevic D, Le Bronec J, Morel P, Robe MC, Maurenas JM, Faivre-Pierret R, Martin D, Sabroux JC and Zeetwoog P, 1991. Eruptive and diffuse emission of CO2 Mt. Etna, Nature 351, 387-391.

Ancochea E. 1982. Evolución espacial y temporal del vulcanismo reciente de España Central. Tesis Doctoral, Univ. Complutense, Madrid. Colección Tesis Doctorales, 203/83. 675 p.

Ancochea E. 1999. El Campo volcánico de Calatrava. Enseñanza de las Ciencias de la Tierra, Vol. 7, nº 3), 237-242.

Ardelan MV, Steinnes E. (2010). Changes in mobility and solubility of the redox sensitive metals Fe, Mn and Co at the seawater-sediment interface following CO_2 seepage. Biogeosciences 7: 569-583

Ardelan MV, Sundeng K, Slinde GA, Gjøsund NS, Nordtug T, Olsen AJ, Torp TA. (2012). Impact of possible CO_2 seepage from sub-seabed storage on trace elements mobility and bacterial distribution at sediment-water interface. En. Proc. 23: 449-461

Bates NR, Astor YM, Church MJ, Currie K, Dore JE, González-Dávila M, Lorenzoni L, et al. (2014). A time-series view of changing ocean chemistry due to ocean uptake of anthropogenic CO2 and ocean acidification. Oceanography 27(1):126–141.
http://dx.doi.org/10.5670/oceanog.2014.16.

Berner R.A., Lasaga A.C., Garrels R.M., 1983. The carbonate-silicate geochemical cycle and its effect on atmospheric carbon dioxide over the past 100 million years. Am. J. Sci.,283, 641-683.

Berner RA and Lasaga AC, 1989. Modelling of the geochemical carbon cycle. Scientific American 260: 74-81.

Birkholzer J, Apps J, Zheng Y, Xu T, Tsang C-F, 2008. Research Project on CO_2 Geological Storage and Groundwater resources: Large-scale Hydrogeological Evaluation and Impact on Groundwater Systems, Annual Report October 1, 2007 to September 30, 2008. Report, Lawrence Berkeley National Laboratory, Berkeley, CA, USA.

Bruno J, 1986. Stoichiometric and structural studies on the Be(II)-H_2O-CO_2(g) system. PhD Thesis Department of Inorganic Chemistry, Royal Institute of Technology. Stockholm.

Bruno J, 1990. The influence of dissolved carbon dioxide on trace metal speciation in seawater. Mar. Chem. 30: 231-240.

Bruno J, de Pablo J, Duro L, Figuerola E, 1995. Experimental study and modelling of the U(VI)-$Fe(OH)_3$ surface precipitation/coprecipitation equilibria. Geochim. Cosmochim. Acta 59: 4113-4123.

Bruno J and Duro L, 2000. Reply to W. Hummel's comment on and correction to "On the influence of carbonate in mineral dissolution I. The thermodynamics and kinetics of hematite dissolution in bicarbonate solutions at 25ºC. Geochim. Cosmochim. Acta 56, 1139-1147." Geochim. Cosmochim. Acta 12: 2173-2176.

Bruno J, Duro L, Grivé M, 2002. The applicability and limitations of thermodynamic geochemical models to simulate trace element behaviour in natural waters. Lessons learned from natural analogue studies. Chemical geology, 190(1): 371-393.

Bruno J, Ferri D, Grenthe I, Sandström M, 1987. Studies on metal carbonate equilibria 15. The Be(II)-H_2O-CO_2(g) system in acidic 3.0 M perchlorate medium, at 25º C. J. Chem. Soc., Dalton Trans. 2445-2449.

Bruno J, Grandia F, Vilanova E, 2009. Trace element behaviour in connection to the geological storage of CO_2. Lessons from natural analogues. Abstracts of the Goldschmidt Conference, 2009, Davos (Switzerland). Geochim Cosmochim Acta 73(13):A167.

Bruno J, Stumm W, Wersin P, Brandberg F, 1992a. On the influence of carbonate in mineral dissolution I. The thermodynamics and kinetics of hematite dissolution in bicarbonate solutions at 25ºC. Geochim. Cosmochim. Acta 56: 1139-1147.

Bruno J, Wersin P, Stumm W, 1992b. On the influence of carbonate in mineral dissolution II.The thermodynamics and kinetics of siderite dissolution in bicarbonate solutions at 25ºC. Geochim. Cosmochim. Acta 56: 1149-1155.

Cahill AG, Jakobsen R, 2013. Hydro-geochemical impact of CO_2 leakage from geological storage on shallow potable aquifers: a field scale pilot experiment. Int. J. Greenhouse Gas Control. http://dx.doi.org/10.1016/j.ijggc.2013.03.015.

Calvo D, Barrancos J, Padilla G, Brito M, Becerra-Ramírez R, González E, Gosálvez R, Escobar E, Melián G, Nolasco D, Padrón E, Marrero R, Hernández PA and Pérez N, 2010. Emisión difusa de CO2 en el Campo de Calatrava, Ciudad Real. En: Aportaciones recientes en volcanología 2005-2008. (E. González, E. Escobar, R. Becerra, R.U. Gosálvez i J. Dóniz, editors), Centro de Estudios Calatravos, Almagro, Ciudad Real, 51-55

Castaldi S and Tedesco D, 2005. Methane production and consumption in an active volcanic environment of Southern Italy. Chemosphere 58, 131–139.

Cebriá JM, López-Ruiz J, 1995. Alkali basalts and leucitites in an extensional intracontinental plate setting: the late Cenozoic Calatrava Volcanic Province (central Spain). Lithos 35, 27-46.

Chaffee E, Dasgupta TP, Harris GM, 1973. Kinetics and mechanism of aquation and formation reactions of carbonato complexes V. Carbon dioxide uptake by hydroxopentaaminecobalt(III) ion. J.Am. Chem. Soc. 95: 4169.

Chiodini G, Cioni R, Magro G, Marini L, Panichi C, Raco B, Russo M, 1996. Chemical and isotopic variation of Bocca Grande fumarole (Solfatara volcano, Phlegrean Fields). Acta Vulcanol., 8, 228.

Chiodini G, Frondini F, Kerrick DM, Rogie J, Parello F, Peruzzi L, Zanzari AR, 1999. Quantification of deep CO2 fluxes from Central Italy: examples of carbon balance for regional aquifers and of soil diffuse degassing. Chem. Geol. 159, 205– 222.

Chiodini G, Avino R, Brombach T, Caliro S, Cardellini C, De Vita S, Frondini F, Granieri D, Marotta E and Ventura G, 2004. Fumarolic and diffuse soil degassing west Mount Epomeo, Ischia (Italy), J. Volcanol. Geotherm. Res., 133, 291– 309.

Cornell R.M. and Schwertmann U. 1996. The iron oxides. Structure, properties, reactions occurrences and uses. VCH publ.

Cornell RM and Schwertmann U, 2003. The iron oxides. Structure, properties, reactions occurrences and uses. VCH publ.

Crespo A, 1992. "Geología, mineralogía y génesis de los yacimientos de manganeso cobaltífero del Campo de Calatrava (Ciudad Real)". Tesis Doctoral. Universidad Complutense, Madrid. 389 p.

Czernichowski-Lauriol I, Rochelle C, Gaus I, Azaroual M, Pearce J, Durst P, 2006. Geochemical interactions between CO_2, pore-waters and reservoir rocks: lessons learned from laboratory experiments, field studies and computer simulations. In: Lombardi S, Altunina LK, Beaubien SE. (Eds.), Advances in the Geological Storage of Carbon Dioxide: NATO Science Series IV. Earth. Environ. Sci. 65: 141–157.

Dasgupta TP, Harris GM, 1977. Kinetics and mechanism of aquation and formation reactions of carbonato complexes. 11. Carbon dioxide uptake and intramolecular carbonato ligand chelation in aqueous solution of cis- and trans-diaquo(1,4,8,11-tetraazacyclotetradecane)cobalt(III) cations. J. Am. Chem. Soc. 99 (8): 2490–2495.

Davison W, Zhang H, 1994. In situ speciation measurements of trace components in natural waters using thin-film gels. Nature 367: 546-548.

Donville B, 1976. Géologie néogene de la Catalogne orientale. Bull. B.R.G.M, Seco 4, 3, 177-210

Dunn RJK, Teasdale PR, Warnken J, Schlich RR, 2003. Evaluation of the diffusive gradient in a thin film technique for monitoring trace metal concentration in estaurine waters. Environ. Sci. Technol. 37: 2794-2800.

Duran H, 1985. El paleozoico de Les Guillereis. PhD thesis. Departament de Geologia, Universitat Autonoma de Barcelona.

Duro L, 1996. Estudio cinético y termodinámico de la interacción entre U(VI) y oxihidróxidos de Fe(III). PhD. Thesis. Universidad Politécnica de Cataluña. Barcelona.

Dzombak DA, Morel FMM, 1990. Surface Complexation Modelling: Hydrous Ferric Oxide. John Wiley and Sons 245-287.

Elío J, Ortega MF, Nisi B, Mazadiego LF, Vaselli O, Caballero J and Grandia F, 2015. CO_2 and Rn degassing from the natural analog of Campo de Calatrava (Spain): Implications for monitoring of CO_2 storage sites. Int. J. Greenh. Gas Control 32, 1-14.

Etiope G, 1999. Subsoil CO_2 and CH_4 and their advective transfer from faulted grassland to the atmosphere, J. Geophys. Res, 104(D14), 16,889– 16,894.

Etiope G, Beneduce P, Calcara M, Favali P, Frugoni F, Schiattarella M, Smriglio G, 1999. Structural pattern and CO2-CH4 degassing of Ustica Island, southern Tyrrhenian basin. J. Volcanol. Geotherm. Res., 88(4), 291– 304.

Etiope G, Klusman RW, 2002. Geologic emissions of methane to the atmosphere. Chemosphere 49, 777–789.

European Commission, 2013. Communication from the Commission to the European Parliament, the Council, the European Economic and Social Committe and the Committe of the Regions on the Future of Carbon Capture and Storage in Europe.

Ferri D, Grenthe I, Hietanen S, Salvatore F, 1987a. Studies on metal carbonate equilibria 17. Zinc (II) carbonate complexes in alkaline solutions. Acta Chem. Scand. A 41:190.

Ferri D, Grenthe I, Hietanen S, Salvatore F, 1987b. Studies on metal carbonate equilibria 18. Lead (II) carbonate complexes in alkaline solutions. Acta Chem. Scand. A 41: 349.

Fischer S, Liebscher A, Wandrey M, CO2SINK Group, 2010. CO_2–brine–rock interaction - first results of long-term exposure experiments at in situ P–T conditions of the Ketzin CO_2 reservoir. Chem. Erde 70(3): 155–164.

Ford RG, Bertsch PM, Farley KJ, 1997. Changes in Transition and Heavy Metal Partitioning during Hydrous Iron Oxide Aging. Environ. Sci. Technol., 31 (7), pp 2028–2033.

Fouillac C, Criaud A, 1984. Carbonate and bicarbonate trace metal complexes: Critical reevaluation of stability constants. Geochem. J. 18, 297–303.

Frye E, Bao C, Li L, Blumsack S, 2012. Environmental controls of cadmium desorption during CO_2 leakage. Environ. Sci. Technol. 46, 4388–4395.

Giffaut E, Grivé M, Blanc P, Vieillard P, Colàs E, Gailhanou H, Gaboreau S, Marty N, Madé B, Duro L, 2014. Andra thermodynamic data for performance assessment: ThermoChimie. Applied Geochemistry (in press).

Gold T and Soter S, 1982. Abiogenic methane and the origin of petroleum. Energy Explor. Exploit 1, pp. 89–104.

Grivé M, 2005. The linkage between uranium, iron and carbon cycling, processes at interfaces: evidences from combined solution chemical and spectroscopic studies. Ph.D. Thesis. Universitat Politècnica de Catalunya, Barcelona.

Grivé M, Duro L, Bruno J, 2013. Fe(III) mobilization by carbonate in low temperature environments: study of the solubility of ferrihydrite in carbonate media and the formation of Fe(III) carbonate complexes. Submitted to Geoch. Cosmoch. Acta.

Grivé M, Duro L, Bruno J, 2014a. Fe(III) mobilization by carbonate in low temperature environments: study of the solubility of ferrihydrite in carbonate media and the formation of Fe(III) carbonate complexes. Applied Geochemistry.

Grivé M, Duro L, Bruno J, 2014b. Fe(III) mobilization by carbonate in low temperature environments 2: the applicability of the thermodynamic scheme including Fe(III) carbonate complexes to explain the increased Fe(III) concentrations in CO2-rich waters (In press).

Grivé M, Duro L, Colàs E, Giffaut L, 2014. Thermodynamic data selection applied to radionuclide and chemotoxic elements: an overview of the ThermoChimie-TDB. Applied Geochemistry (in press).

Harvey OR, Brown CF, Qafoku NP, Cantrell KJ, Lee G, Amonette JE, 2012. Geochemical Implications of Gas Leakage associated with Geologic CO_2 Storage - A Qualitative Review. Environmental Science & Technology.

Hawkesworth CJ, Hergt JM, McDermott F, Ellam RM, 1991. Destructive margin magmatism and the contribution from the mantle wedge and subducted crust. Aust. J. Earth Sci. 38, 577– 594.

Hem JD, 1985. Study and interpretation of the Chemical Characteristics of Natural Water, 3rd ed. Alexandria, VA: Department of the Interior, U.S. Geological Survey, Water-Supply Paper 2254. Hem JD. 1989. Study and interpretation of the chemical characteristics of natural water. USGS Water-Supply Paper 2254; U.S. Geological Survey: Washington, D.C.

Hietanen S, Högfeldt E, 1976. A potentiometric study of the solid phases in the systems Hg(I)-HCO_3^- and Hg(II)-HCO_3^-. Chem. Scripta 9: 24-29.

Houghton JT, Filho LGM, Callander BA, Harris N, Kattenberg A and Makell K, editors, Cambridge University Press, 1996. Climate Change 1995- The Science of climate change.

Huanga D, Makhlynetsb OV, Tanc LL, Leec SC, Rybak-Akimovab EV, Holma RH, 2011. Kinetics and mechanistic analysis of an extremely rapid carbon dioxide fixation reaction. Proc. National Acad. Sciences 108: 1222-1227.

Humez P, Négrel P, Lagneau V, Lions J, Kloppmann W, Gal F, Millot R, Guerrot C, Flehoc C, Widory D, Girard JF, 2013. CO_2–water–mineral reactions during CO2 leakage: Geochemical and isotopic monitoring of a CO_2 injection field test. Chemical Geology 368 (2014) 11–30.

Hummel W, 2000. Comment on "On the influence of carbonate in mineral dissolution: 1. The thermodynamics and kinetics of hematite dissolution in bicarbonate solutions at t= 25ºC" by J. Bruno, W. Stumm, P. Wersin and F. Brandberg. Geochim. Cosmochim. Acta 64(12), 2167–2171.

IGME, 1983. Mapa Geológico de España 1:200.000. Ciudad Real (61). Memoria y mapa. Instituto Geológico y Minero de España (IGME), Ministerio de Industria y Energía, Madrid.

IGME, 1988a. Mapa Geológico de España 1:50.000. Ciudad Real (784). Memoria y mapa. Instituto Geológico y Minero de España (IGME), Ministerio de Industria y Energía, Madrid.

IGME, 1988b. Mapa Geológico de España 1:50.000. Almagro (785). Memoria y mapa. Instituto Geológico y Minero de España (IGME), Ministerio de Industria y Energía, Madrid.

Indermühle A, Stocker TF, Joos F, Fischer H, Smith HJ, Wahlen M, Deck B, Mastroianni D, Tschumi J, Blunier T, Meyer R and Stauffer B, 1999. Holocene carbon-cycle dynamics based on CO_2 trapped in ice at Taylor Dome, Antartica. Nature, 298, pp. 121-126.

IPCC, 2005. Special Report on Carbon Capture and Storage. (Ed C. U. Press), United Kingdom and New York, NY, USA: Intergovernmental Panel on Climate Change Groupe III [Metz, B., Davidson O. De Coninck H. C. Loos M. Meyer L. A.].

Jambor JL and Dutrizac JE, 1998. Occurrence and constitution of natural synthetic ferrihydrite, a widespread iron oxyhydroxide. Chem. Rev. 98, 2549-2585.

Keating E, Fessendem J, Kanjorski N, Koning D, Pawar R, 2010. The impact of CO_2 on shallow groundwater chemistry: Observation at a natural analogue site and implication for carbon sequestration. Environmental Earth Sciences 60, 521-536.

Keating EH, Hakala JA, Viswanathan H, Carey JW, 2013. CO_2 leakage impacts on shallow groundwater: Field-scale reactive-transport simulations informed by observations at a natural analog site. App. Geochem 30: 136-147

Kerrick DM, McKibben MA, Seward TM, Caldeira K, 1995. Convective hydrothermal CO_2 emission from high heat flow region. Chem. Geol., 121, 285-293.

Kerrick, DM, 2001. Present and past nonanthropogenic CO_2 degassing from the solid. Earth Rev. Geophys. 39, 565– 585.

Kharaka YK, Cole DR, Hovorka SD, Gunter WD, Knauss KG, Freifeld BM, 2006. Gas–water–rock interactions in Frio Formation following CO_2 injection: Implications for the storage of greenhouse gases in sedimentary basins. Geology 34: 577–580.

Kharaka YK and Hanor JS, 2007. Deep fluids in the continents: I. Sedimentary Basins. In: Drever J.I, (Ed.).

Kharaka YK, Thordsen JJ, Hovorka SD, Nance HS, Cole DR, Phelps TJ, Knauss KG, 2009. Potential environmental issues of CO_2 storage in deep saline aquifers: geochemical results from the Frio-I Brine pilot test, Texas, USA. Applied Geochemistry 24: 1106-1112.

Kharaka YK, Thordsen JJ, Kakouros E, Ambats G, Herkelrath WN, Beers SR, Birkholzer JT,

Apps JA, Spycher NF, Zheng L, Trautz RC, Rauch HW, Gullickson KS, 2010. Changes in the chemistry of shallow groundwater related to the 2008 injection of CO_2 at the ZERT field site, Bozeman, Montana. Environ. Earth Sci. 60, 273–284.

Kitajima N, Fujisawa K, Koda T, Hikichi S, Morooka Y, 1990. Fixation of atmospheric CO_2 by a copper(II) Complex. Chem Commun 1357–1358.

Kitajima N, Hikuchi S, Tanaka M, Moro-oka Y, 1993. Fixation of atmospheric CO_2 by aseries of hydroxo complexes of divalent metal ions and the implication for the catalytic role of metal ion in carbonic anhydrase Synthesis, characterization, and molecular structure of .LM.OH._n (n . 1 or 2) and LM.μ-CO3.ML (M.II. . Mn, Fe, Co, Ni, Cu, Zn; L . HB.3;5-i Pr2 pz.3). J Am Chem Soc 115: 5496–5508.

Larson TE, 1967. Oxidation of metals and anions in solution. In Principles and Applications of Water Chemistry (eds. D. Faust and J. V. Hunter) J. Wiley and Sons.

Lelieveld J, Crutzen PJ, Dentener FJ, 1998. Changing concentration, lifetime and climate forcing of atmospheric methane. Tellus Ser. B 50B:128–150.

Lewicki JL, and Brantley SL, 2000. CO_2 degassing along the San Andreas fault, Parkfield, California. Geophys. Res. Lett., 27(1), 5 – 8.

Lions J, Devau N, De Lary L, Dupraz S, Parmentier M, Gombert P, Dictor MC, 2014. Potential impacts of leakage from CO_2 geological storage on geochemical processes controlling fresh groundwater quality: A review. International Journal of Greenhouse Gas Control 22:165–175. DOI: 10.1016/j.ijggc.2013.12.019.

Lions J, Humez P, Pauwels H, Kloppmann W, Czernichowski-Lauriol I, 2014. Tracking leakage from a natural CO_2 reservoir (Montmiral, France) through chemistry and iso- tope signatures of shallow groundwaters. GHGS&T, in press.

Little MG, Jackson RB, 2010. Potential impacts of leakage from deep CO_2 geosequestration on overlying freshwater aquifers. Environ. Sci. Technol. 44, 9225–9232.

Loke MH, Barker RD, 1996. Rapid least-squares inversion of apparent resistivity pseudosecions by a quasi-Newton method. Geophys. Prospect. 44 (1), 131-152.

Loke MH, 2014. Tutorial: 2D and 3D electrical imaging surveys. Geotomo Software, Gelugor, Malaysia., pp. 169. Accessed 2014-04-02 from (www.geotomosoft.com).

López-Ruiz J, Cebriá JM, Doblas M, 2002. Cenozoic volcanism I: the Iberian Peninsula. In: Gibbons, W., Moreno, T. (Eds.), The Geology of Spain. The Geological Society, London, pp. 417-438.

Lu JM, Partin JW, Hovorka SD, Wong C, 2010. Potential risks to freshwater resources as a result of leakage from CO_2 geological storage: a batch-reaction experiment. Environ. Earth Sci. 60, 335–348.

Luther GW, Kostka JE, Church TM, Sulzberger B, Stumm W, 1992. Seasonal iron cycling in the salt-marsh sedimentary environment: The importance of ligand complexes with Fe(II) and Fe(III) in the dissolution of Fe(III) minerals and pyrite respectively. Mar. Chem. 40: 81-103.

Mahon WAJ, McDowell GD, Finlayson JB, 1980. Carbon dioxide: its role in geothermal systems. New Zealand Journal of Science 23, 133-148.

Mas-Pla J, 1986. Aportació al coneixement de la dinàmica fluvial en la conca del riu Onyar (Girona). Scientia gerundensis, 12:173-18

Mattigod S and Sposito G, 1977. Estimated association constants for some complexes of trace metals with inorganic ligands. Soil Sci. Soc. Am. J. 41(6), 1092–1097.

McMahon PB and Chapelle FH, 1991. Microbial production of organic acids in aquitard sediments and its role in aquifer geochemistry. Nature. 34, 233-235

McMahon PB and Chapelle FH, 2008. Redox processes and water quality of selected principal aquifers systems. Groundwater 46, 259-271

Menció i Domingo A, 2005. Ph.D. Thesis. Anàlisi multidisciplinaria de l'estat de l'aigua a la depressío de la Selva.

Miller M, Alexander R, Chapman N, McKinley I, Smellie J, 2000. Geological disposal of radioactive wastes and natural analogues. Waste Management Series vol 2. Permagon. The Netherlands.

Minissale A, Magro G, Martinelli G, Vaselli O, Tassi F, 2000. Fluid geochemical transect in the Northern Apennines (central– northern Italy): fluid genesis and migration and tectonic implications. Tectonophysics 319, 199–222.

Minissale A, 2004. Origin, transport and discharge of CO_2 in central Italy. Earth-Science Reviews 66, 89–141

Montes-Hernandez G, Renard F, Lafay R, 2013. Experimental assessment of CO_2–mineral-toxic ion interactions in a simplified freshwater aquifer: implications for CO_2 leakage from deep geological storage. Environmental Science & Technology 47, 6247–6253.

Murthy NN, Karlin KD, 1993. A Dinuclear Zinc-Hydroxide Complex which Traps Atmospheric Carbon Dioxide: Formation of a Tri-Zinc complex with a Triply-Bridging Carbonate group. J. Chem. Soc., Chem. Commun 1236-1238.

Navarre-Sitchler AK, Maxwell RM, Siirila ER, Hammond GE, Lichtner PC, 2013. Elucidating geochemical response of shallow heterogeneous aquifers to CO2 leakage using high-performance computing: implications for monitoring of CO_2 sequestration. Adv. Water Resour. 53, 45–55.
Nordstrom DK and Puigdomenech I, 1986. Redox chemistry of deep ground-waters in Sweden. Technical report, SKB.

Oliver J, 1986. Fluids expelled tectonically from orogenic belts: their role in hydrocarbon migration and other geologic phenomena. Geology 14, 99– 102.

Pallí L, Trilla J, Estalrich J, 1983. Mapa morfològic de la depressió de la Selva. Unitat de Geodinàmica Externa i Hidrogeologia UAB i Dept. De Geologia del Col·legi Universitari de Girona.

Pallí L and Roqué C, 1995. El vulcanisme de les comarques gironines, II: el Gironès. Diputació de Girona. Àrea de Geodinàmica de la Universitat de Girona.

Parkhurst DL and Appelo CAJ, 2013. Description of input and examples for PHREEQC version 3--A computer program for speciation, batch-reaction, one-dimensional transport, and inverse geochemical calculations: U.S. Geological Survey Techniques and Methods, book 6, chap. A43, 497 p.

Payán MC, Verbinnen B, Galan B, Coz A, Vandecasteele C, Viguri JR, 2012. Potential influence of CO_2 release from a carbon capture storage site on release of trace metals from marine sediment. Environmental Pollution 162: 29-39.

Peacock SM, 1990. Fluid processes in subduction zones. Science 248, 329– 337.

Pérez N.M, Nakai S, Wakita H, Albert-Bertrán JF i Redondo R, 1996. Preliminary results on 3He/4He isotopic ratios in terrestrial fluids from Iberian peninsula: seismotectonic and neotectonic implications. Geogaceta, 20, 830-833.

Person M and Baumgartner L, 1995. New evidence for long distance fluid migration within the Earth's crust. Rev. Geophys Suppl., U.S. Nat. Rep. Intern. Union of Geodesy and Geophys. 1991–1994, pp. 1083–1091.

Peter A, Lamert H, Beyer M, Hornbruch G, Heinrich B, 2012. Investigation of the geochemical impact of CO_2 on shallow groundwater: design and implementation of a CO_2 injection test in Northeastern Germany. Environ. Earth Sci. 67: 335-349.

Piqué A, Grandia F, Canals A, 2010. Processes releasing arsenic to groundwater in the Caldes de Malavella geothermal area, NE Spain. Water Res 44: 5618–5630 .

Poblete MA, 1992. Las últimas manifestaciones asociadas al vulcanismo del campo de Calatrava (Ciudad Real). Los manantiales termales. Eusko Ikaskuntza, Donostia. Cuadernos de Sección. Historia, nº 20, 187-201.

Pous J, Sole Sugrañes LL, Badiella P, 1990. Estudio geoelectrico de la depresion de La Selva (Girona). ACTA GEOLOGICA HISPANICA, v. 25, n' 4, pags. 261 - 269

Puigdomènech I, 2013. http://www.kemi.kth.se/medusa/

Rempel KU, Liebscher A, Heinrich W, Schettler G, 2011. An experimental investigation of trace element dissolution in carbon dioxide: Applications to the geological storage of CO_2. Chemical Geology 289: 224–234.

Rillard J, (Thèse de l'université de Lyon 1) 2013. CO_2 Perturbations in Aquifers: Reaction Kinetics and Metal Behavior.

Rolandi M, Barrera JL, 2003. Los volcanes del Campo de Calatrava. In: R. Nuche (Ed.), Patrimonio Geológico de Castilla-La Mancha. Enresa, pp. 478-509.

Romanó de Orte M, Sarmiento AM, Basallote MD, Rodríguez-Romero A, Riba I, DelValls A, 2014. Effects on the mobility of metals from acidification caused by possible CO_2 leakage from sub-seabed geological formations. Science of the Total Environment 470–471, 356–363

Sadler GG, Dasgupta TP, 1987. Dinuclear complexes of transition metals containing carbonate ligands 7. Kinetics and Mechanism of Formation of μ-(carbonato) bis (μ-hydroxo) bis (triamminecobalt(III)) ion in weakly basic aqueous carbonate. Inorg. Chem, 26: 3254-3257.

Schindler P, Michaelis W, Feitknecht W, 1963. Löslichkeitsprodukte von metalloxiden und –hydroxiden. 8. mitt.: Die löslichkeit gealterter eisen (III-hydroxidfällungen. Helv. Chim. Acta. 46, 444–451.

Schultz MF, Benjamin MM, Ferguson JF, 1987. Adsorption and Desorption of Metals on Ferrihydrite: Reversibility of the Reaction and Sorption Properties of the Regenerated Solid. Environ. Sci. Technol., 21, pp. 863-869.

Schwertmann UI and Cornell RM, 1991. Iron oxides in the laboratory. VCH, Weinheim, 137pp.

Seward TM, and Kerrick DM, 1996. Hydrothermal CO_2 emission from the Taupo Volcanic Zone, New Zeland. Earth Planet. Sci. Let., 139, 105-113.

Siirila ER, Navarre-Sitchler AK, Maxwell RM, McCray JE, 2012. A quantitative methodology to assess the risks to human health from CO2 leakage into groundwater. Adv. Water Resour. 36, 146–164.

Spangler LH, Dobeck LM, Repasky KS, Nehrir AR, Humphries SD, 2010. A shallow subsurface controlled release facility in Bozeman, Montana, USA, for testing near surface CO_2 detection techniques and transport models. Environ. Earth Sci. 60: 227–239.

Spitzer U, Van Eldik R, Kelm H, 1982. Mechanistic information from the effect of pressure on the formation and acid-catalyzed aquation reactions of (carbonato)pentaamminecobalt(III), -rhodium(III), and -iridium(III) ions in aqueous solution. Inorg. Chem. 21 (7): 2821–2823.

Stumm W, 1992. Chemistry of the solid-water interface. Processes at the mineral-water and particle-water interface in natural systems. John Wiley & Sons, Inc.

Stumm W and Sulzberger B, 1992. The cycling of iron in natural environments: Considerations base on laboratory studies of heterogeneous redox processes. Geochim. Cosmochim. Acta 56: 3233-3257.

Sverjensky DA, Garven G, 1992. Tracing great fluid migrations. Nature 356, 481– 482.

Tans PT, Kieling R, 2014. NOAA/ESRL (www.esrl.noaa.gov/gmd/ccgg/trends/). Scripps Institution of Oceanography (scrippsco2.ucsd.edu/).

Tassi F, Montegrossi G, Vaselli O, 2004. Metodologie di campionamento ed analisi di fasi gassose. Rapporto Interno n. 1/2003 del CNR-IGG Istituto di Geoscienze e Georisorse, Unità di Firenze.

Tassi F, Vaselli O, Luchetti G, Montegrossi G and Minissale A, 2008. Metodo per la determinazione dei gas disciolti in acque naturali. CNR-IGG Rapporto Interno n. 2/2008, p. 10.

Trautz R, Pugh J, Varadharajan C, Zheng L, Bianchi M, Nico PS, Spycher N, Newell DL, Esposito RA, Wu Y, 2013. Effect of dissolved CO_2 on a shallow groundwater system: a controlled release field experiment. Environ. Sci. Technol. 47, 298–305.

U.S. Environmental Protection Agency, 1998. MINTEQA2/PRODEFA2, A Geochemical Assessment Model for Environmental Systems: User Manual Supplement for Version 4.0

Vaselli O, Nisi B, Tassi F, Gianninni L, Grandia F, Darrah T, Capecchiacci F and Pérez del Villar, L, 2013. Water and gas geochemistry of the Calatrava Volcanic Province (CVP) hydrothermal System (Ciudad Real, central Spain). Geophysical Research Abstracts, Vol. 15, 10th EGU General Assembly, EGU2013-11102.

Vegas R, Rincón-Calero PJ, 1996. Campos de esfuerzos, deformación alpina y volcanismo neógeno-cuaternario asociado en el antepaís bético de la provincia de Ciudad Real (España central). Geogaceta 19, 31-34.

Vilanova E, 2004. Anàlisi dels sistemes de flux a l'àrea Gavarres-Selva-Baix Empordà. PhD thesis, Universitat Autònoma de Barcelona, 337 pp.

Viswanathan H, Dai Z, Lopano C, Keating E, Hakala JA., Scheckel KG, Zheng L, Guthrie GD, Pawar R, 2012. Developing a robust geochemical and reactive trans- port model to evaluate possible sources of arsenic at the CO_2 sequestration natural analog site in Chimayo, New Mexico. J. Greenhouse Gas Control 10, 199–214.

Waite TD, Davis JA, Payne TE, Waychumas GA, Xu N, 1994. Uranium(VI) adsorption to ferrihydrite: Application of a surface complexation model. Geochim. Cosmochim. Acta, 58(24): 5465-5478.

Wang S and Jaffe PR, 2004. Dissolution of a mineral phase in potable aquifers due to CO_2 releases from deep formations; effect of dissolution kinetics. Energ. Convers. Manage. 45, 2833–2848.

Wei Y, Maroto-Valer M, Steven MD, 2011. Environmental consequences of potential leaks of CO_2 in soil. Energy Proc. 4, 3224–3230.

Wigand M, Carey JW, Schütt H, Spangenberg E, Erzinger J, 2008. Geochemical effects of CO_2 sequestration in sandstones under simulated in situ conditions of deep saline aquifers. Appl. Geochem. 23: 2735–2745.

Wilkin RT, DiGiulio DC, 2010. Geochemical impacts to groundwater from geologic carbon sequestration: controls on pH and inorganic carbon concentrations from reaction path and kinetic modeling. Environ. Sci. Technol. 44, 4821–4827.

Wunsch A, Navarre-Sitchler AK, Moore J, Ricko A, McCray JE, 2013. Metal release from dolomites at high partial-pressures of CO2. Applied Geochemistry 38, 33–47.

Yardley B, Bennet A, Banks D, 2003. Controls on the chemical composition of crustal brines. Journal of geochemical Exploration. 78-79, 133-135.

Yélamos JG, Redondo R, De Castro F, Galván A, Martínez-Rubio J, Rebollo L, Ruano P, Senderos A, Villarroya FI, 1999. Hidrogeoquímica y microbiología en Los Hervideros del Campo de Calatrava (Ciudad Real). Geogaceta 26, 115-118.

Zeebe RE and Wolf-Gladrow D, 2001. CO_2 in seawater: equilibrium, kinetics, isotopes. Volume 65 (Elsevier Oceanography Series).

Zhang H and Davison W, 1995. Performance Characteristics of Diffusion Gradients in Thin-Films for the measurement of trace-Metals in Aqueous-Solution. Analytical Chemistry 67: 3391-3400.

Zheng L, Apps JA, Zhang Y, Xu T, Birkholzer JT, 2009. On the mobilization of lead and arsenic in groundwater in response to CO_2 leakage from deep geological storage. Chem. Geol. 268: 281-297.

Zheng L, Apps JA, Spycher N, Birkholzer JT, Kharaka YK, James Thordsen J, Sarah R, Beers SR, Herkelrath WN, Kakouros E, Trautz RC, 2011. Geochemical modeling of changes in shallow groundwater chemistry observed during the MSU-ZERT CO_2 injection experiment. Intern. Journ. Greenh. Gas Cont.

Zheng L, Apps JA, Spycher N, Birkholzer JT, Kharaka YK, Thordsen J, Beers SR, Herkelrath WN, Kakouros E, Trautz RC, 2012. Geochemical modeling of changes in shallow groundwater chemistry observed during the MSU-ZERT CO_2 injection experiment. Int. J. Greenhouse Gas Control 7, 202–217.

Annexes:

Annex 1: Chemistry of the CO_2-bearing springs sampled in Campo de Calatrava (central Spain). Major ions (in mmol·L^{-1}).

Sample	T °C	Ph	Eh	Cond.	HCO_3^- (mmol/l)	F^- (mmol/l)	Cl^- (mmol/l)	Br^- (mmol/l)	NO_3^- (mmol/l)	SO_4^{2-} (mmol/l)	Ca^{2+} (mmol/l)	Mg^{2+} (mmol/l)	Na^+ (mmol/l)	K^+ (mmol/l)	NH_4^+ (mmol/l)
Chorro Glicerio	16.9	6.1	181	3660	40.67	0.022	4.880	0.006	0.082	3.873	11.827	25.345	9.965	1.688	0.011
Chorro Vil Elen	18.8	6.0	180	2390	25.99	0.027	2.200	0.004	0.029	1.291	8.234	16.540	4.221	1.228	0.009
Fontecha 1	18.4	5.9	207	2430	16.33	0.031	5.021	0.005	0.003	5.226	3.289	8.969	13.098	1.120	0.069
Fontecha 2	22.4	5.9	295	2310	16.75	0.038	5.275	0.005	0.005	5.559	3.244	9.134	14.099	1.105	0.085
Fontecha 3	21.5	6.1	313	2440	17.23	0.045	5.811	0.004	0.015	5.455	3.403	9.463	13.621	1.095	0.054
Fontecha 4	27.1	5.9	17	1720	13.61	0.025	3.103	0.004	0.047	3.061	2.780	6.994	8.660	0.921	0.032
Cañada Real	21.8	6.1	282	3910	34.59	0.025	7.926	0.010	0.001	6.350	7.535	19.091	20.279	2.052	0.058
Baño Chico	21.6	6.1	360	1600	16.53	0.030	1.275	0.002	0.001	1.162	3.568	10.533	3.412	0.701	0.027
Baño Chiquillo	25.2	6.4	-52	1714	18.11	0.041	1.391	0.001	0.013	1.272	6.188	9.298	3.695	0.796	0.047
Codo Jabalon	18.2	5.9	2111	1345	15.97	0.031	3.780	0.004	0.001	3.831	3.408	9.381	9.225	0.816	0.018
Barranko Grande	21.0	6.1	167	2000	17.27	0.030	2.905	0.003	0.016	2.790	3.808	10.533	7.224	1.016	0.013
Hervidero Nuevo	21.0	6.0	213	1626	11.08	0.038	2.194	n.d.	0.006	1.924	2.730	5.612	4.830	0.675	0.087

Annex 2: Chemistry of the CO_2-bearing springs sampled in Campo de Calatrava (central Spain). Major ions (in mg·L^{-1})

Sample	T °C	pH	Eh	Cond.	HCO_3^- (mg/l)	F^- (mg/l)	Cl^- (mg/l)	Br^- (mg/l)	NO_3^- (mg/l)	SO_4^{2-} (mg/l)	Ca^{2+} (mg/l)	Mg^{2+} (mg/l)	Na^+ (mg/l)	K^+ (mg/l)	NH_4^+ (mg/l)
Chorro Glicerio	16.9	6.1	181	3660	2482	0.42	173	0.49	5.1	186	237	308	229	66	0.2
Chorro Vil Elen	18.8	6.0	180	2390	1586	0.52	78	0.29	1.8	62	165	201	97	48	0.17
Fontecha 1	18.4	5.9	207	2430	996.74	0.58	178	0.38	0.216	251	65.9	109	301	43.8	1.24
Fontecha 2	22.4	5.9	295	2310	1022.36	0.72	187	0.397	0.303	267	65	111	324	43.2	1.53
Fontecha 3	21.5	6.1	313	2440	1051.64	0.855	206	0.308	0.928	262	68.2	115	313	42.8	0.977
Fontecha 4	27.1	5.9	17	1720	830.82	0.472	110	0.296	2.92	147	55.7	85	199	36	0.58
Cañada Real	21.8	6.1	282	3910	2110.60	0.472	281	0.773	0.052	305	151	232	466	80.2	1.04
Baño Chico	21.6	6.1	360	1600	1009.00	0.57	45.2	0.179	0.065	55.8	71.5	128	78.4	27.4	0.484
Baño Chiquillo	25.2	6.4	-52	1714	1105.32	0.78	49.3	0.08	0.801	61.1	124	113	84.9	31.1	0.841
Codo Jabalon	18.2	5.9	2111	1345	974.78	0.596	134	0.329	0.059	184	68.3	114	212	31.9	0.319
Barranko Grande	21.0	6.1	167	2000	1054.08	0.571	103	0.201	0.964	134	76.3	128	166	39.7	0.233
Hervidero Nuevo	21.0	6.0	213	1626	675.88	0.731	77.8	n.d.	0.373	92.4	54.7	68.2	111	26.4	1.56

Annex 3: Concentration of trace metals and metalloids in CO_2-impacted shallow aquifers in the Campo de Calatrava region (in mol·L^{-1}).

Sample	T °C	pH	Eh	Conduct	Al (mmol/l)	Mn (mmol/l)	Fe (mmol/l)	Cr (µmol/l)	Co (µmol/l)	Ni (µmol/l)	Cu (µmol/l)	Zn (µmol/l)	As (µmol/l)	Cd (µmol/l)	Pb (µmol/l)	Th (µmol/l)	U (µmol/l)
Chorro Glicerio	16.9	6.1	181	3660	0.001	0.080	0.126	0.078	0.716	1.189	< 0.005	1.464	0.025	< 0.005	< 0.005	<0.05	<0.05
Chorro Vil Elena	18.8	6.0	180	2390	0.002	0.022	0.280	0.130	0.234	0.690	< 0.005	0.735	0.025	< 0.005	< 0.005	<0.05	<0.05
Fontecha 1	18.4	5.9	207	2430	0.004	0.014	0.603	0.040	0.275	0.949	0.310	0.915	0.142	< 0.005	< 0.005	<0.05	<0.05
Fontecha 2	22.4	5.9	295	2310	< 0.001	0.013	0.521	0.043	0.175	0.580	0.330	0.382	0.082	< 0.005	< 0.005	<0.05	<0.05
Fontecha 3	21.5	6.1	313	2440	< 0.001	0.005	0.001	0.042	0.064	0.460	0.335	0.405	< 0.005	< 0.005	< 0.005	<0.05	<0.05
Fontecha 4	27.1	5.9	17	1720	< 0.001	0.019	0.047	0.021	0.331	0.784	0.154	1.183	0.017	< 0.005	< 0.005	<0.05	<0.05
Cañada Real	21.8	6.1	282	3910	< 0.001	0.006	0.016	0.100	0.097	0.297	< 0.005	0.438	0.009	< 0.005	< 0.005	<0.05	<0.05
Baño Chico	25.2	6.1	360	1714	< 0.001	0.016	0.025	0.023	0.378	0.620	0.174	0.686	0.041	< 0.005	< 0.005	<0.05	<0.05
Baño Chiquillo	21.6	6.4	-52	1600	< 0.001	0.012	0.000	0.028	0.281	0.973	0.210	0.524	< 0.005	< 0.005	< 0.005	<0.05	<0.05
Codo Javalon	18.2	5.9	2111	1345	< 0.001	0.011	0.389	0.039	0.227	0.740	0.315	0.740	0.076	< 0.005	< 0.005	<0.05	<0.05
Herv. Nuevo	21	6.1	167	1626	0.004	0.018	0.373	0.035	0.316	0.816	0.270	1.030	0.053	< 0.005	< 0.005	<0.05	<0.05
Barranco Grande	21	6.0	213	2000	< 0.001	0.025	0.601	0.036	0.335	0.626	0.297	0.382	0.087	< 0.005	< 0.005	<0.05	<0.05

Annex 4: Concentration of trace metals and metalloids in CO_2-impacted shallow aquifers in the Campo de Calatrava region (in $mg \cdot L^{-1}$ and $\mu g \cdot L^{-1}$).

Sample	T °C	pH	Eh	Conduct	Al (mg/l)	Mn (mg/l)	Fe (mg/l)	Cr (µg/l)	Co (µg/l)	Ni (µg/l)	Cu (µg/l)	Zn (µg/l)	As (µg/l)	Cd (µg/l)	Pb (µg/l)	Th (µg/l)	U (µg/l)
Chorro Glicerio	16.9	6.1	181	3660	0.027	4.4	7.0	4.0	42	70	< 2.5	96	1.9	< 0.5	< 0.5	< 0.5	12
Chorro Villa Elena	18.8	6.0	180	2390	0.055	1.2	16	6.7	14	41	< 2.5	48	1.9	< 0.5	< 0.5	< 0.5	1.1
Fontecha 1	18.4	5.9	207	2430	0.097	0.80	34	2.1	16	56	20	60	11	< 0.5	< 0.5	< 0.5	0.57
Fontecha 2	22.4	5.9	295	2310	0.03	0.72	29	2.2	10	34	21	25	6.1	< 0.5	< 0.5	< 0.5	< 0.5
Fontecha 3	21.5	6.1	313	2440	< 0.025	0.26	0.078	2.2	3.7	27	21	26	< 0.5	< 0.5	< 0.5	< 0.5	0.61
Fontecha 4	27.1	5.9	17	1720	< 0.025	1.0	2.6	1.1	20	46	9.8	77	1.3	< 0.5	< 0.5	< 0.5	< 0.5
Cañada Real	21.8	6.1	282	3910	< 0.025	0.34	0.90	5.2	5.7	17	< 2.5	29	0.66	< 0.5	< 0.5	< 0.5	3.1
Baño Chico	25.2	6.1	360	1714	< 0.025	0.89	1.4	1.2	22	36	11	45	3.0	< 0.5	< 0.5	< 0.5	1.0
Baño Chiquillo	21.6	6.4	-52	1600	< 0.025	0.65	0.025	1.4	17	57	13	34	< 0.5	< 0.5	< 0.5	< 0.5	0.52
Codo Javalon	18.2	5.9	2111	1345	< 0.025	0.63	22	2.0	13	43	20	48	5.7	< 0.5	< 0.5	< 0.5	2.6
Herv. Nuevo	21	6.1	167	1626	0.098	0.99	21	1.8	19	48	17	67	4.0	< 0.5	< 0.5	< 0.5	< 0.5
Barranco Grande	21	6.0	213	2000	< 0.025	1.4	34	1.9	20	37	19	25	6.5	< 0.5	< 0.5	< 0.5	0.54

Annex 5: Chemistry of the Font Groga CO_2-bearing spring (in mol·L^{-1}).

Sample	Distance (m)	T °C	pH	Eh	Cond.	HCO_3^- (mmol/l)	F^- (mmol/l)	Cl^- (mmol/l)	Br^- (mmol/l)	NO_3^- (mmol/l)	SO_4^{2-} (mmol/l)	Ca^{2+} (mmol/l)	Mg^{2+} (mmol/l)	Na^+ (mmol/l)	K^+ (mmol/l)	NH_4^+ (mmol/l)
Spring	0.0	17.1	6.4	168	6470	55.85	0.05	18.79	0.03	0.05	5.98	16.52	6.83	59.09	0.79	0.01
Point 1	13.2	16.3	6.5	189	6620	55.09	0.02	19.72	0.03	<0.05	6.29	16.52	6.83	58.92	0.92	0.01
Point 2	16.2	15.2	6.5	195	6630	56.00	0.02	19.12	0.03	<0.05	6.12	16.52	6.75	58.53	0.82	0.01
Point 3	21.2	15.8	6.7	198	6570	55.90	0.02	19.32	0.03	<0.05	6.18	16.52	6.83	58.92	0.87	0.01
Point 4	27.2	15.5	6.9	188	6640	57.60	0.03	19.41	0.04	<0.05	6.18	16.52	6.75	58.66	0.77	0.02
Point 5	30.9	15.3	6.9	180	6660	56.90	0.02	18.93	0.03	<0.05	6.16	16.52	6.58	57.66	0.82	0.01
Point 6	38.3	15.0	7.0	189	6630	57.29	0.02	19.21	0.03	0.03	6.52	16.52	6.99	60.62	0.87	0.02
Point 7	46.8	14.6	7.1	197	6630	57.47	0.02	19.74	0.03	0.03	6.62	16.52	6.75	58.27	0.79	0.02
Point 8	56.0	13.7	7.2	214	6560	55.95	0.03	18.90	0.03	0.03	6.00	16.52	6.67	58.09	0.77	0.02

Annex 6: Chemistry of the Font Groga CO_2-bearing spring (in $mg \cdot L^{-1}$).

Sample	Distance (m)	T °C	pH	Eh	Cond..	HCO_3^- (mg/l)	F^- (mg/l)	Cl^- (mg/l)	Br^- (mg/l)	NO_3^- (mg/l)	SO_4^{2-} (mg/l)	Ca^{2+} (mg/l)	Mg^{2+} (mg/l)	Na^+ (mg/l)	K^+ (mg/l)	NH_4^+ (mg/l)
Spring	0.0	17.1	6.4	168	6470	3408	0.89	666	2.06	3.22	287	331	83	1358	31	0.14
Point 1	13.2	16.3	6.5	189	6620	3362	0.38	699	2.27	<1.00	302	371	83	1354	36	0.18
Point 2	16.2	15.2	6.5	195	6630	3417	0.46	678	2.10	<1.00	294	340	82	1345	32	0.18
Point 3	21.2	15.8	6.7	198	6570	3411	0.31	685	2.45	<1.00	297	343	83	1354	34	0.23
Point 4	27.2	15.5	6.9	188	6640	3515	0.55	688	2.89	<1.00	297	323	82	1348	30	0.31
Point 5	30.9	15.3	6.9	180	6660	3472	0.29	671	2.17	<1.00	296	344	80	1325	32	0.13
Point 6	38.3	15.0	7.0	189	6630	3496	0.29	681	2.11	1.57	313	338	85	1393	34	0.27
Point 7	46.8	14.6	7.1	197	6630	3507	0.41	700	2.50	2.00	318	318	82	1339	31	0.29
Point 8	56.0	13.7	7.2	214	6560	3414	0.53	670	2.20	2.10	288	320	81	1335	30	0.39

Annex 7: Concentration of trace metals and metalloids in Font Groga stream (in mmol·L^{-1}).

Sample	T °C	pH	Eh	Cond.	Fe (mmol/l)	Mn (µmol/l)	Al (µmol/l)	Co (µmol/l)	Ni (µmol/l)	Cu (µmol/l)	Zn (µmol/l)	As (µmol/l)	Pb (µmol/l)	Th (µmol/l)	U (µmol/l)
Spring	17.1	6.4	168	6470	0.115	11.870	0.111	0.058	0.068	0.025	0.112	0.162	<0.005	<0.05	<0.05
Point 1	16.3	6.5	189	6620	0.068	11.870	0.111	0.057	0.070	0.017	0.106	0.068	<0.005	<0.05	<0.05
Point 2	15.2	6.5	195	6630	0.049	11.870	0.074	0.057	0.073	0.020	0.167	0.064	<0.005	<0.05	<0.05
Point 3	15.8	6.7	198	6570	0.028	11.870	0.074	0.056	0.082	0.017	0.089	0.047	<0.005	<0.05	<0.05
Point 4	15.5	6.9	188	6640	0.013	11.870	0.074	0.057	0.090	0.017	0.086	0.040	<0.005	<0.05	<0.05
Point 5	15.3	6.9	180	6660	0.010	11.870	0.148	0.052	0.109	0.019	0.128	0.034	<0.005	<0.05	<0.05
Point 6	15.0	7.0	189	6630	0.009	11.870	0.185	0.053	0.094	0.019	0.150	0.035	<0.005	<0.05	<0.05
Point 7	14.6	7.1	197	6630	0.004	11.870	0.111	0.050	0.095	0.020	0.223	0.028	<0.005	<0.05	<0.05
Point 8	13.7	7.2	214	6560	0.005	11.870	<0.05	0.047	0.092	0.017	0.203	0.031	<0.005	<0.05	<0.05

Annex 8: Concentration of trace metals and metalloids in Font Groga stream (in mg·L^{-1}).

Sample	T °C	pH	Eh	Cond.	Fe (mg/l)	Mn (µg/l)	Al (µg/l)	Co (µg/l)	Ni (µg/l)	Cu (µg/l)	Zn (µg/l)	As (µg/l)	Pb (µg/l)	Th (µg/l)	U (µg/l)
Spring	17.1	6.4	168	6470	6.45	652	3	3.4	4	1.6	7.3	12.1	0.07	0.018	1.65
Point 1	16.3	6.5	189	6620	3.8	651	3	3.36	4.1	1.1	6.9	5.07	0.03	0.006	1.69
Point 2	15.2	6.5	195	6630	2.72	634	2	3.38	4.3	1.3	10.9	4.78	0.03	0.005	1.65
Point 3	15.8	6.7	198	6570	1.54	649	2	3.31	4.8	1.1	5.8	3.5	0.02	0.004	1.6
Point 4	15.5	6.9	188	6640	0.75	644	2	3.33	5.3	1.1	5.6	2.99	0.01	0.003	1.62
Point 5	15.3	6.9	180	6660	0.56	625	4	3.08	6.4	1.2	8.4	2.55	0.03	0.002	1.61
Point 6	15.0	7.0	189	6630	0.5	620	5	3.13	5.5	1.2	9.8	2.6	0.04	0.003	1.61
Point 7	14.6	7.1	197	6630	0.25	599	3	2.97	5.6	1.3	14.6	2.1	0.03	0.002	1.63
Point 8	13.7	7.2	214	6560	0.29	505	< 2	2.79	5.4	1.1	13.3	2.3	0.02	0.001	1.51

Annex 9: Chemistry of the dissolved gases sampled from the Font Groga stream.

Sample	CO_2 (mmol/L)	N_2 (mmol/L)	Ar (mmol/L)	CH_4 (mmol/L)	O_2 (mmol/L)	Tot (mmol/L)	CO_2 (%)	N_2 (%)	Ar (%)	CH_4 (%)	O_2 (%)
Spring	6.564	0.213	0.006	0.0005	0.043	6.83	96.16	3.12	0.08	0.0073	0.63
Point 1	3.685	0.411	0.010	0.0002	0.015	4.12	89.41	9.97	0.24	0.0049	0.37
Point 2	2.047	0.405	0.010	0.0016	0.052	2.52	81.37	16.10	0.40	0.0636	2.07
Point 3	2.698	0.395	0.010	0.0008	0.041	3.14	85.79	12.56	0.32	0.0254	1.30
Point 4	1.588	0.615	0.015	0.0001	0.208	2.43	65.45	25.35	0.62	0.0041	8.57
Point 5	2.165	0.316	0.008	0.0011	0.057	2.55	85.01	12.41	0.31	0.0432	2.22
Point 6	1.515	0.588	0.014	0.0001	0.116	2.23	67.84	26.33	0.63	0.0045	5.19
Point 7	5.623	0.255	0.006	0.0002	0.022	5.91	95.21	4.32	0.10	0.0034	0.36
Point 8	1.554	0.319	0.008	0.0007	0.0890	1.97	78.86	16.19	0.41	0.0355	4.52

Annex 10: Diffusion coefficients for each metal and temperature within the DGT gel (m^2/sec)

Ref	Name	Temp (ºC)	Al	Cr	Mn	Fe	Co	Ni	Cu	Zn	Cd	Pb
1	Fontecha 1	17	3.7E-10	3.9E-10	4.5E-10	4.7E-10	4.6E-10	4.5E-10	4.8E-10	4.7E-10	4.7E-10	6.2E-10
2	Fontecha 2	13	3.1E-10	3.3E-10	3.9E-10	4.0E-10	3.9E-10	3.8E-10	4.1E-10	4.0E-10	4.0E-10	5.3E-10
3	Fontecha 3	12.6	2.9E-10	3.0E-10	3.5E-10	3.7E-10	3.6E-10	3.5E-10	3.7E-10	3.6E-10	3.7E-10	4.8E-10
4	Hervidero Nuevo	16	3.6E-10	3.8E-10	4.4E-10	4.6E-10	4.5E-10	4.3E-10	4.7E-10	4.6E-10	4.6E-10	6.0E-10
5	Barranco Grande	15.5	2.9E-10	3.1E-10	3.6E-10	3.8E-10	3.7E-10	3.6E-10	3.9E-10	3.8E-10	3.8E-10	5.0E-10
6	Barranco Chico	14	2.7E-10	2.8E-10	3.3E-10	3.4E-10	3.3E-10	3.2E-10	3.5E-10	3.4E-10	3.4E-10	4.5E-10
7	Barranco Chiquillo	14	2.9E-10	3.1E-10	3.6E-10	3.8E-10	3.7E-10	3.6E-10	3.9E-10	3.8E-10	3.8E-10	5.0E-10
8	Río Jabalón	10	2.6E-10	2.7E-10	3.2E-10	3.3E-10	3.2E-10	3.1E-10	3.4E-10	3.3E-10	3.3E-10	4.3E-10
9	Chorrillo	17	3.6E-10	3.8E-10	4.4E-10	4.6E-10	4.5E-10	4.3E-10	4.7E-10	4.6E-10	4.6E-10	6.0E-10
Blanc	Blanc	15	3.6E-10	3.8E-10	4.4E-10	4.6E-10	4.5E-10	4.3E-10	4.7E-10	4.6E-10	4.6E-10	6.0E-10

Annex 11: CO_2-Bearing sampling stations

Barranco Grande

Baño chico

Baño chiquillo

Herviderio Nuevo

Chorro Glicerio

Cañada Real

Fontecha 1

Fontecha 2

Fontecha 3

Jabalon

Annex 12: Published and Submitted papers

The effect of increased CO_2 concentrations on trace metal mobility: field and laboratory experiences.

Marco Agnelli[a], Jordi Bruno[a,*], Lara Duro[a], Fidel Grandia[a], Mireia Grivé[a], Javier Olmeda[a]

[a]*Amphos 21 Consulting SL, Passeig Garcia Faria 49-51, 08109 Barcelona*

*corresponding autor. Tel: +34 93 583 05 00; fax: +34 93 307 59 28; e-mail address: jordi.bruno@amphos21.com (Jordi Bruno)

Abstract

Already in 1990 it was postulated that increased CO_2 concentrations in seawater would affect trace element mobility. Some 24 years later, CO_2 levels have further increased and the acidity of seawater is also increasing. In this article we revise the effects of increased CO_2 concentrations on the iron(III) mobility and associated trace elements with particular emphasis on the environmental consequences of CO_2 geological storage.

The outcome of this work would indicate, by comparison between field and laboratory experiences, that increasing in dissolved CO_2 solubilises Fe(III) oxyhydroxides and triggers secondary mobility of the trace metals associated to these phases with special focus on uranium(VI).

Keywords

Trace metal mobility; Iron solubility; CO_2 geological storage; Carbonate content; Dissolved CO_2; Seawater acidity.

1. Introduction

Back in 1990 it was already postulated that increased CO_2 concentrations would have an effect on trace metal mobility, particularly in seawater (Bruno, 1990). At that time the CO_2 concentrations in the atmosphere as measured in the Manua Loa observatory were around 350 ppmv, while at present they reach the 400 ppmv (Tans and Kieling, 2014). The measured CO_2 concentrations in surface sea water appear to follow the increased trend of atmospheric concentrations with some variability depending on sea water temperature (Bates et al., 2014). This has critical consequences for seawater acidification as the oceans constitute the largest CO_2 sink. An example of the consequences caused by the increase in the atmospheric CO_2 concentration in the surface of the ocean is that its mean pH is approximately 0.1 units lower today than in the preindustrial period (Zeebe and Wolf-Gladrow, 2001) and these trends are confirmed by the multisite oceanographic study by Bates et al. (2014).

Since the publication in 1990, a large number of investigations have been performed in order to determine the influence of increased CO_2 concentrations in the mobility of a number of key trace metals, including Fe(II) (Bruno et al., 1992a) and Fe(III) (Bruno et al., 1992b; Duro, 1996 ; Bruno and Duro, 2000; Grivé et al., 2014a, b) and U(VI) (Bruno et al., 1995; Duro, 1996; Grivé, 2005). The linkage between uranium mobility and the influence of CO_2 on Fe(III) mobility was specifically studied in Duro (1996) and Grivé (2005).

The outcome of these studies was clear in the sense of demonstrating the influence of increased CO_2 concentrations on the dissolution of Fe(III) oxyhydroxides and consequently on the mobilisation of trace metals attached to these very relevant and ubiquitous surfaces.

This was later confirmed by a number of evidences from the geochemical modelling of trace element solubility in a number of sites that were investigated as natural analogues to geological repositories of spent nuclear fuel (Miller et al., 2000), particularly, in the *Poços de Caldas* and the *El Berrocal* sites (Duro, 1996; Bruno et al., 2002; Grivé, 2005).

In recent years, the focus of our research has shifted towards the potential environmental effects of the geological storage of CO_2 and in particular in the metal mobilisation in aquifers affected by potential leakage from the storage complex. In this context, there are two issues to be concerned about. On one hand, increased CO_2 concentrations may induce increased acidity in poorly buffered systems where acidity increases of three orders of magnitude have been observed (Trautz et al., 2013). This increased acidity may result in the release of metals bound on the existing solid phases. On the other hand, the increased CO_2 concentrations will result in the increase of the total carbonate of the system and consequently in the build-up of metal hydroxo carbonate and metal carbonate complexes, which will result in increased metal concentrations. The two effects are difficult to separate in natural system studies, but some dedicated laboratory tests, particularly in relation to effects on marine systems may give some interesting clues.

In this paper the findings from the early publication in the light of the research conducted in these two decades, will be revised and updated with the aim to clearly confirm the link between increased carbon dioxide, iron(III) solubility and trace metal mobility by the comparison of laboratory results and field experiences, discussing the implications for trace metal mobility in the present emissions scenario with constantly increasing CO_2 levels.

2. Field experience:

An illustrative example of the impact of CO_2 dissolution on the iron transport is found in the aquifers affected by CO_2 flows from deep underground sources (i.e., mantle degassing, thermal decarbonation). These gas-water-rock interactions have been recently studied in detail in the environmental impact assessment of potential CO_2 leakage from geological storage (e.g., Zheng et al., 2009; Kharaka et al., 2010; Spangler et al., 2010). In addition, injection tests of high-pressured CO_2 have resulted in an increase of iron and other metals in the reservoir (e.g., Peter et al., 2012; Trautz et al., 2013). In both cases, the metal mobilisation has been commonly related to acidity increase and the relative high solubility of Fe(II). However, the role of carbonate complex formation has also been discussed (Lions et al., 2014).

Many CO_2-bearing aquifers carry high amounts of iron and other metal even at circumneutral pH and oxidising Eh, in which Fe(III) is the dominant redox state. In these cases, the low solubility of iron(III) oxyhydroxide phases should prevent the dissolution of significant amounts of Fe(III) but the formation of aqueous carbonate complexes allows the concentration of Fe(III) to reach values higher than 10^{-4} mol·L^{-1}. (e.g., Agnelli et al., 2013). In order to better understand that increasing in dissolved CO_2 solubilises Fe(III) oxyhydroxides and triggers secondary mobility of the trace metals associated to these phases, a detailed systematic sampling was performed in this work, from the source point to the end, at the Font Groga stream (Spain).

2.1. The case of Font Groga stream (La Selva basin, NE Spain):

In the Miocene-Pliocene La Selva basin, in NE Spain, a large number of CO_2-bearing springs occur, related to mantle degassing. Gas and water discharges are intimately related to deep fault systems. All these ground waters have a circum-neutral pH (between 6 and 7) and relatively oxic Eh (Vilanova, 2004; Piqué et al., 2010). The degree of water-gas-rock interaction is high as proved by the elevated concentration of solutes such as Cl, Na, K, Li and F. Characteristically, these waters are iron rich, with concentration up to 10^{-4} mol·L^{-1}.

One of the best-known CO_2-bearing groundwater in the area is the Font Groga stream, located in the north margin of the basin. This stream allows the observation of the role of CO_2 on the iron transport. The chemistry of the water and solute evolution has been studied in detail in this study.

2.1.2 Sampling*:*

9 water samples in the Font Groga stream have been collected, from the spring (sample 0) and downstream (samples 1 to 8; Fig. 1 and Fig. 2). From each sampling point, 3 aliquots of water were collected: *i)* 125 mL in a plastic bottle for the analysis of anions; *ii)* 50 mL in a plastic bottle for the analysis of cations, previous acidification with 0.5 mL of Suprapur HCl and filtration using 0.45 µm filters; iii) 50 mL in a plastic bottle for the determination of trace metals, previous acidification with 0.5 mL of 1M HNO_3 and filtration using 0.1 µm filters.

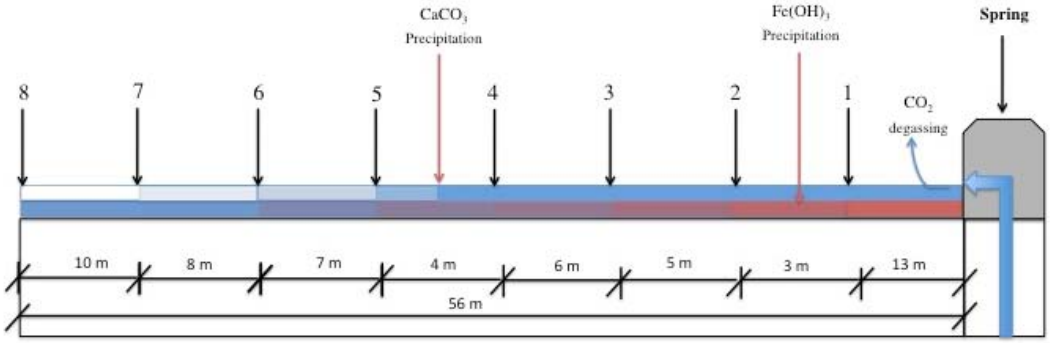

Figure 1: Sketch of the sampling in the Font Groga stream. Observable precipitation of ferrihydrite and calcite has been indicated as a reddish and bluish colour, respectively.

The determination of the dissolved gas concentration in aqueous phase was performed by using a new method setup (Tassi et al., 2008c) for which the collection of dissolved gases is carried out at equilibrium conditions. The sampling is operated by using gas tubes with a capacity of 200-300 mL with a Teflon stopcock. In the laboratory the gas vials are pre-evacuated by a rotary pump with a vacuum value of 10^{-1}-10^{-2} Pa. By submerging the gas vial into the water and opening the Teflon stopcock, the water is forced to enter the vial by decompression. Normally, < 70% of the tube volume has to be filled with water in order to allow the chemical and determination.
The pH-Eh measurements where performed in the field using a Crison portable pH-Eh meter with a platinum electrode for the redox determination.

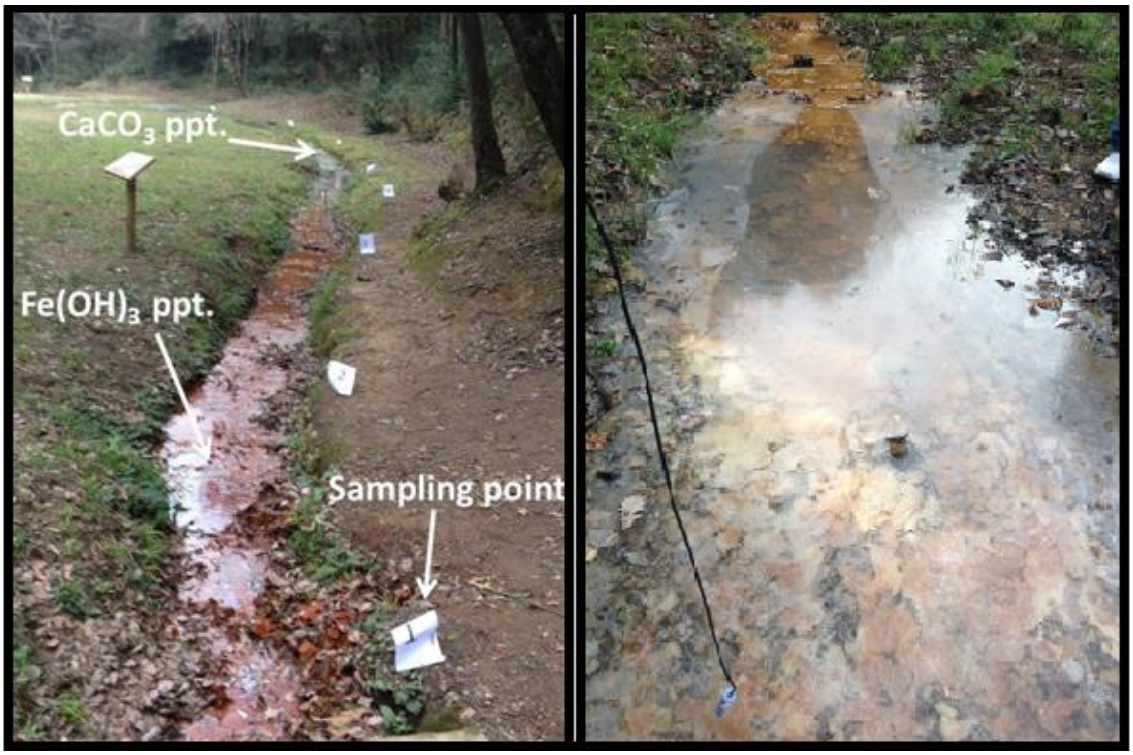

Figure 2: View of the sampling in the Font Groga stream. Precipitation of ferrihydrite and calcite is clearly observed.

2.3. Geochemical modelling:

Water chemistry was interpreted by using the equilibrium chemical-speciation/mass transfer model PHREEQC-3 (Parkhurst and Appelo, 2013). The thermodynamic calculations were performed using the Sit.dat database, based on the ThermoChimie v.7.c dataset (Giffaut et al., 2014) in order to determine both the $Fe(OH)_3$ saturation indexes and the amount of Fe carbonate complexes formed as a function of the pCO_2 and pH.Input data for each sampling point include measured values of metal (Fe_{tot}) and major elements (HCO_3^-, SO_4^{2-}, Cl^-, K^+, Na^+, Mg^{2+}, Ca^{2+}) concentrations, temperature, pH and alkalinity.

For each sampling point a simulation has been performed using both measured pCO_2 values and the recalculated ones by using the HCO_3^- amounts determined in the water. This double step was carried out to verify whether the simulation result obtained with the measured values does not deviate from the theoretical result and to detect any problems caused by sampling. The degree of saturation is expressed as the saturation index (SI), where SI is equal to the difference between logarithms of product ion activity and constant solubility (SI = log IAP − log Ksp). To determine the ferrihydrite SI was used the log K from the Minteq.V4 dataset (log k = 3.19) instead of the original one of the SIT dataset (log k = 1.19). This change was done taking in mind the variability of the thermodynamic properties referring to a poorly crystalline mineral in natural systems.

2.4. Results:

2.4.1 Gas and water chemistry

The sampling was carried out dividing the initial 60 m of the stream into 9 equidistant sampling points starting from the spring and then considering each point as a separated system in equilibrium with a given CO_2 pressure. The physical parameters, the chemical compositions of waters in terms of major, minor and trace elements and an aliquot of dissolved gases were sampled for each point. The results are shown in Table 1. From the spring to the last sample point, the stream is characterized by an electrical conductivity ranging from 6470 $\mu S \cdot cm^{-1}$ up to 6600 $\mu S \cdot cm^{-1}$ and by pH values that increase from 6.4 to 7.3.

Eh ranges from 168 mV to 214 mV. The main metal characterizing the spring is Fe, in a range of $2.5x10^{-1}$ $mg \cdot L^{-1}$ ($4.47x10^{-3}$ $mmol \cdot L^{-1}$) to 6.4 $mg \cdot L^{-1}$ ($1.15x10^{-1}$ $mol \cdot L^{-1}$). The studied samples also show rather high concentrations of Mn (up to 652 $\mu g \cdot L^{-1}$, 11.9 $\mu mol \cdot L^{-1}$), Zn (up to 14.6 $\mu g \cdot L^{-1}$, 2.23 $x10^{-1}$ $\mu mol \cdot L^{-1}$), Ni (up to 6.4 $\mu g \cdot L^{-1}$, 1.09 $x10^{-1}$ $\mu mol \cdot L^{-1}$) and Co (up to 3.38 $\mu g \cdot L^{-1}$, $5.73x10^{-2}$ $\mu mol \cdot L^{-1}$).

The main dissolved gas dominating all the pools is CO_2 (Table 2), with a range from 96.16% (6.56 $mmol \cdot L^{-1}$) to 65,45% (1.58 $mmol \cdot L^{-1}$). The remaining gas portion is mainly characterized by the occurrence of N_2, CH_4 and Ar.

A comparison between CO_2 amount and pH in each sampling station (Fig. 3) shows that as the gas concentration decreases, as a consequence of the degasification, the pH increases. In the field this trend is well evidenced by the precipitation of $CaCO_3$ throughout the stream (Fig. 1 and Fig. 2). The same comparison has been done for CO_2 and Fe concentrations (Fig. 4). As for the pH, the plot shows how Fe reduces its concentration as CO_2 decreases.

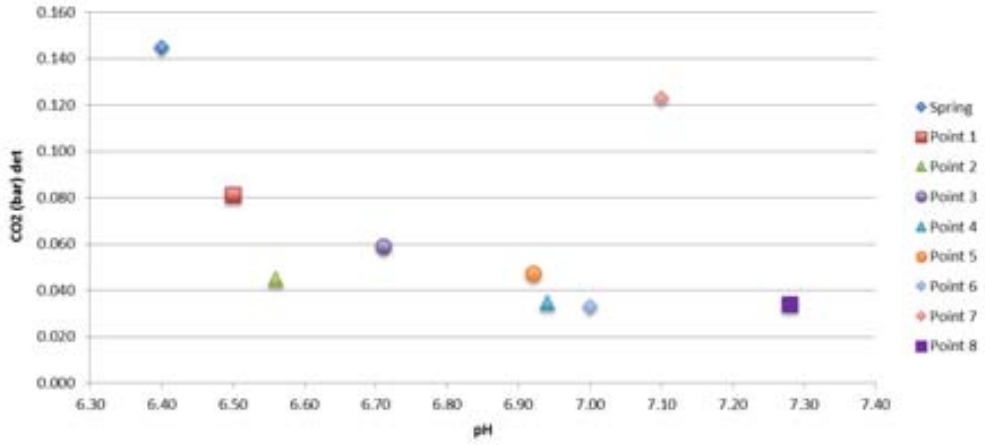

Figure 3: pCO_2 vs pH sampled along the Font Groga stream

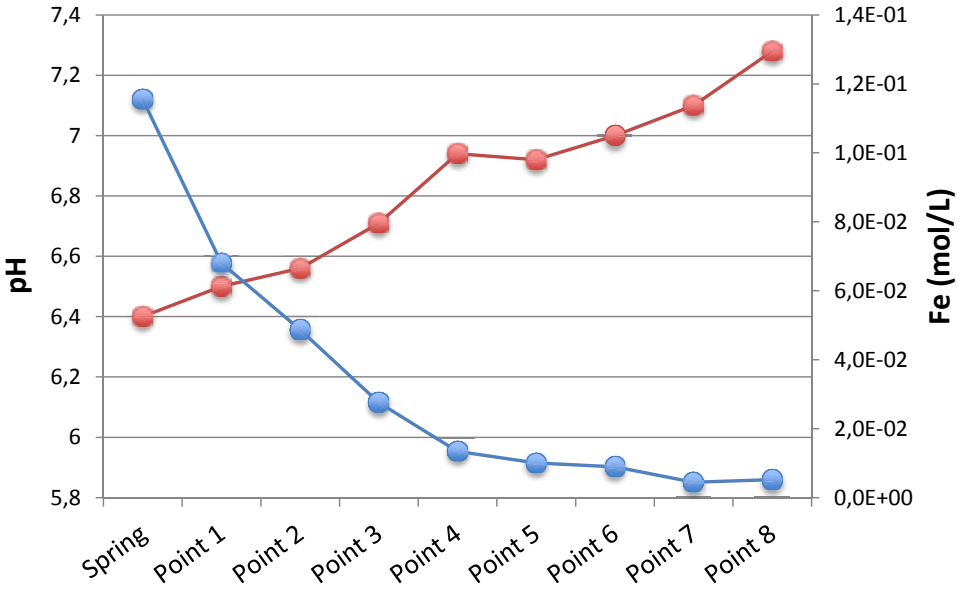

Figure 4: Evolution of pH (red line) and Fe_{tot} concentration (blue line) downstream in the Font Groga River sampling stations.

Table 1: Chemistry of the water samples at Font Groga stream (La Selva basin).

Sample	Distance (m)	T (°C)	pH	Eh (mV)	Cond. ($\mu S \cdot cm^{-1}$)	HCO_3^- (mmol/l)	Cl (mmol/l)	SO_4^{2-} (mmol/l)	Ca (mmol/l)	Mg (mmol/l)	Na (mmol/l)	K (mmol/l)	F (mmol/l)	Fe (mmol/l)
Spring	0.0	17.1	6.4	168	6470	55.9	18.7	3.0	8.3	3.4	59.1	0.8	0.05	0.170
Point 1	13.2	16.3	6.5	189	6620	55.0	19.7	3.1	9.2	3.4	58.9	0.9	0.02	0.068
Point 2	16.2	15.2	6.6	195	6630	56.0	19.1	3.1	8.5	3.4	58.5	0.8	0.02	0.048
Point 3	21.2	15.8	6.7	198	6570	55.9	19.3	3.1	8.6	3.4	58.9	0.9	0.02	0.027
Point 4	27.2	15.5	6.9	188	6640	57.6	19.4	3.1	8.1	3.4	58.7	0.7	0.03	0.013
Point 5	30.9	15.3	6.9	180	6660	56.9	18.9	3.1	8.6	3.3	57.6	0.8	0.02	0.010
Point 6	38.3	15.0	7.0	189	6630	57.3	19.2	3.2	8.4	3.5	60.6	0.8	0.02	0.009
Point 7	46.8	14.6	7.1	197	6630	57.5	19.7	3.3	7.9	3.4	58.3	0.8	0.02	0.004
Point 8	56.0	13.7	7.3	214	6560	55.9	18.9	3.0	8.0	3.3	58.1	0.8	0.03	0.005

Table 2: Chemical composition of the dissolved gases sampled in the Fong Groga stream

Sample	CO_2	N_2	Ar	CH_4	O_2	CO_2	N_2	Ar	CH_4	O_2
Spring	6.564	0.213	0.006	0.0005	0.043	96.16	3.12	0.08	0.0073	0.63
Point 1	3.685	0.411	0.010	0.0002	0.015	89.41	9.97	0.24	0.0049	0.37
Point 2	2.047	0.405	0.010	0.0016	0.052	81.37	16.10	0.40	0.0636	2.07
Point 3	2.698	0.395	0.010	0.0008	0.041	85.79	12.56	0.32	0.0254	1.30
Point 4	1.588	0.615	0.015	0.0001	0.208	65.45	25.35	0.62	0.0041	8.57
Point 5	2.165	0.316	0.008	0.0011	0.057	85.01	12.41	0.31	0.0432	2.22
Point 6	1.515	0.588	0.014	0.0001	0.116	67.84	26.33	0.63	0.0045	5.19
Point 7	5.623	0.255	0.006	0.0002	0.022	95.21	4.32	0.10	0.0034	0.36
Point 8	1.554	0.319	0.008	0.0007	0.0890	78.86	16.19	0.41	0.0355	4.52
	$mmol \cdot L^{-1}$					%				

2.4.2 Thermodynamic modelling results:

From the chemistry data from gas and water analysis, the SI for calcite and ferrihydrite have been calculated. The results shown that the SI calculated using the sampled pCO_2 fit reasonably better with field observations than those obtained using the calculated pCO_2 (Fig. 5 and Fig 6). Moreover, an undersaturation with respect with calcite generally corresponds to an oversaturation in ferrihydrite. This is consistent with the field observation since ferrihydrite precipitation stops between sampling points 3 and 4 and the calcite precipitation starting at the same points (Fig. 1 and Fig. 2).

Under the pH-Eh conditions in the studied samples, iron is present as Fe(III). The solubility of this species is commonly low in shallow aquifers and surface waters due to the precipitation of $Fe(OH)_3$. However, the dissolution of CO_2 allows the enhanced solubilisation of Fe(III) by the formation of aqueous Fe(III) carbonate complexes. The impact of these complexes, especially $FeOHCO_3$, is illustrated in Fig. 7, since the solubility of Fe(III) increases three orders of magnitude. Such an impact is very well illustrated by looking at the ferrihydrite saturation index (SI) (Fig. 8) obtained in the set of simulations performed using the sampled pCO_2 (pCO_2 det) and the calculated one (pCO_2 calc) and with or without the aqueous Fe-carbonate complexes formation. In fact, the SI values calculated without the aqueous Fe-carbonate complexes always show an unrealistic oversaturation of $Fe(OH)_3$ along the stream, independently of the pCO_2 used. Introducing the aqueous carbonate complexes, the SI dramatically decreases to normal saturation values.

Table 3: Sampled CO_2 pressure values and recalculated (PhreeqC) by using the HCO_3^- amounts determined in Font Groga stream stations.

Sample	CO_2 (bar) (sampled)	CO_2 (bar) (PhreeqC)
Spring	0.145	0.662
Point 1	0.081	0.562
Point 2	0.045	0.512
Point 3	0.059	0.407
Point 4	0.035	0.269
Point 5	0.048	0.281
Point 6	0.033	0.239
Point 7	0.123	0.194
Point 8	0.034	0.131

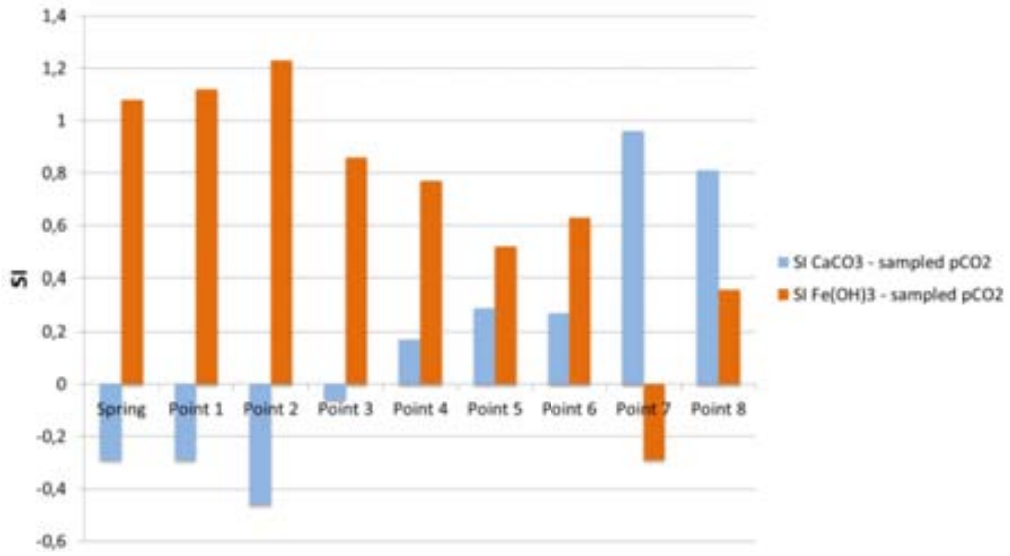

Figure 5: Comparison between SI $Fe(OH)_3$ and SI $CaCO_3$ calculated using the sampled CO_2 pressures.

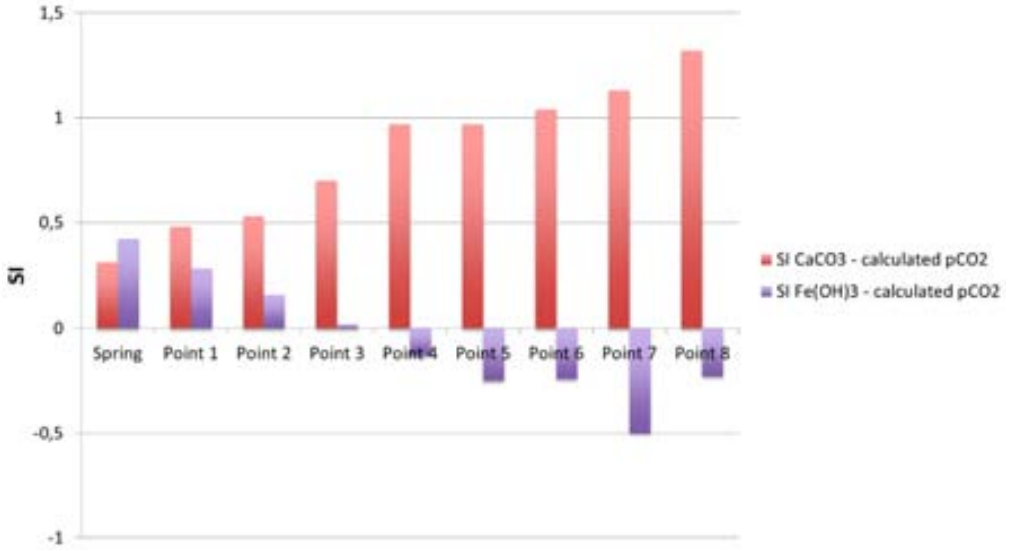

Figure 6: Comparison between SI $Fe(OH)_3$ and SI $CaCO_3$ calculated using the calculated CO_2 pressures.

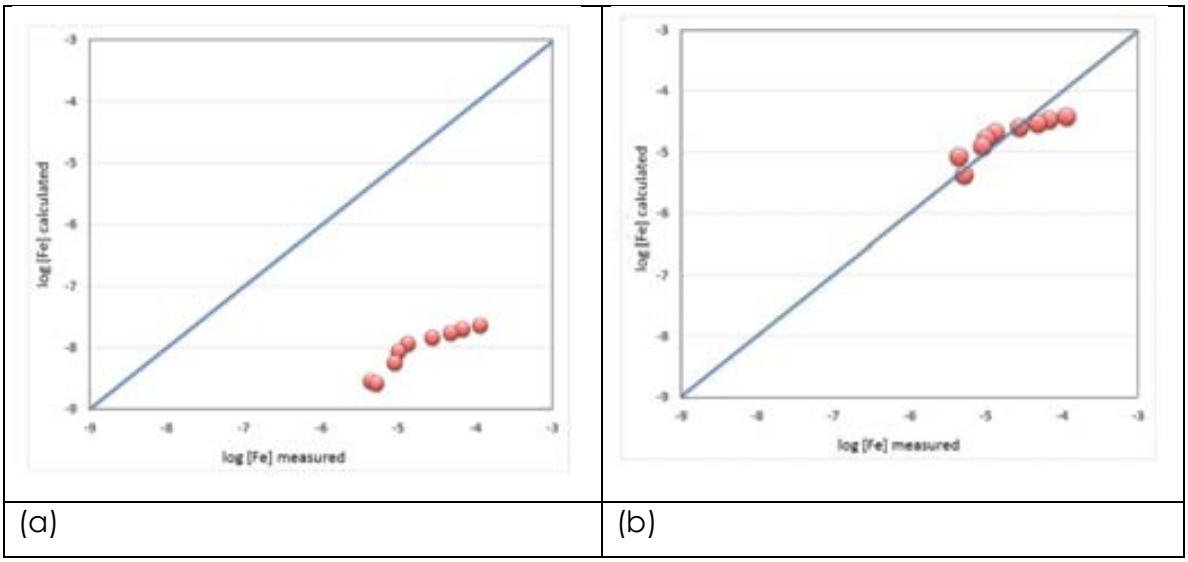

(a) (b)

Figure 7: Plot of the calculated iron (III) concentrations in the samples from the Font Groga stream in front of the iron (III) measured concentrations (a) No iron (III) carbonate species in the thermodynamic database used (b) Effect of the incorporation of iron (III) carbonate species proposed in Grivé (2005) and Grivé et al. (2014a) in the thermodynamic database used in the calculations.

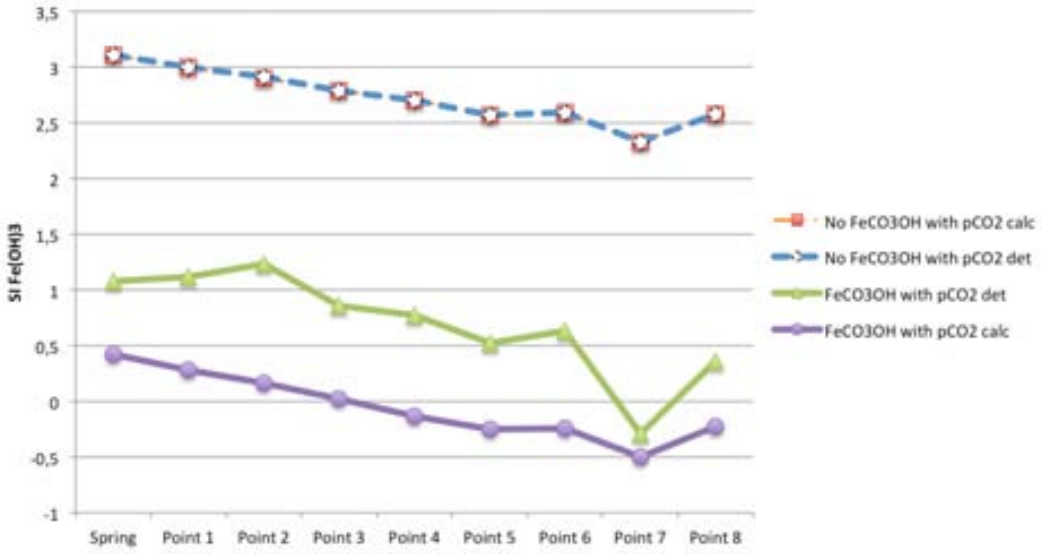

Figure 8: Ferrihydrite saturation index (SI) calculated in the simulation performed with or without considering the Fe(III)-carbon-complexes formation, using the sampled pCO_2 (pCO_2 det) and the calculated one (pCO_2 calc).

3. Evidences from laboratory studies related to CO_2 storage:

3.1 Trace metal behaviour in systems with increased CO_2 concentration.

Ardelan et al. (2012) reported a particularly interesting study in connection with the effects of CO_2 seepage from sub-seabed geological storage. In this study the authors have used a titanium pressure tank, to simulate a high-pressure release of carbon dioxide in a sediment-sea water system. The sediments used in the experiment were extracted from the Trondheimsfjord and placed in contact with seawater extracted from the same site at 90 m depth. The seawater was flown into the tank and out for sampling at a flow rate of 1 l min^{-1}. Pure CO_2 was pumped into the system at 10 bar.

The conditions of the experiment were carefully controlled and the inflowing and outflowing waters were analysed for pH, dissolved inorganic carbonate (DIC), pCO_2 and trace metal concentrations as collected in diffusive gradient thin-film (DGT) units.

The inflow sea water composition was: pH=8.1; $pCO_2=3.38\cdot10^{-3}$ atm and DIC=2.13 milimolar. The outflowing seawater composition was pH=6.9; pCO_2=6.6 atm and DIC=2.635 milimolar. One of the striking observations is that the acidity of the system is rather well buffered, due to the sediment-water interactions that control the pH, in this case most probably through the $CO_2/CaCO_3$(s) buffer system. Cruz Payán et al. (2012) made similar observations in their investigations of the effects of CO_2 interactions with seabed sediments from the Cantabria Sea, where they observed a strong buffering effect of the sediments when put in contact with water at pH between 5 and 7, although they could also observe a substantial release of trace metals contained in the sediments.

In spite of the relative acidity buffering effect, Ardelan et al. (2012) observed a strong mobilisation of Al, Cr, Co, Pb, Ce, As and U when compared with similar high pressure tests run with N_2 as blanks.

In order to discern to which extent this effect is the result of the acidification and/or the carbonate complexation, a simple modelling exercise was performed in this study.

The solubility and speciation of a number of trace metals was calculated as a function of pCO_2 at the outflow pH=6.8 reported by Ardelan et al (2012). The code used was the Spana package developed by Puigdomènech (last update, April 2013) together with the ThermoChimie database (Giffaut et al., 2014; Grivé et al., 2014c; http://www.thermochimie-tdb.com/).

The results of the calculations are shown in Figure 9.

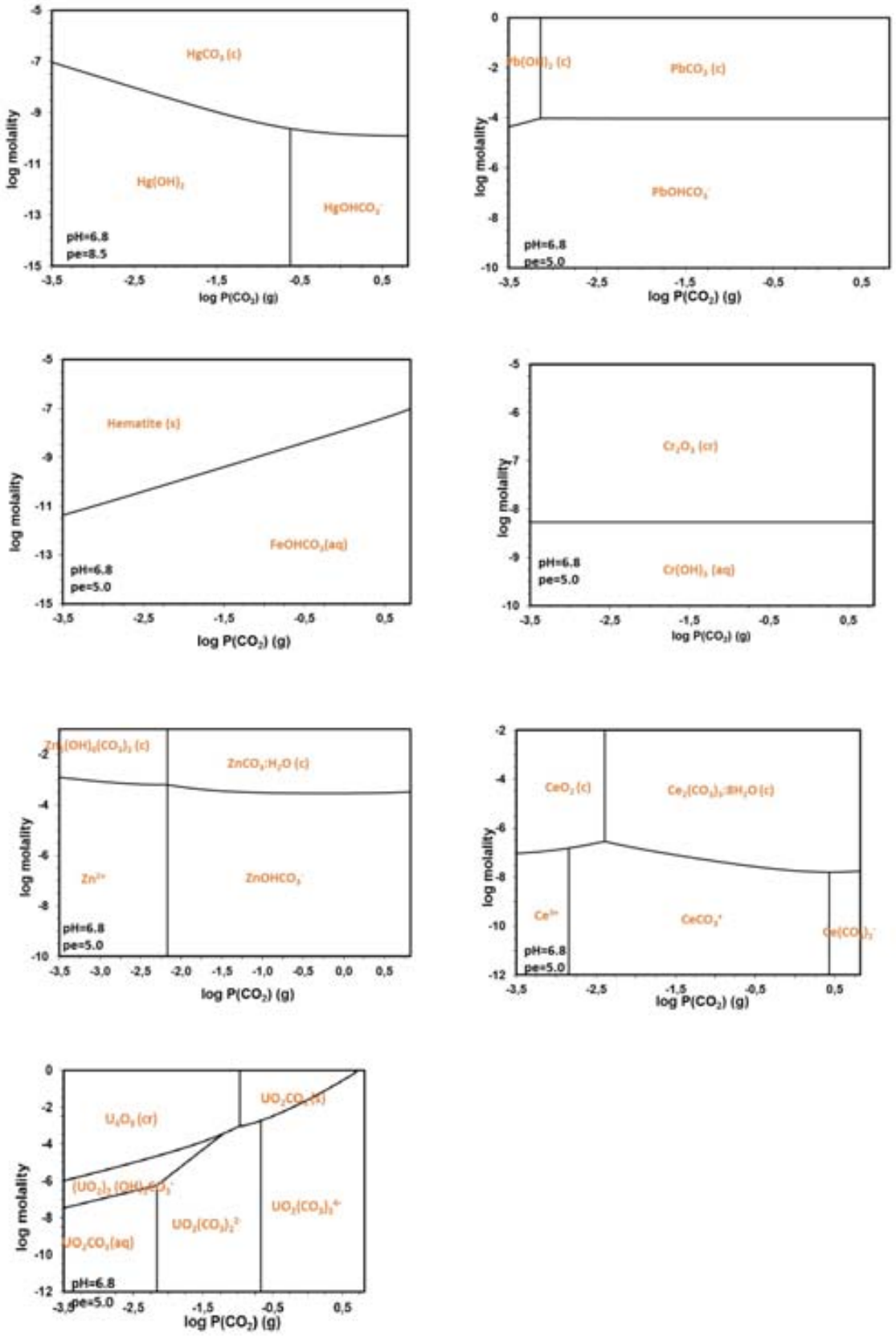

Figure 9: Predominance diagram of Hg(II), Pb(II), Zn(II), Fe(III), Cr(III), U(VI), Ce(III) and Ce(IV) species at pH=6.8 and pe=8.5 as a function of pCO_2, reflecting the outlet conditions of the experiments performed by Ardelan et al. (2012).

The outcome of these simple calculations would indicate that for most trace metals (Hg(II), Pb(II), Zn(II), Ce(III) and Ce(IV)) the increased pCO_2 has a positive effect in terms of stabilising their carbonate or hydroxocarbonato solid phases. This is the result of the formation of carbonate containing solid phases, which are more stable than the aqueous carbonate complexes. In the case of Cr(III) the increased pCO_2 has no effect, as no Cr(III) carbonate complexes have been reported in the literature. It is only in the case of Fe(III), when increased pCO_2 clearly results on a solubilisation of the Fe(III) oxyhydroxide or Fe(III) oxide phases resulting not only into increased iron concentrations but also triggering the dissolution of a number of trace metals sorbed onto the Fe(III) oxyhydroxide phases. This is clearly in line with the observations in the Font Groga stream and other data, previously discussed.

In the case of uranium(VI), the presence of very stable hydroxocarbonate and carbonate complexes results in the increase of uranium solubility as a function of pCO_2. This effect, together with the destabilisation of Fe(III) oxyhydroxides results in a net release of U(VI) in CO_2-rich waters as described in the results here reported, as well as in Grivé (2005) and references therein.

3.2 Secondary trace elemental mobility as a result of Fe(III) dissolution in oxic conditions

The association of trace elements to Fe(III) oxyhydroxides through sorption processes has also been very well established and the compilation by Dzombak and Morel (1990) summarises the rationalisation of these interactions through surface complexation reactions. Therefore, any effect of CO_2 on the solubility of the iron(III) oxyhydroxides cascades into the release of trace metals associated to these solid phases. In addition, for some trace metals, the formation of mixed hydroxocarbonate or carbonate aqueous complexes enhances their dissolution and consequently their mobility.

One of the trace elements that better exemplifies this is uranium. In oxic environments uranium is present in the hexavalent form and is rather soluble in natural water conditions. However, U(VI) has also a strong affinity to sorb onto iron(III) oxyhydroxide phases and depending on the circumstances may even co-precipitate with these solid phases (Bruno et al., 1995). The presence of increased CO_2 concentrations has a double effect on this retention mechanism. In one hand, as we have seen in the previous section, carbon dioxide may destabilise the iron(III) oxyhydroxide (ferrihydrite, Fe(OH)3(am)) releasing the attached uranium(VI) and in addition, increased total carbonate has the result of building stable U(VI) carbonate complexes.

Duro (1996) studied the effect of increased HCO_3^- concentration in the kinetics of dissolution of U(VI)/$Fe(OH)_3$ coprecipitates back in 1996. To this aim, coprecipitates of $Fe(OH)_3$/U(VI) were synthesised at a nominal 3% U:Fe ratio $(2.71\pm0.1)\cdot10^{-2}$ determined by total dissolution and ICP analyses. 5 different experiments with the same solid phase were setup, by contacting 0.4 g of

solid with 200 mL of a 0.1M$NaHCO_3$ solution, previously equilibrated with 1 atm CO_2(g). The experiments were kept under a constant bubbling of 100% CO_2(g) at different pH values (in the range 5 to 7), as shown in Table 4. Another experiment, equilibrated with atmospheric CO_2(g) was set up to reach a more alkaline pH of 9.2. Solution samples were taken at different time intervals for uranium analysis and pH monitoring until steady state uranium concentration was reached. No important pH changes were observed (the uncertainty in Table 4 stands for the maximum pH variation in each experiment). For the sake of comparison with a pure uranium solid phase, an experiment mimicking the previous ones, but by using schoepite ($UO_2(OH)_2$(s)) instead of a $Fe(OH)_3$/U(VI) coprecipitate, was set up.

Table 4. Experimental conditions used in the dissolution experiments of a coprecipitate and schoepite samples.

Exp	**Solid phase**	**Gas**	**pH**
Exp 1	$Fe(OH)_3$/U(VI) coprecipitate	100% CO_2	5.58 ± 0.04
Exp 2	$Fe(OH)_3$/U(VI) coprecipitate	100% CO_2	6.16 ± 0.12
Exp 3	$Fe(OH)_3$/U(VI) coprecipitate	100% CO_2	6.66 ± 0.06
Exp 4	$Fe(OH)_3$/U(VI) coprecipitate	100% CO_2	7.03 ± 0.07
Exp 5	$Fe(OH)_3$/U(VI) coprecipitate	Atmospheric CO_2	9.18 ± 0.04
Exp. 6	Schoepite	100% CO_2	6.03 ± 0.04

The results obtained are shown in Fig. 10, showing an initial stage of fast uranium dissolution is followed by a slow down until a steady-state is established (note the logarithmic scale in the plot). The influence that bicarbonate has on the dissolution of uranium from the coprecipitate can be clearly observed when representing the initial dissolution rates versus the concentration of [HCO_3^-] in the system (Fig. 11 a) from where a direct linear correlation with the dissolved HCO_3^- concentration is observed. The best fit to the data renders a calculated rate constant in the order of 10^{-3} moles U·$g^{-1}h^{-1}$ (see **eq. 1**):

$$R_o = (1.1\pm0.2)\cdot10^{-3}\cdot[HCO_3^-]^{(1.06\pm0.12)} \text{ moles U } g^{-1}h^{-1} \qquad \textbf{eq. 1}$$

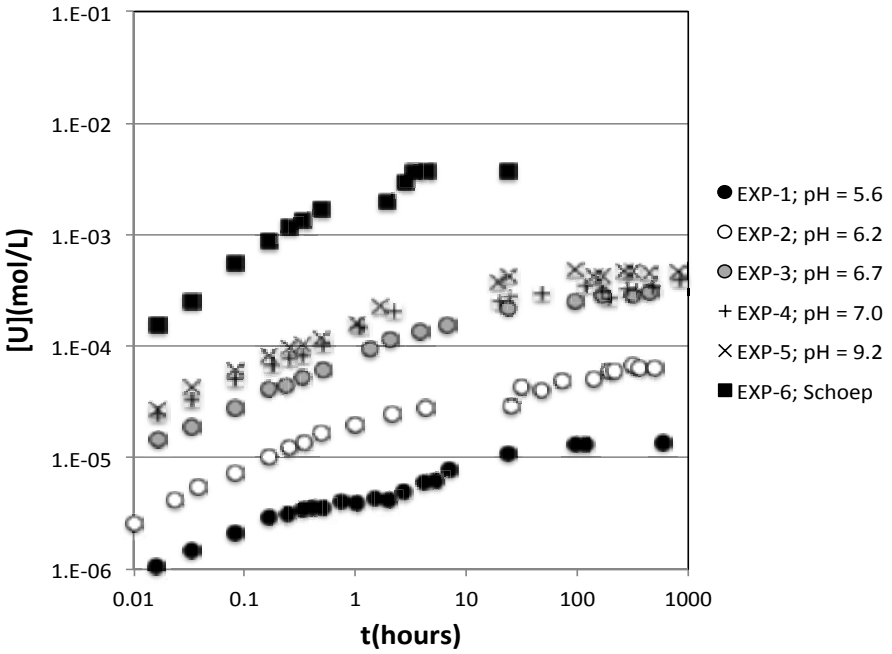

Figure 10: Evolution of the concentration of uranium in solution with time in experiments 1 to 5 in Table 4.

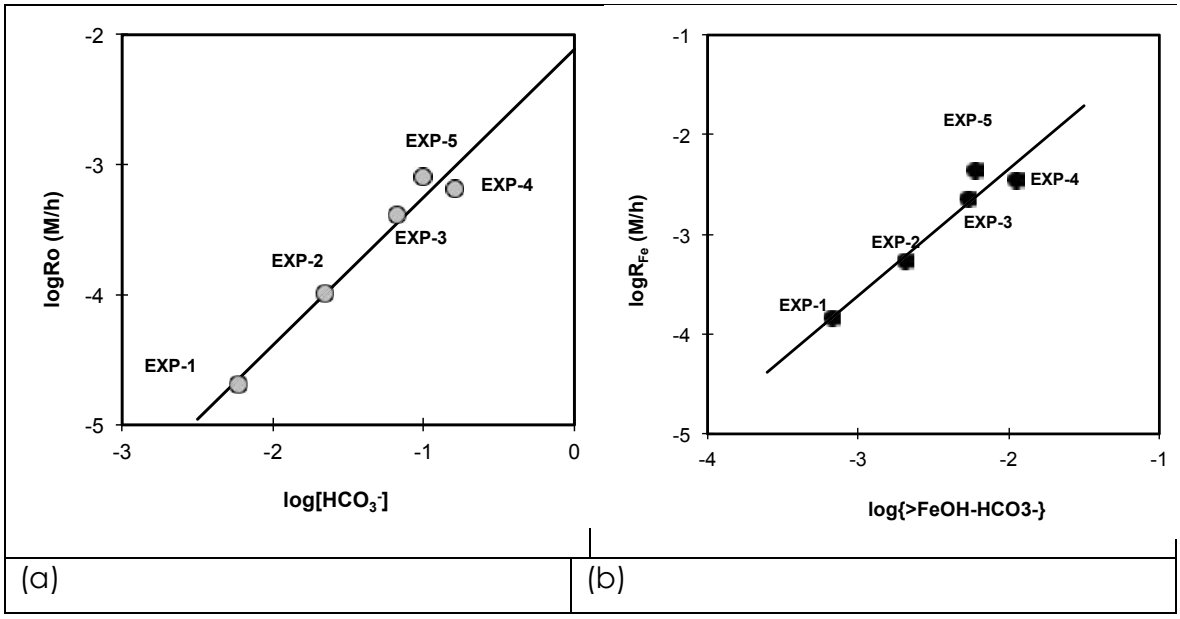

Figure 11: (a) Plot of the initial rates of uranium dissolution from the co-precipitates versus the concentration of bicarbonate in the system; (b) plot of the initial rates of iron dissolution from the co-precipitates versus the calculated concentration of >FeOH-HCO_3^-.

Bruno et al. (1992) established the formation of a surface complex on the surface of ferrihydrite in the presence of CO_2(g): >FeOH-HCO_3^-. According to their study, the rate of dissolution of hematite was linearly dependent on the concentration of this surface complex. By assuming congruent dissolution of the co-precipitate, and calculating the concentration of the surface complex in experiments 1 to 5, it is possible to observe a direct correlation between the rate of

dissolution of iron from the coprecipitate and the concentration of this surface species (see Fig. 11 b).

The comparison of the rates of congruent dissolution of the U/Fe coprecipitate and the pure schoepite indicated that the coprecipitate had a protective action against dissolution. The rates of uranium dissolution in the presence of bicarbonate were three orders of magnitude slower in the case of the coprecipitate than for the pure schoepite phase. Kinetic data for schoepite was only possible to obtain until 120 hours, given that a solid phase transformation to rutherfordine ($UO_2CO_3(s)$) occurred after 200 hours of contact between the solid and the solution, confirmed by XRD (see Fig. 12).

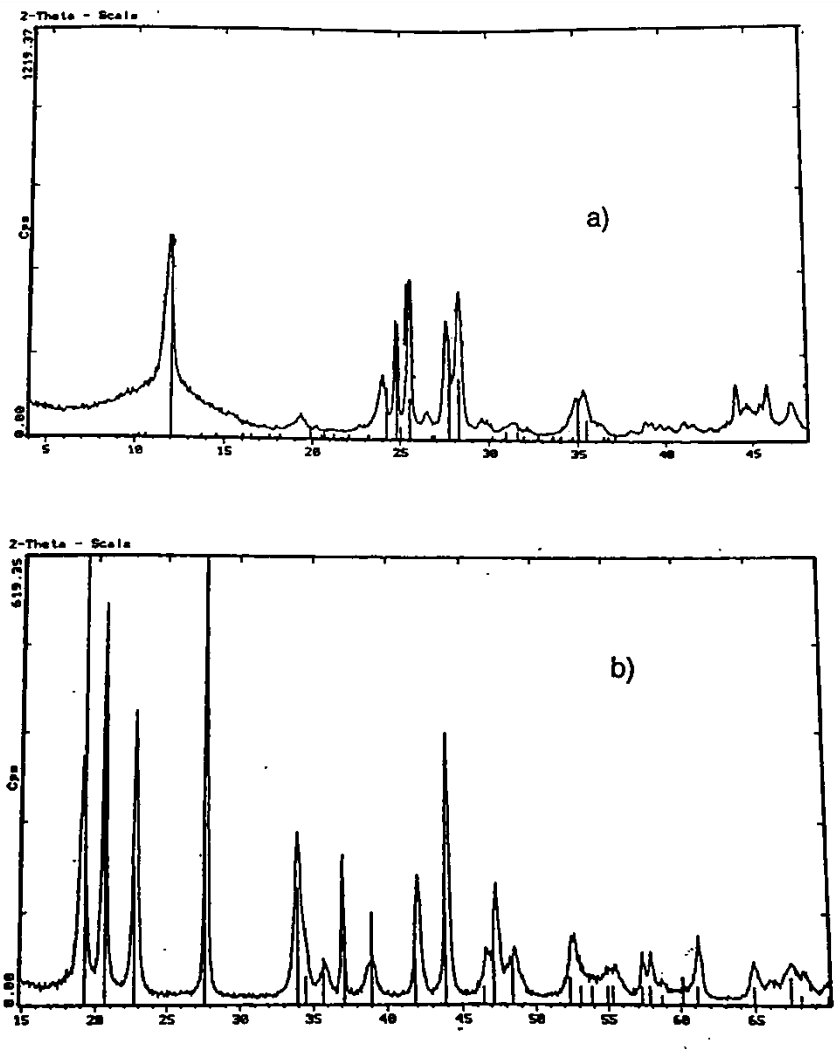

Figure 12: (a) XRD of the initial schoepite solid phase used in Exp-6; (b) XRD of the solid phase in Exp-6 after 200 hours of contact with the solution, showing the pattern of the uranyl carbonate Rutherfordine ($UO_2CO_3(s)$).

The concentrations of uranium reached at steady state from Experiments 1 to 5 in Table 4, could be properly explained by invoking the dissociation of the following carbonate surface complex (**eq. 2**), with its associated equilibrium constant (Fig. 13):

$$FeO\text{-}UO_2OH\text{-}HCO_3^- + 3\ H^+ \Leftrightarrow >FeOH + UO_2^{2+} + CO_2(g) + 2\ H_2O \quad (\log K = 13.42 \pm 0.5) \qquad \textbf{eq.2}$$

which is in agreement with a similar complex defined by Waite et al. (1994) with a log K = 14.43.

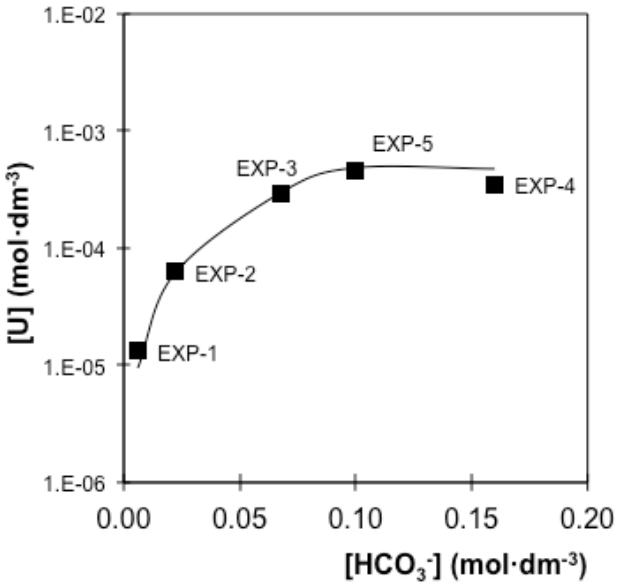

Figure 13: Steady state concentrations of uranium in solution from the dissolution of a coprecipitate (see Table 4) versus the concentration of hydrogenocarbonate in solution. Symbols stand for experimental data and line for the calculated solubility obtained by considering the formation of the surface species in eq. 2.

These results highlight again the relevance of carbonate not only on the kinetics of the release of trace metals associated with major mineral phases, such as U(VI) with ferrihydrite, but also on the equilibrium (or steady-state) concentrations in the system.

In order to remove the effect of phase transformation and to expand the study to lower $pCO_2(g)$, more representative of natural conditions, Grivé (2005) investigated further the previous system by means of flow-through experiments. This author assessed the effect of the carbonate system on the kinetics of dissolution of ferrihydrite, schoepite and U(VI)/$Fe(OH)_3$ co-precipitate in bicarbonate solutions through flow-through experiments. The results suggested a three-step mechanism in the case of ferrihydrite and schoepite, and a two-step mechanism in the case of the co-precipitate. The applicability and validity of the model presented in the case of the co-precipitate was tested against independent data from Duro (1996) (see Grivé, 2005).

4. Discussion

4.1 General aspects:

4.1.1 The effect of CO_2 on trace metal complexation

Already in 1986 it was postulated that trace metal mobility in natural waters is affected by carbon dioxide content through the formation of mixed hydroxo-carbonate complexes (Bruno, 1986), as it had been established by the pioneering work of Hietanen and Högfeldt (1976) on mixed hydroxo-carbonate complexes of Hg(II) and the one by Ferri and co-workers on Zn(II) and Pb(II) (Ferri et al., 1987a, b) mixed hydroxo-carbonate complexes and our own work on the Be(II) hydroxo carbonate system (Bruno et al., 1987).

The co-authors of this paper proposed that mechanism for the transition between metal hydroxo complexes to metal hydroxo carbonate complexes involved the attack of the dissolved CO_2 onto the metal hydroxide bridges to build bicarbonate and carbonate bridges. This was based on the kinetic work performed by Chaffe et al. (1973), Dasgupta and Harris (1977), Spitzer et al. (1982) and Sadler and Dasgupta (1987) on the formation of ternary organo-hydroxo-carbonato complexes in the presence of CO_2.

Later, the reaction of metal bridging OH groups with CO_2 to build carbonate bridges has been further studied for Cu(II) (Kitajima et al. 1990), for Zn(II) (Murthy and Karlin, 1993) and for a series of divalent organometallic(II) complexes, including Mn, Fe, Co, Ni, Cu and Zn, in Kitajima et al. (1993). This research is particularly relevant in the case of zinc since the Zn(II) enzyme carbonic anhydrase catalyses the reversible reaction CO_2 hydration to produce bicarbonate, a process that is essential to remove CO_2 from tissues in mammalian respiration process.

More recently Huanga et al. (2011) have proposed a similar mechanism for the fixation of CO_2 onto a Ni(II) pyridine hydroxo complex by a combination of spectrophotometric measurements and density functional theory (DFT) calculations which occurs at remarkable fast rates (10^6 $M^{-1}s^{-1}$) compared to rates obtained for the transformation of metal hydroxides onto metal carbonates which are 1000 times slower.

From all this information, we can conclude that the formation of metal carbonate complexes is kinetically enhanced by increased CO_2 concentrations and that it is favoured by the occurrence of metal hydroxide complexes normally occurring at the pH ranges of natural water systems. According to the work performed on divalent organometallic complexes, the presence of organic matter could largely accelerate the reaction.

Iron is a key metal ion in biological and geochemical systems as it regulates many key processes, including the scavenging and release of critical trace metals in natural water systems. The cycle of iron is often kinetically coupled with the cycles of P, S, heavy metals, O_2 and C, and depends

on the biota and the energy and intensity of the light (Luther et al., 1992; Stumm and Sulzberger, 1992).

The cycles of iron (Stumm and Sulzberger, 1992) and of carbon (Berner and Lasaga, 1989) are also the drivers of the mobility and retention of trace elements involved in natural weathering processes of minerals as well as in the anthropogenic activities. This is especially critical in the biosphere/geosphere interface, where the atmospheric oxygen and carbon dioxide undergo the main part of the transformation processes. Among them, the coupled dissolution-precipitation of iron (III) hydroxides and calcium carbonate are very dynamic processes in natural water systems with characteristic reaction times which are in the range of days.

The role of the iron cycle on trace metal mobility in natural water systems has been traditionally associated to the oxic/anoxic redox transitions and the effect of increased CO_2 concentrations has been mainly explained by the formation of Fe(II) carbonate complexes in anoxic/reducing conditions. However, already in 1992 , the effect of increased CO_2 on Fe(III) oxyhydroxide dissolution by the formation of mixed Fe(III) hydroxocarbonato complexes was indicated established (Bruno et al., 1992b; Bruno and Duro, 2000). The stoichiometry and stability of the mixed hydroxocarbonato complexes was firmly determined by Grivé in her PhD Thesis (2005) and it has been recently published (Grivé et al., 2014a, b). In this work was shown that the solubility of Fe(III) is enhanced some 3 to 4 orders of magnitude as $CO_2(g)$ is increased from present atmospheric to 1 bar at the pH range of most natural waters. This is mainly due to the formation of one mixed hydroxocarbonato complex, $Fe(OH)CO_3(aq)$, predominant in the circumneutral pH range and a very stable Fe(III) carbonato complex, $Fe(CO_3)_3^{3-}$, in the alkaline pH range.

7. Conclusions

Increased atmospheric CO_2 concentrations have an effect on the aquatic chemistry of seawater by increasing the total carbonate content and increasing the acidity.

The buffering capacity of the oceanic system is quite large but a clear increase of acidity and of the dissolved CO_2 content can be observed, provided a careful date analyses is performed in a long time series (Bates et al., 2014)

The effect of increased acidity in trace elemental solubility is obvious but the net effect of increased carbon dioxide concentrations is more complex. The increased dissolution due to the formation of aqueous carbonate complexes can be balanced by the formation of carbonate solid phases. However, as the kinetics of the carbonate complex formation is faster than the build up of carbonate solid phases, in a dynamic situation a net metal release could be observed when the partial pressure of CO_2 is increased.

Our observations from several CO_2-rich systems would indicate that there is a marked increase of Fe(III) solubility due to the formation of aqueous hydroxo carbonate and carbonate complexes (Agnelli et al., 2013; Grive et al., 2014). This increase on Fe(III) solubility cascades in the release of trace elements associated to Fe(III) oxyhydroxide solid phases.

An analysis of the observations by Ardelan et al. (2012) on the effect of increased CO_2 on increased trace metal dissolution would indicate that most of the trace elemental mobility is due to secondary dissolution as a result of the destabilisation of Fe(III) oxyhydroxides and/or the competing kinetics between aqueous and solid metal carbonate complex formation.

Acknowledgements

This work was initiated during a post-doctoral stay of one of us (JB) some decades ago at EAWAG, where he enjoyed the privilege of acquiring a very wide perspective on aquatic chemistry with a terrific number of enthusiastic and skilful researchers under the lead of Werner Stumm. Laura Sigg was one of this extremely enthusiastic and very skilful chemists that brought robustness to the work of the EAWAG team. It is a real pleasure to contribute to this well-deserved Special Issue in her honour. The review and calculations performed in this research article have been done in the frame of the MetTrans Initial Training Network (2012-2016; http://www.mettrans-itn.eu/) of the Marie Curie Programme of the EC through a grant to M.Agnelli.

References

Agnelli M, Grandia F, Credoz, A, Gasparini A, and Bruno J (2013) Use of diffusive gradients in thin films (DGT) as an early detection tool of low-intensity leakage from CO_2 storage. Greenhouse Gases: Science&Technology 1:1-13.

Ardelan MV, Sundeng K, Slinde GA, Gjøsund NS, Nordtug T, Olsen AJ, Steinnes E, Torp TA (2012) Energy Procedia 23: 449 – 461.

Bates NR, Astor YM, Church MJ, Currie K, Dore JE, González-Dávila M, Lorenzoni L, et al (2014) A time-series view of changing ocean chemistry due to ocean uptake of anthropogenic CO_2 and ocean acidification. Oceanography 27(1):126–141. http://dx.doi.org/10.5670/oceanog.2014.16.

Berner RA, Lasaga AC (1989) Modelling of the geochemical carbon cycle. Scientific American 260: 74-81.

Bruno J (1986) Stoichiometric and structural studies on the Be(II)-H_2O-CO_2(g) system. PhD Thesis Department of Inorganic Chemistry, Royal Institute of Technology. Stockholm.

Bruno J, Ferri D, Grenthe I, Sandström M (1987) Studies on metal carbonate equilibria 15. The Be(II)-H_2O-CO_2(g) system in acidic 3.0 M perchlorate medium, at 25º C. J. Chem. Soc., Dalton Trans. 2445-2449.

Bruno J (1990) The influence of dissolved carbon dioxide on trace metal speciation in seawater. Mar. Chem. 30: 231-240.

Bruno J, Stumm W, Wersin P, Brandberg F (1992a) On the influence of carbonate in mineral dissolution I. The thermodynamics and kinetics of hematite dissolution in bicarbonate solutions at 25ºC. Geochim. Cosmochim. Acta 56: 1139-1147.

Bruno J,Wersin P, Stumm W (1992b) On the influence of carbonate in mineral dissolution II.The thermodynamics and kinetics of siderite dissolution in bicarbonate solutions at 25ºC. Geochim. Cosmochim. Acta 56: 1149-1155.

Bruno J, de Pablo J, Duro L, Figuerola E (1995) Experimental study and modelling of the U(VI)-$Fe(OH)_3$ surface precipitation/coprecipitation equilibria. Geochim. Cosmochim. Acta 59: 4113-4123.

Bruno J, Duro L (2000) Reply to W. Hummel's comment on and correction to "On the influence of carbonate in mineral dissolution I. The thermodynamics and kinetics of hematite dissolution in bicarbonate solutions at 25ºC. Geochim. Cosmochim. Acta 56, 1139-1147." Geochim. Cosmochim. Acta 12: 2173-2176.

Bruno J, Duro L, Grivé M (2002) The applicability and limitations of thermodynamic geochemical models to simulate trace element behaviour in natural waters. Lessons learned from natural analogue studies. Chemical geology, 190(1): 371-393.

Bruno J, Grandia F, Vilanova E (2009) Trace element behaviour in connection to the geological storage of CO_2. Lessons from natural analogues. Abstracts of the Goldschmidt Conference, 2009, Davos (Switzerland). Geochim Cosmochim Acta 73(13):A167.

Chaffee E, Dasgupta TP, Harris GM (1973) Kinetics and mechanism of aquation and formation reactions of carbonato complexes V. Carbon dioxide uptake by hydroxopentaaminecobalt(III) ion. J.Am. Chem. Soc. 95: 4169.

Dasgupta TP, Harris GM (1977) Kinetics and mechanism of aquation and formation reactions of carbonato complexes. 11. Carbon dioxide uptake and intramolecular carbonato ligand chelation in aqueous solution of cis- and trans-diaquo(1,4,8,11-tetraazacyclotetradecane)cobalt(III) cations. J. Am. Chem. Soc. 99 (8): 2490–2495.

Duro L (1996) Estudio cinético y termodinámico de la interacción entre U(VI) y oxihidróxidos de Fe(III). PhD. Thesis. Universidad Politécnica de Cataluña. Barcelona.

Dzombak DA, Morel FMM (1990) Surface Complexation Modelling: Hydrous Ferric Oxide. John Wiley and Sons 245-287.

Ferri D, Grenthe I, Hietanen S, Salvatore F (1987a) Studies on metal carbonate equilibria 17. Zinc (II) carbonate complexes in alkaline solutions. Acta Chem. Scand. A 41:190.

Ferri D, Grenthe I, Hietanen S, Salvatore F (1987b) Studies on metal carbonate equilibria 18. Lead (II) carbonate complexes in alkaline solutions. Acta Chem. Scand. A 41: 349.

Giffaut E, Grivé M, Blanc P, Vieillard P, Colàs E, Gailhanou H, Gaboreau S, Marty N, Madé B, Duro L (2014) Andra thermodynamic data for performance assessment: ThermoChimie. Applied Geochemistry (in press).

Grivé M (2005) The linkage between uranium, iron and carbon cycling, processes at interfaces: evidences from combined solution chemical and spectroscopic studies. Ph.D. Thesis. Universitat Politècnica de Catalunya, Barcelona.

Grivé M, Duro L, Colàs E, Giffaut L (2014) Thermodynamic data selection applied to radionuclide and chemotoxic elements: an overview of the ThermoChimie-TDB. Applied Geochemistry (in press).

Grivé M, Duro L, Bruno J (2014) Fe(III) mobilization by carbonate in low temperature environments: study of the solubility of ferrihydrite in carbonate media and the formation of Fe(III) carbonate complexes. Applied Geochemistry.

Grivé M, Duro L, Bruno J (2014) Fe(III) mobilization by carbonate in low temperature environments 2: the applicability of the thermodynamic scheme including Fe(III) carbonate complexes to explain the increased Fe(III) concentrations in CO2-rich waters (In press).

Huanga D, Makhlynetsb OV, Tanc LL, Leec SC, Rybak-Akimovab EV, Holma RH (2011) Kinetics and mechanistic analysis of an extremely rapid carbon dioxide fixation reaction. Proc. National Acad. Sciences 108: 1222-1227.

Hietanen S, Högfeldt E (1976) A potentiometric study of the solid phases in the systems Hg(I)-HCO_3^- and Hg(II)-HCO_3^-. Chem. Scripta 9: 24-29.

Kharaka YUK, Thordsen JJ, Kakouros E, Ambats G, et al (2010) Changes in the chemistry of shallow groundwater related to the 2008 injection of CO_2 at the ZERT Field Site, Bozeman, Montana. Environ. Earth. Sci. 60: 273-284.

Keating EH, Hakala JA, Viswanathan H, Carey JW, et al (2013) CO_2 leakage impacts on shallow groundwater: Field-scale reactive-transport simulations informed by observations at a natural analog site. App. Geochem 30: 136-147

Kitajima N, Fujisawa K, Koda T, Hikichi S, Morooka Y (1990) Fixation of atmospheric CO_2 by a copper(II) Complex. Chem Commun 1357–1358.

Kitajima N, Hikuchi S, Tanaka M, Moro-oka Y (1993) Fixation of atmospheric CO_2 by aseries of hydroxo complexes of divalent metal ions and the implication for the catalytic role of metal ion in carbonic anhydrase Synthesis, characterization, and molecular structure of .LM.OH._n (n . 1 or 2) and LM.μ-CO3.ML (M.II. . Mn, Fe, Co, Ni, Cu, Zn; L . HB.3;5-i Pr2 pz.3). J Am Chem Soc 115: 5496–5508.

Lions J, Devau N, de Larya L, Dupraza S, et al (2014) Potential impacts of leakage from CO2geological storage on geochemical processes controlling fresh groundwater quality: A review. Intl. J. of Greenhouse Gas Control 22: 165-175.

Luther GW, Kostka JE, Church TM, Sulzberger B, Stumm W (1992) Seasonal iron cycling in the salt-marsh sedimentary environment: The importance of ligand complexes with Fe(II) and Fe(III) in the dissolution of Fe(III) minerals and pyrite respectively. Mar. Chem. 40: 81-103.

Miller M, Alexander R, Chapman N, McKinley I, Smellie J (2000) Geological disposal of radioactive wastes and natural analogues. Waste Management Series vol 2. Permagon. The Netherlands.

Murthy NN, Karlin KD (1993) A Dinuclear Zinc-Hydroxide Complex which Traps Atmospheric Carbon Dioxide: Formation of a Tri-Zinc complex with a Triply-Bridging Carbonate group. J. Chem. Soc., Chem. Commun 1236-1238.

Parkhurst, D.L. and Appelo, C.A.J., (2013) Description of input and examples for PHREEQC version 3--A computer program for speciation, batch-reaction, one-dimensional transport, and inverse geochemical calculations: U.S. Geological Survey Techniques and Methods, book 6, chap. A43, 497 p.

Payán MC, Verbinnen B, Galan B, Coz A, Vandecasteele C, Viguri JR (2012) Potential influence of CO_2 release from a carbon capture storage site on release of trace metals from marine sediment. Environmental Pollution 162: 29-39.

Peter A, Lamert H, Beyer M, Hornbruch G, Heinrich B, et al (2012) Investigation of the geochemical impact of CO_2 on shallow groundwater: design and implementation of a CO_2 injection test in Northeastern Germany. Environ. Earth Sci. 67: 335-349.

Piqué A, Grandia F, Canals A (2010) Processes releasing arsenic to groundwater in the Caldes de Malavella geothermal area, NE Spain. Water Res 44: 5618–5630 .

Stumm W, Sulzberger B (1992) The cycling of iron in natural environments: Considerations base on laboratory studies of heterogeneous redox processes. Geochim. Cosmochim. Acta 56: 3233-3257.

Puigdomènech I (2013) http://www.kemi.kth.se/medusa/

Stumm W (1992) Chemistry of the solid-water interface. Processes at the mineral-water and particle-water interface in natural systems. John Wiley & Sons, Inc.

Sadler GG, Dasgupta TP (1987) Dinuclear complexes of transition metals containing carbonate ligands 7. Kinetics and Mechanism of Formation of μ-(carbonato) bis (μ-hydroxo) bis (triamminecobalt(III)) ion in weakly basic aqueous carbonate. Inorg. Chem, 26: 3254-3257.

Spangler LH, Dobeck LM, Repasky KS, Nehrir AR, Humphries SD (2010) A shallow subsurface controlled release facility in Bozeman, Montana, USA, for testing near surface CO_2 detection techniques and transport models. Environ. Earth Sci. 60: 227–239.

Spitzer U, Van Eldik R, Kelm H (1982) Mechanistic information from the effect of pressure on the formation and acid-catalyzed aquation reactions of (carbonato)pentaamminecobalt(III), -rhodium(III), and -iridium(III) ions in aqueous solution. Inorg. Chem. 21 (7): 2821–2823.

Tans PT, Kieling R (2014) NOAA/ESRL (www.esrl.noaa.gov/gmd/ccgg/trends/). Scripps Institution of Oceanography (scrippsco2.ucsd.edu/).

Tassi, F., Vaselli, O., Luchetti, G., Montegrossi, G. & Minissale, A., (2008c). Metodo per la determinazione dei gas disciolti in acque naturali. CNR-IGG Rapporto Interno n. 2/2008, p. 10.

Trautz RC, Pugh JD, Varadharajan C, Zheng L, et al (2013) Effect of dissolved CO_2 on a shallow groundwater system: a controlled release field experiment. Environ. Sci. Tech. 47: 298-305.

Vilanova E (2004). Anàlisi dels sistemes de flux a l'àrea Gavarres-Selva-Baix Empordà . PhD thesis, Universitat Autònoma de Barcelona, 337 pp.

Waite TD, Davis JA, Payne TE, Waychumas GA, Xu N (1994) Uranium(VI) adsorption to ferrihydrite: Application of a surface complexation model. Geochim. Cosmochim. Acta, 58(24): 5465-5478.

Zeebe RE, Wolf-Gladrow D (2001) CO_2 in seawater: equilibrium, kinetics, isotopes. Volume 65 (Elsevier Oceanography Series).

Zheng L, Apps JA, Zhang Y, Xu T, Birkholzer JT (2009) On the mobilization of lead and arsenic in groundwater in response to CO_2 leakage from deep geological storage. Chem. Geol. 268: 281-297.

Metal enrichment in shallow aquifers due to $CO_{2(g)}$-rich fluids intrusion: the influence of carbonate aqueous species on iron solubility and metal plumes in natural systems

Marco Agnelli [a], Fidel Grandia [a], David Soler [b], Alvaro Sainz [a,c], David Brusi [b], Manel Zamorano [b], Jordi Bruno [a]

[a] *Amphos 21 Consulting S.L., Passeig Garcia i Fària, 49-51, 08019 Barcelona – Spain.*

[b] *Centre de Geologia i Cartografia Ambiental (GEOCAMB), Departament de Ciències Ambientals, Facultat de Ciències, Universitat de Girona. Campus de Montilivi s/n, 17071 Girona – Spain.*

[c] *Université Toulouse III - Paul Sabatier - Route de Narbonne 118, 31062- Toulouse – France*

Abstract

The interaction between carbon dioxide gas flows and groundwater leads to the dissolution, mobilization and re-precipitation of metals and metalloids. The potential for metal release associated with CO_2 leakage from underground storage formations into shallow aquifers is an important aspect in the risk assessment associated with CO_2 sequestration, and the understanding of the persistence of metal plumes is a very concerning aspect. In the Campo de Calatrava region, an old volcanic field in central Spain, CO_2 flows from mantle interact with shallow aquifers resulting in remarkable metal release. 12 sampling stations have been selected for gas and water analysis, 10 as bubbling pools and 2 as episodic "cold" geysers. These samples are characteristically much enriched in trace metals compared to CO_2-free aquifers, being Fe the most abundant, (up to 6.08×10^{-4} mol·L^{-1}). Also, high concentrations of Mn (up 8.01×10^{-5} mol·L^{-1}), Zn (up to 1.46×10^{-6} mol·L^{-1}), Ni (up to 1.19×10^{-6} mol·L^{-1}), Co (up to 7.1×10^{-7} mol·L^{-1}), Cu (up to 3.3×10^{-7} mol·L^{-1}) and As (up to 1.4×10^{-7} mol·L^{-1}). pH range is very close to 6 and Eh is quite oxidising. Gas composition is almost pure CO_2, with no detectable amounts of CH_4 and H_2S.

Thermodynamic calculations reveal that the formation of aqueous Fe(III) carbonate complexes, mainly $FeCO_3OH$, as a result of the CO_2-shallow aquifer interaction causes the dissolution of native $Fe(OH)_3$ releasing iron and all trace metals sorbed onto its charged surface. Then, neither acidification, "reducing" gas impurities, nor low Eh environments (i.e., making Fe(II) as predominant iron form) can be considered as the main drivers for the development of the metal plumes associated to gas inflows into shallow aquifers. The persistence of these metal plumes, which is crucial in the risk assessment studies of CO_2 underground storage, is predicted to be potentially long since $Fe(OH)_3$ is the solubility-limiting phase not only for Fe but also for the other metals with an observed increase in concentration. The effect of the formation of aqueous metal carbonate is not as relevant in metals like Mn, Zn, Cu, Co, Ni, and except for Mn, the

measured concentration in samples from the Campo de Calatrava are far from the saturation in solid carbonates.

Keywords: Carbon storage, leakage, metal transport, natural analogue, Campo de Calatrava

Introduction:

The capture and storage of CO_2 in deep subsurface reservoirs is one of the options currently being considered to lower the industrial emissions of this greenhouse gas to the atmosphere. The site selection of CO_2 storage reservoirs must be accurate enough to minimize the risks to human health and the environment (Rempel et al., 2011; Zheng et al., 2011). However, the possibility of CO_2 leakage cannot be completely ruled out, in which case the stored CO_2 could migrate following preferential pathways upward into overlying shallow groundwater resources. The presence of high carbon dioxide content into an aquifer leads to chemical interactions between the CO_2, brine and reservoir rock, leading the dissolution, mobilization and re-precipitation of metals and metalloids (Czernichowski-Lauriol et al., 2006; Fischer et al., 2010; Kharaka et al., 2006; Kharaka et al., 2009; Wigand et al., 2008). The potential for metal release associated with CO_2 leakage from underground storage formations into shallow aquifers is an important aspect in the risk assessment associated with CO_2 sequestration. The effects of increased CO_2 concentrations on the release of metals like Zn, Cu, Co and Ni in shallow aquifers have been studied using numerical simulation (Apps et al., 2010; Atchley et al., 2013; Navarre-Sitchler et al., 2013; Siirila et al., 2012; Wang and Jaffe, 2004; Wilkin and DiGiulio, 2010; Zheng et al., 2012), laboratory experiments (Frye et al., 2012; Little and Jackson, 2010; Lu et al., 2010; Romanò et al., 2013; Wei et al., 2011) and few field studies (Agnelli et al., 2013; Kharaka et al., 2009; Trautz et al., 2013). In most studies, the exposure of aquifer materials to CO_2 increased the aqueous concentrations of metals, although in some cases such increase was episodic (Lu et al., 2010). In other cases, the concentration of some metals decreased altogether (Little and Jackson, 2010). In principle, the metal transport capacity of CO_2-bearing fluids in shallow aquifers should increase as pH decreases; another potential mechanism is the formation of low Eh environments due to the presence of "reducing" trace gases (e.g., H_2S and CH_4). More recently, Grivé et al. (2014) showed that Fe(III) solubility in CO_2-bearing fluids can significantly increase due to the formation of Fe(III) carbonate complexes that are stable at circumneutral pH's, and, therefore, being more persistent in time and space in geological media. The enhanced solubility of Fe(III) has an additional and unwanted side effect: the inhibition of the precipitation of $Fe(OH)_3$ (am), which is a major sink for many trace and minor elements. The $Fe(OH)_3$ precipitation is favoured when CO_2 starts degassing due to loss of pressure (i.e., fluid ascent to surface through faults or by well production) and, eventually, part of all these metals may precipitate back into solid phases; but

some of the metal load is still dissolved.

The high solubilisation of metals can be used as a monitoring tool of CO_2 leakage episodes. Time-lapse measurement of metal contents in shallow aquifers can help in the early detection of seal failure of CO_2 storage site because the concentration of all these metals in shallow and surface waters is commonly very low, and tiny changes in such a concentration could be indicative of early leakage (Agnelli et al., 2013; Romanò de Orte et al., 2013; Wunsch et al., 2013).

Constraining the duration and intensity of metal release to the aquifer is fundamental in the risk assessment of the geological storage because such metal increase, if fast and intense, can jeopardise the quality of water resources. The rates of metal release due to CO_2(g)-water interaction are believed to be quite fast in view of laboratory experiments and from few pilot plant-scale injection operation. Recently, Romanò de Orte et al. (2013) found, in a laboratory experiment, how Fe content in water increased 85% and persisted in water due to a decrease of pH from 7 to 5.5 in 10 days, showing that short time interaction between CO_2(g) and water is sufficient to dramatically increase the metal concentration in the water. Furthermore, in natural systems, some examples of episodic intrusion of deep natural CO_2 into shallow aquifers provide evidence of quick metal increase in solution (Piqué et al., 2010).

In this research article, the interaction of deep CO_2 fluxes with shallow aquifers is investigated through the geochemistry of CO_2-bearing waters and gas emissions in natural systems in the Campo de Calatrava region in central Spain. A ubiquitous feature of the CO_2-rich waters in this area is the reddish color due to the formation of iron hydroxide colloids. The quality of these springs and aquifers is not acceptable in terms of metal content and represents an illustrative example of the impact of potential leakage from deep geological storage. The role and importance of the aqueous Fe(III) carbonate complexes in metal mobility is assessed and compared against other mechanism of metal solubilisation, such as acidity or reducing gases.

Geology of the Campo de Calatrava Volcanic Province:

The use of natural systems as analogues of geological storage of waste (CO_2, spent nuclear fuel) and energy (H_2, methane) is valuable since it provides evidence for processes occurring at mid and long term, extending in time the observations collected at lab scale. In this work, the impact of CO_2 flows on metal mobility in shallow aquifers has been studied in the Campo de Calatrava volcanic field (CCVF), which hosts a large number of CO_2 emission sites, either as free gas discharges or dissolved in water. The CCVF is a late Cenozoic intraplate volcanic region located in the province of Ciudad Real (south-central Spain). Its geology consists mainly of horst and grabens with folded and thrusted Ordovician-Silurian slates, quartzites and limestones of the

Variscan age, overlaid by late Miocene to Quaternary continental sediments coeval with alkaline mafic volcanic rocks. Location, extension and thicknesses of these grabens are strongly influenced by a complex pattern of normal faults developed after different episodes of weak compressional and extensional stress field conditions since the Oligocene within the Iberian intracratonic crust (Vegas and Rincón-Calero, 1996; López-Ruiz et al., 2002 and references therein). Volcanism took place intermittently between 8.7 and 1.75 Ma BP and formed about 200 monogenetic strombolian and hydromagmatic emission points intimately linked to the fracture network. Magmas have a clear mantellic origin and range from olivine melilites-nephelinites-leucitites to alkaline olivine basalts and basanites (Ancochea, 1992; Cebriá and López-Ruiz, 1995; Ancochea, 1999).

Although the volcanism is presently extinct, CO_2 degassing from mantle is still active. Deep faults are the main conduits of gas ascent to ground surface. A mean diffuse CO_2 emission rate from soil of 2.1 $g \cdot m^{-2} \cdot d^{-1}$ and a total efflux of 2492 ± 282 $t \cdot d^{-1}$ has been estimated for an area of 758 km^2 in CCVF (Calvo et al., 2010), whereas point-source anomalies up to 5000 $g \cdot m^{-2} \cdot d^{-1}$ have also recently been reported (Elío et al., 2015). Where gas interacts with groundwater, it dissolves and migrates following the aquifer hydrodynamics, eventually flowing out at natural or man-made bubbling springs, locally named "hervideros" ("boiling pools", Poblete, 1992; Yélamos et al., 1999). In confined aquifers, well drilling often causes the occurrence of "cold" geysers that may remain active up to several months (Rolandi and Barrera, 2003) (Fig. 1a).

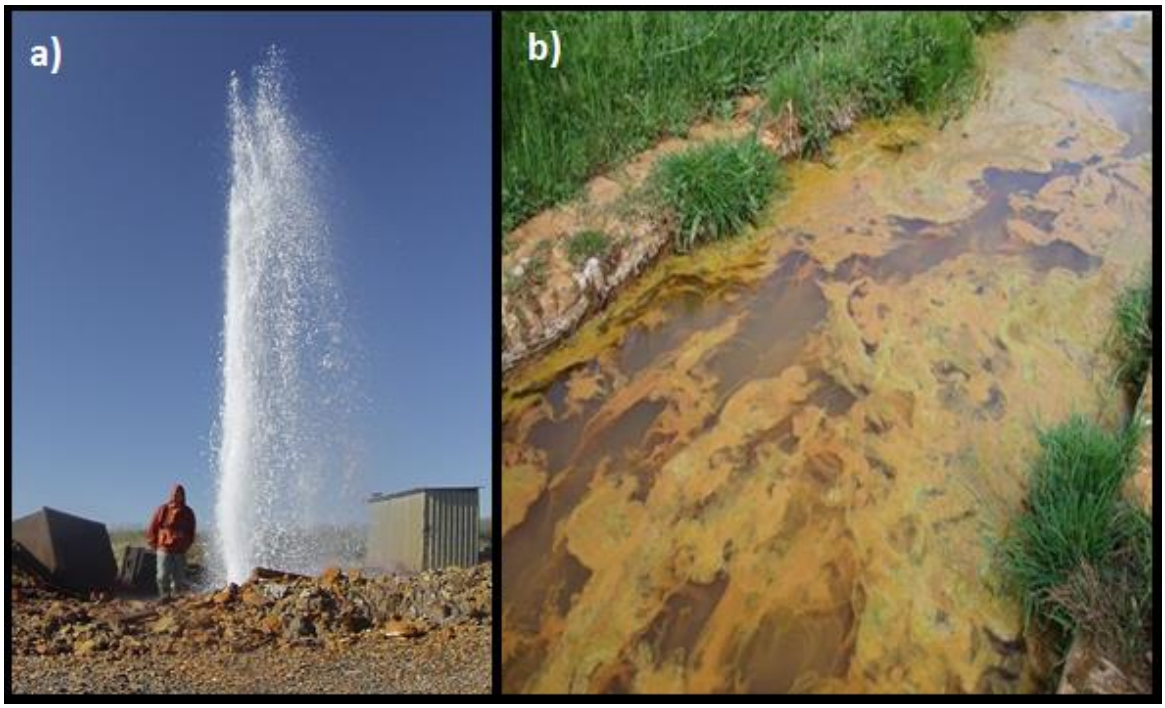

Figure 1: Gas and water eruption at sampling station "Chorro Glicerio" near Almagro village in 2014 (a) and the formation of iron hydroxide colloids and algae growth over the water table (b).

Main aquifers in the region are related to the Miocene-Pliocene sedimentary cover. These waters are commonly fresh and neutral where they are not impacted by deep gases, with conductivities below 500 $\mu S \cdot cm^{-1}$and alkalinity around 5×10^{-3} M (Confederación Hidrográfica del Guadiana, www.chguadiana.es). Where interacted with CO_2(g), they quickly become reddish after the formation of iron hydroxide colloids and causing significant changes in the biogeochemistry of the surface waters (Fig. 1b). Evidence for long-term gas-water-rock interaction in Campo de Calatrava is found in some Miocene-Pliocene rock formations which presently are exposed but were aquifers in the past; these rocks are strongly cemented by iron hydroxides (Fig. 2).

Figure 2: Conglomerate level from Neogene sedimentary cover in the Jabalón river area, in the Campo de Calatrava volcanic field. The black-coloured mineralisation is $Fe(OH)_3$ that cements the rock, related to CO_2-water interaction.

Methodologies:

Electrical Resistivity Tomography:

In order to constrain ground geology and hydrogeology related to the CO_2-bearing water emission points, electrical resistivity tomography (ERT) investigations were carried out at the Cañada Real site (see location in Fig. 3), the largest CO_2 discharge in CCVF. Three profiles between 200 and 600 m long (ERT#1 to ERT#3) were carried out in May 2014 (Fig. 4). The objective was mapping the electrical resistivity distribution in the subsurface i) to delineate the geometry of the geological formations that host the local shallow aquifer and the rock basement, ii) to determine depth and width of the WSW-ENE oriented fault zone that apparently acts as main pathway for the gas

release, and iii) to identify geo-electric anomalies related to the presence and dynamics of gas-rich waters.

Apparent resistivity data acquisition was implemented with a Lund Imaging System (ABEM Instrument AB, Sweden), according to Wenner-Schlumberger configuration. A sequence of two correlative protocols involving all the possible quadripoles from up to 41 available electrodes connected to the ground at the same time was followed (ABEM, 2009). A first ("long") batch considered the full transect length at a constant electrode spacing (i.e., 10 m for ERT#1 and ERT#3, 20 m for ERT#2). A second ("short") one comprised only the two central multicore cable coils and an electrode separation half of the previous. Measurements were done once again in the central segment of lines ERT#1 and ERT#2 where the spring and/or the fault zone are present, by overlapping the same array with a reduced electrode spacing of 5 and 2.5 m in ERT#1 in the case of the "long" and "short" configuration respectively, and 10-5 m in ERT#2. This allowed higher resolution coverage of the most interesting areas of the profiles. Since a certain number of resistivity points were measured twice with a few hours difference, it provided a time-lapsed set of data that afterwards was used to check short term resistivity variations within the water system. Data inversion was performed with Res2DInv package (Geotomo Software, Malaysia). After a pre-processing manual deletion of bad (noisy) data points and a preliminary default inversion to discard some records with excessive difference between measured and calculated values, 96-98% of the data remained valid for the analysis (723 to 1,269 points). Iterative least squares inversion and finite-element forward modelling (Loke and Barker, 1996; Loke, 2014) was applied to apparent resistivity pseudo-sections to get the final resistivity sections, giving a bulk root mean square error (RMS) of 7.3 to 9.2% that reflects an acceptable quality for the models. The maximum investigation depths from the surface ranged between 40 and 91 m.

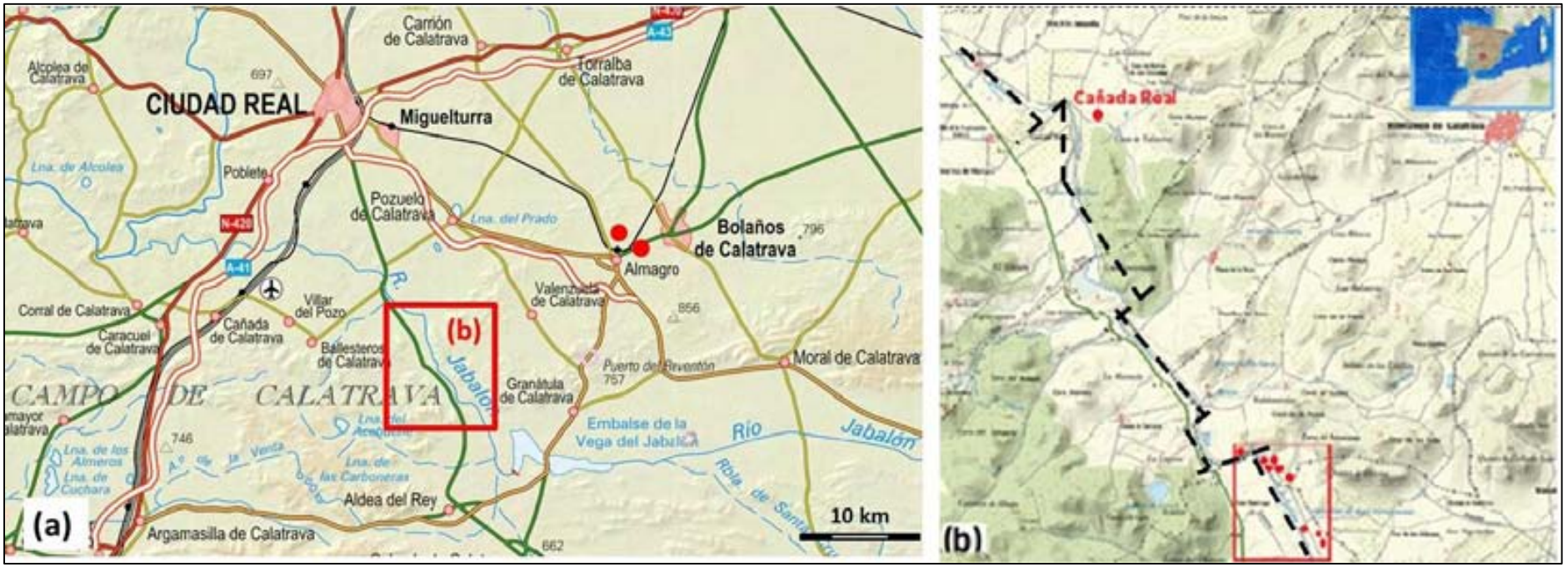

Figure 3: Location of sampling stations in the Jabalón river basin in the Campo de Calatrava region (from Visor Iberpix IGN, http://www.ign.es/iberpix2/visor).

Water and gas sampling:

12 sampling stations have been selected for gas and water analysis, 10 as bubbling pools and 2 as episodic "cold" geysers. The sampling of the two geysers was found relevant because they provide a unique opportunity to collect aquifer waters not affected by a long-term degassing, and, therefore, to collect more pristine water from the impacted aquifer. Degassing leads to the formation of Fe(III) hydroxide colloids that can trap metals by surface sorption, lowering the metal concentration in solution.

From each sampling site, 3 aliquots of water were collected: *i)* 125 mL in a plastic bottle for the anions analysis; *ii)* 50 mL in a plastic bottle for cations; the bottles were previously acidified with 0.5 mL of Suprapur HCl, and collected water was filtered using 0.45 µm filters; iii) 50 mL in a plastic bottle for trace metals analysis; the bottles were previously acidified with 0.5 mL of 1M HNO_3 and collected water was filtered using 0.1 µm filters. The analysis of the dissolved gases in aqueous phase was performed by using a method set up by Tassi et al. (2008) in which the determination of dissolved gases concentration is carried out at equilibrium conditions. The sampling is operated by using gas tubes with a capacity of 200-300 mL with a Teflon stopcock. In the laboratory the gas vials are pre-evacuated by a rotary pump with a vacuum value of 10^{-1}-10^{-2} Pa. By submerging the gas vial into the water and opening the Teflon stopcock, the water is forced to enter the vial by decompression. Normally, >70% of the tube volume has to be filled with water in order to allow the chemical determination. The pH-Eh measurements were performed in the field using a Crison portable pH-Eh meter with a platinum electrode for the redox determination.

Results:

Electrical resistivity tomography

Results of the three electrical resistivity tomography profiles at Cañada Real site provide clues on the subsurface features of shallow aquifers impacted by CO_2(g) flows, and on their hydrodynamics. Three resistivity units can be distinguished according to the resistivity distribution along these profiles (Fig. 4). In the data treatment model, resistivity values have been arbitrarily classified into four categories: very low (<4 Ωm), low (4 - 16 Ωm), medium (16 - 64 Ωm) and high (>64 to ≈650 Ωm). The uppermost resistive unit defines a roughly continuous level parallel to the surface in all the profiles, with a minimum thickness of 5-7 m and a maximum of 15 m. This unit is attributed to Upper Pliocene calcarenites (IGME, 1988a, 1988b). Groundwater table is located within this unit at depths mostly ranging between 4.5 and 5.5 m from the surface. Beneath, a second resistive unit is characterized by very low to low resistivity values with some low-medium resistivity patches in its eastern upper zones. Presumably, it is

formed by Upper Pliocene sediments (IGME, 1988a, 1988b). In accordance with the low resistivity values, it may be assumed that the unit is saturated with groundwater. The bottom of the geo-electrical sections forms a third resistive unit attributed to the Ordovician quartzite basement. However, this third unit is cut by an area with low-medium resistivity values which is considered to be a fracture zone of WSW-ENE orientation and over 50 m wide. This pattern may be attributed to rocky topographic highs located at both sides of a nearly vertical fault zone where materials affected by fracturing and weathering are present. This fault likely is the conduit for the ascent of CO_2 flows in the area. Upward migration of gas would cause a progressive decrease in resistivity of the Neogene sediments as it gradually becomes dissolved into groundwater, increasing its electrical conductivity and hence, giving rise to very low resistivity areas. The size and distribution of these most conductive lenses probably reflect the stratigraphic position of patches of higher porosity (i.e., sand-gravel lenses with lesser fine content) which represent preferential pathways of the CO_2-bearing water to spread across the aquifer. A detailed inspection of resistivity distribution in the vicinity of the spring zone (X coordinates 20 to 40 m in line ERT#1) reveals distinctive features that can be directly linked to the process of groundwater upward migration and gas release (Fig. 5). Here, the uppermost calcarenitic unit hosts a negative anomaly that suddenly disrupts the horizontal continuity of prevailing high resistivity values. Under the first 3-4 m from the surface (18-30 Ωm), resistivity rapidly decreases to 4-16 Ωm, depicting a sort of hemispherical convex shape up to about 8-9 m depth. The anomaly extends even deeper inside the underlying detrital sediments, where it becomes a nearly vertical neck-shaped positive anomaly of low-medium values (8-20 Ωm) horizontally surrounded at both sides by two very low resistivity elliptical zones (<4 Ωm). No more distortion of the resistivity isolines is detected below 20-22 m deep, so the Paleozoic basement does not seem to be involved here in the dynamics that causes this particular anomaly.

Ascent of water across the fractured calcarenites would cause a marked reduction of their resistivity and originate the plume-like shape related to localized elevation of the water table. Finally, near-surface water degassing would increase again resistivity values immediately below the bubbling pond.

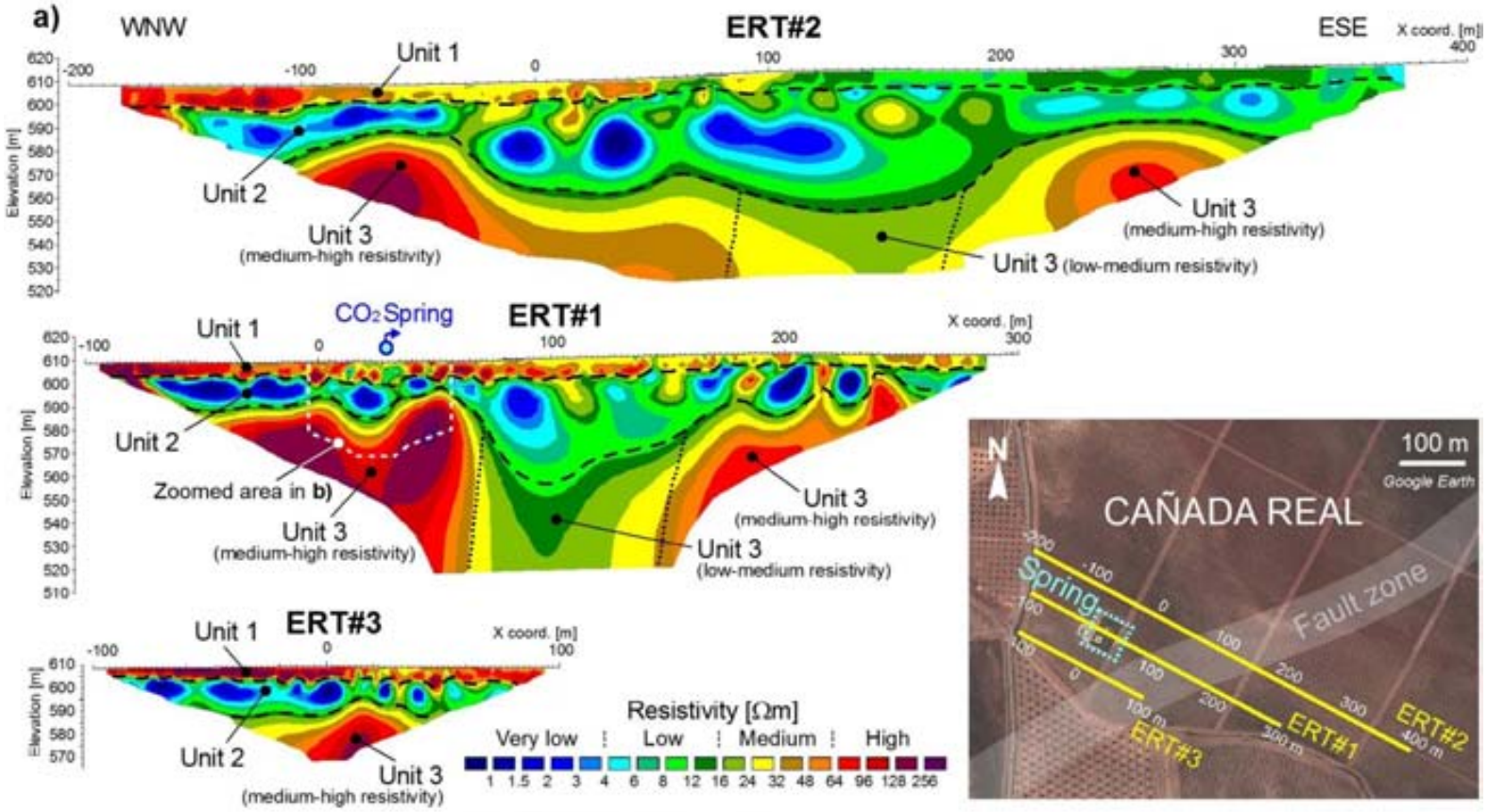

Figure 4 (a): Location and model sections of the three electrical resistivity tomography profiles measured at Cañada Real in May, 2014. The two existing bubbling springs are placed inside a green grassy rectangular area, surrounded by brown vineyard's terrain. The inferred cartographic trace of the CO_2 source fault zone is also indicated in the map. Resistivity scale in the sections is divided into four classes only for descriptive clarity. Black dashed lines delineate contacts between resistivity units 1, 2 and 3, whereas dotted lines indicate different resistivity areas within Unit 3. (b) Zoomed view of the resistivity section ERT#1 along the spring zone. Color scheme is adjusted to four discrete resistivity intervals in order to emphasize different features related to the CO_2 dynamics: (b1) uses the same scale as in Fig. 4a for a more detailed general perception; (b2) highlights very low and low resistivity values in Unit 2; (b3) calls attention to the convex shape defined by the ascending CO_2-bearing water plume across Unit 1; and (b4) illustrates horizontal spreading of gas and water in the near-surface.

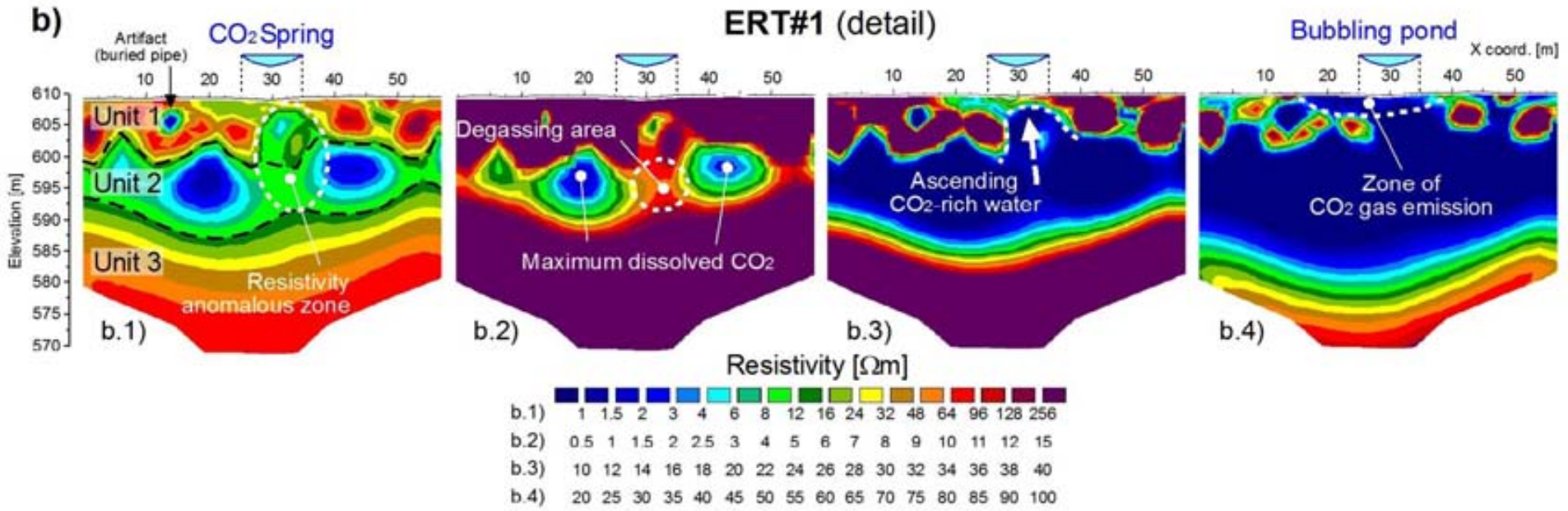

Figure 4 (b) Zoomed view of the resistivity section ERT#1 along the spring zone. Color scheme is adjusted to four discrete resistivity intervals in order to emphasize different features related to the CO_2 dynamics: (b1) uses the same scale as in Fig. 4a for a more detailed general perception; (b2) highlights very low and low resistivity values in Unit 2; (b3) calls attention to the convex shape defined by the ascending CO_2-bearing water plume across Unit 1; and (b4) illustrates horizontal spreading of gas and water in the near-surface.

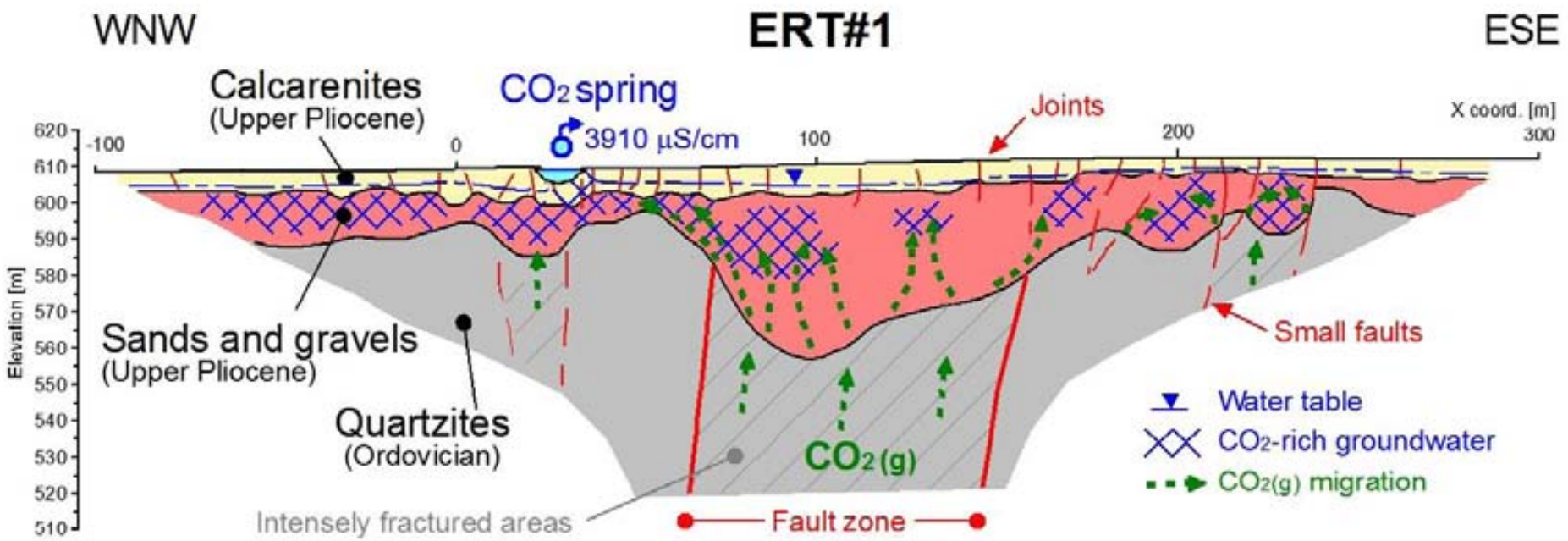

Figure 5: Interpretative model of CO_2 migration and its emanation on profile ERT#1. CO_2 gas ascending across the fractured and fine grained materials of the main fault zone and other minor faults enters the water-saturated Neogene sands and gravels, where it partly dissolves. Emission into the atmosphere at the bubbling spring may be linked to a stationary upward water-gas plume below it.

Water and gas composition:

The temperature and the chemical composition of major, minor and trace elements of the waters have been determined for all the springs (Table 1). Spring waters are characterized by a circumneutral pH in the range of 5.9 to 6.4, an electrical conductivity ranging from 1345 $\mu S \cdot cm^{-1}$ up to 3910 $\mu S \cdot cm^{-1}$ and Eh values in the range of 167.2 mV to 360.2 mV. Only in one station, Baño Chiquillo, a more reduced Eh value has been measured (-52 mV). Temperature at sampling point is 16.9 and 27 ºC. Major ion composition is Mg-Ca-HCO_3, with minor Na-Cl-SO_4 (Fig. 6, and Table 1). Dissolved CO_2 (mainly as bicarbonate) is the main anion in solution (up to 2110 $mg \cdot L^{-1}$, 34.6 $mol \cdot L^{-1}$, in the Cañada Real site) (Fig. 6). These data are quite similar as CO_2-free aquifers in the region (Table 2), although a general increase in the solute content is observed when CO_2 is present, suggesting some degree of water-gas-rock interaction.

Concerning the chemical composition of the dissolved gases (Table 3), CO_2 is by far the most abundant gas species, ranging from 85.77% to 99.92%, followed by N_2 and Ar. H_2S content was always less than the detection limit. These compositions are consistent with those reported in a previous study by Vaselli et al. (2013). The authors suggested that a mantle-sourced signature of these volcanic products is apparently preserved in many CO_2-rich (up to 99% vol) gas discharges in the Calatrava Volcanic Province, whose carbon and helium isotopic signature is characterized by values between -6.8 and -3.2 ‰ (V-PDB) and up to 2.7 R/Ra, respectively. The authors also found that nitrogen and argon are related to an atmospheric component, with values between that of the air (83) and that of ASW (Air Saturated Water).

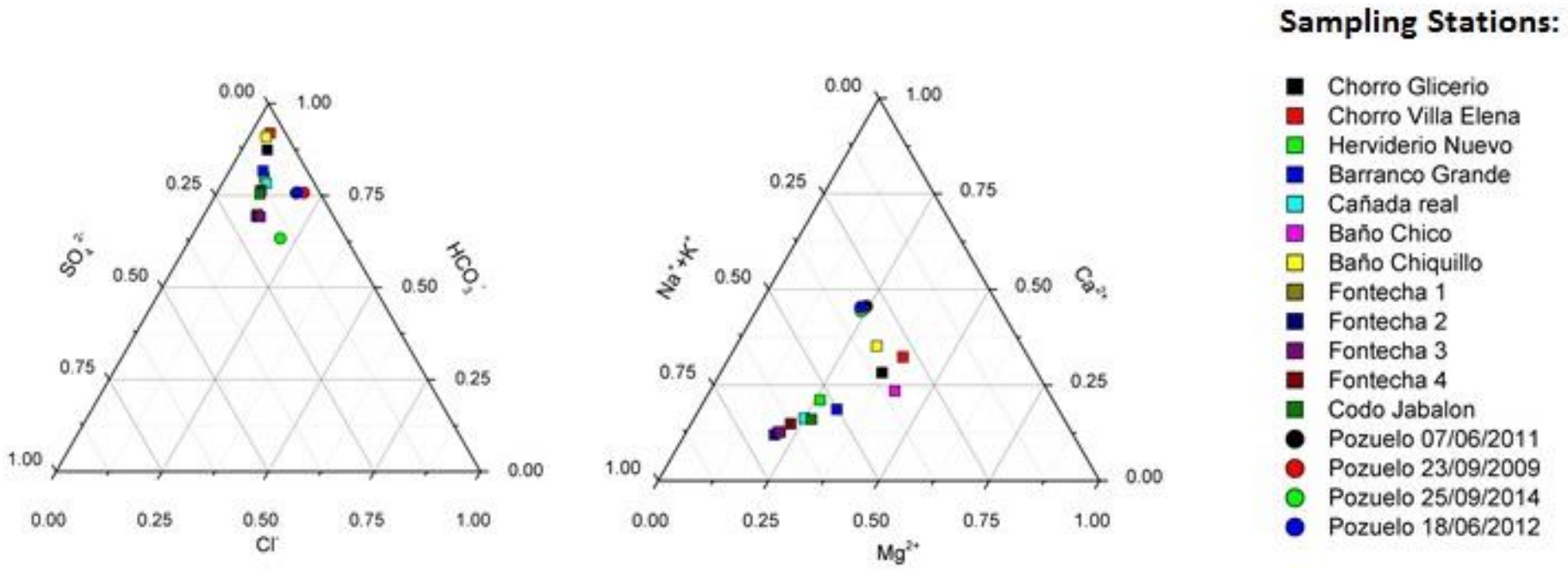

Figure 6: Triangular diagrams showing the chemical composition of the major elements in CO_2-bearing water samples, and in non-impacted aquifers in the Campo de Calatrava region. See Tables 3 and 4 for complete chemistry of these waters.

Table 1: Chemistry parameters of the CO_2-bearing springs sampled in Campo de Calatrava area. All the concentrations are expressed as mg·L^{-1}.

Sample	T °C	pH	Eh (mV)	Cond. El. (µS·cm^{-1})	HCO_3^-	F^-	Cl^-	Br^-	SO_4^{2-}	Ca^{2+}	Mg^{2+}	Na^+	K^+
Chorro Glicerio	16.9	6.2	181	3660	2482	0.42	173	0.49	186	237	308	229	66
Chorro Villa Elena	18.8	6.1	180	2390	1586	0.52	78	0.29	62	165	201	97	48
Fontecha 1	18.4	5.9	207	2430	997	0.58	178	0.38	251	65.9	109	301	43.8
Fontecha 2	22.4	5.9	295	2310	1022	0.72	187	0.40	267	65	111	324	43.2
Fontecha 3	21.5	6.2	313	2440	1052	0.86	206	0.31	262	68.2	115	313	42.8
Fontecha 4	27.1	5.9	17	1720	831	0.47	110	0.30	147	55.7	85	199	36
Cañada Real	21.8	6.1	282	3910	2111	0.47	281	0.77	305	151	232	466	80.2
Baño Chico	21.6	6.1	360	1600	1009	0.57	45.2	0.180	55.8	71.5	128	78.4	27.4
Baño Chiquillo	25.2	6.4	-53	1714	1105	0.78	49.3	0.1	61.1	124	113	84.9	31.1
Codo Jabalon	18.2	5.9	211	1345	975	0.60	134	0.33	184	68.3	114	212	31.9
Barranco Grande	21	6.1	167	2000	1054	0.57	103	0.20	134	76.3	128	166	39.7
Hervidero Nuevo	21	6.0	213	1626	676	0.73	77.8	n.d.	92.4	54.7	68.2	111	26.4

Table 2: Chemistry of the representative spring not affected by CO_2 in Campo de Calatrava. All the concentrations are expressed as mg·L^{-1}. Data from Confederación Hidrográfica del Guadiana (www.chguadiana.es).

Sample	Date	pH	HCO_3^-	Cl^-	SO_4^{2-}	Ca^{2+}	Mg^{2+}	Na^+	K^+
Pozuelo de Calatrava	mar-09	7.2	211	29.1	8.7	42.9	21.2	26.9	3.6
	sep-09	7.1	210	33	8.2	41.3	22.2	24.8	3.9
	aug-10	7.3	123	88.1	168	61.2	33.8	46.7	6.1
	nov-10	7.4	209	23.3	8.3	43.7	22.6	24.6	3.5
	jun-12	7.3	210	30.4	11.4	42.5	21.7	25.6	3.9
	dic-12	7.2	213	26.2	9.9	41.8	20.8	26.5	3.6
	jun-13	7.2	210	27.8	9.3	39.9	22.1	24.2	3.8
	dic-13	7.2	213	28.5	10.9	42.8	22.4	24.6	3.9
	oct-14	7.4	144	44.8	24.9	43.3	14.0	31.6	-
	nov-14	7.3	168.5	66.4	31.1	55.6	16.4	37.4	-

Table 3: Chemical composition of the dissolved gases sampled. All the values are reported in %.

Sample	CO_2	N_2	Ar	O_2
Barranco Grande	85.77	13.41	0.32	0.48
Chorro Glicerio	91.16	8.23	0.20	0.40
Chorro Villa Elena	88.35	11.25	0.16	0.30
Cañada Real	99.53	0.42	0.01	0.01
Hervidero Nuevo	88.50	11.12	0.23	0.14
Fontecha 1	92.00	7.66	0.17	0.16

Determination of alkalinity: CO_2 measured vs calculated

One of the key parameters in the assessment of the mobility of metals in the CO_2-impacted aquifers is the correct determination of the CO_2 pressure once dissolved. Such data are obtained by direct sampling of the gas phase since most sampling stations show gentle bubbling meaning that active degassing is occurring or gas flows are bubbled through the groundwater. In both cases, direct collection of the gas phase may lead to overestimation or underestimation of the CO_2 pressure in equilibrium with water. In this work, gas pressure data from direct sampling has been compared with CO_2 pressure calculated from alkalinity of water samples. The calculation has been done using the PHREEQC-3 code (Parkhurst and Appelo, 1999), and with the ThermoChimie v.9 database (Giffaut et al., 2014), including the SIT approach for ionic strength correction. The compared pressures for each sampling station are shown in Table 4. Calculated pressure is in general similar as measured in the field, although in some stations the difference is remarkable. This suggests that sampling is performed under gas-water disequilibrium, assuming that no degassing occurs after water collection.

Table 4: Sampled CO_2 pressure value vs. calculated (PhreeqC) pressure in the sampling stations.

Sample	Sampled CO_2 pressure (bar)	Calculated CO_2 pressure (bar)
Baño Chico	0.400	0.281
Baño Chiquillo	0.200	0.223
Barranco grande	0.200	0.295
Cañada Real	0.733	0.602
Chorro Glicerio	0.022	0.478
Chorro Villa Elena	0.020	0.457
Fontecha 1	0.029	0.316
Fontecha 3	0.700	0.288
Fontecha 4	0.600	0.281
Hervidero Nuevo	0.024	0.208

Gas pressure is important to quantify the impact of CO_2 on the aquifers in terms of water-gas-rock interaction. The nature of shallow aquifers receiving CO_2 discharges in the Campo de Calatrava region is not well constrained but thermodynamic equilibrium calculation from water chemistry can provide clues on the mineral assemblage. For sample "Pozuelo de Calatrava", considered as a representative example of non-impacted shallow aquifer in the region, the saturation index calculation indicates that these waters are undersaturated with carbonate minerals (calcite and dolomite) but close to saturation (Table 5). This suggests that some carbonate components are part of the mineralogy of the aquifer, and, therefore, some potential of CO_2 buffering could exist. In contrast, equilibrium with silica is not attained, likely due to the very slow dissolution kinetics of silicon-bearing phases at low T and circumneutral pH.

Table 5: Saturation indexes with respect calcite, dolomite, gypsum and silica of the aquifer not affected by CO_2 intrusion in Campo de Calatrava (central Spain). All the concentrations are expressed as mg·L^{-1}. Data from Confederación Hidrográfica del Guadiana (www.chguadiana.es).

Sample	Date	pH	SI Calcite	SI Dolomite	SI Gypsum	SI SiO_2(am)
Pozuelo de Calatrava	mar-09	7.2	-0.22	-0.37	-2.80	-0.57
	sep-09	7.1	-0.34	-0.57	-2.85	-0.54
	aug-10	7.3	-0.28	-0.44	-1.48	-0.90
	nov-10	7.4	-0.02	0.06	-2.82	-0.57
	jun-12	7.3	-0.15	-0.19	-2.68	-0.53
	dic-12	7.2	-0.22	-0.38	-2.76	-0.54
	jun-13	7.2	-0.25	-0.38	-2.80	-0.56
	dic-13	7.2	-0.22	-0.34	-2.71	-0.52
	oct-14	7.4	-0.18	-0.46	-2.32	-0.59
	nov-14	7.3	-0.12	-0.39	-2.16	-0.59

The intrusion of CO_2 (either already dissolved or as a gas phase) into the shallow aquifers in Campo de Calatrava leads to a decrease in pH and dissolution of carbonate phases. However, such dissolution is not significant as a pH buffer since all samples become even more undersaturated in carbonate minerals (Fig. 7).

Trace (transition, post-transition) metals and metalloids

All the studied samples are characteristically much enriched in trace metals compared to CO_2-free aquifers (Table 6). Iron is by far the most abundant, ranging from 2.5×10^{-2} mg·L^{-1} (4.47×10^{-7} mol·L^{-1}) to 34 mg·L^{-1} (6.08×10^{-4} mol·L^{-1}) (Fig. 8). They also show high concentrations of Mn (up to 4.4 mg·L^{-1}, 8.01×10^{-5} mol·L^{-1}), Zn (up to 96 µg·L^{-1}, 1.46×10^{-6} mol·L^{-1}), Ni (up to 70 µg·L^{-1}, 1.19×10^{-6} mol·L^{-1}), Co (up to 42 µg·L^{-1}, 7.1×10^{-7} mol·L^{-1}), Cu (up to 21 µg·L^{-1}, 3.3×10^{-7} mol·L^{-1}) and As (up to 11 µg·L^{-1}, 1.4×10^{-7} mol·L^{-1}) (Fig. 9). In general, uranium is not significantly

enriched except in the sample from the cold geyser called "Chorro Glicerio", with 12 $\mu g \cdot L^{-1}$ (5.1×10^{-8} mol·L^{-1}).

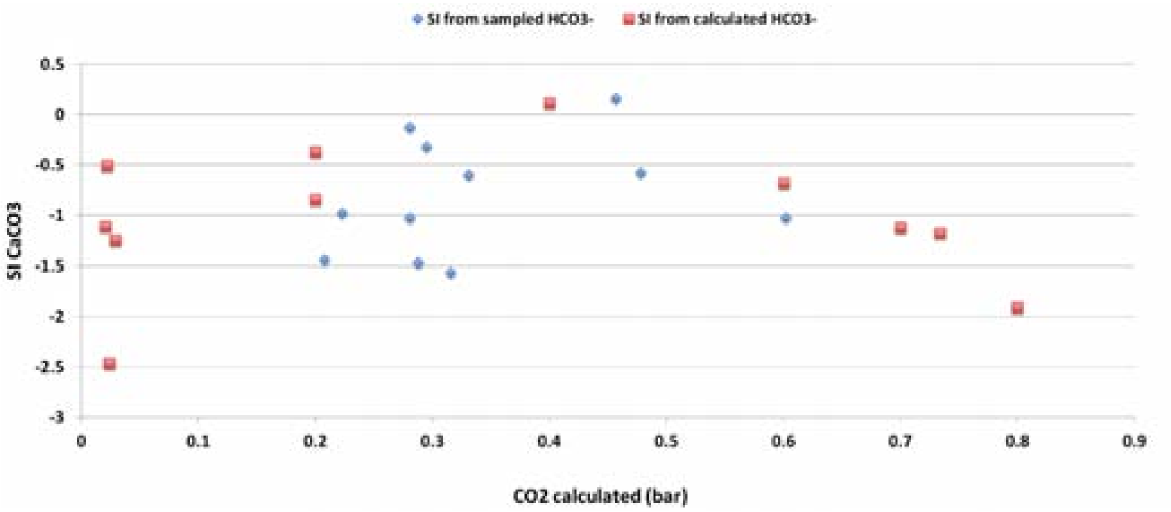

Figure 7: Calcite saturation indexes (SI) trend calculated using the sampled and calculated CO_2 pressure.

Table 6: Concentration of trace metals and metalloids in impacted and non-impacted shallow aquifers.

Sample	Fe (tot) (mg/l)	Mn^{2+} (mg/l)	Cr^{3+} (μg/l)	Ni^{2+} (μg/l)	Co^{2+} (μg/l)	Cu^{2+} (μg/l)
Pozuelo de Calatrava	< 0.05	< 0.1	< 0.02	< 0.05	< 0.05	< 0.05
	< 0.05	< 0.1	< 0.02	< 0.05	< 0.05	< 0.05
	< 0.1	< 0.1	< 0.02	< 0.05	< 0.05	< 0.05
	< 0.1	< 0.1	< 0.02	< 0.05	< 0.05	< 0.05
	< 0.1	< 0.1	< 0.02	< 0.05	< 0.05	< 0.05
	< 0.1	< 0.1	< 0.02	< 0.05	< 0.05	< 0.05
	< 0.1	< 0.1	< 0.02	< 0.05	< 0.05	< 0.05
	< 0.1	< 0.1	< 0.02	< 0.05	< 0.05	< 0.05
	< 0.1	< 0.1	< 0.02	< 0.05	< 0.05	< 0.05
	< 0.1	< 0.1	< 0.02	< 0.05	< 0.05	< 0.05
Chorro Glicerio	7.0	4.4	4.0	70	42	1.3
Chorro Villa Elena	16	1.2	6.7	41	14	1.3
Fontecha 1	34	0.8	2.1	56	16	20
Fontecha 2	29	0.7	2.2	34	10	21
Fontecha 3	0.08	0.26	2.2	27	3.7	21
Fontecha 4	2.6	1.0	1.1	46	20	9.8
Cañada Real	0.9	0.4	5.2	17	5.7	1
Baño Chico	1.4	0.9	1.2	36	22	13
Baño Chiquillo	0.02	0.6	1.4	57	17	11
Codo Jabalon	22	0.6	2.0	43	13	20
Herviderio Nuevo	21	1.0	1.8	48	19	17
Barranco Grande	34	1.4	1.9	37	20	19

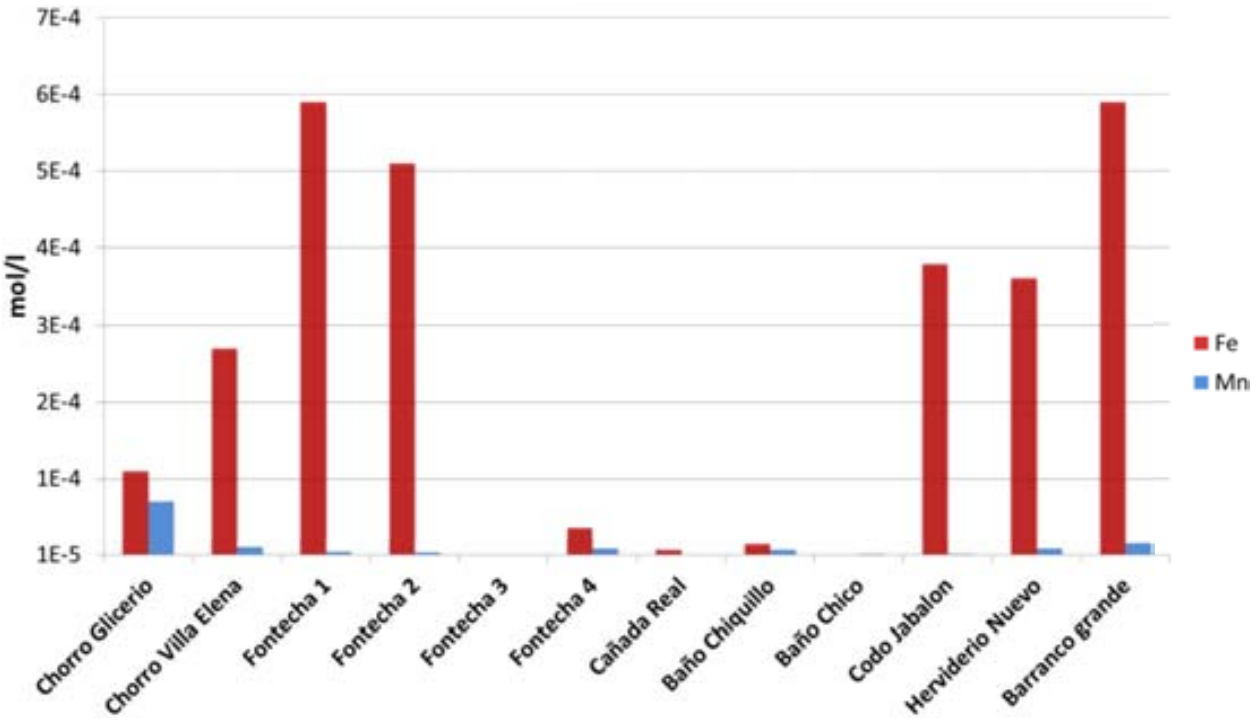

Figure 8: Fe and Mn concentration of the sampled CO_2-bearing sampling stations.

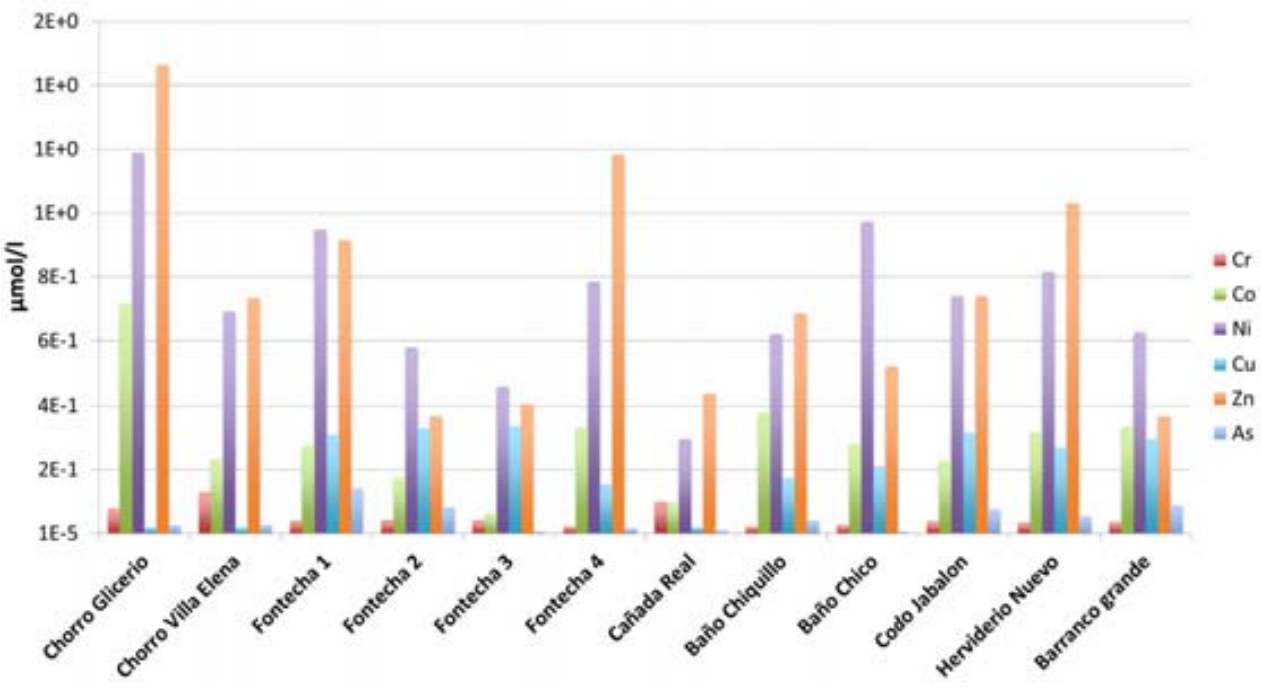

Figure 9: Main trace metal and metalloid concentration of the sampled CO_2-bearing sampling stations.

The increase of iron and trace metals in solution is neither directly correlated with pH or CO_2 pressure (actually both parameters should be strongly related since CO_2 is the main contributor to water acidity) (Fig. 16). In a similar way, trace metals content do not show any positive correlation (Fig.10 to Fig. 12). In contrast, a good linear correlation between Ni, Zn and Co concentrations is observed (Fig. 13), suggesting a similar geochemical behaviour and source for all them.

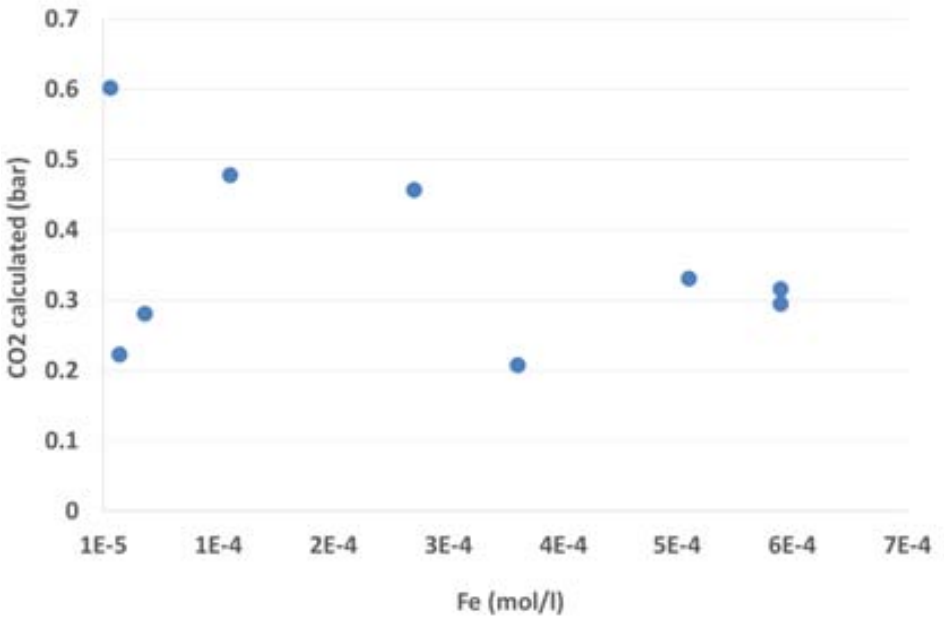

Figure 10: Diagram of Fe_{tot} concentration vs. CO_2 pressure in the CO_2-bearing sampling stations.

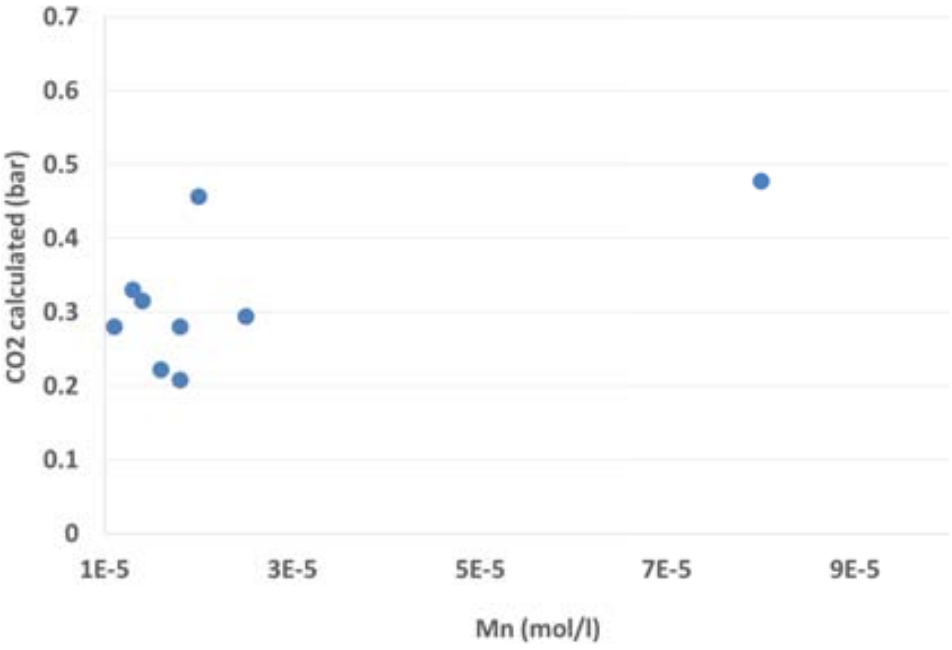

Figure 11: Diagram of Mn concentration vs. CO_2 pressure in the CO_2-bearing sampling stations.

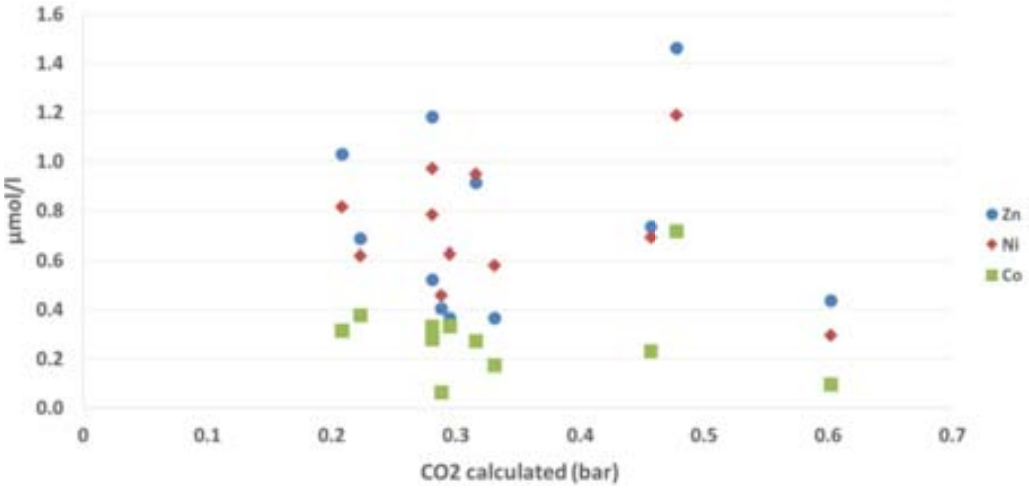

Figure 12: Diagram of Ni, Zn and Co concentration vs. CO_2 pressure in the CO_2-bearing sampling.

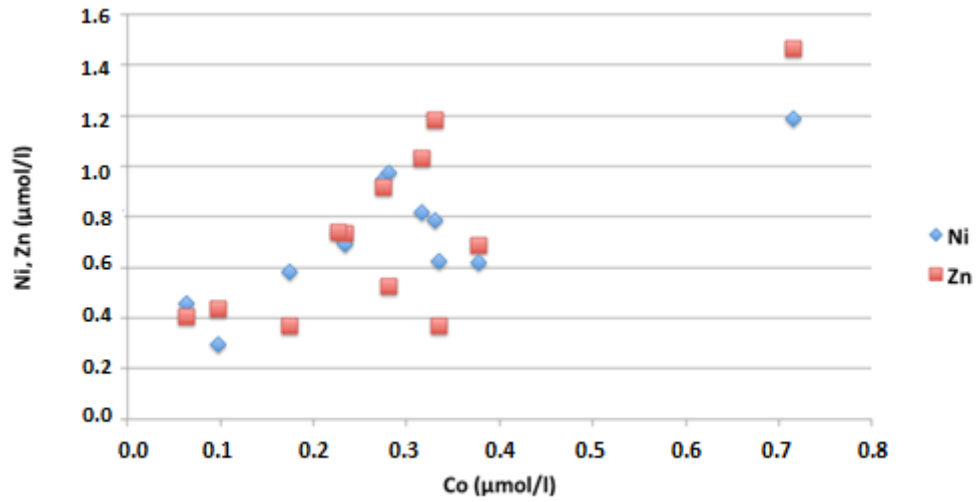

Figure 13: Correlation diagram of Ni, Zn and Co concentration sampled in the CO_2-bearing sampling stations.

Geochemical modelling: release and mobility of Fe(III), Mn and trace metals

The mobility of iron in low-CO_2, surface water and shallow groundwater is very limited due to the slightly solubility of Fe(III) at circumneutral pH and oxidizing conditions. In general, iron concentration under these conditions is lower than 1×10^{-6} mol·L^{-1} due to the equilibrium with iron (III) oxihydroxides. Higher concentrations are commonly observed in acidic environments from oxidative Fe-sulphide dissolution (e.g., acid mine drainage) or in anoxic waters due to the higher solubility of Fe(II). The observation that CO_2-bearing waters are commonly rich in iron has been reported from many natural systems and the formation of Fe(III) carbonate complexes accounts for its enhanced solubility (Grivé et al., 2014; Table 7).

The role of Fe(III) carbonate complexes is illustrated in Table 8 and Fig. 14, which shows the

sharing between main aqueous Fe species in the samples. In all them, almost all Fe is found as carbonate $FeCO_3(OH)$, allowing a much higher iron concentration in equilibrium with $Fe(OH)_3$ existing in the aquifer. Fig. 15 shows the saturation index (SI) with respect to $Fe(OH)_3$ considering the presence and absence of these two Fe(III) carbonate aqueous species. It is clearly observed that the solubility of solid $Fe(OH)_3$ is enhanced up to three order of magnitude if the formation of Fe(III) carbon complexes is taken in account. In general, most shallow groundwaters affected by CO_2 intrusion in Campo de Calatrava are saturated with respect $Fe(OH)_3$. However, it is worth considering that the crystallinity of these Fe(III) minerals is highly changeable, and in turn, its solubility product can also vary from one site to another. Therefore, the calculation of SI is just indicative of the necessary role of aqueous carbonate complexes.

Table 7. Solubility of Fe(III) carbonate aqueous complexes and ferrihydrite ($Fe(OH)_3$ (am)). Data from Grivé et al. (2014) and Schindler et al. (1963).

$FeCO_3OH \leftrightarrow Fe^{3+} + H^+ + CO_3^{2-} + H_2O$, log K= -10.76

$Fe(CO_3)_3^{3-} \leftrightarrow Fe^{3+} + 3CO_3^{2-}$, log K= -24.24

$Fe(OH)_3$ (am) + $3H^+ \leftrightarrow Fe^{3+} + 3H_2O$, log K= 2.54

Table 8. Percentage of iron species in solution in the studied samples.

Stations	**$FeCO_3(OH)$ (%)**	**Fe^{+2} (%)**	**$Fe(CO_3)_{(aq)}$ (%)**	**$Fe(OH)_{3\ (aq)}$ (%)**
Baño chico	93.5	5.9	0.6	0.002
Baño chiquillo	98.4	1.2	0.3	0.003
Barranco Grande	92.2	7.1	0.6	0.002
Cañada Real	94.0	5.3	0.7	0.001
Chorro Glicerio	98.9	0.7	0.3	0.001
Chorro Villa Elena	92.8	6.5	0.7	0.001
Fontecha 1	79.2	19.9	0.8	0.002
Fontecha 2	77.5	21.7	0.9	0.002
Fontecha 3	93.9	5.5	0.6	0.002
Fontecha 4	75.9	23.2	0.8	0.002
Hervidero Nuevo	83.0	16.2	0.7	0.003

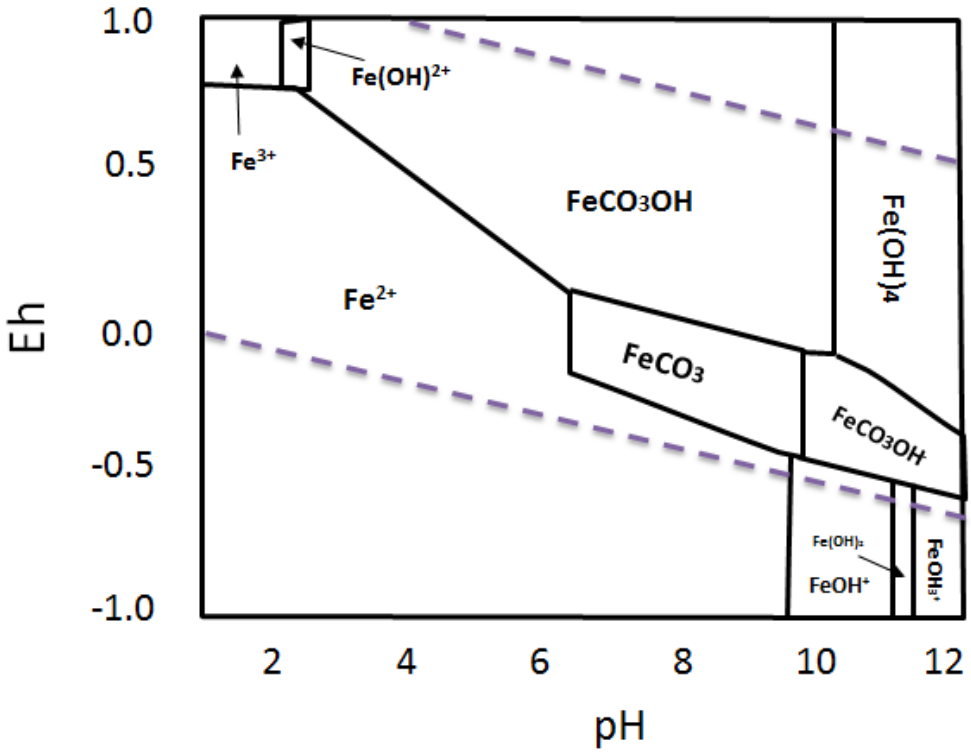

Figure 14: pH-Eh diagram of the aqueous speciation of iron considering the pCO_2 found in shallow groundwaters in Campo de Calatrava.

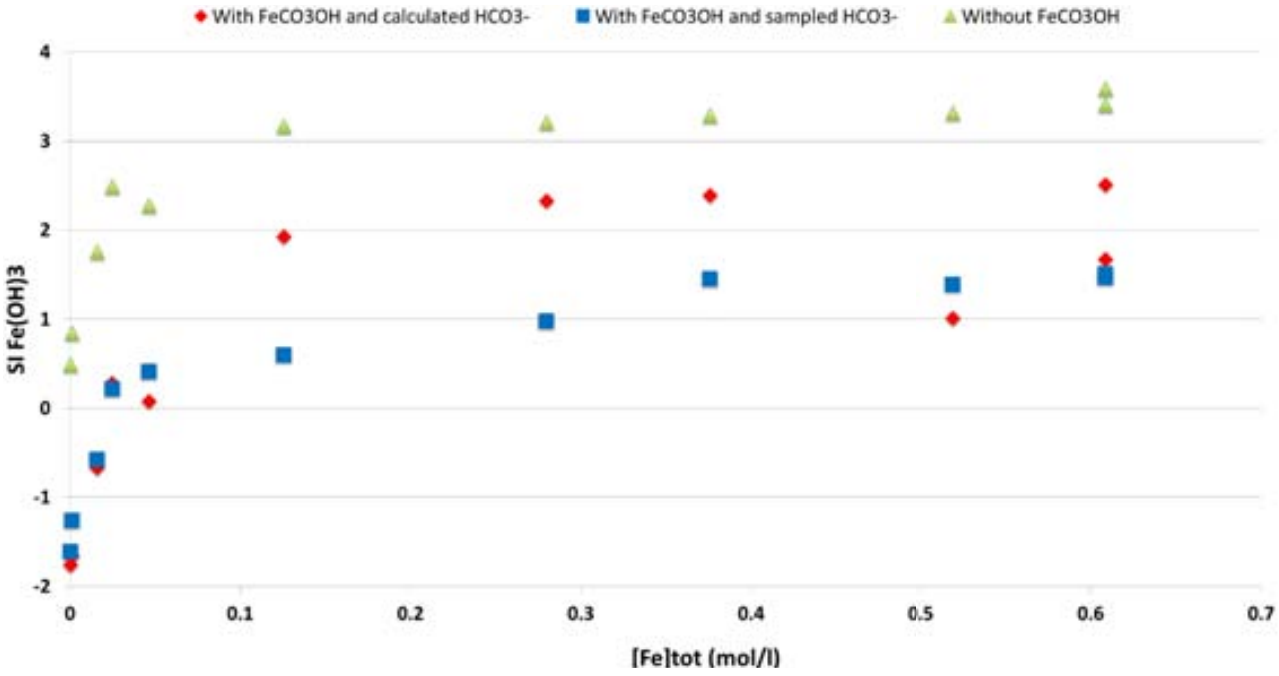

Figure 15: $Fe(OH)_3$(am) saturation indexes (SI) trend calculated using the sampled and calculated pCO_2 compared with the theoretical values obtained excluding the formation of Fe(III) carbonate complexes.

The source of iron in the Campo de Calatrava shallow CO_2-bearing groundwaters is likely the iron(III) oxihydroxides in the aquifer host rocks, which are widespread in sedimentary rocks. A numerical model of a gas-water-rock reaction supports such hypothesis. The impact of pH, CO_2 pressure and iron solubility increase was simulated using PHREEQC. 1 mol of CO_2(g) has been progressively added, in steps of 1×10^{-3} moles, to an aquifer with the initial chemical composition of the water "mar-09" from the regional aquifer (Table 4 above). The aquifer is considered in equilibrium with $Fe(OH)_3$ (am) and to account for the potential variability in the solubility product of $Fe(OH)_3$ (am), a range of Log K has been considered (Log K = 4, 3.5, 3 and 2.2 respectively). The numerical simulation has been compared with the data collected from the CO_2-bearing waters, assuming the sampled CO_2 pressure.

The results indicate that the intrusion of CO_2 gas can account for the observed pH and CO_2 pressure even assuming a significant loss of accuracy in sampling due to the bubbling during the water and gas collection (Fig. 16).

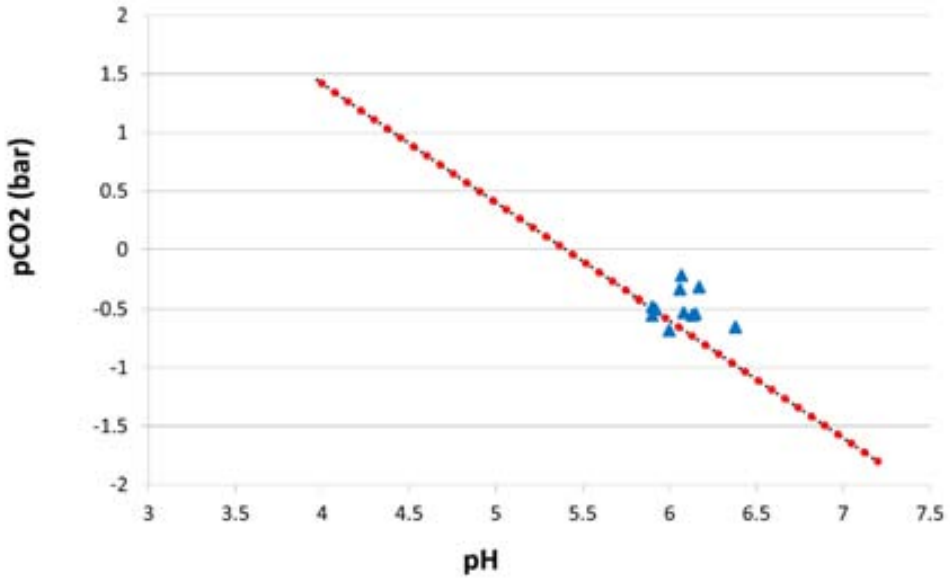

Figure 16: Predicted increase of pCO_2 and decrease in pH in an aquifer as a response of CO_2 gas intrusion. Blue triangles are the data from Campo de Calatrava CO_2-bearing sampling stations.

Concerning the iron release and solubility, the simulation results show that most measured [Fe] can be explained by the dissolution of Fe(III) solids due to the inflow of CO_2(g) (Fig. 17). Again, the role of aqueous Fe (III) carbonate complexes is essential to reach the observed iron concentrations since the decrease in pH is not sufficient (see green dashed line in Fig. 18).

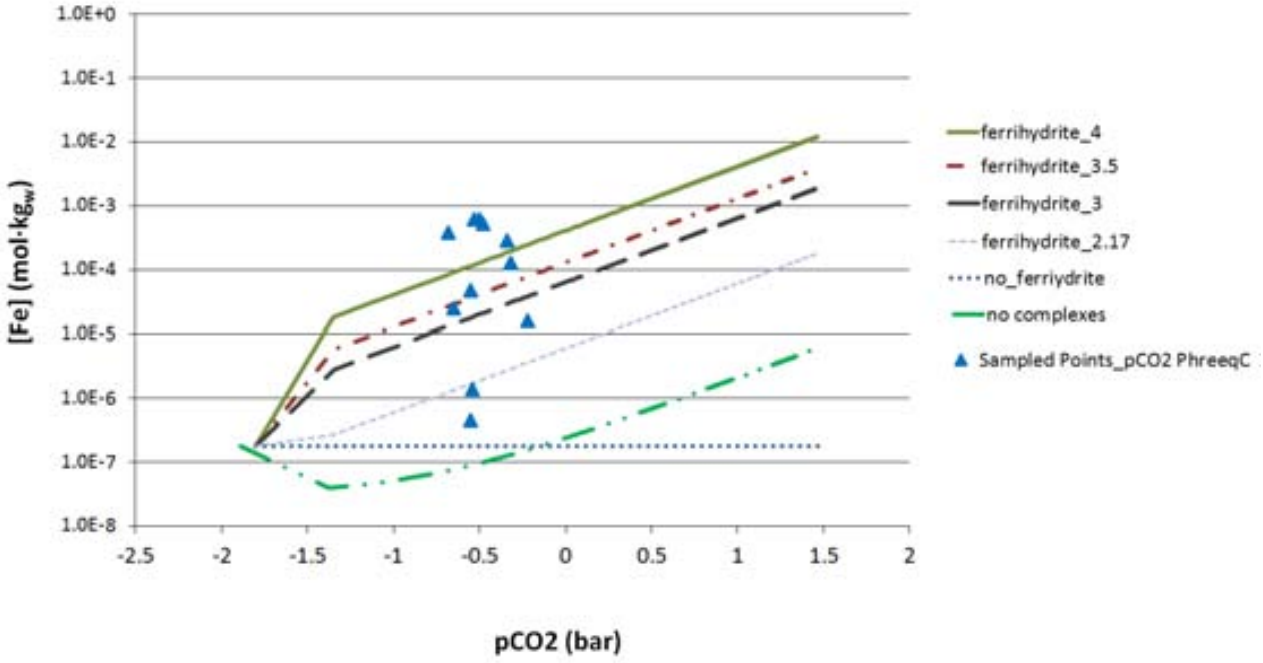

Figure 17: Predicted concentration of iron from $Fe(OH)_3$(am) (ferrihydrite in the label) dissolution due to the intrusion of CO_2(g). Lines are the reaction path considering different $Fe(OH)_3$(am) solubility products (Ksp= 4, 3 and 2.17, respectively). Dashed line corresponds to the simulation with no consideration of aqueous Fe(III) carbonate complexes. Iron concentration and corresponding pCO_2 of sampled shallow groundwaters in Campo de Calatrava are included in the plot for comparison.

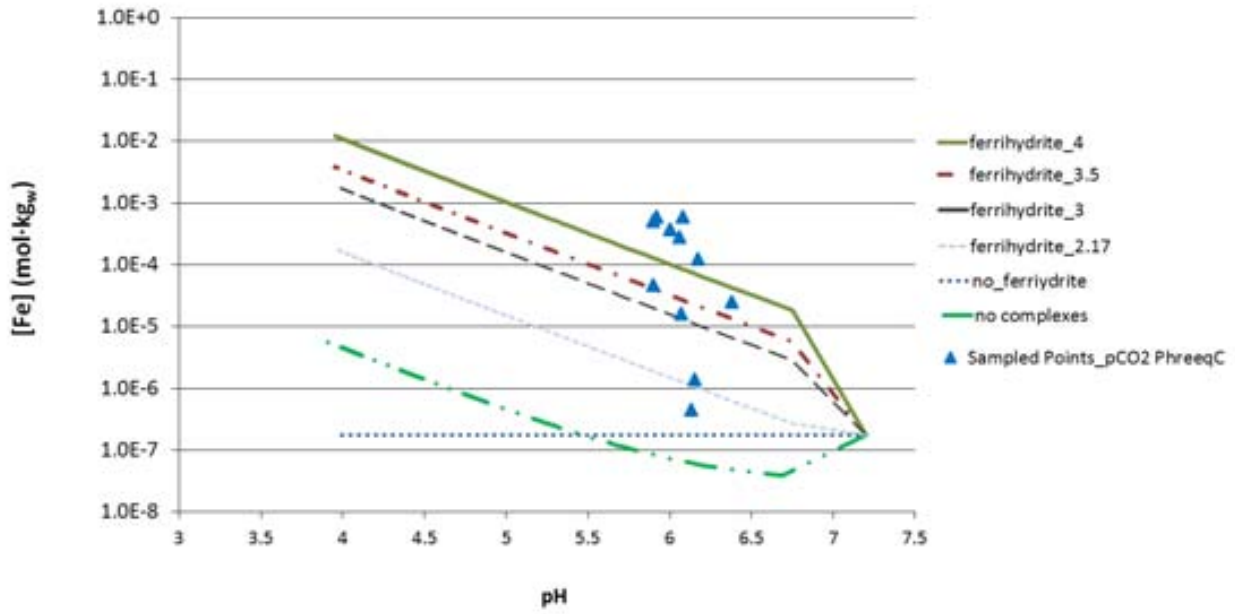

Figure 18: Predicted concentration of iron from $Fe(OH)_3$(am) dissolution due to the intrusion of CO_2(g) vs. pH. Lines are the reaction path considering different $Fe(OH)_3$(am) solubility products (Ksp= 4, 3 and 2.17, respectively). Dashed line corresponds to the simulation with no consideration of aqueous Fe(III) carbonate complexes. Iron concentration and corresponding pH of sampled shallow groundwaters in Campo de Calatrava are included in the plot for comparison.

Manganese is also released in shallow aquifers in Campo de Calatrava. According the existing thermodynamic data, the speciation of Mn in fresh, oxidising waters is essentially as Mn^{2+}. In CO_2-impacted aquifers, the formation of $MnCO_3$(aq) is enhanced (Fig. 19). In the studied waters, carbonate aqueous Mn species are in the same order of magnitude as free Mn^{2+}, being predominant is some samples up to 75% of the dissolved Mn (Table 9). The solubility of Mn is limited by the precipitation of $MnCO_3$(s) (rhodocrosite) as suggested by the SI of these samples; Mn oxides and hydroxides are significantly much soluble.

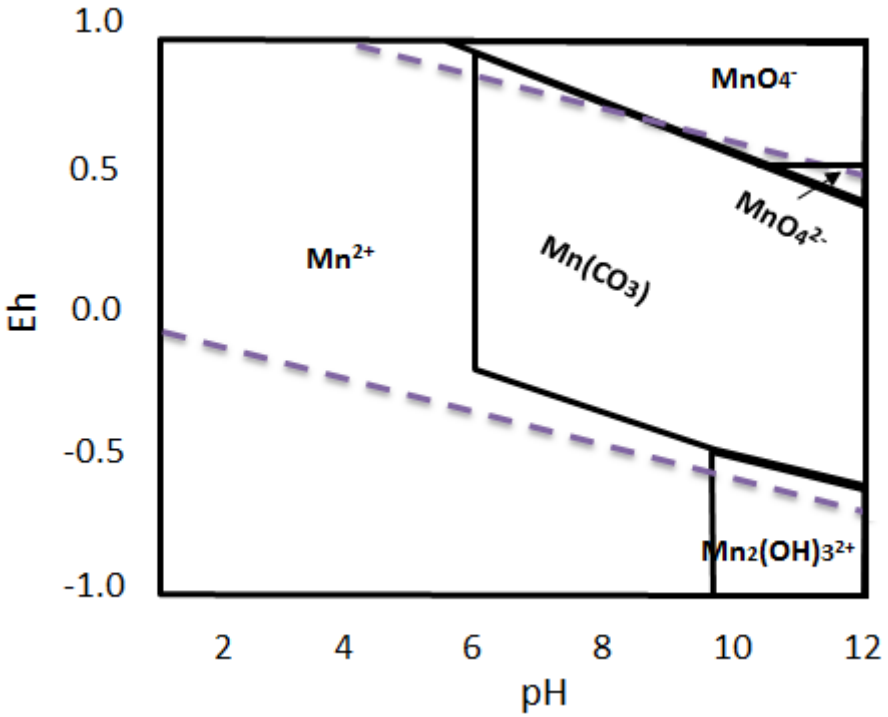

Figure 19: pH-Eh diagram of the aqueous speciation of Mn considering the pCO_2 found in shallow groundwaters in Campo de Calatrava.

Table 9. Percentage of Mn free cations and aqueous carbonate species in the studied samples. Saturation indexes of the solubility-limiting phase (rhodocrosite) are also listed.

Stations	Mn^{2+} %	$MnCO_3$ %	$MnHCO_3^+$ %	SI rhodocrosite ($MnCO_3$) %
Baño chico	56.6	37.7	4.1	-0.59
Baño chiquillo	34.3	61.1	3.6	-0.51
Barranco Grande	57.9	33.3	4.0	-0.44
Cañada Real	48.2	41.3	5.5	-0.97
Chorro Glicerio	23.6	70.8	4.4	0.38
Chorro Villa Elena	55.3	38.5	5.1	-0.44
Fontecha 1	70.1	18.8	3.4	-0.93
Fontecha 2	70.4	17.8	3.4	-1.00
Fontecha 3	53.4	36.1	3.9	-1.14
Fontecha 4	74.0	17.1	3.2	-0.87
Hervidero Nuevo	72.4	20.8	3.0	-0.79

The trace metal contents from the analysis of the CO_2-bearing fluids reveal a clear enrichment mainly in Zn, Co, Ni, Cu and, in a minor extend, U. Unlike Fe (III), whose enhanced concentration is a combination of release from the iron minerals and the formation of soluble Fe(III) aqueous carbonate complexes, the high concentration of these trace metals seems to be only related to a dissolution of the their source, i.e., $Fe(OH)_3$. Considering the aqueous species for Co and Ni included in Thermochimie v.9 database, and Minteq-v4 (U.S. Environmen tal Protection Agency, 1998) for Zn and Cu (since Cu and Zn carbonate and hydrolised species are not defined in Thermochimie v.9). This is the reason behind the selection of Minteq-v4., the impact on transport of the formation of aqueous metal carbonate complexes is less relevant, and divalent free cations are much predominant for Co, Ni and Zn (Table 10). In contrast, Cu carbonate species are predominant in some samples.

Table 10. Percentage of Co, Ni, Cu and Zn free cations and aqueous carbonate species in the studied samples.

Stations	Co^{2+} %	$CoHCO_3^+$ %	Ni^{2+} %	$NiHCO_3^+$ %	Cu^{2+} %	$CuCO_3$ %	$CuHCO_3^+$ %	Zn^{2+} %	$ZnHCO_3^+$ %
Baño chico	75.1	22.3	88.4	8.5	38.1	47.0	9.4	85.6	10.6
Baño chiquillo	67.9	29.3	84.7	11.8	20.6	68.2	7.4	80.3	14.5
Barranco Grande	74.0	20.6	85.8	7.7	38.6	42.1	9.2	83.4	10.0
Cañada Real	63.4	29.6	79.1	11.9	27.4	43.7	11.0	75.5	15.3
Chorro Glicerio	54.2	41.8	75.7	18.9	12.9	72.6	8.7	68.9	23.3
Chorro Villa Elena	71.1	26.8	86.9	10.6	35.9	46.6	11.5	83.4	13.4
Fontecha 1	75.3	14.9	83.2	5.3	46.6	23.7	7.9	82.1	7.0
Fontecha 2	75.1	14.7	82.8	5.3	46.8	22.4	7.9	81.7	6.9
Fontecha 3	70.0	20.7	80.9	7.7	32.7	41.1	8.1	78.7	9.8
Fontecha 4	79.1	13.9	86.8	4.9	53.3	22.9	7.8	85.6	7.2
Hervidero Nuevo	81.0	13.8	89.1	4.9	52.3	28.4	7.5	87.7	6.3

Discussion:

The impact of CO_2 solubilisation on metal transport has been a topic thoroughly studied in the last decade due to the intention of store this greenhouse gas underground. A complete literature review on this topic has recently been performed by Lions et al. (2014). In general, most lab and field studies agree that iron and manganese are easily mobilised when an aquifer is impacted by CO_2, already dissolved in water or as supercritical gas in the storage formation (Kharaka et al., 2010; Trautz et al., 2013; Lu et al., 2010; Little and Jackson, 2010; Humez et al., 2013). However, there is still some debate on the driving processes of this metal mobilisation. Acidification is commonly invoked as a releasing and transport mechanism (Kharaka et al., 2009). Another proposed metal-releasing mechanism is the ascent of low-Eh, deeper fluxes and subsequent displacement of native, oxidising fluids, leading to, e.g., the reduction of Fe(III) to a more mobile Fe(II) form (Hem, 1985; Yardley et al., 2003; Kharaka and Hanor., 2007; Birkholzer et al., 2008; Keating et al., 2010). Finally, the occurrence of minor gases in the gas mixture such as CH_4 or H_2S may favour the development of microbially-driven reactions causing metal reduction (McMahon and Chapelle, 1991, 2008; Lions et al., 2014 and references therein).

The chemistry of the shallow groundwaters affected by CO_2(g) fluxes in Campo de Calatrava reveals that none of the above mechanisms is the main driver for metal release and solubilisation, since (1) all of them have circumneutral pH (close to 6), (2) they have oxidising Eh, and (3) the gas flow is almost pure CO_2 and free of "reducing" minor gases. The measured pH is likely controlled by the dissolution of gas into the shallow aquifer rather than mineral dissolution, as supported by numerical thermodynamic calculations, but gas fluxes are not intense enough to cause very acidic (pH<4) plumes in the affected aquifers. Geophysical profiles reveal that gas mixes at shallow depths with groundwater and part of this gas directly flows to the atmosphere. However, the suspected short interaction time between gas, water and host rocks is enough to dissolve iron hydroxides and form plumes of iron and other trace metals. The source of these trace metals are likely the iron hydroxides themselves since these minerals present charged surfaces where trace metals are immobilised by sorption. The lack of correlation between the concentration of iron and these metals could be found in the variable composition of the surface sites in the sampling stations.

Although part of the metal load precipitates back as colloids if some degree of degassing occurs, the metal concentration is still much higher than expected for circumneutral, oxidising waters. Therefore, the role of aqueous Fe(III) carbonate complexes becomes crucial for the persistence of this metal content in solution. In the samples studied in the Campo de Calatrava area, the theoretical impact of iron mobility calculated from laboratory experiments is well proved, and, contrary to the current opinion in the scientific community, the impact of CO_2 fluxes into shallow aquifers leading to relatively low CO_2 pressure is very significant and worth taking into

consideration in the risk assessment.

Manganese is usually reported to be mobilised along with Fe in CO_2 injection test in aquifers. Interestingly, the role of carbonate complexes in Mn mobilisation is quite different from iron: at high pCO_2, a significant part of dissolved Mn predicted to be found as $MnCO_3(aq)$ but, in turn, the solution is approaching the equilibrium with solid Mn carbonate. Therefore, the competition between the formation of soluble Mn carbonates and the precipitation of solid $MnCO_3$ controls the solubility of Mn in these aquifers.

The general consensus on the release of Fe and Mn is not shared for other trace metals since the reported data shows a disparity of sets of metals released either in laboratory or from field tests (see review in Harvey et al., 2012). According to the analysis performed in this work, the formation of trace transition metal plumes in CO_2-impacted shallow waters is basically related to the occurrence of such metals in surface sorption sites in solid $Fe(OH)_3$, and their transport is eventually controlled by the precipitation of solid carbonates, in a similar way as Mn. In the studied samples in Campo de Calatrava, the thermodynamic calculations predict that these waters are far from the equilibrium with these carbonates (more than 2 orders of magnitude below the saturation) suggesting that the concentration of these metals is actually related to the source rather than to the transport. Their solubilisation is, then, maintained as long as the aquifer system keeps $Fe(OH)_3$ undersaturated.

Compared to results from literature, it is remarkable the similarity with the experimental data from Little and Jackson (2010), obtained from the same pH range. In both datasets, the trace metals with a significant increase are the same, i.e., Fe, Mn, Zn, Co, Ni, Cu and U. Only barium has not found to be mobilised in the present work.

Conclusions:

The CO_2 (g) flows into shallow aquifers cause severe changes in shallow, fresh aquifer chemistry since lead to the release and solubilisation of metals, mainly Fe and Mn but also of a set of many other metals in minor or trace amounts. In most cases, such amounts are not acceptable in terms of water consumption. The persistence of these metal plumes, which is crucial in the risk assessment studies of CO_2 underground storage, is under debate since subsequent water-rock interaction may lead to a decrease of acidity and, in turn, the metal load is then back to the rock. However, the observations from this work reveals that such persistence is clearly enhanced due to the formation of aqueous Fe(III) carbonate complexes, which has not been considered in the past in the risk assessment of the impacts of CO_2 (g) flows into shallow aquifers. These complexes modify the water-rock equilibrium in the aquifer forcing the dissolution of $Fe(OH)_3$, and, in turn,

the release of the sorbed trace metals. These trace metals are dissolved with amounts lower than those necessary to precipitate pure metal carbonate and they are predicted to persist until they sorbed again in iron hydroxides. Consequently, the formation of iron carbonate complexes can be considered as the main driver of metal transport in the CO_2-impacted shallow aquifers.

Acknowledgements

The samplings and calculations performed in this research article have been done in the frame of the MetTrans Initial Training Network (2012-2016; http://www.mettrans-itn.eu/) of the Marie Curie Programme of the EC through a grant to M.Agnelli.
We are very grateful for the technical support during the sampling and geophysical campaignes to Giada Trezzi and Jordi Garcia of the UAB (Universitat autonoma de Barcelona).

Referencies:

ABEM, 2009. Instruction Manual. Terrameter SAS 4000 / SAS 1000. ABEM Instrument AB, Sundbyberg, Sweden. ABEM Printed Matter No. 93109, pp. 136. Accessed 2015-06-09 from (http://www.abem.se/files/upload/manual_terrameter.pdf).

Agnelli M, Grandia F, Credoz, A, Gasparini A, and Bruno J (2013) Use of diffusive gradients in thin films (DGT) as an early detection tool of low-intensity leakage from CO_2 storage. Greenhouse Gases: Science&Technology 1:1-13.

Ancochea E, (Ph.D. thesis), 1982. Evolución espacial y temporal del vulcanismo reciente de España Central. Univ. Complutense, Madrid, Col. Tesis Doctorales 203/83, 675 pp.

Ancochea E, 1999. El campo volcánico de Calatrava. Enseñanza de las Ciencias de la Tierra 7 (3), 237-243.
Apps JA, Zheng L, Zhan Y, Xu T, 2010. Evaluation of potential changes in groundwa- ter quality in response to CO2 leakage from deep geologic storage. Transp. Porous Media 215–246.

Atchley AL, Maxwell RM, Navarre-Sitchler AK, 2013. Using streamlines to simulate transport in CO_2-impacted drinking water aquifers. Adv. Water Resour. 52, 93–106.

Birkholzer J, Apps J, Zheng Y, Xu T, Tsang C-F, 2008. Research Project on CO_2 Geological Storage and Groundwater resources: Large-scale Hydrogeological Evaluation and Impact on Groundwater Systems, Annual Report October 1, 2007 to September 30, 2008. Report, Lawrence Berkeley National Laboratory, Berkeley, CA, USA.

Cahill AG, Jakobsen R, 2013. Hydro-geochemical impact of CO_2 leakage from geological storage on shallow potable aquifers: a field scale pilot experiment. Int. J. Greenhouse Gas Control.

http://dx.doi.org/10.1016/j.ijggc.2013.03.015.

Calvo D, Barrancos J, Padilla G, Brito M, Becerra-Ramírez R, González E, Gosálvez RU, Escobar E, Melián G, Nolasco D, Padrón E, Marrero R, Hernández PA, Pérez N, 2010. Emisión difusa de CO_2 en el Campo de Calatrava, Ciudad Real. In: González E, Escobar E, Becerra R, Gosálvez RU, Dóniz J (Eds.), Aportaciones recientes en volcanología 2005-2008. Centro de Estudios Calatravos, Almagro, Spain, pp. 51-55.

Cebriá JM, López-Ruiz J, 1995. Alkali basalts and leucitites in an extensional intracontinental plate setting: the late Cenozoic Calatrava Volcanic Province (central Spain). Lithos 35, 27-46.

Czernichowski-Lauriol I, Rochelle C, Gaus I, Azaroual M, Pearce J, Durst P. (2006). Geochemical interactions between CO_2, pore-waters and reservoir rocks: lessons learned from laboratory experiments, field studies and computer simulations. In: Lombardi S, Altunina LK, Beaubien SE. (Eds.), Advances in the Geological Storage of Carbon Dioxide: NATO Science Series IV. Earth. Environ. Sci. 65: 141–157.

Elío J, Ortega MF, Nisi B, Mazadiego LF, Vaselli O, Caballero J, Grandia F, 2015. CO_2 and Rn degassing from the natural analog of Campo de Calatrava (Spain): Implications for monitoring of CO_2 storage sites. Int. J. Greenh. Gas Control 32, 1-14, http://dx.doi.org/10.1016/j.ijggc.2014.10.014.

Fischer S, Liebscher A, Wandrey M, CO2SINK Group (2010). CO2–brine–rock interaction - first results of long-term exposure experiments at in situ P–T conditions of the Ketzin CO_2 reservoir. Chem. Erde 70(3): 155–164.

Frye E, Bao C, Li L, Blumsack S, 2012. Environmental controls of cadmium desorption during CO_2 leakage. Environ. Sci. Technol. 46, 4388–4395.
Giffaut E, Grivé M, Blanc P, Vieillard P, Colàs E, Gailhanou H, Gaboreau S, Marty N, Madé B, Duro L (2014). Andra thermodynamic data for performance assessment: ThermoChimie. Applied Geochemistry (in press).

Grivé M, 2005. The linkage between uranium, iron and carbon cycling, processes at interfaces: evidences from combined solution chemical and spectroscopic studies. Ph.D. Thesis. Universitat Politècnica de Catalunya, Barcelona.

Grivé M, Duro L, Colàs E, Giffaut L, 2014. Thermodynamic data selection applied to radionuclide and chemotoxic elements: an overview of the ThermoChimie-TDB. Applied Geochemistry (in press).

Grivé M, Duro L, Bruno J, 2014. Fe(III) mobilization by carbonate in low temperature environments: study of the solubility of ferrihydrite in carbonate media and the formation of Fe(III) carbonate complexes. Applied Geochemistry.

Harvey OR, Brown CF, Qafoku NP, Cantrell KJ, Lee G, Amonette JE, 2012. Geochemical Implications of Gas Leakage associated with Geologic CO_2 Storage - A Qualitative Review. Environmental Science & Technology.

Hem JD, 1985. Study and interpretation of the Chemical Characteristics of Natural Water, 3rd ed. Alexandria, VA: Department of the Interior, U.S. Geological Survey, Water-Supply Paper 2254.

Humez P, Négrel P, Lagneau V, Lions J, Kloppmann W, Gal F, Millot R, Guerrot C, Flehoc C, Widory D, Girard JF, 2013. CO_2–water–mineral reactions during CO2 leakage: Geochemical and isotopic monitoring of a CO_2 injection field test. Chemical Geology 368 (2014) 11–30.

IGME, 1988a. Mapa Geológico de España 1:50.000. Ciudad Real (784). Memoria y mapa. Instituto Geológico y Minero de España (IGME), Ministerio de Industria y Energía, Madrid.

IGME, 1988b. Mapa Geológico de España 1:50.000. Almagro (785). Memoria y mapa. Instituto Geológico y Minero de España (IGME), Ministerio de Industria y Energía, Madrid.

Keating E, Fessendem J, Kanjorski N, Koning D, Pawar R, 2010. The impact of CO_2 on shallow groundwater chemistry: Observation at a natural analogue site and implication for carbon sequestration. Environmental Earth Sciences 60, 521-536.

Kharaka YK, Cole DR, Hovorka SD, Gunter WD, Knauss KG, Freifeld BM, 2006. Gas–water–rock interactions in Frio Formation following CO_2 injection: Implications for the storage of greenhouse gases in sedimentary basins. Geology 34: 577–580.

Kharaka YK and Hanor JS, 2007. Deep fluids in the continents: I. Sedimentary Basins. In: Drever J.I, (Ed.).

Kharaka YK, Thordsen JJ, Hovorka SD, Nance HS, Cole DR, Phelps TJ, Knauss KG, 2009. Potential environmental issues of CO_2 storage in deep saline aquifers: geochemical results from the Frio-I Brine pilot test, Texas, USA. Applied Geochemistry 24: 1106-1112.

Kharaka YK, Thordsen JJ, Kakouros E, Ambats G, Herkelrath WN, Beers SR, Birkholzer JT, Apps JA, Spycher NF, Zheng L, Trautz RC, Rauch HW, Gullickson KS, 2009. Changes in the chemistry of shallow groundwater related to the 2008 injection of CO_2 at the ZERT field site, Bozeman, Montana. Environ. Earth Sci. 60, 273–284.

Lions J, Devau N, De Lary L, Dupraz S, Parmentier M, Gombert P, Dictor MC, 2014. Potential impacts of leakage from CO_2 geological storage on geochemical processes controlling fresh groundwater quality: A review. nternational Journal of Greenhouse Gas Control 22:165–175. DOI: 10.1016/j.ijggc.2013.12.019.

Lions J, Humez P, Pauwels H, Kloppmann W, Czernichowski-Lauriol I, 2014. Tracking leakage from a natural CO_2 reservoir (Montmiral, France) through chemistry and iso- tope signatures of shallow groundwaters. GHGS&T, in press.

Little MG and Jackson RB, 2010. Potential impacts of leakage from deep CO_2 geosequestration on overlying freshwater aquifers. Environ. Sci. Technol. 44, 9225–9232.

Loke MH, Barker RD, 1996. Rapid least-squares inversion of apparent resistivity pseudosecions by a quasi-Newton method. Geophys. Prospect. 44 (1), 131-152.

Loke MH, 2014. Tutorial: 2D and 3D electrical imaging surveys. Geotomo Software, Gelugor, Malaysia., pp. 169. Accessed 2014-04-02 from (www.geotomosoft.com).

López-Ruiz J, Cebriá JM, Doblas M, 2002. Cenozoic volcanism I: the Iberian Peninsula. In: Gibbons, W., Moreno, T. (Eds.), The Geology of Spain. The Geological Society, London, pp. 417-438.

Lu JM, Partin JW, Hovorka SD, Wong C, 2010. Potential risks to freshwater resources as a result of leakage from CO_2 geological storage: a batch-reaction experiment. Environ. Earth Sci. 60, 335–348.

McMahon PB and Chapelle FH, 1991. Microbial production of organic acids in aquitard sediments and its role in aquifer geochemistry. Nature. 34, 233-235

McMahon PB and Chapelle FH, 2008. Redox processes and water quality of selected principal aquifers systems. Groundwater 46, 259-271

Montes-Hernandez G, Renard F, Lafay R, 2013. Experimental assessment of CO_2–mineral-toxic ion interactions in a simplified freshwater aquifer: implications for CO_2 leakage from deep geological storage. Environmental Science & Technology 47, 6247–6253.

Navarre-Sitchler AK, Maxwell RM, Siirila ER, Hammond GE, Lichtner PC, 2013. Elucidating geochemical response of shallow heterogeneous aquifers to CO2 leakage using high-performance computing: implications for monitoring of CO_2 sequestration. Adv. Water Resour. 53, 45–55.

Piqué A, Grandia F and Canals A, 2010. Processes releasing arsenic to groundwater in the Caldes de Malavella geothermal area, NE Spain. Water Res 44:5618–5630.

Poblete MA, 1992. Las últimas manifestaciones asociadas al vulcanismo del Campo de Calatrava (Ciudad Real): los manantiales termales. Cuadernos de Sección. Historia 20, 187-201.

Rempel KU, Liebscher A, Heinrich W, Schettler G, 2011. An experimental investigation of trace element dissolution in carbon dioxide: Applications to the geological storage of CO_2. Chemical Geology 289: 224–234.

Rillard J, (Thèse de l'université de Lyon 1) 2013. CO_2 Perturbations in Aquifers: Reaction Kinetics and Metal Behavior.

Rolandi M, Barrera JL, 2003. Los volcanes del Campo de Calatrava. In: R. Nuche (Ed.), Patrimonio Geológico de Castilla-La Mancha. Enresa, pp. 478-509.

Romanó de Orte M, Sarmiento AM, Basallote MD, Rodríguez-Romero A, Riba I, DelValls A, 2014. Effects on the mobility of metals from acidification caused by possible CO_2 leakage from sub-seabed geological formations. Science of the Total Environment 470–471, 356–363

Schindler P, Michaelis W, Feitknecht W, 1963. Löslichkeitsprodukte von metalloxiden und – hydroxiden. 8. mitt.: Die löslichkeit gealterter eisen (III-hydroxidfällungen. Helv. Chim. Acta. 46, 444–451.

Siirila ER, Navarre-Sitchler AK, Maxwell RM, McCray JE, 2012. A quantitative methodology to assess the risks to human health from CO2 leakage into groundwater. Adv. Water Resour. 36, 146–164.

Tassi, F., Vaselli, O., Luchetti, G., Montegrossi, G. & Minissale, A., 2008. Metodo per la determinazione dei gas disciolti in acque naturali. CNR-IGG Rapporto Interno n. 2/2008, p. 10.

Trautz R, Pugh J, Varadharajan C, Zheng L, Bianchi M, Nico PS, Spycher N, Newell DL, Esposito RA, Wu Y, 2013. Effect of dissolved CO_2 on a shallow groundwater system: a controlled release field experiment. Environ. Sci. Technol. 47, 298–305.

U.S. Environmen tal Protection Agency, 1998. MINTEQA2/PRODEFA2, A Geochemical Assessment Model for Environmental Systems: User Manual Supplement for Version 4.0

Vaselli O, Nisi B, Tassi F, Giannini L, Grandia F, Darrah T, Capecchiacci F, Del Villar P, 2013. Water and gas geochemistry of the Calatrava Volcanic Province (CVP) hydrothermal system (Ciudad Real, central Spain). Geophysical Research Abstracts Vol. 15, EGU2013-11102, 2013.

Vegas R, Rincón-Calero PJ, 1996. Campos de esfuerzos, deformación alpina y volcanismo neógeno-cuaternario asociado en el antepaís bético de la provincia de Ciudad Real (España central). Geogaceta 19, 31-34.

Viswanathan H, Dai Z, Lopano C, Keating E, Hakala JA., Scheckel KG, Zheng L, Guthrie GD, Pawar R, 2012. Developing a robust geochemical and reactive trans- port model to evaluate possible sources of arsenic at the CO_2 sequestration natural analog site in Chimayo, New Mexico. J. Greenhouse Gas Control 10, 199–214.

Wang S, Jaffe PR, 2004. Dissolution of a mineral phase in potable aquifers due to CO_2 releases from deep formations; effect of dissolution kinetics. Energ. Convers. Manage. 45, 2833–2848.

Wei Y, Maroto-Valer M, Steven MD, 2011. Environmental consequences of potential leaks of CO_2 in soil. Energy Proc. 4, 3224–3230.

Wigand M, Carey JW, Schütt H, Spangenberg E, Erzinger J, 2008. Geochemical effects of CO2 sequestration in sandstones under simulated in situ conditions of deep saline aquifers. Appl. Geochem. 23: 2735–2745.

Wilkin RT, DiGiulio DC, 2010. Geochemical impacts to groundwater from geologic carbon sequestration: controls on pH and inorganic carbon concentrations from reaction path and kinetic modeling. Environ. Sci. Technol. 44, 4821–4827.

Wunsch A, Navarre-Sitchler AK, Moore J, Ricko A, McCray JE, 2013. Metal release from dolomites at high partial-pressures of CO2. Applied Geochemistry 38, 33–47.

Yardley B, Bennet A, Banks D, 2003. Controls on the chemical composition of crustal brines. Journal of geochemical Exploration. 78-79, 133-135.

Yélamos JG, Redondo R, De Castro F, Galván A, Martínez-Rubio J, Rebollo L, Ruano P, Senderos A, Villarroya FI, 1999. Hidrogeoquímica y microbiología en Los Hervideros del Campo de Calatrava (Ciudad Real). Geogaceta 26, 115-118.

Zheng L, Apps JA, Spycher N, Birkholzer JT, Kharaka YK, James Thordsen J, Sarah R, Beers SR, Herkelrath WN, Kakouros E, Trautz RC, 2011. Geochemical modeling of changes in shallow groundwater chemistry observed during the MSU-ZERT CO_2 injection experiment. Intern. Journ. Greenh. Gas Cont.

Zheng L, Apps JA, Spycher N, Birkholzer JT, Kharaka YK, Thordsen J, Beers SR, Herkelrath WN, Kakouros E, Trautz RC, 2012. Geochemical modeling of changes in shallow groundwater chemistry observed during the MSU-ZERT CO_2 injection experiment. Int. J. Greenhouse Gas Control 7, 202–217.

In the Field

GREENHOUSE GASES SCIENCE AND TECHNOLOGY

Use of diffusive gradients in thin films (DGT) as an early detection tool of low-intensity leakage from CO_2 storage

Marco Agnelli, Fidel Grandia and Anthony Credoz, Amphos 21 Consulting S.L., Barcelona, Spain
Andrea Gasparini, Istituto Nazionale di Geofisica e Vulcanologia (INGV), Rome, Italy
Jordi Bruno, Amphos 21 Consulting S.L., Barcelona, Spain and Fundaciòn Ciudad de la Energia (CIUDEN), Ponferrada, Spain

Abstract: Diffusive gradients in thin films (DGT) have been tested in CO_2-rich, metal-bearing fluids from springs in the Campo de Calatrava region in Central Spain, to assess their applicability as a monitoring tool in onshore CO_2 storage projects. These films are capable of adsorbing metals and recording changes in their concentration in water, sediments, and soils. Considering that CO_2 dissolution promotes metal solubilization and transport, the use of these films could be valuable as a monitoring tool of early leakage.

A number of DGT have been deployed in selected springs with constant metal concentration. The studied waters show high concentrations of Fe, as high as 1×10^4 $\mu g \cdot L^{-1}$, Ni, Co, Zn, Cu, and Mn. Comparing re-calculated metal concentration in DGT with metal water concentration, two different metal behaviors are observed: (i) metals with sorption consistent with the metal concentration (i.e. plotting close to the 1:1 line in a $[Me]_{DGT}$: $[Me]_{water}$ plot), and (ii) metals with non-linear sorption, with some data showing metal enrichment in DGT compared with the concentration in water. Metals in the first group include Fe, Mn, Co, Ni, and U, and metals in the second group are Zn, Pb, Cr, Cu, and Al. From this research, it is concluded that the metals in the first group can be used to monitor potential leakage by using DGT, providing effective leakage detection even considering low variations of concentrations, episodic metal release, and reducing costs compared with conventional, periodic water sampling.

Keywords: Campo de Calatrava; CO_2 storage and leakage; DGT; metal leakage; metal transport; trace metals.

Introduction

The capture and the storage of CO_2 in deep subsurface reservoirs is one of the options currently being considered to mitigate the rising anthropogenic greenhouse gas (GHG) concentrations in the atmosphere.[1] The site selection of CO_2 storage reservoirs must be accurate enough to minimize the risks to human health and the environment.[2,3] However, even considering a thick, impervious seal

Correspondence to: Marco Agnelli, Pas. Garcia i Faria, 49–51 P.1 Pta.1., 08019, Barcelona, Spain. E-mail: marco.agnelli@amphos21.com
Received July 12, 2013; revised September 12, 2013; accepted September 25, 2013
Published online at Wiley Online Library (wileyonlinelibrary.com). DOI: 10.1002/ghg.1383

formation, the possibility of leakage via preferential pathways (fracture or wells) cannot be completely ruled out, and its early detection is essential to avoid major impacts. In this respect, the changes in the geochemistry of shallow groundwater may provide evidence of CO_2 intrusion in such aquifers. These changes can be promoted by the chemical interactions between the CO_2 and shallow groundwater, leading to the dissolution, mobilization, and re-precipitation of metals and metalloids.[4–8] In principle, the metal transport capacity of CO_2-bearing fluids in shallow aquifers should dramatically decrease as pH increases due the buffering with aquifer rocks and also due to the relative high Eh favoring very low iron solubility. However, the Fe(III) solubility in CO_2-bearing fluids can be significantly increased due to the formation of Fe(III) carbonate complexes that are stable at circum-neutral pHs, and, therefore, being more persistent in time and space in the geological media.[9] The experimental results match observations in natural systems, where high Fe(III) concentration can be found under oxic, circum-neutral solutions where iron concentration is up to 3 orders of magnitude higher than that expected in CO_2-free solutions.[10] The enhanced solubility of Fe(III) has an additional and unwanted side effect: the inhibition of the precipitation of $Fe(OH)_3$(am), which is the main sink for many trace and minor elements in shallow aquifers. Then, CO_2-bearing solutions are particularly rich not only in iron but also in many other metals and metalloids, increasing the pollution impact of affected aquifers. The $Fe(OH)_3$ inhibition is gone due to CO_2 degassing related to fluid ascent to surface, and eventually part of all these metals may be precipitated back into solid phases but still some of the metal load is under solution. Monitoring of metal contents in shallow aquifers can, therefore, be valuable in the early detection of failure of containment of a CO_2 storage site because the concentration of all these metals in shallow and surface waters is commonly very low, and tiny changes in such a concentration could be indicative of early leakage.

DGT have long been used as recorders of ion pollution in waters, soils and sediments.[11] They are commonly used to detect changes of metal concentration through time. Recently, Ardelan and Steinnes (2010) and Ardelan *et al.* (2012) used DGT to record the increase in metal concentration in CO_2-seepage chamber as a test of potential impact of CO_2 leakage on seafloor in offshore storage.[12,13] Their results show that many metals were remarkably increased in their concentration after CO_2 dissolution in seawater, especially U and Ce, whose dramatic increase permits the use of these metals as chemo-indicators for CO_2 seepage. They concluded that the enhanced Fe, Co, and Mn can also be used as supportive chemo-indicators for a possible CO_2 seepage in oxic waters.

In this paper, DGT have been tested in CO_2-rich, metal-bearing fluids from shallow aquifers and springs in the Campo de Calatrava region in Central Spain, to assess its applicability as a monitoring tool in on-shore storage projects.

Diffusive gradients in thin films (DGT)

DGT, invented in Lancaster University in 1993, are devices capable of accumulating dissolved substances and provide the *in situ* concentration at time of deployment, measuring trace metals, phosphate, sulfide and radionuclides in waters, soils and sediments. When deployed in water, DGT measures labile species.[11]

DGT consist of a plastic base (2.5 cm diameter) loaded with a resin gel, a diffusive gel, and filter, and then the plastic top securely push fits over it to leave a 2.0 cm diameter window. The mouldings have been designed to accommodate a 0.4 mm Chelex resin gel layer, 0.8 mm diffusive hydrogel layer and 0.135 mm filter (0.45 μm) (Fig. 1).

The simple plastic DGT is deployed for a known time and then the mass of metal on the resin layer is measured after elution with acid by, for example, AAS or ICP-MS. DGT devices have usually been deployed by simply suspending them from a rope or string. Above a low threshold value, the measurement is independent of solution flow.[14] DGT has been deployed *in situ* in rivers, lakes, estuaries, and the deep sea. Its in-built pre-concentration gives it excellent sensitivity (10^{-12} mol·L^{-1}) and avoids contamination problems. DGT can be kept under water from hours to several weeks, depending on the metal concentration of water and the potential metal saturation of the Chelex resin. While Chelex is a robust and tolerant resin, it works very well in the pH range of 5 to 9 for most metals.[11,15–17] Below or above these values the resin is prone to modify its physical characteristics. For Cu, the resin operates effectively over a broader range of 2–11.

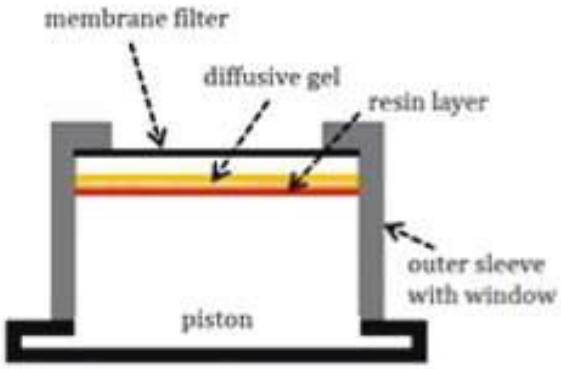

Figure 1. Schematic drawing of DGT device (left; adapted from Zhang and Davison, 1995) and deployment in a monitoring station (right). The device is 2.5 cm in diameter.

DGT provides time-averaged concentrations that are ideal for regulatory monitoring. In water, the determination of the average concentration C_{DGT} of each metal given by DGT device, and the mass m of each metal adsorbed in the Chelex resin, are calculated from Eqn (1):

$$D_{DGT} = \frac{m \times \Delta g}{D \times t \times A} \text{ with } m = Ce \times \frac{(V_{HNO_3} \times V_{gel})}{f_e} \quad (1)$$

where Δg is the thickness of the diffusive gel plus filter (0.8 mm plus 0.14 mm respectively), D is the specific diffusion coefficient in the diffusive gel for each metal at the sampling temperature ($m^2 \cdot s^{-1}$), t is the duration of deployment, A is the area of exposure (3.14 cm^2), Ce is the concentration in the 1.0 M HNO_3 elution solution, V_{HNO3} is the volume for acid elution (average of 1 mL), V_{gel} is the volume of gel (0.15 mL), f_e is the elution factor (0.8).

The diffusion coefficient D used for each metal was selected as a function of the sampling point temperature and are those recommended by DGT Research Ltd (2003) (Table 1).[14]

Scenarios of CO_2 intrusion in shallow aquifers

The changes in the chemistry of shallow aquifers due to early CO_2 leakage from deep storage are not fully understood, since no significant impact has been observed so far in commercial operations. How and

Table 1. Diffusion coefficients (D, x 10^{-6} $cm^2 \cdot s^{-1}$) for each studied elements in the T range between 10 and 27 °C.

Temp	D (10^{-6} cm^2/s)										
°C	Al	Cr	Mn	Fe	Co	Ni	Cu	Zn	Cd	Pb	U
10	3,04	3,23	3,74	3,91	3,80	3,70	3,99	3,89	3,90	5,14	–
12	3,25	3,45	4,00	4,18	4,06	3,94	4,26	4,15	4,16	5,49	–
13	3,35	3,56	4,12	4,31	4,19	4,07	4,39	4,29	4,30	5,67	–
14	3,46	3,67	4,26	4,45	4,32	4,20	4,53	4,42	4,43	5,85	–
15	3,57	3,79	4,39	4,59	4,46	4,33	4,68	4,56	4,57	6,03	–
16	3,68	3,91	4,52	4,73	4,60	4,47	4,82	4,70	4,72	6,21	–
17	3,79	4,03	4,66	4,87	4,74	4,60	4,97	4,85	4,86	6,40	–
20	4,14	4,39	5,09	5,32	5,17	5,02	5,42	5,29	5,30	6,99	–
25	4,75	5,05	5,85	6,11	5,94	5,77	6,23	6,08	6,09	8,03	–
27	5,01	5,32	6,17	6,45	6,27	6,09	6,57	6,41	6,43	8,47	6,41

where such leakage can be detected very early on is then challenging. Natural systems provide evidence of metal increase in solution as a response of CO_2 intrusion but these are in most cases very mature in terms of hydrogeology and water-to-rock interaction processes. Instead, early intrusion may lead to a transient state in which neither CO_2 ascent nor geochemical reactions are constant in time.

The detection of metal changes in shallow aquifers can be done by periodic water collection and analysis in wells within an area that should cover the potential spreading of CO_2 plume in the deep reservoir. In general, the extension of this area should be at least some hundreds of km^2, including dozens of sampling points to be regularly monitored through the operational and post-closure stages. In this context, depending on the nature of early intrusion, there is a chance of not detecting leakage even considering a tight, regular water sampling. To illustrate this, three scenarios could be drawn: (i) No CO_2 intrusion, (ii) episodic intrusion, and (iii) constant intrusion. Assuming that CO_2 dissolution and metal release is fast, the periodic collection and analysis of a particular well close to the intrusion point should yield different results if inputs of CO_2 react with the water aquifer (Fig. 2).

Episodic intrusion of CO_2(g) or CO_2-rich deep groundwater into shallow aquifers has been recently reported by Piqué *et al.* (2010) from the Caldes de Malavella geothermal field (NE Spain).[18] In one of the studied stations (shallow aquifer DW-5), a remarkable increase in bicarbonate concentration was recorded (Fig. 3), coupled with a sharp increase in metal

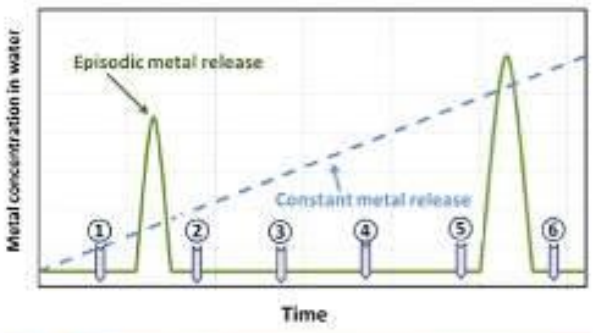

Figure 2. Example of expected metal release from water-to-rock interaction as detected in a well close to a CO_2 intrusion point considering an episodic intrusion and a constant intrusion. Numbers refer to a periodic sampling that misses the detection of the metal release episodes.

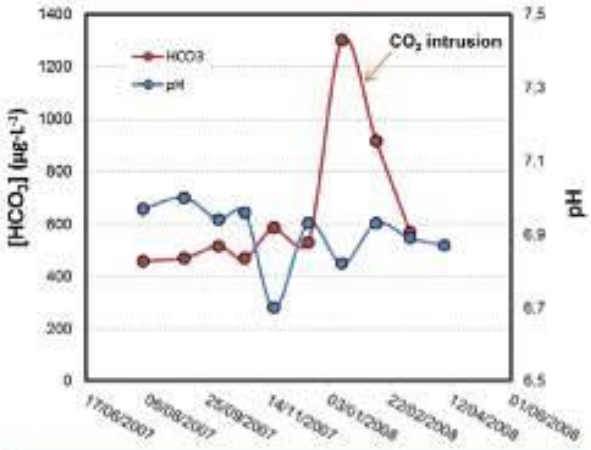

Figure 3. Episodic intrusion of CO_2-rich deep groundwater into a shallow aquifer at Caldes de Malavella geothermal field (station DW-5 from Piqué et al. 2010). Note that pH does not significantly change.

concentration, mainly iron (Fig. 4) but also U, V, Cu, Zn, Th, and Al. In contrast, pH did not significantly change through the sampling period (9 months). The CO_2-rich groundwater was geothermal in origin, showing a very similar chemistry with geothermal springs nearby.

The use of DGT is intended to reduce costs of sampling and to avoid missing metal release episodes. In Fig. 5, the evolution of the metal mass sorbed in

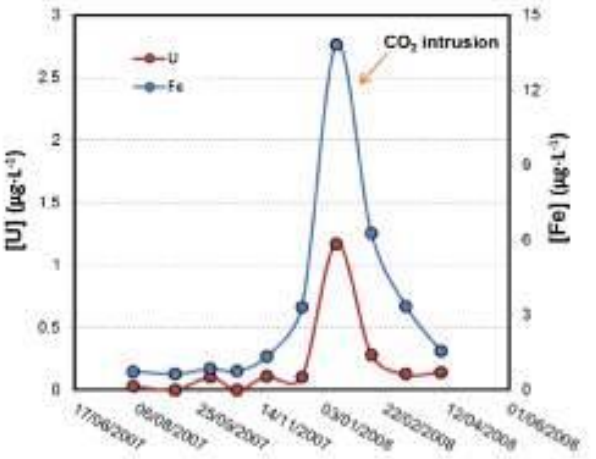

Figure 4. Increase in Fe and U in shallow aquifer as a response of an episodic intrusion of CO_2-rich deep groundwater at Caldes de Malavella geothermal field (station DW-5 from Piqué et al. 2010).

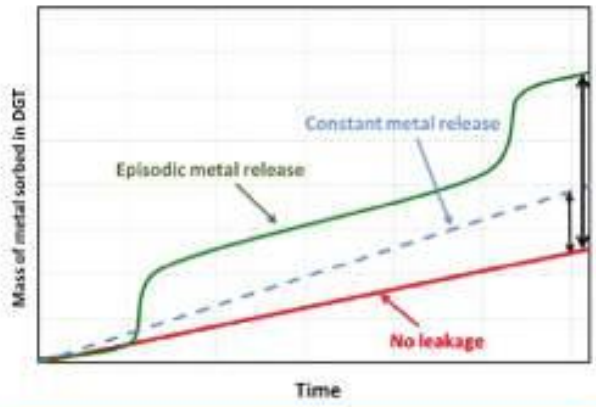

Figure 5. Evolution of the mass of metal sorbed in DGT deployed in a well close to a CO_2 intrusion point in the three scenarios discussed in the text and illustrated in Fig. 2.

DGT in time concerning the scenarios listed above is drawn, and it is clearly shown the capability of DGT to record metal increases any time, even if metal release is episodic.

In a more convenient way, the mass of sorbed metal can be converted to concentration of metal per litre of water following Eqn (1), and plotted against the corresponding metal concentration in water (Fig. 6). All data plotting above the 1:1 line would be indicative of metal excess related, possibly, to an episodic CO_2 intrusion and leakage in the deep reservoir.

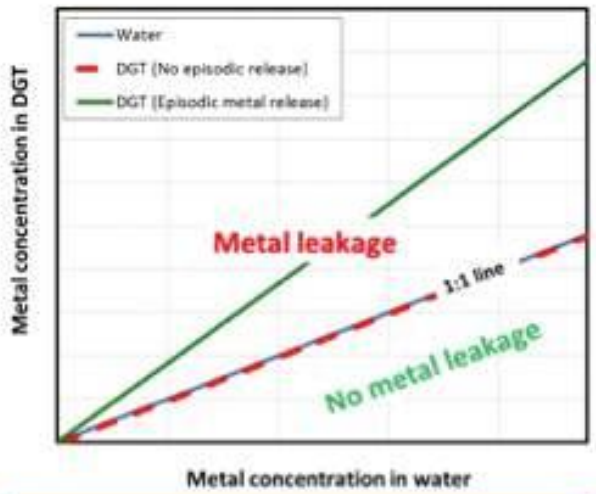

Figure 6. [Me] sorbed in DGT per liter of water vs. [Me] in water plot. Potential leakage will yield data plotting above the 1:1 line.

Beneath this line, data could suggest formation of metal-organic complexes, saturation or clogging of the DGT filters, or formation of metal precipitates before water passing through the resin.

Validation of DGT in natural analog of CO_2 seepage

In this paper, the use of DGT to detect early leakage in commercial storage has been tested in natural CO_2-bearing, metal-rich groundwater in the Campo de Calatrava region in Central Spain. The objective is to quantify the sorption behavior of a number of metals in DGT resins compared to the corresponding concentration in water. This must help to the selection of those metals showing an almost ideal behavior, i.e., 1:1 relationship in a time-averaged $[Me]_{DGT}/L_{water}$ vs $[Me]_{water}/L_{water}$ plot (Fig. 6), that can be later used in monitoring campaigns in commercial storage. In the Campo de Calatrava region, CO_2 intrusion from mantle in shallow aquifers leads to significant changes in the chemistry of the water in terms of metal content. The metal concentration of these fluids can be considered stationary (e.g. no significant changes through time are expected in the fluid chemistry) in individual sampling points, at least in the sampling period. Interestingly, concentration gradients have been observed in these aquifers and a relatively large difference in the metal concentration is measured between sampling points. The reason behind such gradients is likely related to the channeled nature of the CO_2 migration and to particular geochemical reactions at the sampling sites.

The Campo de Calatrava region, located a few hundreds of km south of Madrid (Fig. 7), comprises a series of scattered volcanic vents, mafic lava flows and pyroclastic deposits of alkaline composition in a domain some 4000 km^2 in area, within the Iberian Hercynian Massif, close to the external sectors of the Alpine Betic Cordilleras. This volcanic region has close affinities with the Miocene-Quaternary volcanic regions of western and central Europe,[19] characterized by a intracontinental plate magmatic association of leucitites, melilitites, nephelinites, and olivine basalts extruded during the late Miocene to Quaternary. Concerning the age of the volcanic events, the Campo de Calatrava can be subdivided into two separated events.[20] The first one (ultrapotassic) is less intense and occupies the central part of the region, with ages between 8.7 and 6.4 Ma. The second event (alkaline

Figure 7. Location of sampling stations in the Jabalón river basin in the Campo de Calatrava region. Red lines are major fracture zones.

and ultra-alkaline) ranges between 3.7 and 1.75 Ma. The main eruptive features of the many volcanic edifices that characterize the Campo de Calatrava region are dominated by strombolian and hydromagmatic events.

Natural CO_2 emission consists of a number of CO_2-rich fluid springs, dry CO_2 vents and some leaky wells, often characterized by conspicuous gas bubbling (Fig. 8). Free gas vents can yield fluxes higher than 5000 $g_{CO2} \cdot m^{-2} \cdot d^{-1}$ at the soil-atmosphere interface. The gas composition is largely dominated by CO_2 (>90% vol., up to 99.9% vol.), with minor and trace amounts of nitrogen, argon, H_2S, methane, and other hydrocarbons.

The deployment of DGT and monitoring of trace metals have been studied in nine sampling stations in the Jabalón river basin, in the Ciudad Real province (Fig. 7). All stations, except one corresponding to the Jabalón river bed, are CO_2-bearing springs.

Before deployment DGT devices were preserved in the fridge in a plastic bag filled with deionized water to avoid drying. Under these conditions, they have an optimal life of six months. During the field campaign, they were taken out from the bag, disposed, and kept with a nylon string deep in the sampled spring. They were deployed from 24 h (CO_2-bearing springs) to 30 days (river bed and station 9). After collection, the DGT surface was washed with deionized water, disposed in the original bag, and preserved in the fridge until the laboratory treatment and analysis. In the lab, Chelex resin was submerged 24 h in 1 M Suprapur HNO_3 solution to desorb metals. The mass of metal on the resin layer were measured by ICP-MS.

Figure 8. CO_2-bearing springs in Campo de Calatrava, with clear evidence of Fe(III) oxyhydroxide colloid formation.

In parallel to DGT withdrawal, sampling of spring and river water was performed in the same sites. Since CO_2 degassing at springs leads to formation of Fe(III) oxyhydroxide colloids, special care was taken in collecting colloid-free samples using 0.1μm filters.

Water samples were collected using 50 mL LDPE bottles where 0.5 mL of 1 M Suprapur HNO_3 acid was added for cations determination by ICP-MS.

Results

Metal ratios are quite similar of the nine stations of Jabalón basin for both water and DGT in spite of their different ranges of concentration (Table 2). Metal concentration in the Jabalón River (point 8) and in the Chorrillo site (point 9) are one order of magnitude lower than the CO_2-bearing springs since they are much more diluted waters in spite of the continuous metal release due to CO_2 degassing.

Sampled spring waters are slightly acidic with pH in the range of 5.4 to 5.9. Water from Jabalón river has a pH of 8.16. Electrical conductivity is above 1000 $\mu S \cdot cm^{-1}$ in all the springs except in sampling point 9, reaching values above 2000 μS in points 1, 2 and 3.

The collected samples contain high Fe concentrations, up to 1×10^{4} $\mu g \cdot L^{-1}$ (5.8×10^{-4} $mol \cdot L^{-1}$) (Table 2). The concentration in sample 5 only reaches 60 $\mu g \cdot L^{-1}$ (1.0×10^{-6} $mol \cdot L^{-1}$). This value is not consistent with the whole chemistry of the sample, and it is concluded that some error occurred during analysis. River water (sample 8) has a lower concentration (180 $\mu g \cdot L^{-1}$, 3.2×10^{-6} $mol \cdot L^{-1}$). The redox state of these waters is quite oxidizing and Fe is found under its ferric form. Then, considering the low solubility of Fe(III) in CO_2-free waters, the elevated Fe concentration in these samples illustrates well the role of aqueous Fe(III) carbonate complexes.

The studied samples also show high concentrations of Ni (up to 60 $\mu g \cdot L^{-1}$, 1.1×10^{-6} $mol \cdot L^{-1}$), Co (up to 24 $\mu g \cdot L^{-1}$, 4.1×10^{-7} $mol \cdot L^{-1}$), Zn (up to 157 $\mu g \cdot L^{-1}$, 2.4×10^{-6} $mol \cdot L^{-1}$), Cu (up to 22 $\mu g \cdot L^{-1}$, 3.4×10^{-7} $mol \cdot L^{-1}$), and Mn (up to 1 $mg \cdot L^{-1}$, 1.8×10^{-5} $mol \cdot L^{-1}$). In river

Table 2. Metal concentration in the samples from the Campo de Calatrava CO_2-bearing springs and in DGT devices after collection. All concentrations are µg·L^{-1}.

Ref	Temp (°C)	pH Detection limits	Conductivity (µS)	DGT/ Water	Al (µg·L^{-1}) 2	Cr (µg·L^{-1}) 0.5	Mn (µg·L^{-1}) 0.1	Fe (µg·L^{-1}) 10	Co (µg·L^{-1}) 0.005	Ni (µg·L^{-1}) 0.3	Cu (µg·L^{-1}) 0.2	Zn (µg·L^{-1}) 0.5	Pb (µg·L^{-1}) 0.01	U (µg·L^{-1}) 0.001
1	17	5,9	2170	DGT	479	4,6	204,3	633	5,95	25,8	10,1	65,7	0,61	0,29
				Water	1230	6,4	803,0	>10000	19,20	59,6	21,8	157,0	3,96	0,61
2	13	5,75	2300	DGT	616	5,0	258,5	4100	7,66	24,6	5,3	36,2	0,68	0,01
				Water	66	4,5	745,0	>10000	12,20	40,5	3,4	10,2	0,03	0,04
3	12,6	5,88	2250	DGT	682	5,8	219,7	137	4,89	28,3	4,7	54,3	0,78	0,21
				Water	12	3,8	349,0	190	6,88	39,2	2,4	22,3	0,03	0,29
4	16	5,69	1216	DGT	557	4,8	459,2	4235	13,74	34,9	4,2	94,8	0,63	0,16
				Water	204	3,0	973,0	>10000	22,40	53,8	1,5	81,1	0,07	0,67
5	15,5	5,85	1733	DGT	609	6,5	516,4	4770	15,60	40,2	10,7	70,9	0,67	0,22
				Water	70	4,1	841,0	6860	18,30	43,3	1,8	73,6	0,06	0,30
6	14	6,1	1429	DGT	645	6,2	524,7	122	18,88	58,0	4,1	163,2	0,71	0,25
				Water	27	2,9	693,0	602	23,60	63,8	1,1	55,6	0,06	0,35
7	14	5,88	1421	DGT	623	5,2	445,3	8373	21,65	55,0	19,8	106,7	0,72	0,19
				Water	53	4,7	763,0	8760	24,30	56,7	2,9	63,5	0,17	0,25
8	10	8,16	1244	DGT	23	0,2	50,2	173	0,66	0,7	0,4	2,0	0,03	0,16
				Water	4	4,0	78,9	180	0,56	6,9	3,7	3,8	0,05	3,98
9	17	5,42	960	DGT	30	0,1	2,3	5	0,18	1,1	0,2	2,6	0,05	0,29
				Water	38	4,0	33,2	40	0,48	10,7	1,1	12,8	0,09	0,33
Blanc	15	–	–	DGT	556	4,4	5,9	65	0,05	2,3	3,6	394,5	0,77	0,0002

sample, the concentration of all these elements is at least 1 order of magnitude lower. On the other hand, metals such as Pb, Cr, U (Table 2), and metalloids (As) do not show elevated concentrations.

Comparing re-calculated metal concentration in DGT (from eq.1; Table 2) with metal water concentration, two different groups of metals are observed (Figs 9 and 10): (i) metals with sorption close to the ideality (plotting close to the 1:1 line) or with lower sorption, and (ii) metals with non-linear sorption, with some data with $[Me]_{DGT}$: $[Me]_{water}$ >1. Metals in the first group include Fe, Mn, Co, Ni and U (Fig. 9). Metals in the second group are Zn, Pb, Cr, Cu and Al, with most data showing 'excess' of sorption compared to the concentration in water (Fig. 10).

Discussion

The use of DGT for convencional surface monitoring in the influence area of CO_2 geological storage is apparently cost-effective for operators and regulators. Considering one-year long monitoring campaign, DGT could be deployed during a couple of times with a water sampling at each deployment and collection time. In constrast, a traditional monitoring campaign of periodic water sampling is much more expensive in both sample analysis and field work, and less reliable for detecting slight changes in metal contents.

A strong point of DGT films is their capacity to bear tough environmental conditions (e.g. intensive rainfall and water level increase in river and lake, biological activity). However, the sorption of metals in DGT could not be complete due to a number of processes and this is something to take into consideration during monitoring and in the data interpretation. It is worth mentioning that DGT Chelex resin is selective for labile species that form inorganic complexes or small organic complexes.[21] Large organic complexes diffuse differently through the resin and their presence may underestimate the calculated amount of metals in solution.

It is also remarkable the effect of colloid formation, which can reduce the sorption of mainly Fe and Mn in DGT, since particles larger than 0.45 µm will be excluded. In addition, all metals sorbed onto colloids can not pass through the filters. However, the impact of colloid formation is minimized if a $[Me]_{DGT}/L_{water}$ vs $[Me]_{water}/L_{water}$ plot is used, since water collection also include colloid retention in filters.

The formation of biofilm growth on DGT device can limit metal retention. Dunn *et al.* (2003) observed that DGT labile metal concentrations could be 3 to 5 times

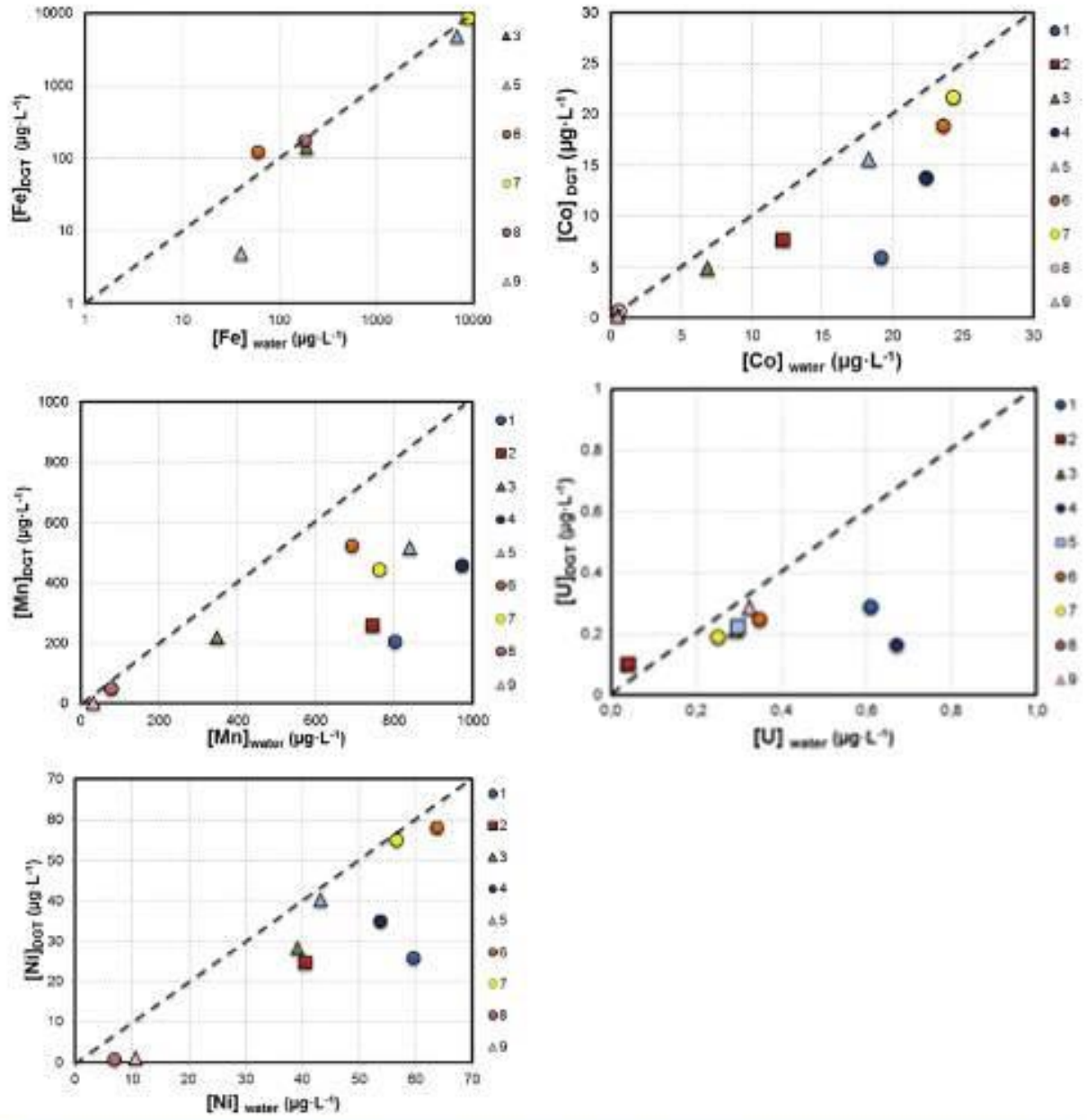

Figure 9. [Me] sorbed in DGT per liter of water vs. [Me] plot in water corresponding to Fe, Mn, Ni, Co and U, in samples collected in the Campo de Calatrava region. These metals show typically data plotting below the 1:1 line. Symbol numbers are the sample station.

below the concentrations of 0.45 µm filtered samples for some elements such as Ni, Pb, Cu and Zn.[22] They suggested that biofilm growth on DGT could act to increase the thickness of the diffusive path-length above that estimated, which would mean that DGT labile metal concentrations calculated are proportionally underestimated. In the time of DGT exposure (24 h to one month) in the studied springs, biofilm did not significantly grow to have a significant retardation effect on metal diffusion into the monitoring device.

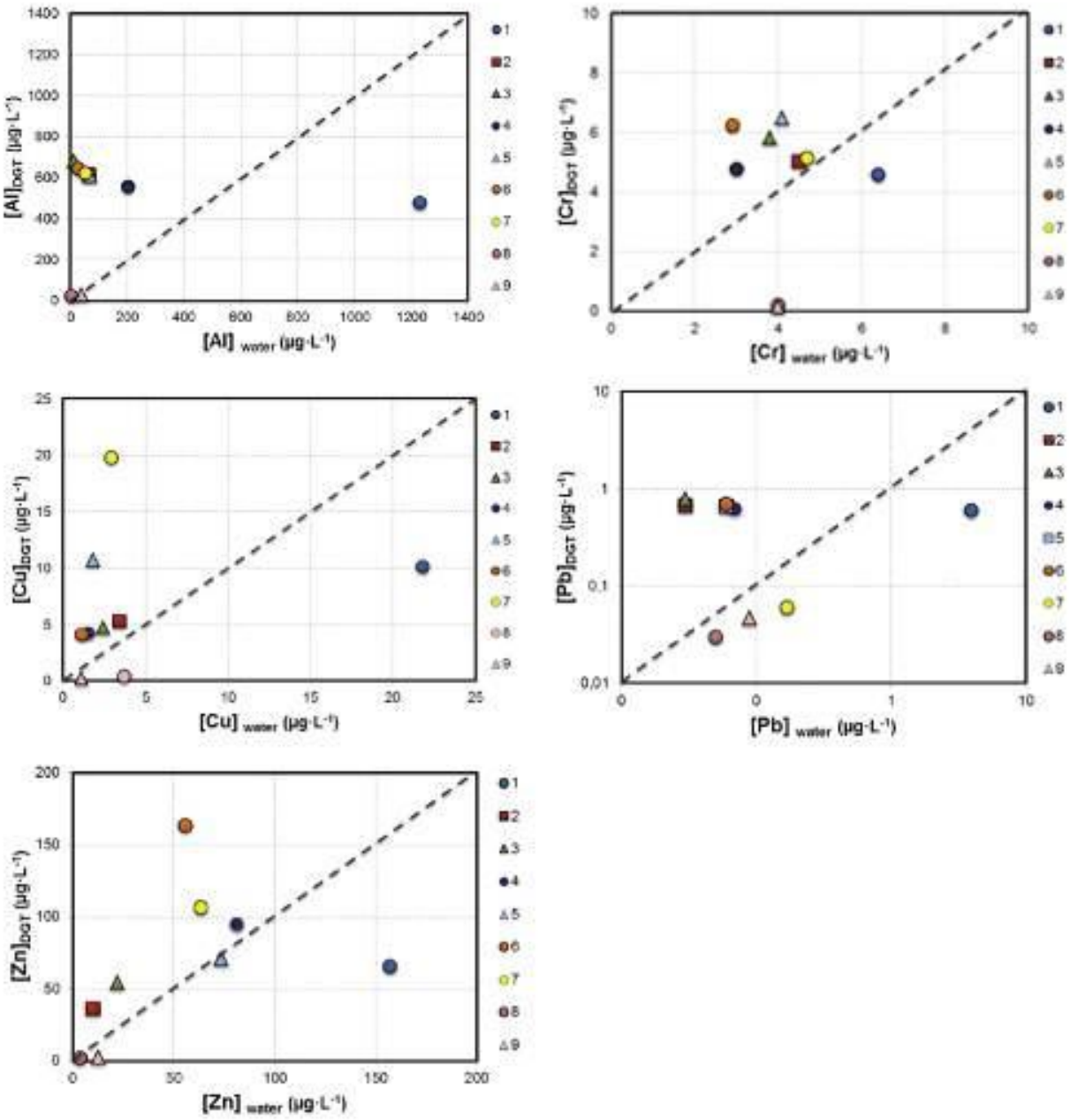

Figure 10. [Me] sorbed in DGT per liter of water vs. [Me] plot in water corresponding to Al, Cr, Zn, Pb and Cu, in samples collected in the Campo de Calatrava region. These metals show most data plotting above the 1:1 line. Symbol numbers are the sample station.

Operators would have to adapt the time of exposure of DGT to potential biofouling effect in backwater.

From the monitoring perspective, the limitation of DGT resins seems to be, thus, the behavior of the metal sorption depending on the metal speciation in the studied waters. The results from the tests in Campo de Calatrava suggest that some metals (Fe, Co, Ni, and U) are basically transported as labile inorganic forms and they are almost fully adsorbed in the DGT, as revealed by the $[Me]_{DGT}/I_{water}$ vs $[Me]_{water}/I_{water}$ ratios close to 1. For these metals, data plotting far below 1:1 line suggest problems with clogging of

the DGT filters or metal uptake by mineral precipitation prior to the sorption in the DGT resin. This could be the case of sample 1 since DGT is always much depleted in any metal.

In contrast, other metals (Zn, Pb, Cr, Al) show large discrepancies between the measured and expected metal sorption in DGT, with $[Me]_{DGT}/L_{water}$ vs $[Me]_{water}/L_{water}$ ratios typically higher than 1. The reason behind such discrepancies is not clear and commonly proposed hypotheses are not conclusive. First of all, the formation of colloidal particles could overestimate the metal concentration in DGT. In this work, two different filters have been used for DGT and for filtering the water samples, 0.45 and 0.1 µm, respectively. Therefore, some colloid-borne metals can be retained and analyzed in DGT and excluded from the water collection. However, since most colloids in the studied samples seem to be Mn-, Fe-oxyhydroxides, the overestimation of metals in DGT should also be seen for iron and manganese, and also for other trace metals sorbed in their surfaces (including U, Ni, and Co), which is not the case. For Al, the presence of clay colloids could account for the excess in the DGT, since these minerals are abundant in the precipitates around the CO_2-rich springs.

Another hypothesis to explain preferential metal sorption on DGT could be a variable metal concentration in water through sampling time (up to one month) due to, for example, dilution in the aquifer. However, this variability also should be seen in all metals. The formation of carbonate mineral precipitates inside the DGT device which could be also dissolved during the laboratory treatment could account for the data for Zn and Pb since calcite may uptake these metals in its lattice. Nevertheless, calcite can also fix metals with similar geochemical properties, i.e. Co and Ni, which are not enriched in excess in the DGT analysis.

Conclusions

The enhanced metal transport due to CO_2 dissolution makes the changes in metal contents in surface waters and shallow aquifers a potential good indicator of leakage from deep geological storage. The early stages of such metal increase may not be constant in time and, consequently, of difficult detection. The use of DGT films appears to be a cost-effective monitoring tool to be used as a regular technique in commercial on-shore projects. Tests in CO_2-bearing, metal-rich springs in the Campo de Calatrava region in Central Spain reveal that DGT record well the concentration of some metals such as Fe, Ni, Co, and U since a remarkable correlation between metal concentration in water and metal contents in DGT is observed. Therefore, these metals can be considered as favourable tracers for detection of early leakage by using DGT films. On the other hand, metals such as Zn, Pb, and Al do not show a clear correlation between adsorbed contents in DGT and water concentration. The reason behind such lack of correlation is not clear and it is suggested that the use of these metals could lead to misinterpretation of early CO_2 leakage from deep sources.

Acknowledgments

We are grateful for the technical support to Hao Zhang from the University of Lancaster in the use of DGT films. Also, we are grateful to CIUDEN for the funding of the project. This study is part of the OXYCFB 300 'Compostilla' EEPR project.

References

1. European Commission, *Communication from the Commission to the European Parliament, the Council, the European Economic and Social Committe and the Committe of the Regions on the Future of Carbon Capture and Storage in Europe*. EC, Brussels.
2. Rempel KU, Liebscher A, Heinrich W and Schettler G, An experimental investigation of trace element dissolution in carbon dioxide: Applications to the geological storage of CO_2. *Chem Geol* **289**:224–234 (2011).
3. Zheng L, Apps JA, Spycher N, Birkholzer JT, Kharaka YK, James Thordsen *J et al.*, Geochemical modeling of changes in shallow groundwater chemistry observed during the MSU-ZERT CO_2 injection experiment. *Int J Greenhouse Gas Control* **60**:273–284 (2011).
4. Czernichowski-Lauriol I, Rochelle C, Gaus I, Azaroual M, Pearce J and Durst P, Geochemical interactions between CO_2, pore-waters and reservoir rocks: lessons learned from laboratory experiments, field studies and computer simulations, in Advances in the Geological Storage of Carbon Dioxide: *NATO Science Series IV*, ed by Lombardi S, Altunina LK and Beaubien SE. *Earth Environ Sci* **65**:141–157 (2006).
5. Kharaka YK, Cole DR, Hovorka SD, Gunter WD, Knauss KG and Freifeld BM, Gas–water–rock interactions in Frio Formation following CO_2 injection: Implications for the storage of greenhouse gases in sedimentary basins. *Geology* **34**:577–580 (2006).
6. Kharaka YK, Thordsen JJ, Hovorka SD, Nance HS, Cole DR, Phelps TJ and Knauss KG, Potential environmental issues of CO2 storage in deep saline aquifers: Geochemical results from the Frio-I Brine pilot test, Texas, USA. *Appl Geochem* **24**:1106–1112 (2009).
7. Wigand M, Carey JW, Schütt H, Spangenberg E and Erzinger J, Geochemical effects of CO_2 sequestration in sandstones

under simulated in situ conditions of deep saline aquifers. *Appl Geochem* **23**:2735–2745 (2008).
8. Fischer S, Liebscher A, Wandrey M and CO2SINK Group. CO_2–brine–rock interaction - first results of long-term exposure experiments at in situ P–T conditions of the Ketzin CO_2 reservoir. *Chem Erde* **70(3)**:155–164 (2010).
9. Grivé M, Duro L and Bruno J, Fe(III) mobilization by carbonate in low temperature environments: Study of the solubility of ferrihydrite in carbonate media and the formation of Fe(III) carbonate complexes. Submitted to *Geoch. Cosmochim Acta* (2013).
10. Bruno J, Grandia F and Vilanova E, Trace element behaviour in connection to the geological storage of CO_2. Lessons from natural analogues. Abstracts of the Goldschmidt Conference 2009, Davos (Switzerland). *Geochim Cosmochim Acta* **73(13)**:A167 (2009).
11. Zhang H and Davison W, Performance characteristics of diffusion gradients in thin-films for the measurement of trace-metals in aqueous-solution. *Anal Chem* **67**:3391–3400 (1995).
12. Ardelan MV and Steinnes E, Changes in mobility and solubility of the redox sensitive metals Fe, Mn and Co at the seawater-sediment interface following CO_2 seepage. *Biogeosciences* **7**:569–583 (2010).
13. Ardelan MV, Sundeng K, Slinde GA, Gjøsund NS, Nordtug T, Olsen AJ and Torp TA, Impact of possible CO_2 seepage from sub-seabed storage on trace elements mobility and bacterial distribution at sediment-water interface. *Energ Procedia* **23**:449–461 (2012).
14. DGT Research Ltd, *DGT-for measurements in water, soils and sediments: Users guide for DGT technique*. DGT Research Ltd, Lancaster, UK (2003).
15. Gimpel J, Zhang H, Hutchinson W and Davison W, Effect of solution composition, flow and deployment time on the measurement of trace metals by the diffusive gradient in thin films technique. *Anal Chim Acta* **448**:93–103. (2001)
16. INAP (International Network for Acid Prevent), *Diffusive gradients in thin-film (DGT). A technique for determining bioavailable metal concentration*. INAP (2002).
17. Chelex 100 and Chelex 20 Chelating Ion, *Exchange resin instruction manual*. Bio-Rad Laboratories, Hercules, CA (2000).
18. Piqué A, Grandia F and Canals A, Processes releasing arsenic to groundwater in the Caldes de Malavella geothermal area, NE Spain. *Water Res* **44**:5618–5630 (2010).
19. Wilson M and Downes H, Tertiary—quaternary extension-related alkaline magmatism in Western and Central Europe. *J Petrol* **32(4)**:811–849 (1991).
20. Ancochea E, Huertas MJ, Cantagrel JM, Coello J, Fúster JM, Arnaud N and Ibarrola E, Evolution of the Cañadas edifice and its implications for the origin of the Cañadas Caldera (Tenerife, Canary Islands). *J Volcanol Geoth Res* **88**:177–199 (1999).
21. Davison W and Zhang H, In situ speciation measurements of trace components in natural waters using thin-film gels. *Nature* **367**:546–548 (1994).
22. Dunn RJK, Teasdale PR, Warnken J and Schlich RR, Evaluation of the diffusive gradient in a thin film technique for monitoring trace metal concentration in estaurine waters. *Environ Sci Technol* **37**:2794–2800 (2003).

Marco Agnelli

Marco Agnelli a PhD student in Geochemistry. Contracted with Amphos 21 Consulting S.L., he is in charge of the project 10 (Tracing metal-CO_2(aq)-solid interactions from deep sources to shallow aquifers) of the Met-Trans project, a European project about the metal transoport in the environment. His research focuses on the metal transport in fluids that are characterized by an high amount of dissolved CO_2. The expected results should be taken into consideration in the risk assessment programs of present-day and future commercial projects of CO_2 storage.

Jordi Bruno

Jordi Bruno is CEO and Chairman of the Board of Amphos 21 Consulting and Amphos 21 Group. He is also Director of the Chair Enresa-Amphos 21 on Sustainability and Waste Management in the Universitat Politecnica de Catalunya (UPC). He holds a PhD in Inorganic Chemistry from the Royal Institute of Technology (KTH), Stockholm, and an Executive MBA from Stanford University. With over 30 years of experience in the field of waste management, risk analysis, and environmental management strategies, his main areas of expertise include sustainability, chemical risk assessment and evaluation of performance and safety of nuclear waste repositories, toxic/hazardous and geological storage of CO_2.

Anthony Credoz

Anthony Credoz is a senior consultant in Amphos 21 on experimental, modeling and monitoring activities for performance and safety of radioactive wastes and gases (CO_2, CH_4) geological storage for national and international clients and R&D consortiums. Currently, he is managing the commercial development of Amphos 21 Consulting in France.

A graduate in Agronomic Sciences from the National Institute of Agronomy, Toulouse-France (2006), he holds a PhD in Geochemistry-Energy-Environment from Toulouse University, France.

Fidel Grandia

Fidel Grandia is currently the Project Manager of the Carbon Capture and Storage Group at Amphos 21, and former Associate Professor on Environmental Geology at the Technical University of Catalonia. He has a PhD in Geology by the Universitat Autonoma de Barcelona (2001). His research is focused on the modeling of the geochemical behavior of fluids in both present-day and fossil environments. He is currently involved in a number of 7th EC FP projects on CO_2 injection and storage, including Compostilla (Spain), MUSTANG and CarbFix (Iceland).

Andrea Gasparini

Andrea Gasparini is a PhD student studying CO_2 storage at the Univeritat Politècnica de Cataluña and Amphos 21 Consulting. He holds a degree in Geological Science from the University of Roma Tre, specializing in underground geological investigation. After that he qualified as a geologist. With the Istituto Nazionale di Geofisica e Vulcanologia (INGV), he worked in the Fluid Geochemistry, Geological Storage and Geothermal research team. With this team he started to work on soil gases (CO_2 and Radon mainly) and 3D modeling.